FROM CROSS FAULTS TO LAKE DEPOSITS: GEOLOGIC EVIDENCE OF PAST AND PRESENT HAZARDS

by

Bibek Giri

A dissertation submitted in partial fulfillment
of the requirements for the degree

of

Doctor of Philosophy

in

Earth Sciences

MONTANA STATE UNIVERSITY
Bozeman, Montana

July 2023

DEDICATION

I dedicate this work to my late grandparents, Krishna Lal Giri and Padma Kumari Giri.

ACKNOWLEDGEMENTS

I am indebted to numerous individuals who have made selfless and invaluable contributions to my work. First, I would like to express my gratitude to my supervisor, Dr. Mary Hubbard, whose support, encouragement, and guidance have been instrumental in this journey. Many thanks to my esteemed committee members, Dr. Devon Orme, Dr. Ananta Gajurel, and Dr. Andrew Laskowski, for their feedback and direction.

I am also deeply grateful to my parents, Arjun Giri and Ambika Giri, and my brother, Ashesh Giri, for their assistance with field logistics. Additionally, I would like to extend my appreciation to Samir Dhungel, Bishal KC, Nirman Lama, Thakur Kumar Lama, and Raju Lama for their involvement during my field study. Thanks to the locals of the region for welcoming me with open arms. Assistance provided by Sanjita Mishra and Ravi Acharya with necessary paperwork is also acknowledged. I extend my sincere gratitude to Dr. Dave Lageson, Dr. Xiangmei Li, Dr. John Childs, and Nischal Baral for their invaluable personal and professional support throughout these years.

The analytical work for my dissertation research was conducted at Arizona State University, Geosep Services, Lamont-Doherty Earth Observatory, Petrographic Services, and Utah State University.

I would also like to acknowledge the support received from the National Geographic Society, the Explorers Club, the Geological Society of America, and Montana State University. Their financial assistance has been crucial in the successful completion of this work.

TABLE OF CONTENTS

TABLE OF CONTENTS CONTINUED

TABLE OF CONTENTS CONTINUED

LIST OF TABLES

LIST OF FIGURES

LIST OF FIGURES CONTINUED

ABSTRACT

The Everest region in the eastern Nepal Himalaya is a natural laboratory for Earth sciences research as it consists of spectacular rock exposures, glaciers, lakes, rivers, and rockslide zones. While a plethora of research has been conducted in the region, a geomorphic and a tectonic feature remained unnoticed until recently. In 2017, a segment of a young (<12 Ma), NNE-striking cross fault, later named the Benkar Fault Zone (BFZ), was recognized and examined within the Everest region. Cross faults are faults that strike at a high angle to the trend of the orogen. The BFZ remained unexplored towards the south. Secondly, there are a number of layered, sandy deposits, around the Namche-Phortse areas, perched high on hillsides with no obvious connection to a modern depositional basin. The goals of my dissertation are to explore these unanswered questions in order to: 1) understand the southern continuity and genesis of the BFZ; and 2) constrain depositional ages for those sandy deposits and understand their depositional settings. To achieve my first goal, I mapped the BFZ towards the south from the Everest region and augmented the mapping results with kinematic and petrographic analysis. I find that the BFZ is a ~100 km long, segmented cross fault zone that possibly cuts across the entire width of the eastern Nepal Himalaya. The BFZ is a composite of a series of deformational events and might continue further towards the south into the foreland basin. This fault, like other Himalayan cross faults, likely contributes to seismic and landslide hazards. Through an extensive literature review, I have synthesized the occurrences and drivers of cross faults and lateral heterogeneity in several mountain belts around the world. For my second goal, I constrained the depositional ages of six sedimentary deposits by utilizing infrared stimulated luminescence analysis and integrated the ages (~13-42 ka) with their geomorphic setting. I interpret that some of them were likely deposited in localized, landslide- and/or moraine-related, ephemeral lakes/ponds. Such deposits provide invaluable agricultural land in these extreme topographies.

CHAPTER ONE

INTRODUCTION

The Khumbu region, also known as the Everest region, in the eastern Nepal Himalaya, is home to 4 peaks greater than 8000 m, including the highest summit on earth, Mt. Everest (8848 m). Within these areas of high altitude (>4000 m), the geomorphology is primarily defined by the spectacular exposures of high-grade metamorphic rocks, which have been reshaped by alpine glaciers and their deposits. It is not surprising that most of the work to date has been focused on hard rock geology (e.g.; Hubbard, 1989; Carosi et al., 1999; Searle et al., 2003; Jessup et al., 2006; Cottle et al., 2009; Carrapa et al., 2016), glaciology (e.g.; Wessels et al., 2002; Kang et al., 2004; Owen et al., 2009; Quincey et al., 2009; Bolch et al., 2011; Kaspari et al., 2011; Sherpa et al., 2017), and glacial geomorphology (e.g.; Benedict, 1976; Iwata, 1976; Fushimi, 1978; Muller, 1980; Aoki & Imamura, 1999; Richards et al., 2000; Finkel et al., 2003; Barnard et al., 2006). While voluminous research across multiple disciplines has already been conducted in the region, our research group recently identified previously unrecognized tectonic and geomorphic features in the region.

Hubbard et al. (2018) recognized a NNE-striking topographic lineament feature near Benkar village. Subsequently, Seifert (2019) conducted structural mapping and petrographic kinematic analysis in the Everest region and interpreted the lineament to be a segment of a cross fault, later named the Benkar Fault Zone (BFZ). Hubbard et al. (2018) and Seifert (2019) have interpreted the BFZ as a NNE-striking, SE-dipping, right-lateral, normal cross fault that runs along and adjacent to the Dudh Koshi valley in the Everest region (Figure 1.1). I am defining cross fault as faults that strike at a high angle to the trend of the orogen. The BFZ is the only

Himalayan cross fault documented in high mountain regions other than the graben-bounding faults such as along the Thak Khola Graben. Seifert (2019) recognized that the BFZ likely continued to the south, but mapping in that direction was beyond the scope of his work. One of the goals of my dissertation research was to take the mapping and kinematic and petrographic analysis southward to understand the southern continuity and mode of formation of the BFZ. Although in recent years, researchers have documented several cross faults in the lower regions of the Himalaya (e.g.; Wu et al., 1998; Sahoo et al., 2000; Hurtado et al., 2001; Mukul, 2010; Harvey et al., 2015; Divyadarshini & Singh, 2019; Duvall et al., 2020), a comprehensive understanding, in terms of timing of movement, genesis, and tectonic implications, of these structures is still lacking. Therefore, I reviewed literature on cross faults in other mountain belts around the world to gain structural and tectonic understanding of cross faults. The review work (Giri & Hubbard, 2023) forms the second chapter of my dissertation. In the third chapter, I have presented my mapping and structural work on the BFZ to the south of Seifert (2019)'s map area.

A geomorphic puzzle in the Everest region is that around Namche-Phortse-Tyangboche areas there are a number of well-bedded, sandy deposits perched high on hillsides with no obvious connection to a modern depositional basin (Figure 1.1). Terraces along river valleys generally serve as possible depositional zones for glacial, landslide, aeolian, fluvial, and debris flow deposits but these deposits are located at elevations >100 m from the river beds. The Everest region has an erosional exhumation rate of ~1mm/yr (Hubbard et al., 1991; Streule et al., 2012). If these deposits were river terrace deposits, then they would have to be >100 ka in age. In general, erosion strongly outpaces deposition at these extreme topographies and such a

Figure 1.1: Map of the Everest region. The map frame area is shown in the inset map. Solid red lines indicate the extent of the Benkar Fault Zone. Rectangles show the extent of map area in Figures 4.2 and 4.3.

prolonged preservation of deposits is not very likely. The second goal of my dissertation is to constrain the timing of deposition for these deposits and to explore the possible depositional setting in light of the contemporaneous geomorphic processes. This research effort forms the fourth chapter of my dissertation.

Together, my research contributes to our understanding of structures and geomorphic features that are products of the Himalayan mountain building process. The results presented here also provide a basis from which we may be able to better understand features in other mountains as well.

References

Aoki, T., & Imamura, M. (1999). *Reconstructing the glacial chronology based on the 10Be exposure age in the Khumbu glacier, eastern Nepal Himalayas-a problem on the production rate of in-situ cosmogenic radionuclides.* Paper presented at the Proc. the Korea-Japan/Japan-Korea Geomorphological Conference.

Barnard, P. L., Owen, L. A., & Finkel, R. C. (2006). Quaternary fans and terraces in the Khumbu Himal south of Mount Everest: their characteristics, age and formation. *Journal of the Geological Society, 163*(2), 383-399. doi:https://doi.org/10.1144/0016-764904-157

Benedict, J. (1976). Khumbu glacier series, Nepal. *Radiocarbon, 18*(2), 117-178.

Bolch, T., Pieczonka, T., & Benn, D. (2011). Multi-decadal mass loss of glaciers in the Everest area (Nepal Himalaya) derived from stereo imagery. *The Cryosphere, 5*(2), 349-358.

Carosi, R., Musumeci, G., & Pertusati, P. C. (1999). Extensional tectonics in the higher Himalayan crystallines of Khumbu Himal, eastern Nepal. *Geological Society of America Special Paper, 328*, 211-223.

Carrapa, B., Robert, X., DeCelles, P. G., Orme, D., Thomson, S., & Schoenbohm, L. (2016). Asymmetric exhumation of the Mount Everest region: Implications for the tectono-topographic evolution of the Himalaya. *Geology, 44*(8), 611-614.

Cottle, J. M., Searle, M. P., Horstwood, M. S., & Waters, D. J. (2009). Timing of midcrustal metamorphism, melting, and deformation in the Mount Everest region of southern Tibet revealed by U (-Th)-Pb geochronology. *The Journal of Geology, 117*(6), 643-664.

Divyadarshini, A., & Singh, V. (2019). Investigating topographic metrics to decipher structural model and morphotectonic evolution of the Frontal Siwalik Ranges, Central Himalaya, Nepal. *Geomorphology, 337*, 31-52. doi:10.1016/j.geomorph.2019.03.028

Duvall, M. J., Waldron, J. W. F., Godin, L., & Najman, Y. (2020). Active strike-slip faults and an outer frontal thrust in the Himalayan foreland basin. *Proceedings of the National Academy of Sciences, 117*(30), 17615-17621. doi:doi:10.1073/pnas.2001979117

Finkel, R. C., Owen, L. A., Barnard, P. L., & Caffee, M. W. (2003). Beryllium-10 dating of Mount Everest moraines indicates a strong monsoon influence and glacial synchroneity throughout the Himalaya. *Geology, 31*(6), 561-564.

Fushimi, H. (1978). Glaciations in the Khumbu Himal (2). *Journal of the Japanese Society of Snow and Ice, 40*(Special), 71-77.

Giri, B., & Hubbard, M. (2023). Lateral Heterogeneity in Compressional Mountain Belt Settings. In E. J. Catlos & I. Cemen (Eds.), *Compressional Tectonics: Plate Convergence to Mountain Building* (Vol. 1, pp. 47-86): AGU Books.

Harvey, J. E., Burbank, D. W., & Bookhagen, B. (2015). Along-strike changes in Himalayan thrust geometry: Topographic and tectonic discontinuities in western Nepal. *Lithosphere, 7*(5), 511-518. doi:10.1130/l444.1

Hubbard, M., Gajurel, A. P., Mukul, M., & Seifert, N. (2018). *Cross faults and their role in Himalayan Structural Evolution*. Paper presented at the Geological Society of America Abstracts with Programs.

Hubbard, M., Royden, L., & Hodges, K. (1991). Constraints on unroofing rates in the High Himalaya, eastern Nepal. *Tectonics, 10*(2), 287-298. doi:https://doi.org/10.1029/90TC02777

Hubbard, M. S. (1989). Thermobarometric constraints on the thermal history of the Main Central Thrust Zone and Tibetan Slab, eastern Nepal Himalaya. *Journal of Metamorphic Geology, 7*(1), 19-30.

Hurtado, J. M., Jr, Hodges, K. V., & Whipple, K. X. (2001). Neotectonics of the Thakkhola graben and implications for recent activity on the South Tibetan fault system in the central Nepal Himalaya. *GSA bulletin, 113*(2), 222-240. doi:10.1130/0016-7606(2001)113<0222:Nottga>2.0.Co;2

Iwata, S. (1976). Late pleistocene and holocene moraines in the Sagarmatha (Everest) Region, Khumbu Himal. *Journal of the Japanese Society of Snow and Ice, 38*(Special), 109-114.

Jessup, M., Law, R., Searle, M., & Hubbard, M. (2006). Structural evolution and vorticity of flow during extrusion and exhumation of the Greater Himalayan Slab, Mount Everest Massif, Tibet/Nepal: implications for orogen-scale flow partitioning. *Geological Society, London, Special Publications, 268*(1), 379-413.

Kang, S., Mayewski, P. A., Qin, D., Sneed, S. A., Ren, J., & Zhang, D. (2004). Seasonal differences in snow chemistry from the vicinity of Mt. Everest, central Himalayas. *Atmospheric Environment, 38*(18), 2819-2829.

Kaspari, S. D., Schwikowski, M., Gysel, M., Flanner, M., Kang, S., Hou, S., & Mayewski, P. A. (2011). Recent increase in black carbon concentrations from a Mt. Everest ice core spanning 1860–2000 AD. *Geophysical Research Letters, 38*(4).

Mukul, M. (2010). First-order kinematics of wedge-scale active Himalayan deformation: Insights from Darjiling–Sikkim–Tibet (DaSiT) wedge. *Journal of Asian Earth Sciences, 39*(6), 645-657. doi:https://doi.org/10.1016/j.jseaes.2010.04.029

Muller, F. (1980). *Present and late Pleistocene equilibrium line altitudes in the Mt. Everest region-An application of the glacier inventory.* Paper presented at the Proceedings of the Riederalp Workshop.

Owen, L. A., Robinson, R., Benn, D. I., Finkel, R. C., Davis, N. K., Yi, C., Putkonen, J., Li, D., & Murray, A. S. (2009). Quaternary glaciation of Mount Everest. *Quaternary Science Reviews, 28*(15-16), 1412-1433.

Quincey, D., Luckman, A., & Benn, D. (2009). Quantification of Everest region glacier velocities between 1992 and 2002, using satellite radar interferometry and feature tracking. *Journal of Glaciology, 55*(192), 596-606.

Richards, B. W., Benn, D. I., Owen, L. A., Rhodes, E. J., & Spencer, J. Q. (2000). Timing of late Quaternary glaciations south of Mount Everest in the Khumbu Himal, Nepal. *Geological Society of America Bulletin, 112*(10), 1621-1632.

Sahoo, P. K., Kumar, S., & Singh, R. P. (2000). Neotectonic study of Ganga and Yamuna tear faults, NW Himalaya, using remote sensing and GIS. *International Journal of Remote Sensing, 21*(3), 499-518. doi:10.1080/014311600210713

Searle, M. P., Simpson, R. L., Law, R. D., Parrish, R. R., & Waters, D. J. (2003). The structural geometry, metamorphic and magmatic evolution of the Everest massif, High Himalaya of Nepal–South Tibet. *Journal of the Geological Society, 160*(3), 345-366. doi:doi:10.1144/0016-764902-126

Seifert, N. (2019). *Structural analysis of the Benkar Fault Zone, a cross structure in the Higher Himalaya of the Khumbu Region, eastern Nepal.* (MS). Montana State University, Bozeman, Montana.

Sherpa, S. F., Wagnon, P., Brun, F., Berthier, E., Vincent, C., Lejeune, Y., Arnaud, Y., Kayastha, R. B., & Sinisalo, A. (2017). Contrasted surface mass balances of debris-free glaciers observed between the southern and the inner parts of the Everest region (2007–15). *Journal of Glaciology, 63*(240), 637-651. doi:https://doi.org/10.1017/jog.2017.30

Streule, M. J., Carter, A., Searle, M. P., & Cottle, J. M. (2012). Constraints on brittle field exhumation of the Everest-Makalu section of the Greater Himalayan Sequence: Implications for models of crustal flow. *Tectonics, 31*(3). doi:https://doi.org/10.1029/2011TC003062

Wessels, R. L., Kargel, J. S., & Kieffer, H. H. (2002). ASTER measurement of supraglacial lakes in the Mount Everest region of the Himalaya. *Annals of Glaciology, 34*, , 399-408.

Wu, C., Nelson, K. D., Wortman, G., Samson, S. D., Yue, Y., Li, J., Kidd, W. S. F., & Edwards, M. A. (1998). Yadong cross structure and South Tibetan Detachment in the east central Himalaya (89°–90°E). *Tectonics, 17*(1), 28-45. doi:https://doi.org/10.1029/97TC03386

CHAPTER TWO

LATERAL HETEROGENEITY IN COMPRESSIONAL MOUNTAIN BELT SETTINGS

Contribution of Authors and Co-Authors

Manuscript in Chapter 2

Author: Bibek Giri
Contributions: Investigation, Writing – original draft and figures
Co-Author: Mary Hubbard
Contributions: Conceptualization, Validation, Writing – review and editing

Manuscript Information

Bibek Giri and Mary Hubbard

Geophysical Monograph Series

Status of Manuscript
____ Prepared for submission to a peer-reviewed journal
____ Officially submitted to a peer-reviewed journal
____ Accepted by a peer-reviewed journal
__x_ Published in a peer-reviewed journal

The American Geophysical Union
April 2023
Compressional Tectonics: Plate Convergence to Mountain Building
https://doi.org/10.1002/9781119773856.ch3

Abstract

Analysis of convergent orogens reveals important orthogonal/cross structures and laterally heterogenous deformation style, igneous activity, metamorphic grade, geomorphology and seismic activity. To assess the occurrence, causal mechanisms, and implications of these lateral heterogeneities, we review a selection of convergent orogens, with different tectonic settings and history. We find that heterogeneities are primarily driven by the pre-existing deformational history of the cratonic blocks involved, lateral change in lithology of crustal rocks, variations in rheologic properties, or changes in plate kinematics. The Appalachian orogenic front mimics the Iapetan rift margin. As seen in the Zagros and the Cordillera, pre-existing basement structures have control on pre- and syn- orogenic sedimentation, which subsequently impact how the orogenic wedge evolves. Several cross faults in the Himalaya spatially coincide with basement structures on the down-going plate. Similarly, physiography of the subducting oceanic plate influences deformation in the overriding plate of Andean-type margins. Orogenic extension in the Alps has been accompanied by a system of orogen-parallel strike slip faults and extensional cross faults. It is evident that lateral heterogeneities can form crucial control on the evolution of orogenic belts and can influence seismic rupture patterns, resource occurrence, and landslide hazards.

Introduction

Many of the world's major mountain belts are found along modern or former convergent plate boundaries and they are typically dominated by major thrust structures (Elliott, 1976; Chapple, 1978; Boyer & Elliott, 1982; Dahlen, 1990). The terms 'continental collision or terrane accretion' have been used for convergent boundaries when both the involved plates are continental, though mountain building also occurs along convergent plate boundaries where an oceanic plate is subducting beneath continental crust (e.g.; Dewey & Bird, 1970). In both tectonic settings, compressive stress is accommodated through imbrication and shortening of upper crustal material as thrust sheets and/or nappes, within a system of fault surfaces, which generally strike perpendicular to the direction of compression (or parallel to the orogen). In general, these faults and related structures are laterally continuous both temporally and spatially. Detailed geological and geophysical research, however, has found that while these convergent mountain belts exhibit overall lateral continuity, there are also lateral heterogeneities that have made an important contribution to the development of the mountain belt. Driven by various mechanisms, these lateral changes serve to induce important structural, geological, and geomorphological lateral heterogeneities along mountains belts that may (or may have) influence(d) igneous or seismic processes or even the occurrence of economic resources. Commonly, significant along-strike changes are known to occur across structures, which strike orthogonal to the overall trend of the orogen. In this article, the term 'cross structure' has been utilized to refer to all generic, syn and post orogenic structural features that bound lateral changes along a mountain belt, though the terms 'cross-strike structural discontinuities' (CSD), 'transverse zones', and 'cross faults' have all been utilized to describe large-scale structures that strike across convergent mountain belts (Drahovzal & Thomas, 1976; Wheeler, 1980; Hubbard et al., 2018; Hubbard et al., 2021). Thomas (1990) suggested that transverse zones (TZ) along fold and thrust belts are domains of several, structurally aligned ‘lateral connectors’, which encompass transverse/tear faults, lateral ramps, and displacement transfer faults/zones. In general, the term ‘transverse zone’ has been used in the literature to denote large-scale, inherited basement features with a high-angled orientation to the evolving orogen. Lateral connecters like tear faults, lateral ramps, and transfer faults/zones form during thrust propagation and are rather localized, only spanning across a few thrust sheets. Formed during the propagation of thrust belts, these lateral connectors could be spatially controlled by the inherited structures in the crystalline basement as well as the overlying stratigraphy of the evolving thrust sheet (Thomas, 1990). During orogenesis, inherited basement structures are commonly reactivated or inverted and impart a great control on the tectonic and structural evolution of mountain belts (e.g.; Tavarnelli et al., 2004; Butler et al., 2006). Evidence has also been presented suggesting that oceanic transform faults or seamounts in a subducting oceanic plate can influence the structural development of the mountain belt in the overriding continental plate, thus causing lateral heterogeneity or the presence of cross structures (e.g.; Gutscher et al., 2000; Chapin, 2012).

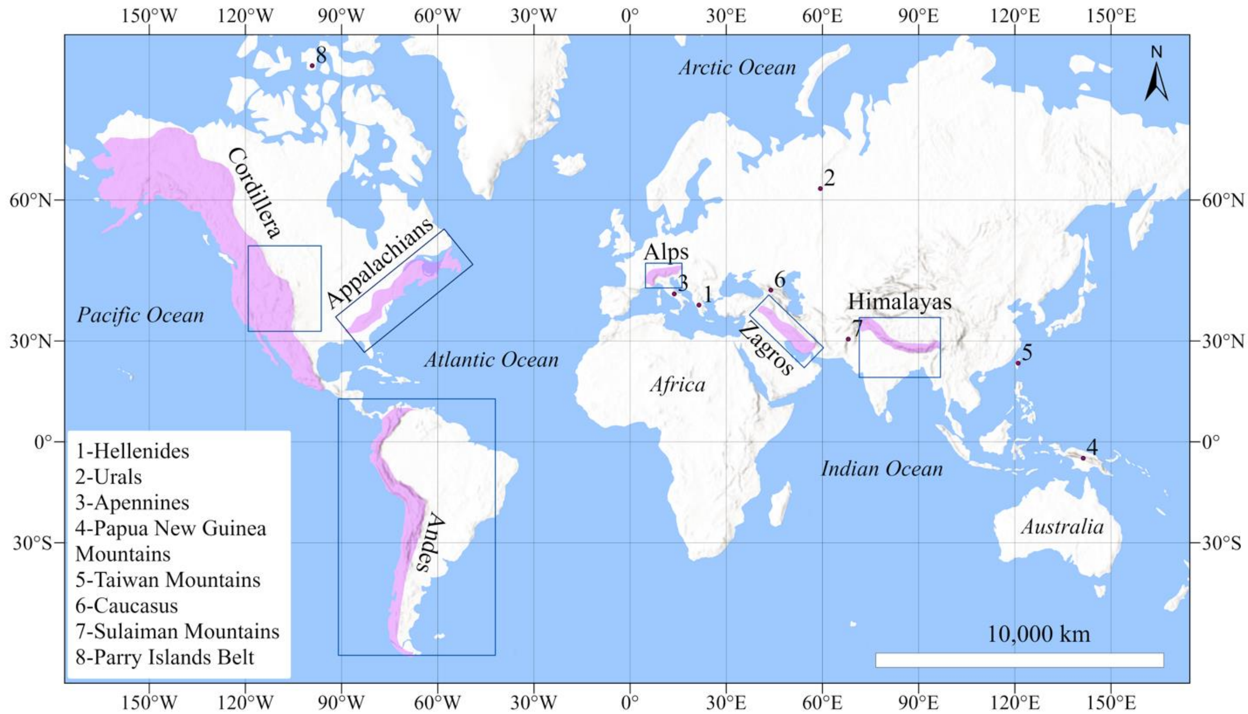

Figure 2.1: Map of the world showing locations of mountain belts described in this review. The pink shades are spatial extent of respective orogenic belts. Rectangular boxes indicate the extent of tectonic maps presented in the following sections. Numbered areas are other convergent orogens mentioned in the text.

Mountain belts formed in convergent plate tectonic settings at different time periods in Earth's history all exhibit some degree of lateral heterogeneity. The following review explores a selection of mountain belts from convergent boundaries, examining the proposed driving mechanisms and implications of lateral heterogeneities and the presence of cross structures during and after orogenesis. The Appalachians, the North American Cordillera, the Alps, the Himalaya, the Zagros, and the Andes have been looked at in detail, and several other mountain belts are briefly discussed (Figure 2.1). This selection represents some of the most well studied and prominent mountain belts around the world and presents a wide array of tectonic settings. Within each mountain belt, presented examples of lateral heterogeneities and cross structures are representative of the lateral variability for that orogen. For each mountain belt, we present a brief introduction of the tectonic setting, observed lateral heterogeneities, and proposed causal factors for those heterogeneities. It is noted that lateral heterogeneities can be expressed in several ways including: 1) along-strike changes in deformation style; 2) variation in igneous activity or metamorphic grade; 3) variation in seismic activity; 4) changes in geomorphology; or 5) abrupt lateral stratigraphic change. Drivers of these along-strike changes can include irregularities along continental margin, inherited basement structures of an overriding plate, features from a subducting plate (oceanic) or footwall block (continental), lateral variation in lithospheric or crustal properties, lateral changes in thickness and facies of the deforming sedimentary sequence, lateral variation in dynamic plate tectonic setting or a combination of these factors. Apart from their influence in the structural/tectonic evolution of the mountain belt, the lateral heterogeneity may also have important seismic, geomorphic, and economic implications.

Appalachians

Tectonic Setting and Lateral Heterogeneities

The Appalachian orogenic belt, along the eastern margin of the North American continent, is the structural culmination of a prolonged tectonic history consisting of multiple episodes of subduction, terrain accretion, continental collision, and rifting (Figure 2.2). The prominent Grenville orogeny (1.3-0.9 Ga; Li et al., 2008; Hynes & Rivers, 2010; Rivers, 2012)) was the coalescence of the Laurentian (modern day North American continent) and Amazonian cratons, which formed the Rodinia supercontinent (Li et al., 2008; Rivers, 2008, 2015). Following the Grenville orogeny, the Laurentian craton remained tectonically inactive for about 250 Ma before being detached from the Rodinia craton in various episodes from 759±12 Ma to 530 Ma (Thomas, 1991; Aleinikoff et al., 1995; Hogan & Gilbert, 1998). The Iapetan rifting, during which the Iapetus ocean opened between the Laurentian and Amazonian (Gondwana) cratons (Domeier, 2016), marked the end of this series of tectonic events (Rankin, 1976; Thomas, 1977; O'Brien & van der Pluijm, 2012). The Middle Ordovician to Late Silurian Taconian orogeny represents the aggregate contractional tectonic activity along the boundary between the Laurentian and Iapetan plates (Hatcher, 1972; Drake et al., 1989; van Staal et al., 2007; Hatcher, 2010). The Late Silurian to Devonian Acadian orogeny has been interpreted to have formed along an Andean-type margin (flat slab subduction) following the accretion of Avalonia to the Laurentia margin (Keppie & Krogh, 1999; Murphy & Keppie, 2005). The youngest event in the building of the Appalachians was the Late Mississippian to Late Permian Alleghenian orogeny (Laurentia and Gondwana) (Hatcher et al., 1989), which also marked the formation of the Pangean supercontinent. In the Mesozoic, the modern day North American plate rifted westward from the African continent. Dominant structures from all of these convergent and divergent tectonic events are range-parallel faults and fold axes. Close inspection, however, reveals lateral heterogeneity that includes changes in the mountain belt orientation, structural style, metamorphic grade, and the presence of cross structures.

One of the obvious heterogeneities in topography is the fact that the NE-trending Appalachian Mountain front curves around a series of recesses and salients along the length of its western margin (Figure 2.2). These recesses and salient are proposed to be bound by broad transverse structures that offset or truncate thrust structures (Thomas, 1990). In the southern Appalachians, the large-scale thrust faults and related structures are predominantly striking northeast and verging towards the northwest (Bayona et al., 2003). Abrupt along-strike terminations of these structures are known to spatially coincide with these transverse zones (TZ). In the Alabama recess (Figure 2.3a), major TZs include the Bessemer TZ, the Happersville TZ, the Anniston TZ, and the Rising Fawn TZ from southwest to northeast respectively (Thomas, 1990; Bayona et al., 2003; Brewer, 2004). In general, these transverse zones are tens of kilometers wide, hundreds of kilometers long, and cut into the Proterozoic basement rocks (Thomas & Bayona, 2002; Brewer, 2004). Thrust-related structures plunge into these TZs, abruptly terminate at lateral or oblique ramps, show offsets along transverse faults (tear faults), or break into en-echelon segments of transfer zones (Thomas & Bayona, 2002; Thomas, 2007; Cook & Thomas, 2009). Structural strike deviates within these TZs, while propagating over oblique/lateral ramp and irregular basement and at junctions between lateral/oblique and frontal ramps (Bayona et al., 2003). Above a lateral/oblique ramp, hanging wall rocks are generally folded into upright, isoclinal folds driven by local-scale, ramp perpendicular contraction in the hanging wall due to crowding of materials along that trend (Cook and Thomas 2009). Across the Cartersville TZ, deformation style, metamorphic grade, and thrust sheet stratigraphy show sharp contrast between the Alabama recess and the Tennessee salient (Tull & Holm, 2005). In the salient, passive margin and foreland sedimentary sequences are much thicker and have been deformed and metamorphosed (biotite grade of the Barrovian metamorphic series) more strongly than in the recess (Tull & Holm, 2005). Towards the adjoining Virginia recess, a section of the Pine Mountain belt, bounded by the left-lateral Jacksboro tear fault and the right lateral Russel Fork tear fault (Figure 2.3a), demonstrates a double ramp geometry in the middle section, while a single ramp geometry around the edges (Mitra, 1988). Presence of the orogen-parallel, large-scaled (about 35 km wide, (Brewer, 2004)) Birmingham graben beneath the southern Alleghenian thrust belt also had major controls on the foreland sedimentation and subsequent propagation of the thrust sheet (Thomas, 2007). Transverse zones in the southern Appalachians have been interpreted as inherited transform fault related to the Iapeton rifting along the continental margin of Laurentia (e.g.; Figure 2.4) (Rankin, 1976; Thomas, 1977, 2014).

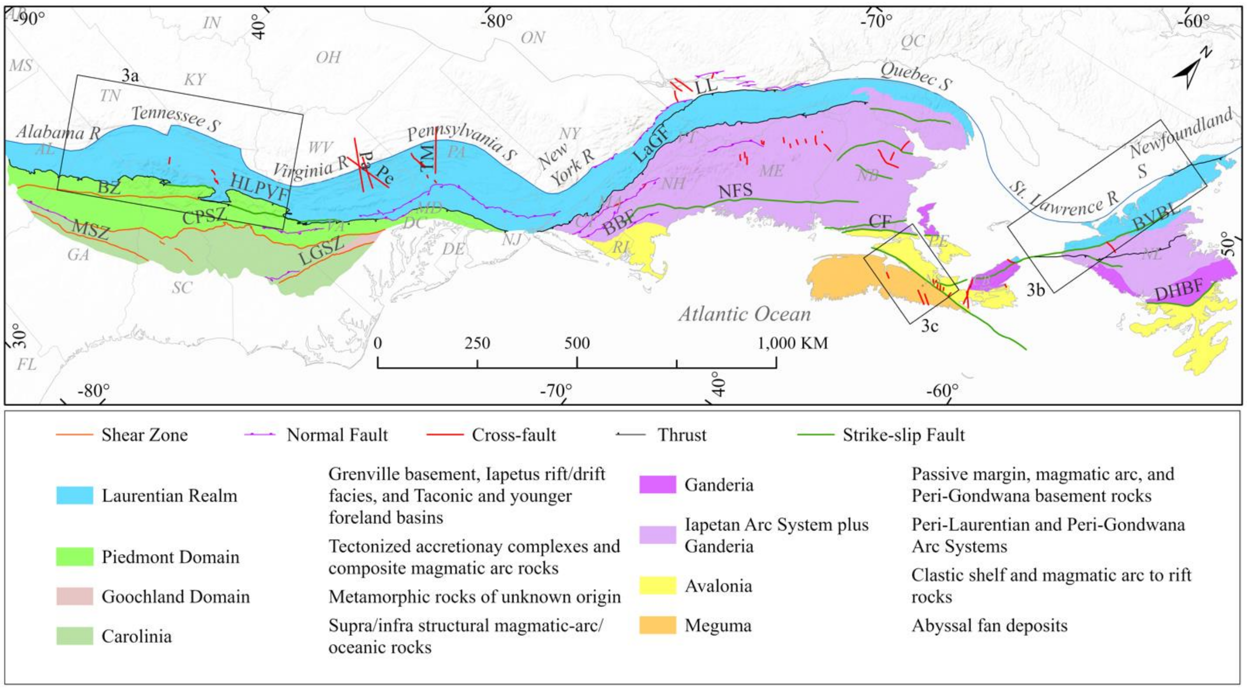

Figure 2.2: Simplified tectonic map of the Appalachian showing the major faults, the salient (S) and recesses (R), and the extent of the Appalachian deformation front. Insets show the locations of figures 2.3a, 2.3b, and 2.3c (simplified from: Southworth, 1986; Hibbard et al., 2006; Waldron et al., 2015). Acronyms: BBF: Bloody Bluff Fault; BVBL: Baie Verte-Brompton Line; BZ: Brevard Zone; CF: Caledonia Fault; CPSZ: Central Piedmont Shear Zone; DHBF: Dover Hermitage Bay Fault; HLPVF: Hollins Line-Pleasant Valley Fault System; LaGF: La Gaudaloupe Fault; LGSZ: Lake Gordon Shear Zone; LL: Logan's Line; MSZ: Modoc Shear Zone; NFS: Norumbega Fault System; Pa: Parson's Lineament; Pe: Petersburg Lineament; TM: Tyrone-Mount Union lineament.

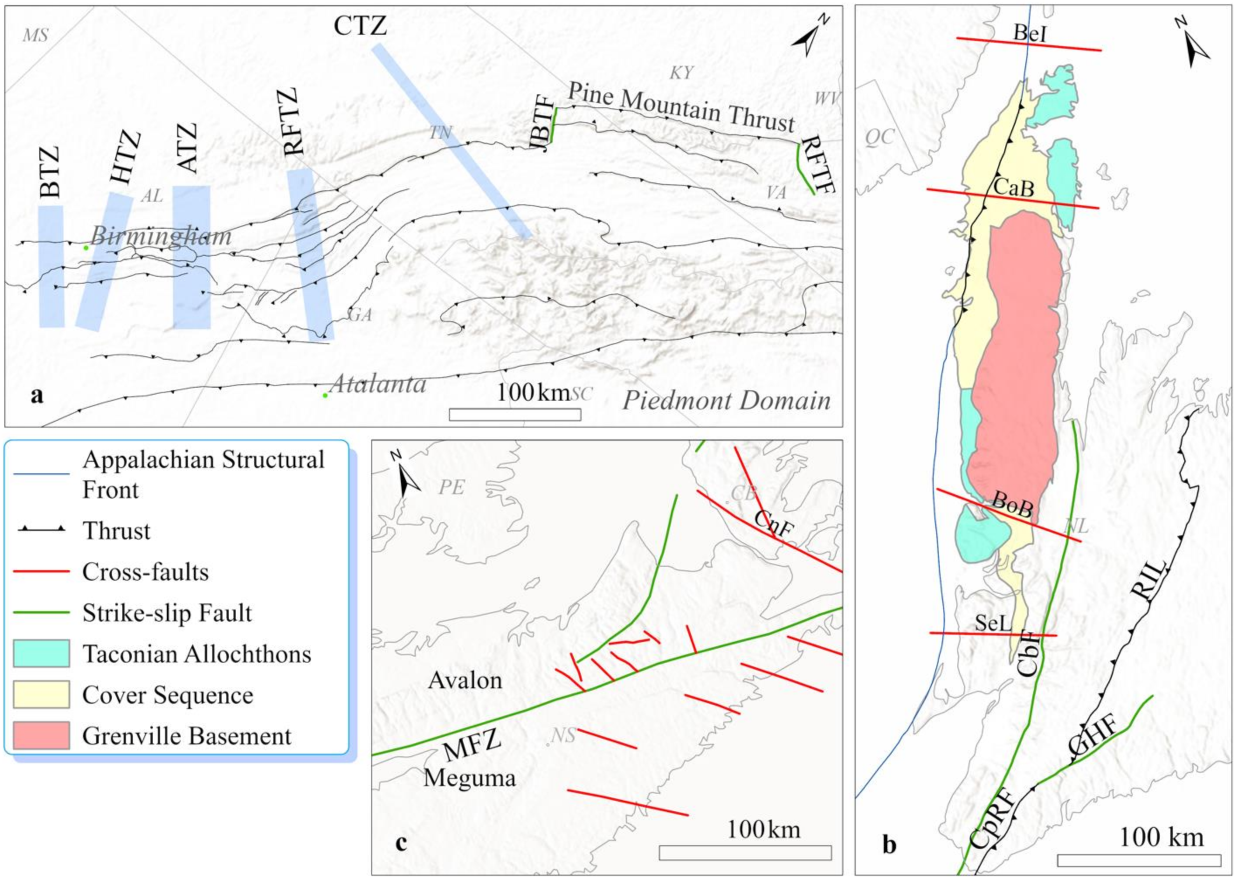

Figure 2.3: Cross structures along the Appalachians. a) Map of the Alleghenian fold and thrust belt in the Alabama recess and the Tennessee salient showing the major transverse zones (light blue rectangles) and the tear faults on either side of the Pine Mountain (source:Mitra, 1988; Cook & Thomas, 2009). b) Tectonic-sketch map of the Newfoundland Island showing the major cross-faults. Note the lateral termination of the Grenville basement inliers at the Bonne Bay cross-strike discontinuity (BoB) and the Canada Bay (CaB) cross-strike discontinuity. (source: Cawood & Botsford, 1991; Hibbard et al., 2006; Waldron et al., 2015). c) The Minas Fault Zone (MFZ) between the Avalon and Meguma terranes and its conjugate faults including the Canso Fault (CnF) (source: Hibbard et al., 2006; Waldron et al., 2015). Acronyms: ATZ: Anniston Transverse Zone; BeI: Belle Isle cross-strike discontinuity; BoB: Bonne Bay cross-strike discontinuity; BTZ: Bessemer Transverse Zone; CaB: Canada Bay cross-strike discontinuity; CbF: Cabot Fault; CnF: Canso Fault; CpRF: Cape Ray Fault; CTZ: Cartersville Transverse Zone, GHF: Gunflap Hills Fault; HTZ: Happersville Transverse Zone; JBTF: Jacksboro Tear Fault; MFZ: Minas Fault Zone; RFTF: Russel Fork Tear Fault; RFTZ: Rising Fawn Transverse Zone; RIL: Red Indian Line; SeL: Serpentine Lake cross-strike discontinuity.

Cross-structures in the Appalachians of Pennsylvania and West Virginia (central Appalachians) such as the Parsons, Petersburg, and Tyrone-Mount Union lineaments (Figure 2.2) also have similar effects on the orogen-parallel structures as is seen in the southern Appalachians (Wheeler, 1980; Southworth, 1986). In the northern Appalachians, however, genesis of cross-structures presents much more diversity. The Serpentine Lake cross-strike discontinuity (CSD), the Bonne Bay CSD, the Canada Bay CSD, and Belle Isle CSD in Newfoundland mark the

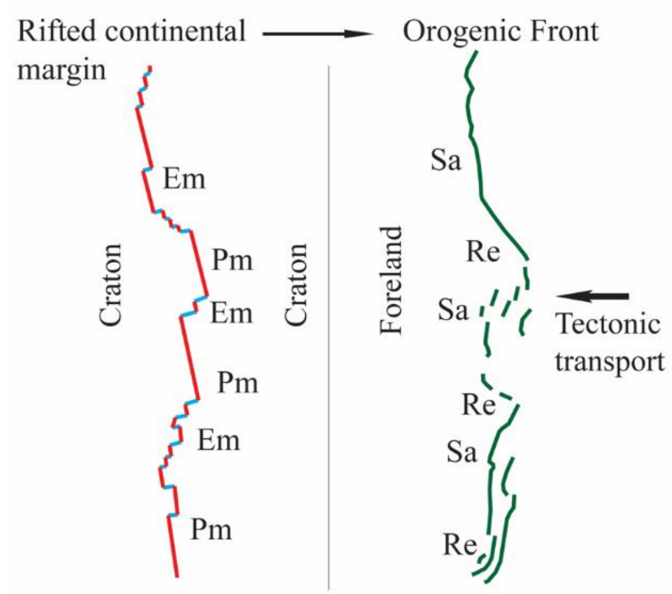

Figure 2.4: Impacts of the continental margin geometry on the geometry of an orogenic front. Embayments (Em) evolve into salients (Sa) and Promontories (Pm) evolve into recesses (Re).

boundaries of second-order salients and recesses and had controls on the Taconic and younger orogenic events (Figure 2.3b) (Cawood & Botsford, 1991). Across these structures, the depositional facies and structural style of the rock units overlying the Grenville basement change abruptly suggesting these faults have Precambrian roots. The Grenville basement inlier terminates southward at the Bonne Bay CSD (Figure 2.3b), which also delineates the southern limit of the Acadian uplift of the Grenville Inlier (Cawood & Botsford, 1991). North of the Bonne Bay CSD, thrusts and associated structures are west verging, while towards the south the vergence reverses (Williams & Cawood, 1986). In southern Newfoundland and the Cape Breton islands, the Silurian tectonic wedging of the Avalon craton into the Laurentian craton has resulted in a very narrow Appalachian central mobile belt characterized by stronger syncollisional deformation, high-grade Barrovian metamorphism (‘Kyanite and Sillimanite grade, 700-750 ˚C at 6-10 kbar (Plint & Jamieson, 1989), 5 kbar elsewhere’), and a greater volume of Silurian magmatism than elsewhere (Lin et al., 1994). This intensely deformed and metamorphosed narrow band is bound by the NW-striking Canso fault (Figure 2.3c) to the southwest and the E-striking Gunflap Hills fault to the northwest, interpreted as transverse, right lateral wrench faults that accommodated the differential movement on either side of the wedging (Lin et al., 1994). In its western end, the Gunflap Hills fault (Colman-Sadd et al., 1992) merges with the NW-striking Cape Ray fault zone (Figure 2.3b). In eastern Nova Scotia, several NW-striking, transverse, left-lateral strike-slip faults (e.g. the Country Harbour Fault) have been described as conjugates of the Minas Fault Zone (Figure 2.3c) (Waldron et al., 2015), which is an E-W striking 300 km long, continental transform fault in New Brunswick and Nova Scotia that marks the boundary between the Avalon and Meguma terranes (Murphy et al., 2011). Towards the west, the Paleozoic Norumbega Fault System (Figure 2.2) demonstrates the effect of the subducting plate physiography on the upper plate structures. This NE-striking, 300 km long, transpressive, dextral fault system (West Jr & Hubbard, 1997; Hubbard, 1999) has recently been interpreted to be a result of subduction of an oceanic ridge and related transform fault (Kuiper, 2016; Kuiper & Wakabayashi, 2018). Around the orogenic front in Quebec and northern

Vermont, cross structures were formed due to reactivation of earlier-formed transverse, normal faults with an oblique thrust-sense or served as an oblique ramp during the westward thrusting of the Lower to Middle Ordovician shelf-carbonates (Séjourné & Malo, 2007).

Proposed Factors Controlling Lateral Heterogeneities

Lateral heterogeneity along the Appalachians has largely been controlled by the irregularities along pre-collisional continental margins and by inherited basement structures. The eastern continental margin of Laurentia went through a series of rifting events including the Iapetan rifting, all of which acted in concert to develop a series of embayments (concave oceanward) and promontories (convex oceanward) separated by transform faults (Rankin, 1976; Thomas, 1977, 2014). During subsequent orogenic events (Taconic, Acadian, and Alleghenian orogenies), embayments evolved into salients (convex towards the foreland), promontories evolved into recesses (concave towards the foreland), and the transform fault boundaries evolved into transverse zones (Figure 2.4). As Tull and Holm (2005) noted, foreland sedimentary sections along salients are much thicker than along recesses, which has a great control on the geometry and deformation style of the evolving thrust sheets (discussed in detail in the North American Cordillera section of this article). Irregularity along continental margins also has another important control, which results in a sharp lateral heterogeneity along an orogen. A collisional event between two promontories (of two different landmasses) results in a narrower but stronger orogenic deformation and a higher grade of metamorphism that a promontory-embayment collision (Lin et al., 1994). The evolution of rift-related transform faults into transverse zones also had a profound impact on the evolution of the Appalachians mountains by creating barriers or zones that truncated or offset major thrust faults. Along the range front, transverse zones have served as nucleation sites for cross structures in the form of lateral ramps or tear faults.

Cordillera

Tectonic Setting and Lateral Heterogeneities

The North American Cordilleran orogenic system records the Jurassic (and possibly earlier) to Paleogene history of terrane accretion and the eastward convergence of the Farallon and Kula plates beneath the western margin of Laurentia (North American continent) (Oldow et al., 1989; Burchfiel et al., 1992; Saleeby et al., 1992; DeCelles, 2004; Dickinson, 2004). This convergence resulted in a number of different ranges including the Sierra Nevada, the Rocky Mountains, and the various mountain systems of Alaska (Figure 2.5a). Changing plate dynamics has resulted in varied deformation style and distribution throughout the Cordilleran evolution. The Late Cretaceous (Beck et al., 1988; Decelles et al., 1991) transition of deformation style from the thin-skinned, taper-wedge in the US Sevier fold-thrust belt to predominantly thick-skinned, basement-involved Laramide orogenesis is one of the remarkable changes. Initiation of the Laramide system uplifts has generally been correlated to the subduction of a flat-slab segment (e.g.; Coney & Reynolds, 1977; Dickinson & Snyder, 1978; Saleeby, 2003; Chapin, 2012). North of the Canadian border, the Laramide-style deformation is absent. Orogenic collapse of the Cordilleran system, focused on the Sevier belt, initiated during Middle to Late Eocene due to the change in relative plate kinematics and has resulted in the active Basin and Range province of extensional deformation (e.g.; Constenius, 1996; Yonkee & Weil, 2015). The contractional phase of deformation resulted in spectacular range-parallel fold and thrust belts

(Yonkee & Weil, 2015), yet there are important lateral heterogeneities and a number of cross structures along the Cordillera.

Basement provinces and their suture zones and major faults along the western margin of the North American continent include the Snowbird Tectonic Zone (Ross et al., 1991; Hope & Eaton, 2002), the Archean Hearne Province (Hope & Eaton, 2002), the Archean Medicine Hat Block (Ross et al., 1991; Lemieux et al., 2000); the Archean Wyoming Province (Wooden & Mueller, 1988; Mogk et al., 1992), and the Paleoproterozoic Yavapai and Mazatzal Provinces (Foster et al., 2006; Whitmeyer & Karlstrom, 2007), from north to the south (Figure 2.5b). The Trans-Hudson Orogen and the Superior Craton lie towards the east, around the central region of the North America. Towards the west, the basement block include the Archean Grouse Creek Block and the Selway Terrane (Foster et al., 2006).

Transverse crustal boundaries between these provinces and the other Archean/Paleoproterozoic transverse basement structures are one of the primary causes of lateral heterogeneity in the Cordillera due to their influence in the subsequent sedimentary and deformational history (e.g.; Paulsen & Marshak, 1999; Sears & Hendrix, 2004; McMechan, 2012). Significant crustal-scale, transverse boundaries around the southeastern Canadian Cordilleran front (Alberta) include the Thorsby Low, a crustal suture within the Snowbird tectonic zone (Ross et al., 1991; Hope & Eaton, 2002), the Red Deer zone, the northern boundary of the Hearne Province (Hope & Eaton, 2002), and the Vulcan Low, a crustal suture between the Medicine Hat Block and Hearne Province (Figure 2.5b) (Hoffman, 1988; Ross et al., 1991). These structures and terrane boundaries served as loci for activation of transverse zones during the deposition of the Mesoproterozoic Belt-Purcell sequence (Benvenuto & Price, 1979; Foo, 1979; Root, 1987; Anderson & Davis, 1995; McMechan, 2012). Multiple other transverse structures were also initiated in Mississippian and Triassic as normal faults above these transverse boundaries (Cooley et al., 2011; McMechan, 2012). Segments of some of these transverse zones were reactivated as dextral, oblique reverse faults or as tear faults during Jurassic to Eocene in response to compressional stresses (Bielenstein, 1969; Foo, 1979; Price, 1981; McMechan & Price, 1982; McMechan, 2000; Cooley et al., 2011). Similar impacts of basement structures on the evolution of thrust belts have been reported from other domains in the Canadian Cordillera (e.g.; Pride et al., 1986; Thompson, 1989; Pilkington et al., 2000; Berger et al., 2008). In northern British Columbia, a geometric inversion of the northern end of a NW-trending “basement uplift” during the Sevier contraction resulted in the formation of NE to E-trending (transverse) contractional structures, which were superimposed on the regional NW-striking structures (McMechan, 2007). Aside from their influence in the sedimentary and deformational history, these basement structures and terrane boundaries also formed suitable conduits for melt transport and served as loci for igneous intrusions and mineralization (McMechan, 2012).

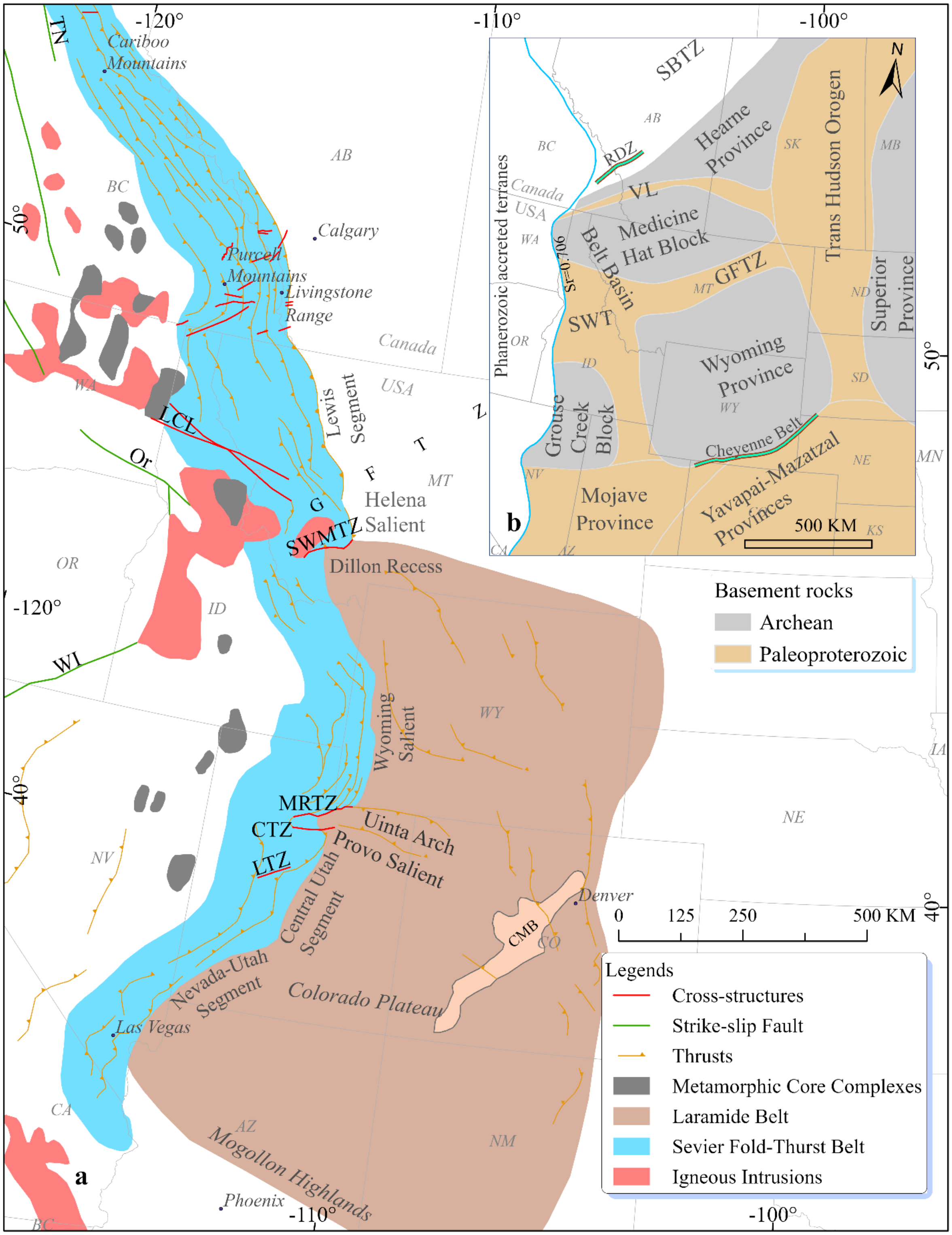

Figure 2.5: Simplified tectonic and basement map of the Cordillera. a) Tectonic map of the US and Southern Canadian Cordillera showing the major orogenic curvature and the major cross-

structures (modified from: Moffat & Spang, 1984; McGugan, 1987; Kwon & Mitra, 2006; Cooley et al., 2011; McMechan, 2012; Whisner et al., 2014; Yonkee & Weil, 2015) b) Generalized basement map of the western North America. The Sr=0.706 line represents the eastern boundary of the accreted terranes (source: Foster et al., 2006; Whitmeyer & Karlstrom, 2007; McMechan, 2012; Yonkee & Weil, 2015; Ronemus et al., 2020). Acronyms: CMB: Colorado Mineral Belt; CTZ: Charleston Transverse Zone; GFTZ: Great Falls Tectonic Zone; LCL: Lewis and Clark Line; LTZ: Leamington Transverse Zone; MRTZ: Mount Raymond Transverse Zone; Or: Orfino Shear Zone; RDZ: Red Deer Zone; SBTZ: Snowbird Tectonic Zone (the Thorsby Low is located within the SBTZ); SWMTZ: Southwestern Montana Transverse Zone; SWT: Selway Terrance; TN: Tintina-Rocky Mountain Shear Zone; VL: Vulcan Low; WI: West-Idaho Fault.

The Sevier FTB is generally classified into the Main Ranges, the Front Ranges, and the Foothills, from the hinterland to the foreland, in the northern US and the southern Canada. Cross structures have been observed in all these sub-divisions at different scales. In the Main Ranges of British Columbia (Purcell Mountains), Mesoproterozoic and Eocambrian synsedimentary faults have been reactivated as dextral, east-striking, transverse, thrust faults (Figure 2.5a) during Mesozoic and Cenozoic (Höy & Heyden, 1988; Larson et al., 2006; McMechan, 2012). Several transverse faults have also been identified in the Front Ranges (e.g.; Moffat & Spang, 1984; McGugan, 1987; Fermor, 1999; McMechan, 2001; Norris, 2001). In the foothills, the north to NW-trending Livingstone Range anticlinorium consists of en-echelon, chevron-style fault-propagation folds, which have been compartmentalized by multiple tear faults and transverse zones of intense fracturing (Cooley et al., 2011). Anticlines plunge into these tear faults and form domal culminations. Tear faults also mark along-strike changes in fold-style, from chevron to concentric and changes in the presence or absence of back-thrusts. These tears are thought to be the results of syn-thrusting reactivation of preexisting NE-striking Paleoproterozoic basement faults, some of which were active during Mississippian (Cooley et al., 2011).

The Great Falls Tectonic Zone (GFTZ; Figure 2.5) in Montana is a NE-trending, transverse (in relation to the Cordillera) crustal suture between the Medicine Hat Block and the Wyoming Craton (O'Neill & Lopez, 1985). This deformation zone was initiated prior to ~1.9 Ga as a convergent boundary and subsequently evolved into a transpressive boundary in response to the eastward movement of the Wyoming Craton (Dahl et al., 1999; Mueller et al., 2002; Gifford et al., 2014). Cenozoic alkali magmatism, belonging to the Montana Alkali Province, occurred within this zone (Gifford et al., 2014). In central Montana and Idaho, the Mesoproterozoic Belt rifting most likely led to the initiation of the Lewis and Clark fault zone from the southern margin of the GFTZ (Harrison et al., 1974; Reynolds, 1979; Wallace et al., 1990; Sears & Hendrix, 2004; Foster et al., 2006). The Lewis and Clark fault zone (Figure 2.5a) is a WNW-trending, >800 km long, system of 'steeply dipping strike-slip, oblique-slip, and dip-slip faults', which obliquely cuts across the Sevier belt (Foster et al., 2007). During the Mesozoic-Cenozoic Cordilleran orogeny, this fault zone deformed as a ca. 40 km wide, sinistral shear zone with 'transpressional flower structures' (Hyndman et al., 1988; Sears et al., 2000; Sears & Hendrix, 2004). With the onset of the Basin and Range extension in the Eocene, polarity of the fault movement reversed, and this zone served as a dextral, extensional, TZ that facilitated the exhumation of metamorphic core complexes (Figure 2.5a) (Foster et al., 2007).

In the Sevier FTB (USA), the geometry of basement structures had first-order control on the formation of orogenic curvatures and on the evolution of their transverse boundaries (e.g.; Paulsen & Marshak, 1999). A deeper basin generally corresponds to a thicker sedimentary column and more material available to be incorporated into the deforming taper, which results in a wider wedge (salient) (e.g.; Marshak & Wilkerson, 1992; Boyer, 1995). The Helena salient likely formed over an E-trending, asymmetrical depositional trough of the Middle Proterozoic Belt basin called the Helena embayment (Figure 2.5b) (Harrison et al., 1974). A north-dipping Middle Proterozoic normal fault on the southern edge of the embayment probably evolved into the Southwest Montana Transverse Zone (SWMTZ), which forms the southern boundary of the salient with the Dillon recess (Whisner et al., 2014). Thrusts and related structures in the southern domain of this salient are strongly converging into the right-lateral, reverse faults within the SWMTZ, due to a gradual clockwise rotation of the shortening direction during their evolution (Whisner et al., 2014).

Further south, controls of the basin boundary geometry on the evolution of transverse zones have been exemplified by the Mount Raymond Transverse Zone (MRTZ) and the Charleston TZ. The MRTZ and the Charleston TZ form the northern and the southern boundaries of the Uinta/Cottonwood arch (recess) with the Wyoming Salient and the Provo Salient respectively (Figure 2.5a) (Paulsen & Marshak, 1997, 1998). Paulsen and Marshak (1999) noted contrasting structural styles between these two zones and explained this contrast in light of corresponding basement structures. An east-west trending asymmetric basement high, with a gentle northern flank and a steep southern flank, existed just north of the present Uinta/Cottonwood arch, along the boundary between the Archean Wyoming province (north) and Proterozoic terranes (south) (Paulsen & Marshak, 1999). A gentler northern flank meant that the sedimentary thickness gradually increased northwards from the Uinta recess into the Wyoming Salient. The MRTZ initiated above this flank as NNE-trending thrusts along the southern margin of the Wyoming salient, which were later tilted northward creating an E-W strike during the uplift of the Uinta/Cottonwood arch (Paulsen & Marshak, 1997). The steeper southern flank, however, marked an abrupt increase in sedimentary thickness towards the south and thereby formed the boundary between two contrasting taper wedges. The Charleston TZ (Figure 2.5a) served as zone of lateral ramp between the two contrasting tapers and gradually evolved into a left-lateral strike slip zone, which accommodated the differential motion between the Uinta recess and the Provo salient (Paulsen & Marshak, 1998 and references therein). The southern boundary of the Provo salient with the central Utah segment is the Leamington TZ, which is an ENE trending, >50 m long, complex, cross structure (Lawton et al., 1997; Kwon & Mitra, 2006). In the salient, an initial E-directed vergence over the TZ rotated clockwise during subsequent deformational phases, which likely reflects the interaction between a deforming wedge and an oblique ramp (Lawton et al., 1997; Paulsen & Marshak, 1999; Kwon & Mitra, 2006).

In southern Wyoming, the E- to NE-trending Cheyenne belt (Figure 2.5b) represents the transverse, crustal suture/ transpressional shear zone between the Wyoming and Yavapai-Mazatzal Provinces, across which the Precambrian geology, metamorphism, and metallogenesis abruptly change between adjacent blocks (Karlstrom & Houston, 1984). During the Laramide orogeny, this weak crustal zone was reactivated as a left-lateral transpressional structure and subsequently as a right-lateral transtensional zone during the Tertiary extension (Bader, 2008). Just to the south, east-west trending Precambrian basement fault zones, genetically linked to the Cheyenne belt (Sims et al., 2001; Whitmeyer & Karlstrom, 2007), have been identified to influence Laramide uplift resulting in accumulation of oil and gas resources (Bader, 2009).

A peculiar feature in the Laramide belt of Colorado is a 500-km long, 25-50 km-wide, linear zone of numerous magmatic intrusions, known as the Colorado Mineral Belt (Figure 2.5a).

This zone marks an abrupt along-strike change in: 1) the structural trend of the Laramide uplifts (north-trending in the southern region versus NW-trending northwards); 2) the thickness of the Late Cretaceous and Paleogene sedimentary sequences; and 3) the composition of the Laramide plutons (Chapin, 2012). This economically valuable belt has been interpreted to have formed over an extensional boundary between two adjacent segments of the underlying Farallon flat slab (Chapin, 2012), which serves to demonstrate the effects of the down-going plate features and processes on the upper plate structures. In the Laramide belt, preexisting basement structures and lateral heterogeneities are suggested to have a control on the stress-field and thereby led to the development of structures with an orientation different from the regional trend (Weil et al., 2016).

Proposed Factors Controlling Lateral Heterogeneities

Along the Cordillera (primarily along the Sevier FTB), pre-existing basement features/structures likely had the greatest impact on creating lateral heterogeneity, which has generally manifested as curvatures along the orogenic front and as variation in the geometry of cross structures. Prior to the Cordilleran orogeny, transverse crustal boundaries served as loci for activation of transverse zones during various rift-related extensional features (McMechan, 2012). Subsequently, these transverse zones were reactivated as cross structures during the orogenic contraction/extension and served to partition or distort deformation of the evolving crustal wedge. Both transverse structures and irregular basement topography further added lateral heterogeneity through their profound control on the lateral continuity of facies and thickness of the pre and syn orogenic sedimentary succession. Abrupt lateral changes in the facies and thickness of the sedimentary column caused the deforming wedge to partition into segments, which are separated by cross structures of various geometries and genesis. As Paulsen and Marshak (1999) explained, a thicker sedimentary column corresponds to a farther propagation of the deforming wedge (salients) than a thinner column (recesses). Further the geometry of the basement irregularities and transverse structures dictate the geometry of cross structures. A near vertical transverse structure is more likely to evolve into a tear fault, whereas, an inclined structure evolves into a lateral ramp (Paulsen & Marshak, 1999). And finally, features of the subducting plate (Farallon) may have influenced the development of cross structures and lateral heterogeneity along the range (e.g.; Chapin, 2012).

Alps

Tectonic Setting and Lateral Heterogeneities

The European Alps formed during a Late Cretaceous collision between the European and African plates following the closure of the Alpine Tethys, which consisted of the northern Valais ocean and the southern Piemont-Liguria ocean, separated by continental crust in the middle known as the Brianconnais (Tricart, 1984; Stampfli & Borel, 2002; Schmid et al., 2004; Handy et al., 2010). The European side of the collision was the lower plate with the Apulian/Adriatic blocks of the African plate forming the upper plate (Dewey et al., 1998; Handy et al., 2010). The Apulian plate refers to all continental domains located south of the Alpine Tethys. The Adriatic micro-plate or Adriatic indenter, a part of the Apulian plate, is situated south of the modern-day Periadriatic Fault System (PA; Stampfli & Borel, 2002; Schmid et al., 2004; Handy et al., 2010). Today this orogen trends approximately east-west in the Eastern and Central Alps and has a NE-SW orientation in the Western Alps (Figure 2.6). Major range-parallel lithotectonic units of the Alpine orogen are from north to south, the European foreland, Jura Mountains, Molasse Basin

(Oligocene-Miocene Foreland), Helvetics, Penninic zone, Austroalpine, Southern Alpine, and Po Basin (retro-arc basin for the Alps and foreland basin for the Apennines) (Pfiffner, 2014). The Helvetic domains are derived from the Mesozoic and Cenozoic shelf and upper slope deposits along the southern European plate margin, and in places include the Pre-Triassic basement (Zerlauth et al., 2014). For simplicity, the classic term ‘Penninic nappes/zone’ has been largely used in the literature to denote the tectonic units derived from the subducted European margin, the Valais ocean, the Piemont-Liguria ocean, and the Brianconnais continental crust (e.g.; Schmid et al., 2004; Pfiffner, 2014). Parts of the Apulian plate to the north and south of the PA are represented by the Austoalpine and Southern Alpine units respectively (Polinski & Eisbacher, 1992; Schmid et al., 2004). While the Austroalpine unit dominates the eastern Alps, this unit has fully eroded away in the Western Alps, exposing up to blueschist to eclogite facies rocks of the Penninic unit and sub-greenschist facies rocks of the Helvetics (Pfiffner, 2014). The rheologically strong Dolomites, the Adriatic indenter, lie within the Southern Alpine unit. Following the initial collision, the eastern Alps underwent E-W directed orogen parallel extension in the Miocene (Oligocene; Ring, 1994; Steck, 2008). This extension has been referred to as “lateral extrusion” (Ratschbacher et al., 1991). The lateral extrusion has been interpreted as; i) coupling of compression and gravitational collapse (Ratschbacher et al., 1991), ii) upper plate extension due to roll back of a subduction zone beneath the Carpathian orogen (Royden et al., 1983; Royden, 1993; Horváth & Cloetingh, 1996; Sperner et al., 2002), iii) northward indentation of the southern Dolomites (Rosenberg et al., 2004; Rosenberg & Garcia, 2011; Reiter et al., 2018), and iv) an extension related to the roll back of the Mediterranean plate in the west (Ring & Gerdes, 2016). This Miocene extension has been accommodated along a series of orogen-parallel, strike-slip faults and orogen-perpendicular, normal faults. Modern-day topographic evolution was largely controlled by these faults as much of the lateral heterogeneity we see along the range (Bartosch et al., 2017). Major orogen-parallel strike-slip faults in the Eastern and Central Alps are the Periadriatic Fault System (PA), the Defreggen-Antholz-Vals Fult (DAV), Salzach-Ennstal-Mariazell-Puchberg Fault (SEPM), Inntal Fault (IN), and Mur-Murz Valley Fault (MM) (Figure 2.6). The PA trends E-W for ~700 km and forms a rheological boundary between the weaker Eastern Alps and the relatively stronger Southern Alps (Robl & Stüwe, 2005). From the west to east, the PA consists of the Tonale (or Insubric) Line, Giudicarie Fault System, Mauls, Puresetral, and Gailtal segments (Figure 2.6). Different segments of the PA were active during 32-29 Ma and 22-16 Ma (Müller et al., 2001). North of the PA (Pustertal and Mauls segments), the sinistral, normal DAV runs E-W, for ~80 km and forms the southern boundary of alpine metamorphism (Müller et al., 2000; Bartosch et al., 2017). Within the Austroalpine domain, the EW-striking, ~400 km long, SEPM has a cumulative left-lateral slip of about 60 km (Urbanek et al., 2002) and separates the Mesozoic Northern Calcareous Alps (NCA) from the Middle Austroalpine basement rocks (Bartosch et al., 2017). The NE-striking, sinistral MM was active during 17-13 Ma (Dunkl et al., 2005) as a conjugate of the NNW-striking, dextral Pols-Lavanttal fault system (PL) (Bartosch et al., 2017).

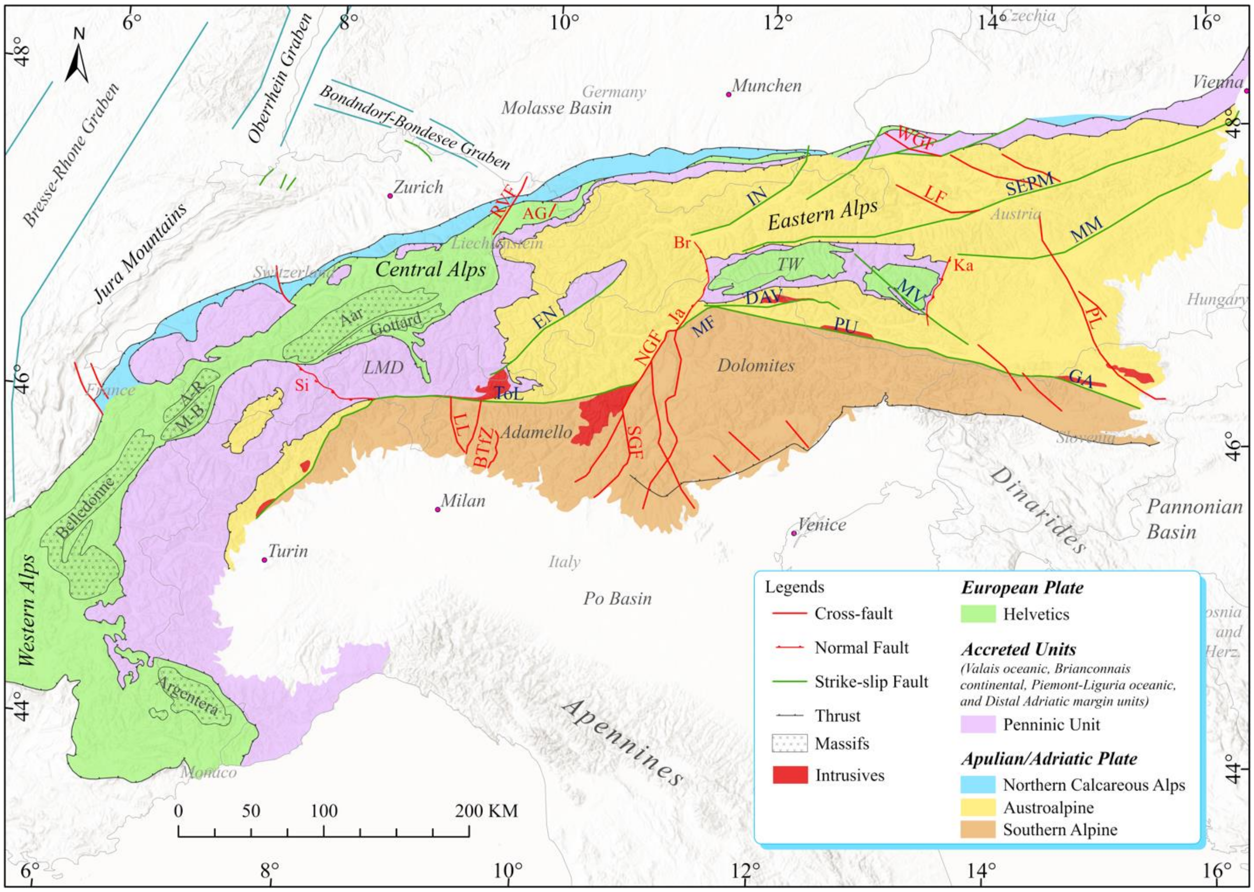

Figure 2.6: Geological map of the Alps showing the major lithotectonic units, major strike-slip faults (green lines), and major cross-faults (red lines) (after Laubscher, 1985; Polinski & Eisbacher, 1992; Schönborn, 1992; Linzer et al., 1995; Castellarin et al., 2006; Pfiffner, 2014; Zerlauth et al., 2014; Ring & Gerdes, 2016; Bartosch et al., 2017). Acronyms: AG: Alpenrhein Graben; A-R: Aiguilles Rouges Massif; Br: Brenner Fault; BTfZ: Ballabio-Barzio Transfer Zone; EN: Enagdin Fault; GA: Gailtal Fault; IN: Inntal Fault; Ja: Jaufen Fault; Ka: Katschberg Faults; LF: Lammertal Fault; LL: Lecco Line; LMD: Lepontine Metamorphic Dome; M-B: Mont-Blanc Massif; MF: Meran-Mauls Fault; MM: Murz-Valley Fault; MV: Moll Valley Fault; NGF: North Giudicarie Fault System; PL: Pols-Lavanttal fault system; PU: Purestal Fault; RVF: Rhine Valley Fault; SEPM: Salzach-Ennstal-Mariazell-Puchberg Fault; SGF: South Giudicarie Fault System; Si: Simplon Fault Zone; ToL: Tonale (Insurbic) Line; TW: Tauern Window; WGF: Wolfgangsee Fault.

Cross Structures in the Eastern and Central Alps Major transverse, normal faults in the eastern and central Alps are the Simplon Fault Zone (Si), the Pols-Lavanttal fault system (PL), the Brenner Fault (Br), the Moll Valley Fault (MV), and the Katschberg Faults (Ka) (Figure 2.6).

The Brenner and Katschberg Faults mark the western and eastern edges of the Tauern Window respectively (Behrmann, 1988; Selverstone, 1988; Fiigenschuh et al., 1997), where blue-schist and eclogitic facies rocks of the Penninic zone have been exposed (Pfiffner, 2014). Exhumation of the Tauern Window has been widely linked to Miocene extension. Rosenberg and Garcia (2011) argue that localized intensive folding deformation due to an irregular geometry of the Dolomite indenter coupled with erosion can also exhume deep-seated rocks without a significant crustal extension. The southern edge of the window has been cut by the NW-striking dextral, normal MV fault. Gently west-dipping mylonitic fabric, with top-to-the-west shear along the Brenner Fault (Behrmann, 1988; Selverstone, 1988), has been overprinted by steeply west-dipping cataclastic zones (Prey, 1989). Much like the Brenner Fault, the Simplon Fault zone is a low-angle, SW-dipping, extensional fault that exhumes the Lepontine Metamorphic Dome in its footwall. Mylonitic shearing that formed the Simplon Fault zone initiated at 30 Ma (Campani et al., 2010) and was overprinted by brittle detachment faults of the Simplon Line from 14.5-10 Ma until 3-5 Ma (Hubbard & Mancktelow, 1992; Mancktelow, 1992; Grosjean et al., 2004; Campani et al., 2010). Both the Brenner and Simplon Faults expose a telescoped crustal section via an initial ductile shearing and subsequent brittle faulting (Grosjean et al., 2004; Campani et al., 2010; Mancktelow et al., 2015). It has been proposed that Brenner and Simplon extension may be related to step-overs in the range-parallel dextral strike-slip deformation in the Neogene (Schmid et al., 1989; Hubbard & Mancktelow, 1992).

Around the eastern Alpine periphery, the NW-trending, NE-verging, Paleogene folds in Permo-Mesozoic cover of the Austroalpine are cut by sets of NE-striking, high-angle, cross-faults (Figure 2.6) (Polinski & Eisbacher, 1992). In the Miocene, both the Austroalpine and

Southern Alpine units were folded into NE-trending folds, which are dissected by a system of NW-trending high angle, dextral cross-faults, which includes the 150 km long PL. These Miocene cross faults either offset or merge into the PA and partition deformation between the contractional Alpine domain and the extensional Pannonian basin (Polinski & Eisbacher, 1992). In the western Alps, NE to E-striking transverse faults are represented by the Neogene normal faults with a few faults showing minor left-lateral reactivation (Sue & Tricart, 2003) and the late to post Oligocene right-lateral, strike-slip faults (Malusà, 2004; Perello et al., 2004; Perrone et al., 2011). Anti-clockwise rotation of the Apulian plate has been attributed as the cause of the orogen-parallel dextral displacement and the NE to SW extension (Hubbard & Mancktelow, 1992; Calais et al., 2002).

The Giudicarie Fault System (GFS) is a system of WNW-NW dipping fault-links between the Tonale and Pustertal line of the PA (Castellarin & Cantelli, 2000; Mancktelow et al., 2001; Müller et al., 2001; Viola et al., 2001). The Meran-Mauls (MF) and the Northern Giudicarie Fault (NGF) within the GFS form the trace of the PA, while the Southern Giudicarie Fault (SGS) is entirely located in the Southern Alps. The Jaufen Fault, as a secondary fault within the GFS, has been considered as a potential continuity of the Brenner Fault (Rosenberg & Garcia, 2011). An explanation of the genesis of the GFS assumes evolution of an initially curved section of the PA, which underwent Neogene sinistral transpression over an inherited NE-trending horst and graben structure (Castellarin & Cantelli, 2000; Müller et al., 2001; Viola et al., 2001). A second explanation, however, considers an initially straight PA bent by the Late Oligocene to Early Miocene, northward movement of the Dolomite indenter. The MF represents a section of the bend, which was subsequently cut by the NGS (Laubscher, 1971; Schmid et al., 1996; Frisch et al., 1998; Pomella et al., 2012). The SGF has been interpreted as a Serravallian-Tortonian transfer fault between the Guidicarie belt and the pre-Adamello belt of the Southern Alps (Castellarin et al., 2006). The Adamello batholith is an Upper Eocene and Lower Oligocene batholith, the northern rim of which has been sheared by the Tonale line (Brack, 1981; Laubscher, 1985; Zanchetta et al., 2011). Just to the east of the NGS, a shallow, NNE-striking, sinistral transpressive fault has been mapped in the Southern Alps (Fondriest et al., 2015).

<u>Cross Structures in the Southern Alps</u> Basement rocks in the Southern Alps have undergone extension in the Permian, resulting in ENE-trending faults in Triassic, NS-trending faults, and in Jurassic and Cretaceous EW-trending faults (Gaetani et al., 1986; Schumacher, 1990; Bertotti et al., 1993; Picotti et al., 1997; Festa et al., 2020). During the south-verging tectonic transport, these basement structures acted as lateral/oblique ramps, initiated more lateral ramps, and produced complex geometries like en-echelon ramp folds and back thrusting (Schönborn, 1992). In the central Southern Alps, inherited transverse zones cut through decoupling surfaces, partition thrust sheets into discrete blocks, and thereby serve to generate a laterally heterogenous deformation style (Laubscher, 1985; Schönborn, 1992). Several transverse structures that have been identified in this area include the Lecco Line and Ballabio-Barzio TfZ (Figure 2.6) (Laubscher, 1985; Schönborn, 1992; Zanchi et al., 2012). The central Southern Alpine thrust belt has been compartmentalized by these transverse zones (Schönborn, 1992). Moreover, many upper Triassic to Jurassic (Bernoulli, 2007), orogen-perpendicular (e.g.; Berra & Carminati, 2010), normal faults were reactivated during the Neo-Alpine deformation (Oligocene-Miocene; Castellarin & Cantelli, 2000) along with nucleation of several transverse, sinistral, strike-slip faults (Prosser, 1998; Zanchi et al., 2012).

Cross Structures in the Northern Calcareous Alps (a subdivision of the Austroalpine unit) The Permo-Mesozoic sedimentary succession (3-5 km thick) of the Northern Calcareous Alps were deformed into roughly NE-trending contractional structures during Early Cretaceous to Late Eocence (Gaupp & Batten, 1983; Kralik et al., 1987). The synchronous, en echelon, WNW-striking dextral, tear/transfer faults cut these contractional structures at all scales (Linzer et al., 1995). Some examples include the Lammertal and Wolfgangsee fault systems in the northeastern Alps (Figure 2.6). Linzer et al. (1995) observed a peculiar deformation decoupling between the sedimentary cover and basement during the ongoing oblique convergence. The sedimentary cover accommodated the convergence obliquity via deformation partitioning between the contractional and strike-slip structures, while the basement deformed through 'crystal-plastic flow' (Linzer et al., 1995). Together these displacement transfer faults and deformation decoupling caused a 30˚ clockwise rotation of the entire NCA belt about a vertical axis (Linzer et al., 1995). Moreover, tear faults related to the synorogenic inversion of a Jurassic rift-related graben shoulder have also been identified in the NCA (Oswald et al., 2019). The Miocene, extensional, NE-trending, sinistral, strike-slip faults, such as the SEPM and IN, cut all the earlier structures and divide the NCA into a number of rhombohedral crustal blocks (Linzer et al., 1995).

Cross Structures in the Helvetics In the Helvetic units, NW to N-striking tear faults were formed due to lateral variation in shortening of the nappe stack, primarily during 35-30 Ma (Hunziker et al., 1986). Nappe imbrication in the Helvetics changes laterally due to the absence or presence of a decoupling layer (Zerlauth et al., 2014). The Permo-Carboniferous and Jurassic extensional structures along the European margin resulted in these along-strike facies changes, which subsequently controlled the deformation style. During the nappe formation, syn-sedimentary normal faults were also reactivated as lateral ramps (e.g.; the Rhine Valley Fault) and tear faults (Zerlauth et al., 2014). In the Oligocene, the NW-trending, sinistral, transtensional Alpenrhein graben was formed in the Helvetics (Ring & Gerdes, 2016). It's conjugate, the Bonndorf-Bodensee in the Jura Mountains is a NE-trending graben formed due to dextral transtension prior to 18 Ma (Hofmann et al., 2000; Ring & Gerdes, 2016). The Bresse-Rhone and Oberrhien grabens in the Alpine foreland are related to the European Cenozoic Rift System (Ring & Gerdes, 2016).

Proposed Factors Controlling Lateral Heterogeneities

The Eastern and Western Alps show remarkable heterogeneity in timing of major orogenic events (Late Cretaceous in the Eastern Alps Cenozoic in the Western Alps), timing of the regional metamorphism (older in the Eastern Alps and younger in the Western Alps), and overall direction of tectonic transport (NW- to W-directed in the Eastern Alps vs N to NW directed transport in the Western Alps) (Handy et al., 2010, page 123 and references therein). Within each lateral sub-division of the Alps, several factors have contributed to the development of cross structures and lateral heterogeneity. Extension of the upper plate has given rise to several cross faults such as the Simplon and Brenner Faults, which serve as a large-scale, displacement transfer faults between major, range-parallel, strike-slip faults (e.g.; Selverstone, 1988; Hubbard & Mancktelow, 1992). Lateral connecters (tear faults, lateral ramps, and displacement transfer faults) are common in most of the tectonic units of the Alps. As observed in the North American Cordillera and the Appalachians, extension related basement structures, in both the European and Apulian plates, had controls on the lateral continuity of facies and thicknesses of sedimentary rocks and thereby on subsequent deformation, primarily in the Southern Alps and Helvetics (e.g.; Laubscher, 1985; Schönborn, 1992; Zanchi et al., 2012; Zerlauth et al., 2014). Lateral variability in the composition of the sedimentary section has influenced deformation style based on the presence or absence of decollement horizons. Oblique convergence coupled with partitioning of deformation between the basement and sedimentary cover has resulted in multiple cross faults in the Northern Calcareous Alps (Linzer et al., 1995).

Himalaya

Tectonic Setting and Lateral Heterogeneities

The Himalaya is our planet's most prominent example of a collisional mountain belt. While the geology of this orogen is generally presented in the context of range-parallel thrust faults that separate lithotectonic units of differing metamorphic grade (Figure 2.7; Hodges, 2000), there is also lateral heterogeneity in various aspects of the geology along the range and in some areas cross structures have played a role in the segmentation of the Himalaya (Mukul, 2010; Godin & Harris, 2014). Early geological and geophysical studies on the Indo-Gangetic plain presented evidence for lateral variations in sediment thickness and geophysical properties along the Himalayan foreland (Burrard, 1915; Oldham, 1917). In the 1970's new data from the oil and gas industry connected these lateral variations to a series of NE-trending basement ridges (Sastri, 1971; Rao, 1973; Raiverman, 1983). It was also proposed that these transverse basement structures may influence Himalayan deformation (Valdiya, 1976). In recent years, evidence from field surveys and laboratory analyses confirms the lateral heterogeneity and locates structural transfer zones and cross structures (Mugnier et al., 1999; Mukul, 2010; Godin & Harris, 2014; Hubbard et al., 2018; DeCelles et al., 2020; Duvall, 2020).

The Himalaya is characterized by range-parallel zones of differing geologic characteristics separated by north-dipping thrust faults (Figure 2.7). From south to north, the Indo-Gangetic plain is separated from the Sub-Himalaya by the active Main Frontal Thrust (MFT). The Sub-Himalaya is bound to the north by the Main Boundary Thrust (MBT). The hanging wall to the MBT is the Lesser Himalayan zone, which is bound to the north by the Main Central Thrust (MCT). The unit that includes the highest peaks of the range is the Greater Himalayan Sequence (GHS). Geophysical data supports the merging of these thrusts into a master fault known as the Main Himalayan Thrust (Zhao, 1993; Avouac, 2003; Nabelek, 2009). There is an extensional fault system bounding the northern GHS, the South Tibetan Detachment System (STDS; Hodges, 2000). The hanging wall of the STDS is the Tibetan or Tethyan Sedimentary Sequence (Gansser, 1964; DeCelles et al., 2020). Each of these zones from the Sub-Himalaya to the Tibetan Sedimentary Sequence and their bounding structures exhibits some degree of lateral heterogeneity along the length of the range in either the expression of structural style, depositional history, geomorphology, or seismicity.

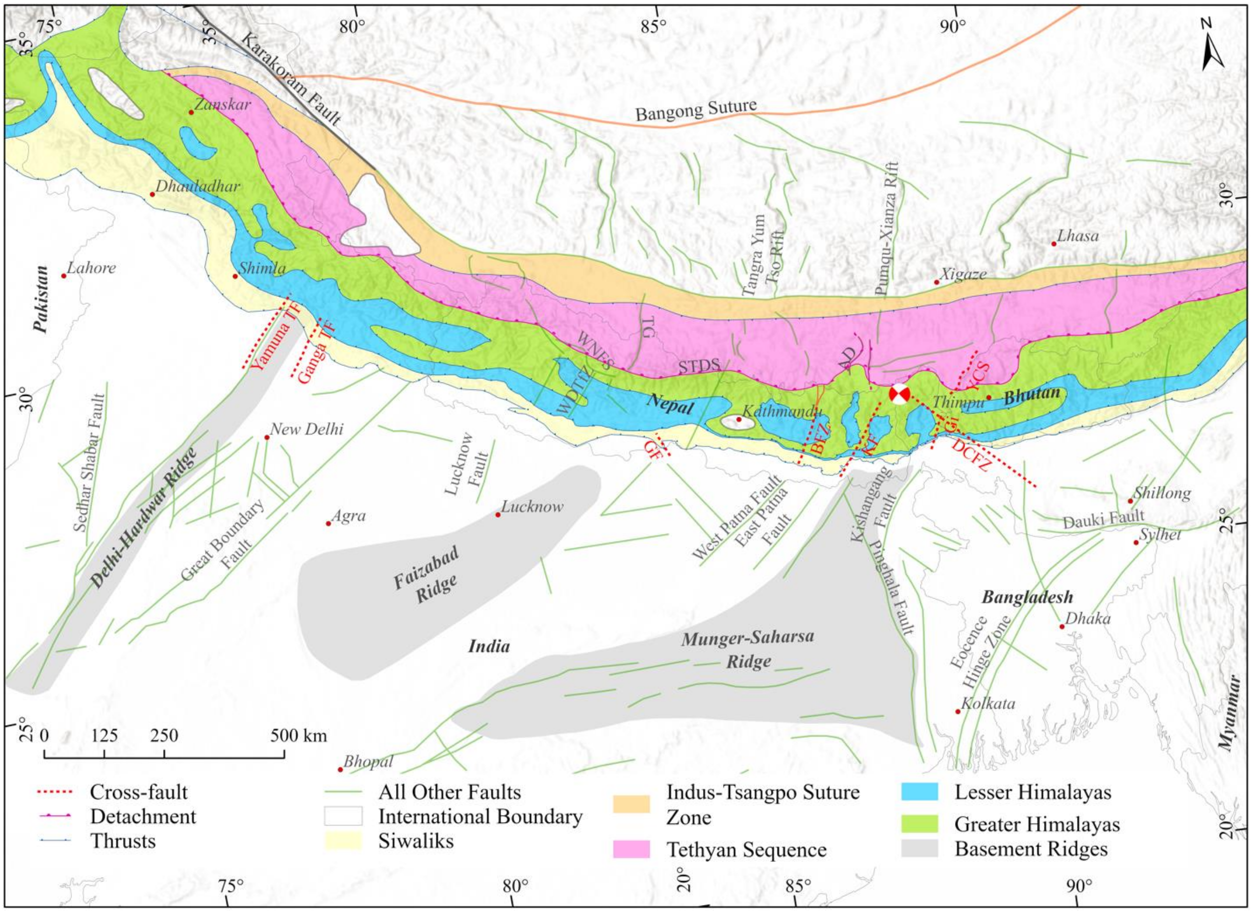

Figure 2.7: Simplified tectonic map of the Himalaya showing the major cross structures. The beach ball shows focal mechanism of the 2011 Mw 6.9 Sikkim Earthquake (source: the Department of Mines and Geology, Nepal; the Geological Survey of India; Gansser, 1964; Sastri, 1971; Mugnier et al., 1999; Sahoo, 2000; Searle et al., 2003; Guillot et al., 2008; Jessup et al., 2008; Godin & Harris, 2014; Silver et al., 2015; Diehl, 2017; Mukul, 2018; Divyadarshini, 2019; Seifert, 2019). Acronyms: AD: Ama Drime Detachment; BFZ: Benkar Fault Zone; DCFZ: Dhurbi-Chungthan Fault Zone; GF: Gardi Tear Fault; Gi: Gish Fault; KF: Kosi Fault; MBT: Main Boundary Thrust, MCT: Main Central Thrust, MFT: Main Frontal Thrust, MMT: Main Mantle Thrust, MZB: Main Zanskar Back Thrust, STDS: South Tibetan Detachment System; TF: Tear Fault; WDTfZ: Western Dang Transfer Zone; WNFS: Western Nepal Fault System; YCS: Yadong Cross Structure.

In the Sub-Himalayan there is notable variability in the morphology of the range front including the local presence of dun structures and a series of recesses and salients (Yeats, 1991; Mukul, 2010). In some areas the irregular mountain front has been linked to differences in shortening (Dubey, 2001) and in other areas there is a connection with cross faults that mark the transitions from salients to recesses. Examples of cross faults in the Sub-Himalaya include the Yamuna and Ganga Tear Faults in the NW Himalaya and the Kosi and Gish faults in eastern Nepal and Sikkim (India), respectively (Figure 2.7) (Sahoo, 2000; Srivastava, 2018). In the Lesser Himalaya, lateral heterogeneity is seen in topographic data, seismic data, and cooling history data (Harvey, 2015; van der Beek, 2016; Soucy La Roche, 2019). In western Nepal there is a zone of change in a variety of parameters that has led researchers to conclude that the MHT may have a ramp at that location, possibly coupled with a change in strike (Harvey, 2015; van der Beek, 2016; Soucy La Roche, 2019). This change also aligns with the proposed West Dang Transfer Zone (Figure 2.7) (Mugnier et al., 1999). Soucy La Roche (2019) propose a connection between this structural change and the NE-striking Lucknow fault in the Indian basement. In several areas, along-strike changes in the geometry of duplex structures in the Lesser Himalaya have also been noted (Hauck, 1998; DeCelles et al., 2001; Grujic, 2002; Long, 2011).

In the Greater Himalaya there is lateral heterogeneity in exhumation rates (Eugster, 2018), topographic profiles (Duncan et al., 2003), the presence of leucogranitic intrusions (Weinberg, 2016), and the presence or absence of discontinuities (Carosi, 2010; Larson, 2014). Hubbard et al. (2018) recently recognized a cross structure, the Benkar Fault zone, in the Greater Himalaya of eastern Nepal (Figure 2.7). This structure has dextral normal displacement and was active in the past ~12 Ma. The Benkar Fault zone may continue into the Lesser Himalaya, however it is yet to be mapped to the south.

Microseismicity in the Himalaya has occurred along cross-strike trends, has terminated at cross-strike zones, and has made other changes along cross-strike boundaries (Rajaure, 2013;

Mugnier et al., 2017; Bilham, 2019; Mendoza, 2019). The aftershock seismicity from the 2015 Gorkha earthquake terminates along a sharp NE-striking boundary east of Kathmandu in Nepal (Hubbard et al., 2016; Mendoza, 2019). In the eastern Himalaya, several seismic events have been consistent with strike-slip displacement on transverse structures (Drukpa, 2006; Paul, 2015; Diehl, 2017). While a number of these events are minor, there have also been major earthquakes such as the 2011 M_w 6.9 Sikkim event that was interpreted to have occurred along a NW-striking (cross-strike) plane with dextral kinematics (Figure 2.7) (Paul, 2015). The Sikkim event and a number of the smaller events have originated at depths of ~50-60 km suggesting that rupture initiation was below the MHT (Drukpa, 2006; Paul, 2015) but possibly penetrating the hanging wall. Major historic thrust-related earthquake events are known to have had a finite rupture area (Bilham et al., 2001) and tracking of these areas has facilitated the recognition of seismic gaps that may represent regions with higher risk (Bilham, 2019). It has been proposed that cross structures may limit the seismic rupture area, thus contributing to the lateral heterogeneity in seismic activity (Mugnier et al., 2017; Hubbard et al., 2021).

Proposed Factors Controlling Lateral Heterogeneities

The combination of pre-existing transverse basement structures and the lateral variation in sedimentary history may both contribute to the lateral heterogeneity and cross structures that we see today in the Himalaya. Godin and Harris (2014) proposed a connection between variations in gravity data across a broad region in the Himalaya and Tibet to ridges in the Indian basement detected in the foreland. Soucy La Roche (2019) demonstrated lateral variations in cooling histories in western Nepal and proposed a cross structure in the form of a lateral ramp or tear fault separating the regions with differing cooling histories. This cross structure aligns with the Lucknow basement fault in the Indian foreland and these authors propose that the Himalayan cross structure is linked to the basement fault. Boundaries between salient and recesses in range front geomorphology has also been linked to basement faults (Hubbard et al., 2021). These basement faults in the foreland may also separate down-dropped blocks with thicker sedimentary sequences from higher blocks and these differences in sedimentary thickness may continue into the Himalaya, thus influencing lateral variations in structural style (DeCelles et al., 2020). Understanding the nature of segmentation and segment boundaries may shed light on details of the mountain building process in collisional orogens but may also help us understand how convergence is accommodated and factors that control seismic energy propagation.

Zagros

Tectonic Setting and Lateral Heterogeneities

The Zagros orogenic belt runs for about 2000 km along the northeastern margin of the Arabian plate (Figure 2.8) and is the product of Miocene collision between the Arabian and Iranian continental plates and subsequent convergence (Allen & Armstrong, 2008; McQuarrie & van Hinsbergen, 2013). The eastern boundary is the dextral Zagros-Makran Transfer Zone (Regard et al., 2005), and it’s western boundary is the sinistral East Anatolian Fault (Falcon, 1974; Haynes & McQuillan, 1974). During Permian to lower Cretaceous, the Neo-Tethys Ocean opened between the Arabian and Iranian plates. Closure of this short-lived ocean began in Late Cretaceous along with the tectonic emplacement of ophiolites and trench sediments on the Arabian plate (Haynes & Reynolds, 1980; Berberian & King, 1981). While there are dominant range-parallel thrust faults, there are also several important cross structures and other geologic features that vary along the length of the range.

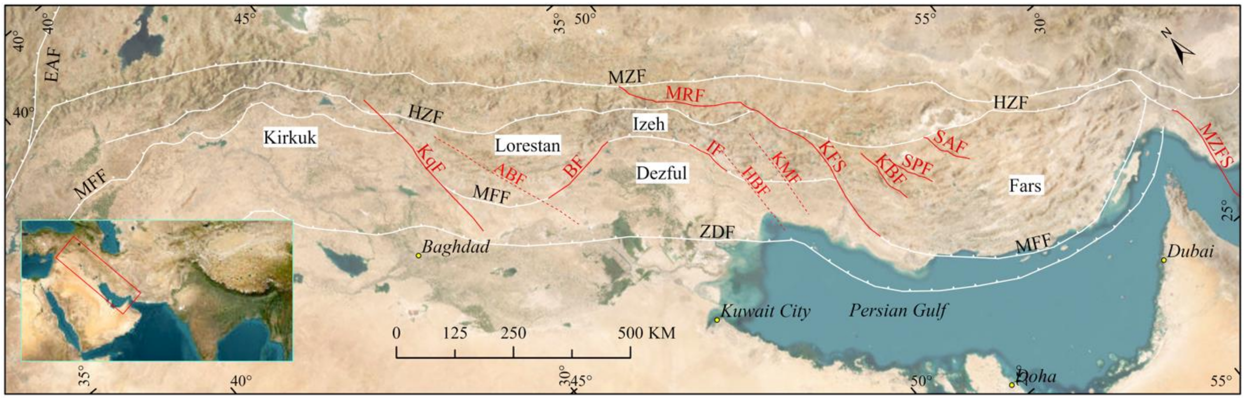

Figure 2.8: Simplified tectonic map of the Zagros mountains showing the major faults and the recesses and salients. The inset on the bottom-left corner shows the location of the larger map. The Minab-Zendan Fault System (MZFS) is a major fault of the Zagros-Makran Transfer Zone (modified from Authemayou et al., 2006; Farzipour-Saein et al., 2013; Joudaki et al., 2016; Le Garzic et al., 2019). The white lines are range parallel faults and red lines indicate cross structures. Background imagery adapted from the Environmental Systems Research Institute Online Resources. Acronyms: ABF: Anaran Basement Fault; BF: Belarud Fault; EAF: East Anatolian Fault; HBF: Hendijan-Izeh Basement Fault; HZF: High Zagros Fault; IF: Izeh Fault; KBF: Kareh-Bas Fault; KFS: Kazerun Fault System; KMF: Khark-Mish Basement Fault; KqF: Khanequin Fault; MRF: Main Recent Fault; MZFS: Minab-Zendan Fault System; MZF: Main Zagros Reverse Fault; SAF: Saverstan Fault; SPF: Sabz Pushan Fault; ZDF: Zagros Deformation Front (also known as the Zagros Foredeep Fault).

The major, range-parallel tectonic elements in the Zagros have a NW-SE trend (Figure 2.8) and include the Main Zagros Reverse Fault (the continental suture), the Zagros Imbricate Zone, the High Zagros Faults, the Zagros Folded Belt, Mountain Front Fault, the Zagros Foredeep, and the Zagros Foredeep Fault, from NE to SW (Stocklin, 1968; Berberian, 1995). A peculiar feature in the Zagros is that crustal shortening has been accommodated by deep seated, high-angled reverse faults, which have been interpreted as reactivated, basement normal-faults initiated during the Neotethyan rifting and spreading (Falcon, 1974; Jackson, 1980; Chauvet et al., 2004; Mouthereau et al., 2012). Generally, these faults are segmented with about 85-100 km gaps in between segments and are confined in the Precambrian basement and the lower stratigraphic levels of the overlying sedimentary cover (Berberian, 1995; Bigi et al., 2018). The

Cambrian to Pliocene sedimentary cover (~5-13 km thick) overlies the Proterozoic to early Cambrian Hormoz Salt (Stocklin, 1968; Falcon, 1974; Colman-Sadd, 1978). This incompetent salt unit acted as a decollement horizon between the thick-skinned deformation in the basement and the thin-skinned deformation in the sedimentary cover (e.g.; Berberian, 1995; Lacombe et al., 2006). Deformation initiated in the Zagros Imbricate Zone at about 20 Ma or earlier (Fakhari et al., 2008)**,** propagated towards the SW and reached the Zagros Folded belt at 14 Ma (Khadivi et al., 2010).

Since the Neogene, a system of strike-slip faults has also been active in the Zagros (Berberian, 1995). The Main Recent Fault (MRF) was initiated in late Pliocene, which is an active, orogen-parallel, strike-slip fault that follows the trace of the Main Zagros Reverse Fault (Tchalenko & Braud, 1974; Berberian, 1995; Authemayou et al., 2006). Oblique convergence between the Iranian and Arabian plate is partially accommodated along this hinterland fault (Authemayou et al., 2006). At its southeastern end, the MRF diffuses into a series of N to NNW-striking right-lateral, basement-inherited faults, grouped as the Karezun Fault System (Authemayou et al., 2006). Major faults belonging to this zone are the Saverstan, Sabz Pushan, and Kareh-Bas Faults (Figure 2.8) with an offset of about 100-150 km along each one (Berberian, 1995; Authemayou et al., 2006). During rifting of the Proto-Tethys and initial stages of the Neo-Tethys, these faults were activated as right-lateral transform faults in the basement rocks (Talbot & Alavi, 1996). Neogene reactivation of these transverse faults has produced a dragging effect on the earlier-formed, orogen-parallel folds. These faults serve to transmit and distribute the slip along the MRF towards the southeast into the Zagros Folded Belt and the Foredeep (Berberian, 1995; Authemayou et al., 2006). Salt diapirs have been intruded along these faults at multiple locations, which suggests that these faults cut into the top of the basement (e.g.; Kent, 1979; McQuillan, 1991; Talbot & Alavi, 1996). A certain degree of seismic hazard is associated with these transverse faults (Berberian, 1995; Authemayou et al., 2006). West of the Karezun Fault System, important transverse faults are the Izeh, Balarud Fault (E-W, 130 km left lateral), the Anaran Basement Fault, and the Khanequin Fault (Figure 2.8) (Hessami et al., 2001; Joudaki et al., 2016; Sadeghi & Yassaghi, 2016). All these transverse faults were active basin-bounding, normal faults, reactivated as strike-slip faults, and had controls on pre and syn-orogenic sedimentation and subsequent deformation in the Zagros (Sepehr & Cosgrove, 2004).

Along its strike, the Zagros curves into a series of salients and recesses bounded by the transverse faults (Figure 2.8). Generally, these curvatures are grouped into domains and include the Fars salient, the Dezful embayment, the Izeh zone (juxtaposed with the Dezful embayment in the north), the Lorestan salient, and the Kirkuk recess from SE to NW (e.g.; Stocklin, 1968; Falcon, 1974; McQuarrie, 2004). The deformation zone is widest in the Fars salient and narrows towards the NW. The style and distribution of deformation changes notably along these curvatures, mostly driven by the presence or absence of decollement layers (e.g.; Bahroudi & Koyi, 2003).

Lateral heterogeneity in the Zagros is expressed through the transverse faults, the presence of salt diapirs, and the salient and recesses on the mountain front as discussed above. Further heterogeneity is also expressed in changes in fold geometry and the amount of shortening in adjacent regions. The Fars salient is characterized by a very low taper angle, several salt intrusions, and concentric folds with large amplitude (Talbot & Alavi, 1996; Sepehr et al., 2006; Mukherjee et al., 2010). Towards the west, box folds and large concentric folds are dominant in the Izeh zone. In the Dezful embayment, however, exposed folds are concentric folds with small wavelengths and probably overlie large concentric folds beneath a detachment surface (Sepehr et al., 2006). The presence of a paleo-basement high, bounded by the N-striking, Hendijan-Izeh and Khark-Mish basement faults, has been suggested beneath the Izeh and Dezful domains (Farzipour-Saein et al., 2013 and references therein). In the Lorestan salient, folds are rounded but with much smaller wavelength than in the Fars salient (Sepehr et al., 2006). Several small-scale transverse faults have also been identified around the inflection zone between the Lorestan salient and the Kirkuk recess (e.g.; Sadeghi & Yassaghi, 2016). Amount of shortening in the Fars, Dezful, and Lorestan segments are 67 km, 85 km, and 57 km respectively (McQuarrie, 2004).

Spatial changes in folding style have been linked to the mechanical anisotropy within the deforming sedimentary column and the depth at which those anisotropies occur (e.g.; Sepehr et al., 2006). Mechanical anisotropy (presence of an incompetent layer) has a major control on the shape of the folds (lower anisotropy equals more rounded folds) and the depth of anisotropy controls the fold wavelength (deeper anisotropy equals large folds) (Sepehr et al., 2006). The deep-seated Cambrian Hormuz Salt is about 1-2 km thick beneath the Fars salient, and possibly present in the Izeh zone, but absent beneath the sedimentary columns in the Lorestan and Dezful domains (Bahroudi & Koyi, 2003). In contrast, the Mesozoic Kazhumdi shales or the Dashtak Evaporites in the Lorestan, and the Miocene Gachsaran Formation in the Dezful Embayment act as higher level decoupling surfaces, while the overlying sedimentary cover has a uniform mechanical stratigraphy (Sepehr & Cosgrove, 2004; Sepehr et al., 2006). The presence of decollement horizons at different structural levels in the Dezful and Izeh domains has generated a peculiar ramp and flat geometry in the sedimentary cover in the central Zagros (McQuarrie, 2004; Sepehr et al., 2006).

Stratigraphy and deformation style are also generally different from the recesses to the salients (Sepehr et al., 2006). It has been suggested that the Zagros foreland in the salient deform by both thin-skinned and thick-skinned deformation, whereas, the foreland deformation in recesses is accommodated only by thin-skinned tectonics (Malekzade et al., 2016). Around the central Zagros foreland, both the intensity of deformation and the amount of shortening increases towards the west and the deformation has been partitioned by left-lateral, blind tear faults reactivated on preexisting basement structures (Sarkarinejad et al., 2018; Pash et al., 2020).

Proposed Factors Controlling Lateral Heterogeneities

Several ideas have been proposed to explain the sinuosity and lateral heterogeneity of deformation style in the Zagros. These ideas include: 1) rotations of crustal blocks (Hessami et al., 2001; Edey et al., 2020); 2) along strike variations in a viscous decollement horizon between the basement and the sedimentary cover (Bahroudi & Koyi, 2003; McQuarrie, 2004); 3) the presence of a lateral buttress that serves to partition deformation (Cotton & Koyi, 2000; Bahroudi & Koyi, 2003); 4) lateral variation in the degree of oblique convergence (McQuarrie et al., 2003; Vernant et al., 2004; Vernant & Chéry, 2006); and 5) heterogenous rigidity along the plate margin (Malekzade et al., 2016). The block rotation model suggests that adjacent crustal blocks rotate with a reverse polarity along a vertical axis, driven by movements along strike-slip faults and the presence of a rigid backstop (e.g.; Hessami et al., 2001; Edey et al., 2020). These strike-slip faults were activated along N-S trending, inherited basement structures attributed to the Pan-African tectonics (Koop & Stoneley, 1982; Husseini, 1988; Hessami et al., 2001) and subsequent Tethyan rifting (Talbot & Alavi, 1996).

Along strike variation in the distribution of the Cambrian salt unit has a major control in the deformation along the Zagros Fold Belt. The presence of this incompetent unit served as a viscous detachment and deformation propagated much further where the salt was present than in the domains where it is missing (Bahroudi & Koyi, 2003; McQuarrie, 2004; Farzipour-Saein et al., 2013). The patchy arrangement of salt deposition has been attributed to the aforementioned, inherited basement structures, which could have also created tear fault-type transverse structures in the hanging walls of the thrust sheets. The style of deformation is also dependent on the nature of detachment horizons. Above a viscous decollement, the overlying units generally deform by ductile thickening, whereas above a frictional detachment, imbrication and folding deformation dominates (Bahroudi & Koyi, 2003). During deformation, the presence of transverse basement faults or a lateral change in facies can act as a lateral buttress and reorient local kinematics (Cotton & Koyi, 2000; Bahroudi & Koyi, 2003). Obliquity of plate convergence and the frictional strength along the MRF (a hinterland fault) together dictate if strike-slip partitioning initiates or not and thereby can have controls on internal deformation in the Zagros belt (McQuarrie et al., 2003; Vernant et al., 2004; Vernant & Chéry, 2006). Moreover, heterogenous plate-margin rigidity along with the presence of embayments and indenters, can cause along-strike changes in deformation patterns by affecting the local obliquity angle and favoring the escape of the upper crustal material into adjacent reentrants (Malekzade et al., 2016).

It is likely that a number of factors have contributed to lateral heterogeneity in the Zagros. The stratigraphy has played a role in terms of thickness changes causing differences in folding patterns and fault geometry. The presence of localized salt layers and salt diapirs further contributes to differences in thrust displacement and local geology. The geometry of the extensional or rifts structures that pre-date collision may have impacted the geometry of post-collisional faults.

Andes

Tectonic Setting and Lateral Heterogeneities

The Andean mountain belt is a classic example of an active subduction margin and likely represents processes that were active in the world's collisional mountain belts prior to collision. Modern-day Andean topography is largely the manifestation of crustal shortening and thickening in response to the ongoing oblique subduction of the Nazca oceanic plate beneath the South American plate (e.g.; Mpodozis & Ramos, 1989). The two plates are currently converging along a N78˚E vector at a rate of about 66 mm/yr (Angermann et al., 1999; Kendrick et al., 2003). The Andean orogen follows a north-south trend along the western margin of the South American plate, except in the Central Andes, where the orogen makes a curve known as the Arica bend (Figure 2.9a). Along the length of the mountain belt there is lateral heterogeneity exhibited at several scales. Lateral heterogeneity along the range has been observed in terms of the upper and lower plate dynamics, topography and deformation style of the retro-arc belt, nature of the foreland basin, and igneous activity.

At a coarse scale, the Andes exhibit lateral heterogeneity in topographic changes from north to south that has led to the characterization of the Northern Andes, the Central Andes, and the Southern Andes (Figure 2.9a). The major visible difference is in the width of the mountain belt where the Northern and Southern Andes are narrow while the Central Andes is much wider and includes the Altiplano and Puna plateau regions. These general topographic differences are the product of differences in their terrane accretion history and subduction zone dynamics. Other broad differences seen along the range include the presence or absence of active volcanism which is likely related to changes in the dip angle of the subduction slab (Ramos & Folguera, 2009). During early Paleozoic, the southwestern margin of South America had a history of exotic terrane accretion and subduction (e.g.; Ramos, 1988). The modern-day subduction margin initiated in late Paleozoic (Giambiagi et al., 2012). The Late Permian to Early Jurassic tectonic history was characterized by crustal extension and the associated volcanism (Llambías et al., 1993). In the Southern Andean front, there was backarc extension from late Triassic to Early Jurassic (Vergani et al., 1995; Giambiagi et al., 2012) while the Central Andes experienced extension from late Jurassic to Early Cretaceous (Galliski & Viramonte, 1988; Salfity & Marquillas, 1994). The resulting orogen-parallel, rift-related, normal faults and/or transfer faults were reactivated as reverse faults with strike-slip components in Cretaceous to Paleogene (Kley et al., 2005; Mescua & Giambiagi, 2012). In the Southern Andes, this Neogene inversion of the extensional basins led to lateral variations in the thickness and facies of the sedimentary sequences, which were subsequently reflected in heterogeneities of the deforming fold and thrust belt (e.g.; Ghiglione et al., 2009; Likerman et al., 2013).

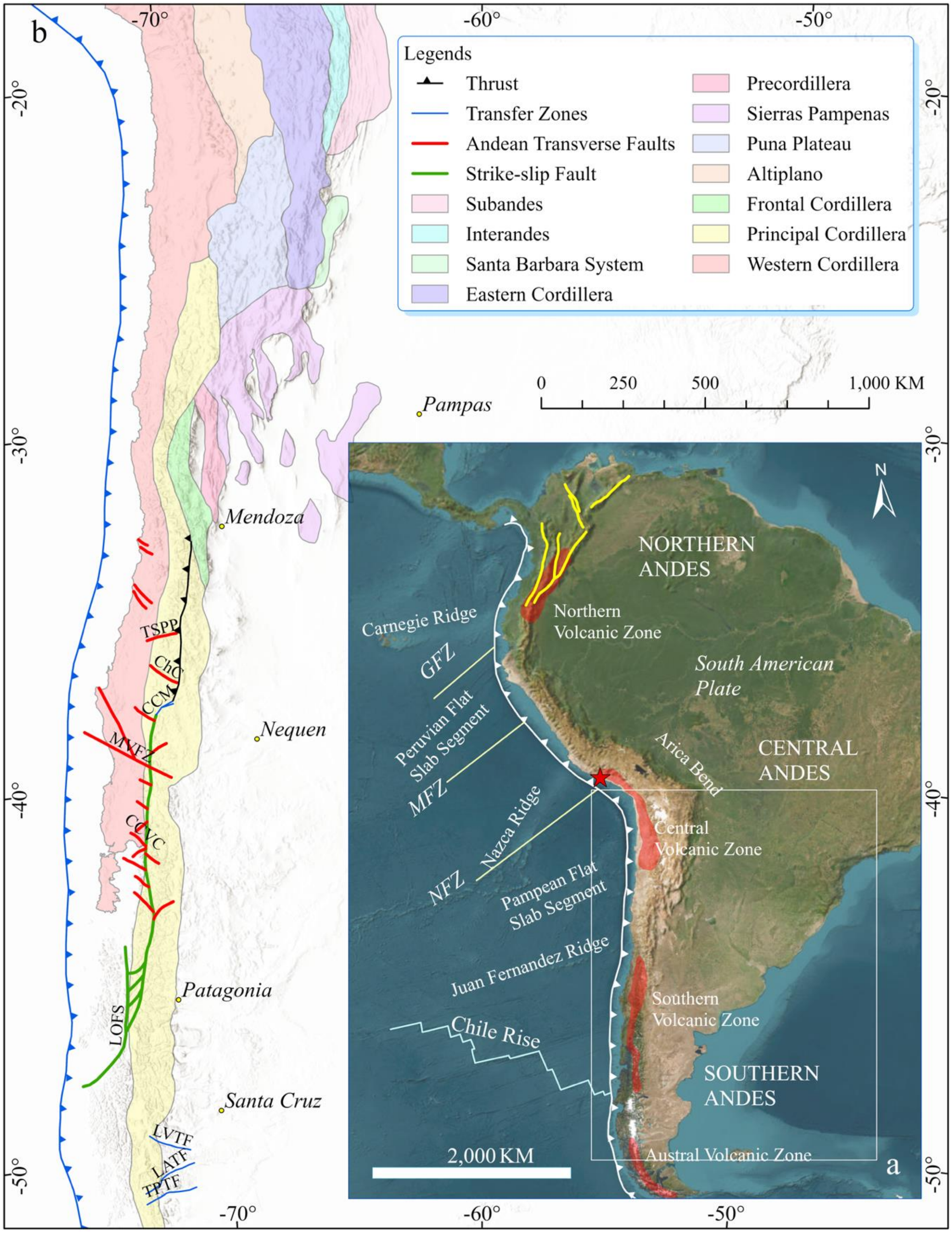

Figure 2.9: Tectonic map of the Andes. a) Map of the South American plate and the Nazca oceanic plate (west) showing major transverse features on the subducting Nazca oceanic plate.

The red star shows the epicenter of the Mw 8.4 2001 Peru earthquake. Red shades indicate volcanic zones. Note the large-scale strike slip faults, indicated by yellow lines, in the Northern Andes. The inset shows the extent of the 'Figure 2.9b' (modified from Gutscher et al., 2000; Robinson et al., 2006; Egbue & Kellogg, 2010; Schepers et al., 2017). b) Geological map of the Central and Southern Andes showing the location of major cross structures. The deformation style and distribution are quite different from the Central to the Southern Andes. (modified from Ghiglione et al., 2009; Stanton-Yonge et al., 2016; Schepers et al., 2017). The red lines in the 'Figure 2.9b' represent the Andean Transverse Faults. Acronyms: CCM: Calliqui-Copahue-Mandolegue Transfer Zone; CCVC: Cordon Caulle Volcanic Complex; ChC: Chillan-Cortaderas Lineament; GFZ: Grijalva Fracture Zone; LATF: Lago Argentino Transfer Fault; LOFS: Liquine-Ofqui Fault System; LVTF: Lago Videma Transfer Fault; MFZ: Mendana Fracture Zone; MVFZ: Mocha-Villarrica Fault Zone; NFZ: Nazca Fracture Zone; TPTF: Torres del Paine Transfer Fault; TSPP: Tarta-San Pedro-Pellado Volcanic Alignment.

The style of subduction of the down-going Nazca Plate in the Central Andean margin differs greatly from the adjacent margins to the north and south. The Central segment has had a steep subducting plate while to the north and south the oceanic plate has been subducting at a low angle since 12 Ma in the respective trench segments namely, the northern Peruvian and southern Pampean flat slabs (Schepers et al., 2017). The trench retreat has greatly outpaced the slab roll back and this difference has generated the 200-300 km long flat slab segments. The slab is thought to have been anchored at the 660 km discontinuity, which is preventing the roll back (Schepers et al., 2017; Chen et al., 2019). The crustal shortening along the Arica bend in the Central Andes is 420 km, which is much greater than shortening values of 160 km and 150 km in the Southern and Northern respectively (Arriagada et al., 2008; Schepers et al., 2017). There are also differences in the style of deformation related to flat slabs including the inland development of thick-skinned deformation east of the crest of the Andes. Another lateral variation related to the flat slab zones is the absence of active volcanism. Several causes for the flattening of the slab have included subduction of buoyant oceanic crust around the Nazca and Juan Fernandez

Ridges or possible changes in the thermal thickness of the overriding lithosphere (Pilger, 1981; Manea et al., 2012; Schepers et al., 2017).

At a finer scale, there are lateral differences in the timing and nature of deformation along the Andes. In the Northern Andes, crustal blocks are “escaping” northeastwards towards the free Caribbean-North Andes boundary and away from the rigid South American Plate along the system of large-scaled, strike-slip faults (Figure 2.9a) (Audemard et al., 2005; Audemard, 2009; Egbue & Kellogg, 2010; Monod et al., 2010). The trench-parallel component of the oblique plate convergence has been driving this escape for the last 1.8 Ma. This escape was likely triggered by an increase in coupling between the upper and lower plate when the Carnegie Ridge entered the subduction zone (Egbue & Kellogg, 2010).

The Central Andes segment is dominated by anomalous topography of the Altiplano-Puna plateau, which was uplifted due to thermal softening of the lithosphere followed by crustal shortening and accompanying arc magmatism during the orogeny (Allmendinger et al., 1997; Coutand et al., 2001). Within the plateau region researchers have documented significant differences in the timing of the surface uplift and crustal structure of adjacent blocks (e.g.; Bianchi et al., 2013; Leier et al., 2013; Canavan et al., 2014). The fault boundaries of these blocks are thought to be related to inherited basement faults, possibly bounding older accreted terranes (Jordan et al., 1983) Towards the foreland, spatial location of the Cenozoic fault systems were likely controlled by the presence of Paleozoic and Mesozoic basement structures (Coutand et al., 2001; Gillis et al., 2006). The plateaus and the adjacent ranges in the Central Andes, define the highest topographic features in the world within a non-collisional setting (Isacks, 1988).

Another feature unique to the southern Central Andes is the fragmentation and exhumation of the retro-arc foreland basin (Sierras-Pampeanas) along inherited structures (Figure 2.9b) (Jordan et al., 1983; Japas et al., 2016). Stronger coupling between the upper and lower plates in the flat-slab segments has been described as the driver behind inland propagation of deformation and subsequently the basin uplift (Ramos et al., 2002; Oriolo et al., 2014). Just to the south of the flat-slab segment, Giambiagi et al. (2012) documented an abrupt southward decrease in topographic uplift and crustal shortening. This sharp, lateral variation is driven by a strong lateral change in the upper plate rheology, which controls the degree of coupling between the upper and lower crust, such that a thick and more felsic crust has strongly coupled upper and lower slabs (Giambiagi et al., 2012).

Thick-skin deformation in the Central Andes terminates towards the south at the northern segment of the Southern Andes, which is characterized by trench-parallel, thin-skinned, fold and thrust deformation. The southern segment, however, is dominated by a system of strike-slip fault systems. The ENE-striking, transverse, dextral Callaqui-Copahue Mandolegue (CCM) fault is thought to decouple the contrasting deformation styles between the retro-arc thrust belt (north) and the Liquine-Ofqui Fault System (LOFS) in south (Folguera et al., 2004).The LOFS (Figure 2.9b) is a ~1200 km long, NNE-striking, right-lateral, reverse, intra-arc fault in the southern segment (Cembrano et al., 1996; Thomson, 2002; Vargas et al., 2013). Here, a series of NE-striking, en echelon, dextral, normal faults splay off from the LOFS and form a strike slip duplex between two sub-parallel fault branches of the LOFS (Cembrano et al., 1996). Another set of strike-slip faults cut the LOFS and associated faults and are called the Andean Transverse Faults (ATF). The ATF (Figure 2.9b) are NW-striking, reverse, sinistral faults, primarily formed on inherited basement structures (e.g.; Roquer et al., 2017; Sielfeld et al., 2019). Deformation partitioning occurs within these faults, whereby the trench-parallel component of the oblique convergence is accommodated by the LOFS and its splay faults and the ATFs accommodate the trench-perpendicular component (e.g.; Stanton-Yonge et al., 2016). In the northern termination of the LOFS, the strike-slip dominated domain sharply transitions into margin-parallel fold and thrust deformation (Figure 2.9b) (Stanton-Yonge et al., 2016). These strike-slip fault systems also form excellent conduits as well as reservoirs for magma and hydrothermal fluids and thereby control the locus of volcanic complexes (e.g.; Petrinovic et al., 2006; Pérez-Flores et al., 2016; Roquer et al., 2017; Sielfeld et al., 2019; Lupi et al., 2020; Piquer et al., 2020).

Effects of the subduction of oceanic fracture zones on seismic activity has also been observed in the central Andes. In the subducted Peruvian slab, generally deeper earthquakes are generated around a subducted segment boundary, the Mendana Fracture Zone (Figure 2.9a) (Gutscher et al., 2000). Towards the south, a fracture zone in the down-going Nazca plate (most likely the Nazca Fracture zone) is thought to have induced a fracture in the over-riding plate that acted as a temporary lateral barrier during the initial seismic rupture propagation but subsequently allowed energy to pass through this vertical plane releasing the energy of the M_w 8.4 2001 Peru earthquake (Robinson et al., 2006). These examples indicate that transverse discontinuities in the lower plate (or subducting plate) can influence structures in the upper plate and can have great seismic implications.

Proposed Factors Controlling Lateral Heterogeneities

Along the Andean belt, lateral heterogeneities have been primarily expressed as variation in crustal shortening and topographic uplift (e.g.; Allmendinger et al., 1997; Arriagada et al., 2008; Giambiagi et al., 2012; Schepers et al., 2017), along-strike changes in the styles and timing of deformation (e.g.; Ramos et al., 2002; Bianchi et al., 2013; Leier et al., 2013; Canavan et al., 2014; Oriolo et al., 2014; Stanton-Yonge et al., 2016), laterally contrasting seismicity (Gutscher et al., 2000; Robinson et al., 2006), and as changes in volcanic activity (e.g.; Pérez-Flores et al., 2016; Roquer et al., 2017; Sielfeld et al., 2019; Lupi et al., 2020; Piquer et al., 2020). Researchers interpret that these heterogeneities are governed by the angle of lower plate subduction (flat versus steep slab), physiography of the lower plate, obliquity of the subduction vector, preexisting basement structures in the upper plate, and the rheology of the upper plate. The angle of the lower plate subduction controls the degree of coupling between the lower and upper plates (lower angle equals stronger coupling), which in turn impacts the nature and distribution of the upper plate deformation (e.g.; Ramos et al., 2002; Oriolo et al., 2014). Subduction of physiographical features in the lower plate also can change the amount of plate coupling and generate respective topographic and seismic signatures in the upper plate or it can influence the development of cross structures (Gutscher et al., 2000; Robinson et al., 2006). Oblique plate convergence in the Southern Andes has been accommodated by a system of strike-slip and transverse faults (e.g.; Stanton-Yonge et al., 2016). In the Northern Andes, however, the dynamic plate setting has favored crustal escape (e.g.; Egbue & Kellogg, 2010). Rheology of the upper plate dictates the amount of plate coupling and therefore, has controls on the rate and amount of crustal shortening and the overall topographic uplift (Giambiagi et al., 2012).

Other Orogens

Lateral heterogeneities have been documented in several other mountain belts around the world (Figure 2.1). While there are groups of along-strike variations common across multiple mountain belts, some of the heterogeneities are the result of the broad tectonic setting and the nature of the sedimentary cover, and therefore can be unique to only a few mountain belts. Comparable to the Appalachians, , the Mesozoic rift structures in the External Hellenides thrust belt in Greece were reactivated as transverse zones (e.g.; the Corinth Gulf, Ierapetra, and Omalos transverse zones), which partitioned the belt into a series of salients, recesses, and linear segments (Skourlis & Doutsos, 2003; Kokkalas & Doutsos, 2004; Chatzaras et al., 2013). These inherited structures also disrupted the lateral continuity of the foreland sedimentary sequences and served as crustal-scale lateral/oblique ramps during thrust propagation and thereby had a significant control on the nature and deformation style of the evolving taper wedge (Robertson et al., 1991; Doutsos et al., 2006; Chatzaras et al., 2013). Similarly, in the Urals, Precambrian aulacogens (failed rift arms) served as transverse basement structures, above which tear-faults and lateral ramps were developed during fold-thrust propagation (Rodgers, 1990; Brown et al., 1997; Perez-Estaun et al., 1997). Cross faults are common in the Apennines and are generally called anti-Apennine Faults (e.g.; Coltorti et al., 1996; Sorgi et al., 1998; Butler et al., 2006; Elter et al., 2011). The NNW-striking Apennine belt is underlain by the NNE-trending crustal tectonic lineaments (Valnerina Line, Ancona-Anzio Line, Ortona-Rocca Monfina Line). These large-scale lineaments act as structural barriers (zones of abrupt lateral changes in tectonic and structural style, wedge stratigraphy, and topography) during tectonic transport and laterally limit the propagation of seismic fault rupture (Pizzi & Galadini, 2009; Satolli et al., 2014). There are also smaller-scaled transverse basement structures, that may either serve as seismic segment boundaries/seismic loci or get reactivated as transfer zones (Valensise & Pantosti, 2001; Pizzi & Galadini, 2009). Furthermore, transfer zones in the Apennines are also known to form suitable loci for magma emplacement (Dini et al., 2008). On a much larger scale, the differential retreat along the adjacent segments of the Adriatic plate during the last 5 Ma has been manifested as a lithospheric tear/transfer zone across the Appennines (Scrocca, 2006), which may share a similar genesis to the Colorado Mineral Belt in the Cordilleran belt.

Cross structures have also been interpreted to have great economic and seismic impacts besides their influence in tectonic, stratigraphic, and structural evolution (e.g.; Mahoney et al., 2017). In the Papua New Guinea fold-thrust belt, the Jurassic, extensional, transverse, crustal structures evolved as zones of economically significant copper-gold mineralization during their Late Miocene-Pliocene inversion (Davies, 1991; Corbett, 1994; Hill et al., 2002). Like in the Apennines and the Himalaya, active cross faults in the Taiwan mountains are known to serve as earthquake nucleation sites and as rupture segment boundaries (Deffontaines et al., 1997; Lacombe et al., 2001; Ching et al., 2011). These cross faults have genetically been linked to changing deformation style (thick-skinned vs thin-skinned) and to a lateral change in thickness of the deforming sedimentary sequences (Lacombe et al., 2001; Mouthereau et al., 2002; Mouthereau & Lacombe, 2006; Ching et al., 2007). Much similar to the Zagros belt, controls of the presence or absence of a decoupling layer on the style of the evolving taper wedge (narrow wedge with a high-taper angle, when decoupling layer is absent and vice-versa) have been noted in the Caucasus belt (Upper Jurassic salt and Middle-Lower Jurassic shales) in Russia (Sobornov, 1996), the Sulaiman belt (Paleozoic, Lower Cretaceous, and Eocene strata) in Pakistan (Jadoon et al., 1994), and the Parry Island belts (Ordovician salt) in the Canadian Arctic (Harrison & Bally, 1988).

Discussion

Despite the general temporal and spatial continuity of crustal deformation along convergent mountain belts, significant lateral heterogeneities have been observed in several orogenic belts from around the world. There are certain lateral variations, which are unique to only a few orogens such as the lithospheric tear in the Apennines and the asynchronous orogenic events in the Alps. More frequently, however, similar groups of lateral variations have been observed across multiple mountain belts. Generally, lateral heterogeneity in convergent mountain belt settings have been expressed as: 1) an along-strike change in deformation style (thick-skinned vs thin-skinned, imbrication vs duplexing/changes in ramp geometries); 2) variation in igneous activity and metamorphic grade; 3) variation in seismic activity; 4) differential topographic uplift/features along the strike; and/or 5) abrupt changes in thickness and facies of sedimentary sequences in both foreland basins and within the fold-thrust belt. Oftentimes such lateral variations are abrupt rather than gradual and are marked by geological structures, mostly faults, that are nearly orthogonal to the strike of the orogen, generically referred to as cross structures in this review. The causal factors/mechanisms behind the observed lateral heterogeneities are discussed in this section.

Irregular Continental Margins

The geometry of the continental margin(s), prior to the collision/convergence, has a profound effect on the geometry of the evolving orogenic belt. The orogenic front may mimic the continental margin geometry (Figure 2.4) such that any irregularities along the margin are reflected along the deformational font. This phenomenon has been proposed in the Appalachians. During the Iapetan rifting (plus the other rifting events) along the Laurentian margin, a series of embayments (concave oceanward) and promontories (convex oceanward) separated by transform faults were produced (Thomas, 2014). Along such an irregular margin, the depositional environment is bound to vary laterally. During subsequent orogenic events, promontories evolved into recesses (concave towards the foreland), embayments evolved into salients (convex towards the foreland), and the transform fault boundaries evolved into transverse zones or cross structures (Thomas, 2014). Kwon and Mitra (2004) have compiled five end-member models for the kinematic development of salients as a function of principal transport direction, amount of shortening, degree of vertical axis rotation, thrust displacement, and presence or absence of tear faults or lateral/oblique ramp boundaries. These models, however, can be viewed as second-order, structural controls on formation of orogenic curvatures.

Lin et al. (1994) further noted that a collisional event between two promontories (of two different landmasses) results in a narrower but stronger orogenic deformation and a higher grade of metamorphism than a promontory-embayment collision. It can be concluded that an irregularity along a continental margin may serve as a nucleation site for lateral heterogeneity.

Inherited Basement Structures

Inherited basement structures form a first-order control on formation of cross structures. Basement structures are primarily related to continental rifting, hyper-extension of rifted margins (e.g.; Ribes et al., 2019) , crustal sutures, or back-arc extension (Figure 2.10). Furthermore, it has been noted that a failed rift-arm (aulacogen) can also serves as an inherited basement structure and control structural evolution (Rodgers, 1990; Brown et al., 1997; Perez-Estaun et al., 1997). Crustal sutures mark boundaries between two continental blocks and form as a result of collisional tectonics or terrane accretion. Generally, suture zones consist of highly deformed rock units and form weaker zones within the crust (Hope & Eaton, 2002; Whitmeyer & Karlstrom, 2007). These zones are known to be intruded by igneous bodies during the subsequent crustal stabilization (Whitmeyer & Karlstrom, 2007), and these intrusion boundaries can also behave as zone of weaknesses during various tectonic events (Simony & Carr, 1997; Bader, 2009).

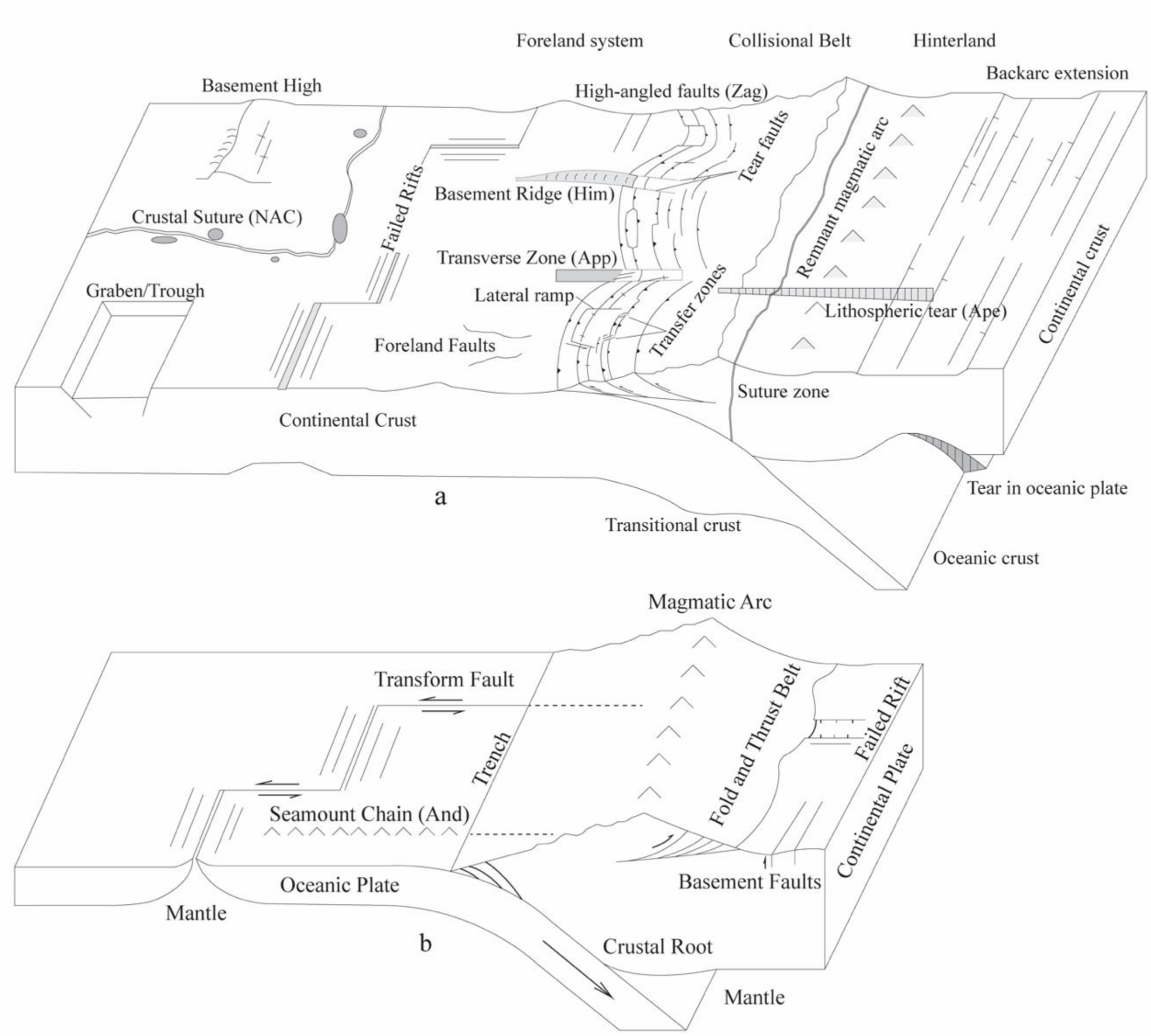

Figure 2.10: Inherited basement structures and oceanic plate physiography in contractional settings. The gray ellipses in the 'Figure10a' represent igneous intrusions. The mountain belt that, in general, represents a certain structure are denoted in parenthesis. And: Andes; Ape: Apennines; App: Appalachians; Him: Himalaya; NAC: North American Cordillera; Zag: Zagros.

Impacts of Basement Structures on Subsequent Sedimentation and Deformation The presence of basement structures can greatly affect the foreland sedimentation and thereby have a strong control on the evolution of mountain belts as is seen in the Zagros, the Cordillera, and the Himalaya. Basement structures can isolate deposition centers in the foreland, which induces sharp lateral variations in both the thickness and facies of the sedimentary strata. A thicker foreland sedimentary sequence, when incorporated into the evolving taper wedge, will propagate much farther (salient) than a wedge consisting of a thinner sequence (recess) (e.g.; Paulsen & Marshak, 1999). Differential tectonic transport between the adjacent segments (salients and recesses) is often accommodated by cross structures such as tear faults, lateral ramps, and displacement transfer zones (Paulsen & Marshak, 1999). Orogen-parallel faults and folds are generally truncated at, or dragged into cross structures as seen in the Appalachians and the Cordillera (e.g.; Thomas, 2007; Whisner et al., 2014).

Similarly, lateral variations in sedimentary facies will also have a significant impact on the wedge evolution. An abrupt change in the structural elevation of decoupling layers results in lateral ramps (Thomas, 1990). Since thrust-ramp geometry is governed by the nature of the sedimentary column, any lateral variation in sedimentary facies is likely to be reflected in the thrust geometry (e.g.; Mitra, 1988). In a broader stratigraphic framework, if the presence of regional decollement horizons (units of salts, evaporites, and shales) varies laterally, then the deformation style in adjacent segments of the mountain belts will be very different. If a decollement horizon is present, then the taper angle will be low and propagate further than adjacent areas. Likewise, in the absence of such a horizon, the taper will build up to a larger angle in a narrower belt as in the Zagros (e,g,; Jadoon et al., 1994; Sobornov, 1996; Bahroudi &

Koyi, 2003). The depth of these decollement horizons will also have a first order control on the fold geometry, such that a deeper horizon will result in folds with larger amplitude (Sepehr et al., 2006). Furthermore, the stratigraphic variation boundaries will also act as a lateral buttress to locally deflect the transport trajectories (Bahroudi & Koyi, 2003). If basement structures are reactivated during deposition, then syn-sedimentary faults and/or drape folds can form in the overlying sedimentary column (Thomas, 1990). These structures will also impact the fold-thrust belt evolution in a similar fashion to other cross-structures (e.g.; Zerlauth et al., 2014).

Reactivation of Basement Structures Regardless of their origin, inherited basement structures can be broadly categorized into three groups: orogen-parallel, oblique, and transverse/cross basement structures. Various styles of preferential reactivation and inversion of basement structures have been discussed in the Apennines (Tavarnelli et al., 2004; Butler et al., 2006), and are also seen in other mountain belts. When orogen-parallel basement structures/faults are present, it is possible for them to be reactivated as reverse faults during orogenic compression (Figure 2.10a). It has, however, been noted that basement faults can be deformed under compression without inversion or reactivation (Pantet et al., 2020). In a reactivation scenario, the deformation between the basement and the overlying sedimentary cover is partially decoupled, whereby the basement deforms in thick-skinned style and the cover deforms as thin-skinned, fold and thrust belts (e.g.; Berberian, 1995; Lacombe et al., 2006). Discontinuities along the orogen-parallel basement structures will eventually result in laterally heterogeneous deformation style along the range. If the basement faults are steeply-dipping, then they often cut into the thin-skinned decollement faults of the sedimentary cover and act as frontal ramps during the upper, brittle deformation (e.g.; Bahroudi & Koyi, 2003). These orogen-parallel basement structures also accommodate convergence via strike-slip faulting under a favorable plate kinematic setting (e.g.; Authemayou et al., 2006). Margin perpendicular and oblique structures, however, either serve as lateral/oblique ramps or get reactivated as strike-slip faults with a dip-slip component based on their orientation in the stress field. Based on their aerial extent, these inherited structures can affect a few thrust sheets, or they can partition the entire mountain belt (Scrocca, 2006; Pizzi & Galadini, 2009; Satolli et al., 2014). Cross faults in the Himalaya may have had an origin in reactivated, margin-perpendicular basement faults and basement highs such as the Delhi-Hardwar ridge (Sahoo, 2000; Godin & Harris, 2014; Hubbard et al., 2018; Hubbard et al., 2021).

Rheology of the Crust

Variation in crustal rheology is another significant element in inducing lateral heterogeneities in orogenic belts, which itself is a function of its composition and thermal structure. In general, a weaker crust is more likely to buckle under contraction resulting in a high crustal relief, whereas a stronger crust will distribute deformation in more brittle manner (Allmendinger et al., 1997; Coutand et al., 2001). It has also been proposed that rheological heterogeneities along a continental margin front could result in orogenic curvatures, such that a stronger segment better resists deformation and evolves as a salient (e.g.; Malekzade et al., 2016). As seen in the Zagros, frictional strength in hinterland faults, which is governed by crustal rheology, can influence the mode of deformation partitioning in the orogenic belt and thereby have a control on the style and distribution of deformation (e.g.; Vernant & Chéry, 2006). Thermal structure and rheology of the crust can vary laterally due to variations in arc magmatism. Therefore, previous tectonic events will also have an indirect impact on lateral heterogeneity of an orogen.

Giambiagi et al. (2012) proposed that a stronger coupling between the upper and lower crust deformation corresponds to a higher, surficial topography and greater crustal shortening. Crustal coupling is thought to be governed by crustal composition such that a thick and more felsic crust has a stronger coupling between the upper and lower units than a thin and mafic crust. Thus, if there is strong lateral variation in crustal properties due to tectonic events such as terrane accretion or rifting then such variation will be manifested as laterally heterogenous deformation segments.

In the Alps, intensive folding and uplift of the Tauern window has been linked to the northward encroachment of the Dolomite acting as an indenter (Rosenberg & Garcia, 2011), which indicates that rheology of both converging crustal blocks have an impact on the morpho-tectonic evolution of an orogen.. As Butler et al. (2006) pointed out, the correlation between precise lithospheric strength profiles and orogenic deformation would further elucidate our understanding about the role of upper crustal rheology during orogenesis.

Plate Dynamics and Physiography of the Lower Plate

Plate dynamics between the upper and lower plate as well as the lower plate structures can disrupt the lateral homogeneity of orogenic belt (Figure 2.10b). Effects of lateral change in the style of subduction in the deforming orogen have contributed to lateral heterogeneity in the Andes. Any transverse structure in the lower plate is likely to be inherited in the upper plate, such as the Colorado Mineral Belt and the lithospheric tear in the Apennines (e.g.; Figure 2.10a) (Scrocca, 2006; Chapin, 2012). These structures in the lower plate impartially dissect the orogen rather than controlling the deformation style. The dynamics of the lower plate, however, generally differs across these transverse structures, which impacts the foreland sedimentation and fold-thrust belt evolution (Chapin, 2012). A similar phenomenon has been observed in cases where oceanic fracture zones (Figure 2.10b), orthogonal to the subduction zone, get subducted and result in the occurrence of cross faults in the over-riding plate. This scenario has been proposed on the Juan de Fuca plate subduction (Goldfinger, 1997), in Sumatra (Graindorge, 2008), and in the Andes (Robinson et al., 2006). Although not a cross structure, the Norumbega Fault System in the Appalachians has been regarded as a surface manifestation of a subducted oceanic ridge-transform system (Kuiper, 2016; Kuiper & Wakabayashi, 2018).

In orogens associated with oceanic subduction, variations in the relative rates of subduction versus convergence can create lateral heterogeneity in the over-riding plates as is seen in the Andes. When subduction outpaces convergence such that the convergent boundary retreats, back-arc extension occurs. These areas may have contrasting evolution when compared to adjacent areas where there is a better balance of the subduction versus convergence rates.

<u>Obliquity of Plate Convergence</u>

Lateral heterogeneity induced by oblique convergence is scale dependent. Obliquity of the plate convergence is generally accommodated by arrays of transtensional, transpressional, and strike-slip faults. In the Andes, transpressional cross faults are associated with mafic volcanism, while transtensional faults are linked with felsic magmatism as driven by magmatic viscosity difference (Petrinovic et al., 2006). At the scale of individual faults, these cross-faults disrupt the continuity of the fold-thrust belt as noted in the southern Andes and the Northern Calcareous Alps (Zerlauth et al., 2014; Stanton-Yonge et al., 2016). Lateral variation in the degree of oblique convergence itself, however, will also induce lateral heterogeneity in the orogenic belt due to an overall change in the stress field (McQuarrie et al., 2003; Vernant et al., 2004; Vernant & Chéry, 2006).

Further Implications of Cross Structures

Besides their role in foreland sedimentation and tectonic evolution of orogens, cross faults also have implications in the seismicity, mineralization, igneous activity, numerical modelling, and in topography of mountain belts. In the Zagros, a small seismic hazard has been linked to cross-faults (Berberian, 1995; Authemayou et al., 2006). Cross-faults in the Apennines are known to either serve as seismic segment boundaries or seismic loci (Valensise & Pantosti, 2001; Pizzi & Galadini, 2009). Similarly, in Taiwan, cross-faults are known to act as earthquake nucleation sites and as rupture segment boundaries (Deffontaines et al., 1997; Ching et al., 2011). Micro-seismicity in the Himalaya has occurred along cross-strike trends, has terminated at cross-strike zones, and has made other spatial changes along cross-strike boundaries (Rajaure, 2013; Mugnier et al., 2017; Bilham, 2019; Mendoza, 2019). A transverse fault in the down-going Nazca plate had an enormous impact during the 2001 Peru earthquake (Robinson et al., 2003). From the economic standpoint, cross-faults form excellent conduits as well as reservoirs for magma and hydrothermal fluids (McMechan, 2012), which makes them target sites for economic mineral deposits. In the Papua New Guinea fold-thrust belt, transverse zones form sites of economically significant copper-gold deposits (Davies, 1991; Corbett, 1994; Hill et al., 2002). The Colorado Mineral Belt is another example of valuable mineral accumulation along a cross-structure (Chapin, 2012). Moreover, cross-structures can form potential traps for oil and gas accumulation, which, in some areas makes them an important site for hydrocarbon exploration

(Wheeler, 1980; Séjourné & Malo, 2007; Bader, 2009). Fault systems can form excellent conduits and reservoirs for magmatic fluids and therefore can control the locus of volcanic complexes in convergent settings (e.g.; Petrinovic et al., 2006; Pérez-Flores et al., 2016; Roquer et al., 2017; Sielfeld et al., 2019; Lupi et al., 2020; Piquer et al., 2020). Thermo-mechanical tectonic models could potentially be rectified by changing the lithospheric parametric values along the strike such that they agree with the lateral variation in crustal deformation, as can be observed on the surface. Finally, cross-structures also have a major control on the geomorphologic evolution of mountain belts. In the Himalayan front, cross faults spatially coincide with river channels (Sahoo, 2000; Srivastava, 2018). The anti-Apennine faults have distinct topographic signatures (Coltorti et al., 1996). Cross-faults can be zones of weaknesses, and therefore, can also amplify erosional hazards, especially in active mountain belts.

Conclusions

While convergent mountain belts are dominated by spatially and temporally continuous orogen-parallel structures, geological and geophysical data shows that various forms of lateral heterogeneity, often marked by cross structures, are ubiquitous in most orogenic settings. In general, lateral heterogeneities along orogens have been manifested as: 1) along-strike changes in deformation style; 2) variation in igneous activity or metamorphic grade; 3) variation in seismic activity; 4) changes in topography and geomorphology; and 5) abrupt lateral stratigraphic changes. Common drivers behind these lateral heterogeneities include the geometry of the continental margin, inherited basement structures, lateral variation in stratigraphy of deforming sedimentary sequences, variation in crustal rheology, along-strike changes in plate tectonic setting, physiography of the lower plate, and obliquity of plate convergence. In most settings, these factors are interrelated and simultaneously influence the morpho-tectonic evolution of an orogen. Apart from their influence on foreland sedimentation and orogenic evolution, lateral heterogeneity and cross structures can have an impact on patterns of seismicity, natural resource occurrence, and natural hazards. We therefore stress the importance of documenting heterogeneity, mapping cross structures, and understanding the role these lateral changes play in mountain belt development along convergent margins.

References

Aleinikoff, J. N., Zartman, R. E., Walter, M., Rankin, D. W., Lyttle, P. T., & Burton, W. C. (1995). U-Pb ages of metarhyolites of the Catoctin and Mount Rogers Formations, central and southern Appalachians: Evidence for two pulses of Iapetan rifting. *American Journal of Science*, *295*(4), 428-454. doi:https://doi.org/10.2475/ajs.295.4.428

Allen, M. B., & Armstrong, H. A. (2008). Arabia–Eurasia collision and the forcing of mid-Cenozoic global cooling. *Palaeogeography, Palaeoclimatology, Palaeoecology, 265*(1-2), 52-58. doi:https://doi.org/10.1016/j.palaeo.2008.04.021

Allmendinger, R. W., Jordan, T. E., Kay, S. M., & Isacks, B. L. (1997). The evolution of the Altiplano-Puna plateau of the Central Andes. *Annual Review of Earth and Planetary Sciences*, *25*(1), 139-174. doi:https://doi.org/10.1146/annurev.earth.25.1.139

Anderson, H. E., & Davis, D. W. (1995). U–Pb geochronology of the Moyie sills, Purcell Supergroup, southeastern British Columbia: implications for the Mesoproterozoic geological history of the Purcell (Belt) basin. *Canadian Journal of Earth Sciences*, *32*(8), 1180-1193. doi:https://doi.org/10.1139/e95-097

Angermann, D., Klotz, J., & Reigber, C. (1999). Space-geodetic estimation of the Nazca-South America Euler vector. *Earth and Planetary Science Letters*, *171*(3), 329-334. doi:https://doi.org/10.1016/S0012-821X(99)00173-9

Arriagada, C., Roperch, P., Mpodozis, C., & Cobbold, P. (2008). Paleogene building of the Bolivian Orocline: Tectonic restoration of the central Andes in 2-D map view. *Tectonics, 27*(6). doi:https://doi.org/10.1029/2008TC002269

Audemard, F. A. (2009). Key issues on the post-Mesozoic southern Caribbean plate boundary. In K. James, M. Lorente, & J. Pindell (Eds.), *Origin and Evolution of the Caribbean Plate* (Vol. 328, pp. 569-586). London: Geological Society, Special Publications.

Audemard, F. A., Romero, G., Rendon, H., & Cano, V. (2005). Quaternary fault kinematics and stress tensors along the southern Caribbean from fault-slip data and focal mechanism solutions. *Earth-Science Reviews, 69*(3-4), 181-233. doi:https://doi.org/10.1016/j.earscirev.2004.08.001

Authemayou, C., Chardon, D., Bellier, O., Malekzadeh, Z., Shabanian, E., & Abbassi, M. R. (2006). Late Cenozoic partitioning of oblique plate convergence in the Zagros fold-and-thrust belt (Iran). *Tectonics, 25*(3). doi:https://doi.org/10.1029/2005TC001860

Avouac, J.-P. (2003). Mountain building, erosion, and the seismic cycle in the Nepal Himalaya. *Advances in geophysics, 46*, 1-80. doi:https://doi.org/10.1016/S0065-2687(03)46001-9

Bader, J. W. (2008). Structural and tectonic evolution of the Cherokee Ridge arch, south-central Wyoming: implications for recurring strike-slip along the Cheyenne Belt suture zone. *Rocky Mountain Geology, 43*(1), 23-40. doi:https://doi.org/10.2113/gsrocky.43.1.23

Bader, J. W. (2009). Structural and tectonic evolution of the Douglas Creek arch, the Douglas Creek fault zone, and environs, northwestern Colorado and northeastern Utah Implications for petroleum accumulation in the Piceance and Uinta basins. *Rocky Mountain Geology, 44*(2), 121-145. doi:https://doi.org/10.2113/gsrocky.44.2.121

Bahroudi, A., & Koyi, H. A. (2003). Effect of spatial distribution of Hormuz salt on deformation style in the Zagros fold and thrust belt: an analogue modelling approach. *Journal of the Geological Society, 160*(5), 719-733. doi:https://doi.org/10.1144/0016-764902-135

Bartosch, T., Stüwe, K., & Robl, J. (2017). Topographic evolution of the Eastern Alps: The influence of strike-slip faulting activity. *Lithosphere, 9*(3), 384-398. doi:https://doi.org/10.1130/L594.1

Bayona, G., Thomas, W. A., & Van der Voo, R. (2003). Kinematics of thrust sheets within transverse zones: a structural and paleomagnetic investigation in the Appalachian thrust belt of Georgia and Alabama. *Journal of Structural Geology, 25*(8), 1193-1212. doi:https://doi.org/10.1016/S0191-8141(02)00162-1

Beck, R. A., Vondra, C. F., Filkins, J. E., & Olander, J. D. (1988). Syntectonic sedimentation and Laramide basement thrusting, Cordilleran foreland; timing of deformation. In C. J. Schmidt Jr & W. J. Perry (Eds.), *Interaction of the Rocky Mountain Foreland and the Cordilleran Thrust Belt* (Vol. 171, pp. 465-488): Geological Society of America Memoir.

Behrmann, J. H. (1988). Crustal-scale extension in a convergent orogen: the Sterzing-Steinach mylomte zone in the Eastern Alps. *Geodinamica Acta, 2*(2), 63-73. doi:https://doi.org/10.1080/09853111.1988.11105157

Benvenuto, G. L., & Price, R. A. (1979). Structural evolution of the Hosmer thrust sheet, southeastern British Columbia. *Bulletin of Canadian Petroleum Geology, 27*(3), 360-394.

Berberian, M. (1995). Master "blind" thrust faults hidden under the Zagros folds: active basement tectonics and surface morphotectonics. *Tectonophysics, 241*(3-4), 193-224. doi:https://doi.org/10.1016/0040-1951(94)00185-C

Berberian, M., & King, G. C. P. (1981). Towards a paleogeography and tectonic evolution of Iran. *Canadian Journal of Earth Sciences, 18*(2), 210-265. doi:https://doi.org/10.1139/e81-019

Berger, Z., Boast, M., & Mushayandebvu, M. (2008). The contribution of integrated HRAM studies to exploration and exploitation of unconventional plays in North America. *Reservoir, Canadian Society of Petroleum Geologist, 35*(10), 42-48.

Bernoulli, D. (2007). The pre-Alpine geodynamic evolution of the Southern Alps: a short summary. *Bulletin für angewandte Geologie, 12*(2), 3-10.

Berra, F., & Carminati, E. (2010). Subsidence history from a backstripping analysis of the Permo-Mesozoic succession of the Central Southern Alps (Northern Italy). *Basin Research, 22*(6), 952-975. doi:https://doi.org/10.1111/j.1365-2117.2009.00453.x

Bertotti, G., Picotti, V., Bernoulli, D., & Castellarin, A. (1993). From rifting to drifting: tectonic evolution of the South-Alpine upper crust from the Triassic to the Early Cretaceous. *Sedimentary Geology, 86*(1-2), 53-76. doi:https://doi.org/10.1016/0037-0738(93)90133-P

Bianchi, M., Heit, B., Jakovlev, A., Yuan, X., Kay, S., Sandvol, E., Alonso, R. N., Coira, B., Brown, L., & Kind, R. (2013). Teleseismic tomography of the southern Puna plateau in Argentina and adjacent regions. *Tectonophysics, 586*, 65-83. doi:http://dx.doi.org/10.1016/j.tecto.2012.11.016

Bielenstein, H. U. (1969). *The Rundle thrust sheet, Banff, Alberta—a structural analysis.* (Ph.D.). Queen's University, Kingston, Ontario.

Bigi, S., Carminati, E., Aldega, L., Trippetta, F., & Kavoosi, M. A. (2018). Zagros fold and thrust belt in the Fars province (Iran) I: Control of thickness/rheology of sediments and pre-thrusting tectonics on structural style and shortening. *Marine and Petroleum Geology, 91*, 211-224. doi:https://doi.org/10.1016/j.marpetgeo.2018.01.005

Bilham, R. (2019). Himalayan earthquakes: a review of historical seismicity and early 21st century slip potential. In P. J. Treloar & M. P. Searle (Eds.), *Himalayan Tectonics: a Modern Synthesis* (Vol. 483, pp. 423-482). London: Geological Society of London Special Publication.

Bilham, R., Gaur, V. K., & Molnar, P. (2001). Himalayan seismic hazard. *Science, 293*. doi:https://doi.org/10.1126/science.1062584

Boyer, S. E. (1995). Sedimentary basin taper as a factor controlling the geometry and advance of thrust belts. *American Journal of Science*, *295*(10), 1220-1254. doi:https://doi.org/0.2475/ajs.295.10.1220

Boyer, S. E., & Elliott, D. (1982). Thrust systems. *AAPG Bulletin, 66*(9), 1196-1230. doi:https://doi.org/10.1306/03B5A77D-16D1-11D7-8645000102C1865D

Brack, P. (1981). Structures in the southwestern border of the Adamello intrusion (Alpi Bresciane, Italy). *Schweizerische Mineralogische und Petrographische Mitteilungen, 61(1)*, 37-50. doi:http://pascal-francis.inist.fr/vibad/index.php?action=getRecordDetail&idt=PASCALGEODEBRGM8220070062

Brewer, M. C. (2004). *Geometric and Kinematic Evolution of the Bessemer Transverse Zone, Alabama Alleghanian Thrust Belt.* (Ph.D.). University of Kentucky,

Brown, D., Alvarez-Marrón, J., Perez-Estaun, A., Gorozhanina, Y., Baryshev, V., & Puchkov, V. (1997). Geometric and kinematic evolution of the foreland thrust and fold belt in the southern Urals. *Tectonics, 16*(3), 551-562. doi:https://doi.org/10.1029/97TC00815

Burchfiel, B. C., Cowan, D. S., & Davis, G. A. (1992). Tectonic overview of the Cordilleran orogen in the western United States. In B. C. Burchfiel, W. Lipman, & M. L. Zoback (Eds.), *The Cordilleran Orogen: Conterminous US* (Vol. G3, pp. 107-168): Geoogical Society of America.

Burrard, S. G. (1915). Origin of the Indo-Gangetic trough, commonly called Himalayan foredeep. *Proceedings of the Royal Society of Londong, 91A*, 220-238. doi:https://doi.org/10.1098/rspa.1915.0014

Butler, R. W. H., Tavarnelli, E., & Grasso, M. (2006). Structural inheritance in mountain belts: an Alpine–Apennine perspective. *Journal of Structural Geology*, *28*(11), 1893-1908. doi:https://doi.org/10.1016/j.jsg.2006.09.006

Calais, E., Nocquet, J.-M., Jouanne, F., & Tardy, M. (2002). Current strain regime in the Western Alps from continuous Global Positioning System measurements, 1996–2001. *Geology, 30*(7), 651-654. doi:https://doi.org/10.1130/0091-7613(2002)030<0651:CSRITW>2.0.CO;2

Campani, M., Mancktelow, N., Seward, D., Rolland, Y., Müller, W., & Guerra, I. (2010). Geochronological evidence for continuous exhumation through the ductile-brittle transition along a crustal-scale low-angle normal fault: Simplon Fault Zone, central Alps. *Tectonics, 29*(3). doi:https://doi.org/10.1029/2009TC002582

Canavan, R. R., Carrapa, B., Clementz, M. T., Quade, J., DeCelles, P. G., & Schoenbohm, L. M. (2014). Early Cenozoic uplift of the Puna Plateau, Central Andes, based on stable isotope paleoaltimetry of hydrated volcanic glass. *Geology, 42*(5), 447-450. doi:https://doi.org/101130/G35239.1

Carosi, R., Montomoli, C., Rubatto, D., Visoná, D. (2010). Late Oligocene high-temperature shear zones in the core of the Higher Himalayan Crystallines (lower Dolpo, Western Nepal). *Tectonics, 29*. doi:https://doi.org/10.1029/2008TC002400

Castellarin, A., & Cantelli, L. (2000). Neo-Alpine evolution of the southern Eastern Alps. *Journal of Geodynamics, 30*(1-2), 251-274. doi:https://doi.org/10.1016/j.tecto.2005.10.019

Castellarin, A., Vai, G. B., & Cantelli, L. (2006). The Alpine evolution of the Southern Alps around the Giudicarie faults: A Late Cretaceous to Early Eocene transfer zone. *Tectonophysics, 414*(1), 203-223. doi:https://doi.org/10.1016/j.tecto.2005.10.019

Cawood, P. A., & Botsford, J. W. (1991). Facies and structural contrasts across Bonne Bay cross-strike discontinuity, western Newfoundland. *American Journal of Science, 291*(8), 737-759. doi:https://doi.org/10.2475/ajs.291.8.737

Cembrano, J., Hervé, F., & Lavenu, A. (1996). The Liquiñe Ofqui fault zone: a long-lived intra-arc fault system in southern Chile. *Tectonophysics, 259*(1-3), 55-66. doi:https://doi.org/10.1016/0040-1951(95)00066-6

Chapin, C. E. (2012). Origin of the Colorado mineral belt. *Geosphere, 8*(1), 28-43. doi:https://doi.org/10.1130/GES00694.1

Chapple, W. M. (1978). Mechanics of thin-skinned fold-and-thrust belts. *Geological Society of America Bulletin, 89*(8), 1189-1198. doi:https://doi.org/10.1130/0016-7606(1978)89<1189:MOTFB>2.0.CO;2

Chatzaras, V., Xypolias, P., Kokkalas, S., & Koukouvelas, I. (2013). Tectonic evolution of a crustal-scale oblique ramp, Hellenides thrust belt, Greece. *Journal of Structural Geology, 57*, 16-37. doi:https://doi.org/10.1016/j.jsg.2013.10.003

Chauvet, A., Onézime, J., Charvet, J., & Barbanson, L. (2004). Syn-to late-tectonic stockwork emplacement within the spanish section of the iberian pyrite belt: Structural, textural, and mineralogical constraints in the tharsis and la zarza areas. *Economic Geology, 99*(8), 1781-1792. doi:https://doi.org/10.2113/gsecongeo.99.8.1781

Chen, Y.-W., Wu, J., & Suppe, J. (2019). Southward propagation of Nazca subduction along the Andes. *Nature, 565*(7740), 441-447. doi:https://doi.org/10.1038/s41586-018-0860-1

Ching, K.-E., Johnson, K. M., Rau, R.-J., Chuang, R. Y., Kuo, L.-C., & Leu, P.-L. (2011). Inferred fault geometry and slip distribution of the 2010 Jiashian, Taiwan, earthquake is consistent with a thick-skinned deformation model. *Earth and Planetary Science Letters, 301*(1-2), 78-86. doi:https://doi.org/10.1016/j.epsl.2010.10.021

Ching, K.-E., Rau, R.-J., Lee, J.-C., & Hu, J.-C. (2007). Contemporary deformation of tectonic escape in SW Taiwan from GPS observations, 1995–2005. *Earth and Planetary Science Letters, 262*(3-4), 601-619. doi:https://doi.org/10.1016/j.epsl.2007.08.017

Colman-Sadd, S. P. (1978). Fold development in Zagros simply folded belt, Southwest Iran. *AAPG Bulletin, 62*(6), 984-1003. doi:https://doi.org/10.1306/C1EA4F81-16C9-11D7-8645000102C1865D

Colman-Sadd, S. P., Cawood, P. A., Dunning, G. R., Hall, J. M., Kean, B. F., O'Brien, B. H., & O'Brien, S. J. (1992). *Lithoprobe East in Newfoundland (Burgeo Transect): A cross-section through the southwest New- foundland Appalachians* (Vol. 92-A7).

Coltorti, M., Farabollini, P., Gentili, B., & Pambianchi, G. (1996). Geomorphological evidence for anti-Apennine faults in the Umbro-Marchean Apennines and in the peri-Adriatic basin, Italy. *Geomorphology, 15*(1), 33-45. doi:https://doi.org/10.1016/0169-555X(95)00117-N

Coney, P. J., & Reynolds, S. J. (1977). Cordilleran benioff zones. *Nature, 270*(5636), 403-406. doi:https://doi.org/10.1038/270403a0

Constenius, K. N. (1996). Late Paleogene extensional collapse of the Cordilleran foreland fold and thrust belt. *Geological Society of America Bulletin, 108*(1), 20-39. doi:https://doi.org/10.1130/0016-7606(1996)108<0020:LPECOT>2.3.CO;2

Cook, B. S., & Thomas, W. A. (2009). Superposed lateral ramps in the Pell City thrust sheet, Appalachian thrust belt, Alabama. *Journal of Structural Geology, 31*(9), 941-949. doi:https://doi.org/10.1016/j.jsg.2009.06.001

Cooley, M. A., Price, R. A., Dixon, J. M., & Kyser, T. K. (2011). Along-strike variations and internal details of chevron-style, flexural-slip thrust-propagation folds within the southern Livingstone Range anticlinorium, a paleohydrocarbon reservoir in southern Alberta Foothills, Canada. *AAPG Bulletin, 95*(11), 1821-1849. doi:https://doi.org/10.1306/01271107097

Corbett, G. J. (1994). *Regional structural control of selected Cu/Au occurrences in Papua New Guinea.* Paper presented at the Proceedings of the Papua New Guinea Geology, Exploration and Mining Conference, Melbourne.

Cotton, J. T., & Koyi, H. A. (2000). Modeling of thrust fronts above ductile and frictional detachments: Application to structures in the Salt Range and Potwar Plateau, Pakistan. *Geological Society of America Bulletin, 112*(3), 351-363. doi:https://doi.org/10.1130/0016-7606(2000)112<351:MOTFAD>2.0.CO;2

Coutand, I., Cobbold, P. R., de Urreiztieta, M., Gautier, P., Chauvin, A., Gapais, D., Rossello, E. A., & López-Gamundí, O. (2001). Style and history of Andean deformation, Puna plateau, northwestern Argentina. *Tectonics*, *20*(2), 210-234. doi:https://doi.org/10.1029/2000TC900031

Dahl, P. S., Holm, D. K., Gardner, E. T., Hubacher, F. A., & Foland, K. A. (1999). New constraints on the timing of Early Proterozoic tectonism in the Black Hills (South Dakota), with implications for docking of the Wyoming province with Laurentia. *Geological Society of America Bulletin*, *111*(9), 1335-1349. doi:https://doi.org/10.1130/0016-7606(1999)111<1335:NCOTTO>2.3.CO;2

Dahlen, F. A. (1990). Critical taper model of fold-and-thrust belts and accretionary wedges. *Annual Review of Earth and Planetary Sciences, 18*(1), 55-99. doi:https://doi.org/10.1146/annurev.ea.18.050190.000415

Davies, H. L. (1991). *Regional geologic setting of some mineral deposits of the New Guinea Orogen.* Paper presented at the Papua New Guinea Geology, Exploration and Mining Conference; Rabaul, Papua New Guinea, 1991.

DeCelles, P. G. (2004). Late Jurassic to Eocene evolution of the Cordilleran thrust belt and foreland basin system, western USA. *American Journal of Science, 304*(2), 105-168. doi:https://doi.org/10.2475/ajs.304.2.105

DeCelles, P. G., Carrapa, B., Ojha, T. P., Gehrels, G. E., & Collins, D. (2020). Structural and thermal evolution of the Himalayan thrust belt in midwestern Nepal. *Geological Society of America Special Paper, 547*, 1-77. doi:https://doi.org/10.1130/2020.2547(01)

Decelles, P. G., Gray, M., Ridgway, K., Cole, R., Pivnik, D., Pequera, N., & Srivastava, P. (1991). Controls on synorogenic alluvial-fan architecture, Beartooth Conglomerate (Palaeocene), Wyoming and Montana. *Sedimentology, 38*(4), 567-590. doi:https://doi.org/10.1111/j.1365-3091.1991.tb01009.x

DeCelles , P. G., Robinson, D. M., Quade, J., Ojha, T. P., Garzione, C. N., Copeland, P., & N., U. B. (2001). Stratigraphy, structure, and tectonic evolution of the Himalayan fold-thrust belt in western Nepal. *Tectonics, 20*, 487-509. doi:https://doi.org/10.1029/2000TC001226

Deffontaines, B., Lacombe, O., Angelier, J., Chu, H., Mouthereau, F., Lee, C., Deramond, J., Lee, J., Yu, M., & Liew, P. (1997). Quaternary transfer faulting in the Taiwan Foothills: evidence from a multisource approach. *Tectonophysics*, *274*(1-3), 61-82. doi:https://doi.org/10.1016/S0040-1951(96)00298-3

Dewey, J. F., & Bird, J. M. (1970). Mountain belts and the new global tectonics. *Journal of Geophysical Research, 75*(14), 2625-2647. doi:https://doi.org/10.1029/JB075i014p02625

Dewey, J. F., Holdsworth, R. E., & Strachan, R. A. (1998). Transpression and transtension zones. In R. E. Holdworth, R. A. Strachan, & J. F. Dewey (Eds.), *Continental Transpressional and Transtensional Tectonics* (Vol. 135, pp. 1-14): Geological Society, London, Special Publications.

Dickinson, W. R. (2004). Evolution of the North American cordillera. *Annual Reviwe of Earth and Planetary Sciences, 32*, 13-45. doi:https://doi.org/10.1146/annurev.earth.32.101802.120257

Dickinson, W. R., & Snyder, W. S. (1978). Plate tectonics of the Laramide orogeny. In V. W. Matthews (Ed.), *Laramide folding associated with block faulting in the Western United States* (Vol. 151, pp. 355-366): Geoloical Society of America Memoir.

Diehl, T., Singer, J., Hetényi, G., Grujic, D., Clinton, J., Giardini, D., Kissling,E., GANSSER Working Group. (2017). Seismotectonics of Bhutan: Evidence for segmentation of the Eastern Himalayas and link to foreland deformation. *Earth and Planetary Science Letters, 471*, 54-65. doi:https://doi.org/10.1016/j.epsl.2017.04.038

Dini, A., Westerman, D., Innocenti, F., & Rocchi, S. (2008). Magma emplacement in a transfer zone: the Miocene mafic Orano dyke swarm of Elba Island, Tuscany, Italy. *Geological Society, London, Special Publications, 302*(1), 131-148. doi:https://doi.org/10.1144/SP302.10

Divyadarshini, A. a. S., Vi. (2019). Investigating topographic metrics to decipher structural model and morphotectonic evolution of the Frontal Siwalik Ranges, Central Himalaya, Nepal. *Geomorphology, 337*, 31-52. doi:10.1016/j.geomorph.2019.03.028

Domeier, M. (2016). A plate tectonic scenario for the Iapetus and Rheic oceans. *Gondwana Research, 36*, 275-295. doi:https://doi.org/10.1016/j.gr.2015.08.003

Doutsos, T., Koukouvelas, I., & Xypolias, P. (2006). A new orogenic model for the External Hellenides. In A. H. F. Robertson & D. Mountrakis (Eds.), *Tectonic development of the Eastern Mediterranean Region* (Vol. 260, pp. 507-520): Geological Society, London, Special Publications.

Drahovzal, J. A., & Thomas, W. A. (1976). *Cross-strike structural discontinuities in the Appalachians of Alabama: Geological Society of America Abstracts with Programs* (Vol. 8).

Drake, A. A. J., Sinha, A. K., Larid, J., & Guy, R. E. (1989). The Taconian Orogen. In R. D. Hatcher Jr, W. A. Thomas, & G. W. Viele (Eds.), *The Appalachian-Ouachita Orogen in the United States, The Geology of North America* (Vol. F-2, pp. 101-177): Geological Society of America.

Drukpa, D., Velasco, A.A., Doser, D. (2006). Seismicity in the Kingdom of Bhutan (1937–2003): Evidence for crustal transcurrent deformation. *Journal of Geophysical Research, 111*, B06301. doi:https://doi/org/10.1029/2004JB003087

Dubey, A. K., Mishra, R and Bhakuni, S.S. (2001). Erratic shortening from balanced cross sections of the western Himalayan foreland basin causes and implications for basin evolution. *Journal of Asian Earth Sciences*, *19*, 765-777. doi:https://doi.org/10.1016/S1367-9120(01)00010-4

Duncan, C., Masek, J., & Fielding, E. (2003). How steep are the Himalaya? Characteristics and implications of along-strike topographic variations. *Geology, 31*(1), 75-78. doi:https://doi.org/10.1130/0091-7613(2003)031<0075:HSATHC>2.0.CO;2

Dunkl, I., Kuhlemann, J., Reinecker, J., & Frisch, W. (2005). Cenozoic relief evolution of the Eastern Alps—constraints from apatite fission track age-provenance of Neogene intramontane sediments. *Austrian Journal of Earth Sciences, 98*, 92-105.

Duvall, M. J., Waldron, J.W.F., Godin, L., Najman, Y. (2020). Active strike-slip faults and an outer frontal thrust in the Himalayan foreland basin. *Proceedings of the National Academy of Sciences, 117*(30), 17615-17621. doi:https://doi.org/10.1073/pnas.2001979117

Edey, A., Allen, M., & Nilfouroushan, F. (2020). Kinematic variation within the Fars Arc, eastern Zagros, and the development of fold-and-thrust belt curvature. *Tectonics, 39*(8), e2019TC005941. doi:https://doi.org/10.1029/2019TC005941

Egbue, O., & Kellogg, J. (2010). Pleistocene to present North Andean "escape". *Tectonophysics, 489*(1-4), 248-257. doi:https://doi.org/10.1016/j.tecto.2010.04.021

Elliott, D. (1976). The motion of thrust sheets. *Journal of Geophysical Research, 81*(5), 949-963. doi:https://doi.org/10.1029/JB081i005p00949

Elter, F. M., Piero, E., Claudio, E., Elena, E., Katharina, K. R., Matteo, P., & Stefano, S. (2011). Strike-slip geometry inferred from the seismicity of the Northern-Central Apennines (Italy). *Journal of Geodynamics, 52*(5), 379-388. doi:https://doi.org/10.1016/j.jog.2011.03.003

Eugster, P., Thiede, R.C., Scherler, D., Stubner, K., Sobel, E.R., Strecker, M.R. (2018). Segmentation of the Main Himalayan Thrust Revealed by Low-Temperature Thermochronometry in the Western Indian Himalaya. *Tectonics, 37*, 2710-2726. doi:https://doi.org/10.1029/2017TC004752

Fakhari, M. D., Axen, G. J., Horton, B. K., Hassanzadeh, J., & Amini, A. (2008). Revised age of proximal deposits in the Zagros foreland basin and implications for Cenozoic evolution of the High Zagros. *Tectonophysics, 451*(1-4), 170-185. doi:https://doi.org/10.1016/j.tecto.2007.11.064

Falcon, N. L. (1974). Southern Iran: Zagros Mountains. *Geological Society, London, Special Publications, 4*(1), 199-211. doi:https://doi.org/10.1144/GSL.SP.2005.004.01.11

Farzipour-Saein, A., Nilfouroushan, F., & Koyi, H. (2013). The effect of basement step/topography on the geometry of the Zagros fold and thrust belt (SW Iran): an analog modeling approach. *International Journal of Earth Sciences*, *102*(8), 2117-2135. doi:https://doi.org/10.1007/s00531-013-0921-5

Fermor, P. (1999). Aspects of the three-dimensional structure of the Alberta Foothills and Front Ranges. *GSA bulletin, 111*(3), 317-346. doi:https://doi.org/10.1130/0016-7606(1999)111<0317:AOTTDS>2.3.CO;2

Festa, A., Balestro, G., Borghi, A., De Caroli, S., & Succo, A. (2020). The role of structural inheritance in continental break-up and exhumation of Alpine Tethyan mantle (Canavese Zone, Western Alps). *Geoscience Frontiers, 11*(1), 167-188. doi:https://doi.org/10.1016/j.gsf.2018.11.007

Fiigenschuh, B., Seward, D., & Mancktelow, N. (1997). Exhumation in a convergent orogen: the western Tauern window. *Terra nova, 9*(5-6), 213-217. doi:https://doi.org/10.1111/j.1365-3121.1997.tb00015.x

Folguera, A., Ramos, V. A., Hermanns, R. L., & Naranjo, J. (2004). Neotectonics in the foothills of the southernmost central Andes (37–38 S): Evidence of strike-slip displacement along the Antiñir-Copahue fault zone. *Tectonics, 23*(5). doi:https://doi.org/10.1029/2003TC001533

Fondriest, M., Aretusini, S., Di Toro, G., & Smith, S. A. (2015). Fracturing and rock pulverization along an exhumed seismogenic fault zone in dolostones: The Foiana Fault Zone (Southern Alps, Italy). *Tectonophysics, 654*, 56-74. doi:http://dx.doi.org/10.1016/j.tecto.2015.04.015

Foo, W. K. (1979). *Evolution of transverse structures linking the Purcell Anticlinorium to the western Rocky Mountains near Canal Flats, British Columbia.* (MSc). Queen's University, Kingston,

Foster, D. A., Doughty, P. T., Kalakay, T. J., Fanning, C. M., Coyner, S., Grice, W. C., & Vogl, J. (2007). Kinematics and timing of exhumation of metamorphic core complexes along the Lewis and Clark fault zone, northern Rocky Mountains, USA. *Special Papers-Geological Society of America, 434*, 207. doi:https://doi.org/10.1130/2007.2434(10)

Foster, D. A., Mueller, P. A., Mogk, D. W., Wooden, J. L., & Vogl, J. J. (2006). Proterozoic evolution of the western margin of the Wyoming craton: Implications for the tectonic and magmatic evolution of the northern Rocky Mountains. *Canadian Journal of Earth Sciences, 43*(10), 1601-1619. doi:https://doi.org/10.1139/E06-052

Frisch, W., Kuhlemann, J., Dunkl, I., & Brügel, A. (1998). Palinspastic reconstruction and topographic evolution of the Eastern Alps during late Tertiary tectonic extrusion. *Tectonophysics, 297*(1-4), 1-15. doi:https://doi.org/10.1016/S0040-1951(98)00160-7

Gaetani, M., Gianotti, R., Jadoul, F., Ciarapica, G., & Cirilli, S. (1986). Carbonifero superiore, Permiano et Triassico nell'area Lariana. *Memorie della Società Geologica Italiana, 32*, 5-

48. doi:http://pascal-francis.inist.fr/vibad/index.php?action=getRecordDetail&idt=7204188

Galliski, M., & Viramonte, J. (1988). The Cretaceous paleorift in northwestern Argentina: a petrologic approach. *Journal of South American earth sciences, 1*(4), 329-342. doi:https://doi.org/10.1016/0895-9811(88)90021-1

Gansser, A. (1964). *Geology of the Himalayas*. New York: Wiley Interscience.

Gaupp, R., & Batten, D. (1983). Depositional setting of middle to Upper Cretaceous sediments in the Northern Calcareous Alps from palynological evidence. *Neues Jahrbuch für Geologie und Paläontologie-Monatshefte*, 585-600. doi:https://doi.org/10.1127/njgpm/1983/1983/585

Ghiglione, M. C., Suarez, F., Ambrosio, A., Da Poian, G., Cristallini, E. O., Pizzio, M. F., & Reinoso, R. M. (2009). Structure and evolution of the Austral Basin fold-thrust belt, southern Patagonian Andes. *Revista de la Asociación Geológica Argentina, 65*(1), 215-226.

Giambiagi, L., Mescua, J., Bechis, F., Tassara, A., & Hoke, G. (2012). Thrust belts of the southern Central Andes: Along-strike variations in shortening, topography, crustal geometry, and denudation. *Bulletin, 124*(7-8), 1339-1351. doi:https://doi.org/10.1130/B30609.1

Gifford, J. N., Mueller, P. A., Foster, D. A., & Mogk, D. W. (2014). Precambrian crustal evolution in the Great Falls tectonic zone: Insights from xenoliths from the Montana Alkali Province. *The Journal of Geology, 122*(5), 531-548. doi:https://doi.org/10.1086/677262

Gillis, R. J., Horton, B. K., & Grove, M. (2006). Thermochronology, geochronology, and upper crustal structure of the Cordillera Real: Implications for Cenozoic exhumation of the central Andean plateau. *Tectonics*, *25*(6). doi:https://doi.org/10.1029/2005TC001887

Godin, L., & Harris, L. B. (2014). Tracking basement cross-strike discontinuities in the Indian crust beneath the Himalayan orogen using gravity data – relationship to upper crustal faults. *Geophysical Journal International, 198*, 198-215. doi:https://doi.org/10.1093/gji/ggu131

Goldfinger, C., Kulm, L.D., Yeats, R.S., McNeill, L., and Hummon, C. (1997). Oblique strike-slip faulting of the central Cascadia submarine forearc. *Journal of Geophysical Research, 102*(B4), 8217-8243. doi:https://doi.org/10.1029/96JB02655

Graindorge, D., Klingelhoefer, F., Sibuiet, J.C., McNeill, L., Henstock, T., Dean, S., Gutscher, M., Dessa, J.X., Permana, H., and 15 others. (2008). Impact of lower plate structure on upper plate deformation at the NW Sumatran convergent margin from seafloor morphology. *Earth and Planetary Science Letters, 275*, 201-210. doi:https://doi.org/10.1016/j.epsl.2008.04.053

Grosjean, G., Sue, C., & Burkhard, M. (2004). Late Neogene extension in the vicinity of the Simplon fault zone (central Alps, Switzerland). *Eclogae Geologicae Helvetiae, 97*(1), 33-46. doi:https://doi.org/10.1007/s00015-004-1114-9

Grujic, D., Hollister, L.S., and Parrish, R.P. (2002). Himalayan metamorphic sequence as an orogenic channel: Insight from Bhutan. *Earth and Planetary Science Letters, 198*, 177-191. doi:https://doi.org/10.1016S0012-821X(02)00482-X.

Guillot, S., Mahéo, G., De Sigoyer, J., Hattori, K., & Pecher, A. (2008). Tethyan and Indian subduction viewed from the Himalayan high-to ultrahigh-pressure metamorphic rocks. *Tectonophysics, 451*(1-4), 225-241. doi:https://doi.org/10.1016/j.tecto.2007.11.059

Gutscher, M. A., Spakman, W., Bijwaard, H., & Engdahl, E. R. (2000). Geodynamics of flat subduction: Seismicity and tomographic constraints from the Andean margin. *Tectonics, 19*(5), 814-833. doi:https://doi.org/10.1029/1999TC001152

Handy, M. R., Schmid, S. M., Bousquet, R., Kissling, E., & Bernoulli, D. (2010). Reconciling plate-tectonic reconstructions of Alpine Tethys with the geological–geophysical record of spreading and subduction in the Alps. *Earth-Science Reviews, 102*(3-4), 121-158. doi:https://doi.org/10.1007/s00531-014-1060-3

Harrison, J., & Bally, A. (1988). Cross-sections of the Parry Islands fold belt on Melville Island, Canadian Arctic Islands: Implications for the timing and kinematic history of some thin-skinned decollement systems. *Bulletin of Canadian Petroleum Geology, 36*(3), 311-332.

Harrison, J. E., Griggs, A. B., & Wells, J. D. (1974). *Tectonic features of the Precambrian Belt basin and their influcence on post-Belt structures* (Vol. 886): United States Geological Survey Professional Paper.

Harvey, J. E., Burbank, D.W., Bookhagen, B. (2015). Along-strike changes in Himalayan thrust geometry: Topographic and tectonic discontinuities in western Nepal. *Lithosphere, 7*(5), 511-518. doi:https://doi.org/10.1130/L444.1

Hatcher, J. R. D. (1972). Developmental model for the southern Appalachians. *Geological Society of America Bulletin, 83*(9), 2735-2760.

Hatcher, J. R. D. (2010). The Appalachian orogen: A brief summary. In R. P. Tollo, M. J. Bartholomew, J. P. Hibbard, & P. M. Karabinos (Eds.), *From Rodinia to Pangea: The Lithotectonic Record of the Appalachian Region: Geological Society of America Memoir 206* (pp. 1-19).

Hatcher, J. R. D., Thomas, W. A., Geiser, P. A., Snoke, A. W., Mosher, S., & Wiltschko, D. V. (1989). Alleghanian orogen. In R. D. Hatcher Jr, W. A. Thomas, & G. W. Viele (Eds.), *The Appalachian-Ouachita Orogen in the United States, The Geology of North America* (Vol. F-2, pp. 233-319): Geological Society of America.

Hauck, M. L., Nelson, K.D., Brown, L.D., Wenjin, Z., and Ross, A.R. (1998). Crustal structure of the Himalayan orogen at ~90° east longitude from Project INDEPTH deep reflection profiles. *Tectonics, 17,* 481-500. doi:https://doi.org/10.1029/98TC01314

Haynes, S. J., & McQuillan, H. (1974). Evolution of the Zagros suture zone, southern Iran. *Geological Society of America Bulletin, 85*(5), 739-744. doi:https://doi.org/10.1130/0016-7606(1974)85<739:EOTZSZ>2.0.CO;2

Haynes, S. J., & Reynolds, P. (1980). Early development of Tethys and Jurassic ophiolite displacement. *Nature, 283*(5747), 561-563. doi:https://doi.org/10.1038/283561a0

Hessami, K., Koyi, H. A., & Talbot, C. J. (2001). The significance of strike-slip faulting in the basement of the Zagros fold and thrust belt. *Journal of petroleum Geology, 24*(1), 5-28. doi:https://doi.org/10.1111/j.1747-5457.2001.tb00659.x

Hibbard, J. P., van Staal, C. R., Rankin, D. W., & Williams, H. (2006). *Lithotectonic map of the Appalachian orogen, Canada–United States of America, Geological Survey of Canada, Map 2096A, scale 1:1,500,000*.

Hill, K. C., Kendrick, R. D., Crowhurst, P. V., & Gow, P. A. (2002). Copper-gold mineralisation in New Guinea: Tectonics, lineaments, thermochronology and structure. *Australian Journal of Earth Sciences, 49*(4), 737-752. doi:https://doi.org/10.1046/j.1440-0952.2002.00944.x

Hodges, K. V. (2000). Tectonics of the Himalaya and southern Tibet from two perspectives. *Geological Society of America Bulletin, 112*(3), 324-350. doi:https://doi.org/10.1130/0016-7606(2000)112<324:TOTHAS>2.0.CO;2

Hoffman, P. F. (1988). Early Proterozoic Assembly. *Annual Review of Earth and Planetary Sciences, 6*, 543-603. doi:https://doi.org/10.1146/annurev.ea.16.050188.002551

Hofmann, F., Schlatter, R., & Weh, M. (2000). Erläuterungen zu Blatt 97: Beggingen (LK 1011) des Geologischen Atlas der Schweiz 1: 25,000. *Bundesamt für Wasser und Geologie, Bern*, 113.

Hogan, J. P., & Gilbert, M. C. (1998). The Southern Oklahoma aulacogen: A Cambrian analog for Mid-Proterozoic AMCG (anorthosite-mangerite-charnockite-granite) complexes? In H. J.P. & G. M.C (Eds.), *Basement tectonics 12. Proceedings of the International Conferences on Basement Tectonics* (Vol. 6, pp. 39-78): Springer.

Hope, J., & Eaton, D. (2002). Crustal structure beneath the Western Canada Sedimentary Basin: constraints from gravity and magnetic modelling. *Canadian Journal of Earth Sciences, 39*(3), 291-312. doi:https://doi.org/10.1139/e01-060

Horváth, F., & Cloetingh, S. A. P. L. (1996). Stress-induced late stage subsidence anomalies in the Pannonian Basin. *Tectonophysics, 266*, 287-300.

Höy, T., & Heyden, P. v. d. (1988). Geochemistry, geochronology, and tectonic implications of two quartz monzonite intrusions, Purcell Mountains, southeastern British Columbia. *Canadian Journal of Earth Sciences, 25*(1), 106-115. doi:https://doi.org/10.1139/e88-011

Hubbard, J., Almeida, R., Foster, A., Sapkota, S. N., Burgi, P., & Tapponnier, P. (2016). Structural segmentation controlled the 2015 MW 7.8 Gorkha earthquake rupture in Nepal. *Geology, 44*(8), 639-642. doi:https://doi.org/10.1130/G38077.1

Hubbard, M., Gajurel, A. P., Mukul, M., & Seifert, N. (2018). *Cross faults and their role in Himalayan Structural Evolution*. Paper presented at the Geological Society of America Abstracts with Programs.

Hubbard, M., Mukul, M., Gajurel, A. P., Ghosh, A., Srivastava, V., Giri, B., Seifert, N., & Mendoza, M. M. (2021). Orogenic Segmentation and Its Role in Himalayan Mountain Building. *Frontiers in Earth Science*, *9*(259). doi:https://doi.org/10.3389/feart.2021.641666

Hubbard, M. S. (1999). Norumbega fault zone: part of an orogen-parallel strike-slip system, northern Appalachians. In A. Ludman & D. P. J. West (Eds.), *Normumberga Fault System of the Northern Appalachians* (Vol. 331, pp. 155-166). Boulder, Colorado: Geological Society of America Special Paper.

Hubbard, M. S., & Mancktelow, N. S. (1992). Lateral displacement during Neogene convergence in the western and central Alps. *Geology, 20*(10), 943-946. doi:https://doi.org/10.1130/0091-7613(1992)020<0943:LDDNCI>2.3.CO;2

Hunziker, J. C., Frey, M., Clauer, N., Dallmeyer, R. D., Friedrichsen, H., Flehmig, W., Hochstrasser, K., Roggwiler, P. T., & Schwander, H. (1986). The evolution of illite to muscovite: mineralogical and isotopic data from the Glarus Alps, Switzerland. *Contributions to Mineralogy and Petrology, 92*(2), 157-180. doi:https://doi.org/10.1007/BF00375291

Husseini, M. I. (1988). The Arabian infracambrian extensional system. *Tectonophysics, 148*(1-2), 93-103. doi:https://doi.org/10.1016/0040-1951(88)90163-1

Hyndman, D. W., Alt, D., & Sears, J. W. (1988). Post-Archean metamorphic and tectonic evolution of western Montana and northern Idaho. In W. G. Ernst (Ed.), *Metamorphism and crustal evolution of the western United States* (Vol. 7, pp. 332-361). Englewood Cliffs, New Jersey: Prentice Hall.

Hynes, A., & Rivers, T. (2010). Protracted continental collision—Evidence from the Grenville orogen. *Canadian Journal of Earth Sciences, 47*(5), 591-620. doi:https://doi.org/10.1139/E10-003

Isacks, B. L. (1988). Uplift of the central Andean plateau and bending of the Bolivian orocline. *Journal of Geophysical Research: Solid Earth, 93*(B4), 3211-3231. doi:https://doi.org/10.1029/ JB093iB04p03211

Jackson, J. A. (1980). Reactivation of basement faults and crustal shortening in orogenic belts. *Nature, 283*(5745), 343-346. doi:https://doi.org/10.1038/283343a0

Jadoon, I. A. K., Lawrence, R. D., & Lillie, R. J. (1994). Seismic data, geometry, evolution, and shortening in the active Sulaiman fold-and-thrust belt of Pakistan, southwest of the Himalayas. *AAPG Bulletin, 78*(5), 758-774. doi:https://doi.org/10.1306/A25FE3AB-171B-11D7-8645000102C1865D

Japas, M. S., Ré, G. H., Oriolo, S., & Vilas, J. F. (2016). Basement-involved deformation overprinting thin-skinned deformation in the Pampean flat-slab segment of the southern Central Andes, Argentina. *Geological Magazine, 153*(5-6), 1042-1065. doi:https://doi.org/10.1017/S001675681600056X

Jessup, M. J., Newell, D. L., Cottle, J. M., Berger, A. L., & Spotila, J. A. (2008). Orogen-parallel extension and exhumation enhanced by denudation in the trans-Himalayan Arun River gorge, Ama Drime Massif, Tibet-Nepal. *Geology, 36*(7), 587-590. doi:https://doi.org/10.1130/g24722a.1

Jordan, T. E., Isacks, B., Ramos, V. A., & Allmendinger, R. W. (1983). Mountain building in the Central Andes. *Episodes, 3*(3), 20-26.

Joudaki, M., Farzipour-Saein, A., & Nilfouroushan, F. (2016). Kinematics and surface fracture pattern of the Anaran basement fault zone in NW of the Zagros fold–thrust belt. *International Journal of Earth Sciences, 105*(3), 869-883. doi:https://doi.org/10.1007/s00531-015-1209-8

Karlstrom, K. E., & Houston, R. S. (1984). The Cheyenne belt: Analysis of a Proterozoic suture in southern Wyoming. *Precambrian Research, 25*(4), 415-446. doi:https://doi.org/10.1016/0301-9268(84)90012-3

Kendrick, E., Bevis, M., Smalley Jr, R., Brooks, B., Vargas, R. B., Lauría, E., & Fortes, L. P. S. (2003). The Nazca–South America Euler vector and its rate of change. *Journal of South American earth sciences, 16*(2), 125-131. doi:https://doi.org/10.1016/S0895-9811(03)00028-2

Kent, P. E. (1979). The emergent Hormuz salt plugs of southern Iran. *Journal of petroleum Geology, 2*(2), 117-144. doi:https://doi.org/10.1111/j.1747-5457.1979.tb00698.x

Keppie, J. D., & Krogh, T. E. (1999). U-Pb Geochronology of Devonian Granites in the Meguma Terrane of Nova Scotia, Canada: Evidence for Hotspot Melting of a Neoproterozoic Source. *The Journal of Geology, 107*(5), 555-568. doi:10.1086/314369

Khadivi, S., Mouthereau, F., Larrasoaña, J. C., Vergés, J., Lacombe, O., Khademi, E., Beamud, E., Melinte-Dobrinescu, M., & Suc, J. P. (2010). Magnetochronology of synorogenic Miocene foreland sediments in the Fars arc of the Zagros Folded Belt (SW Iran). *Basin Research, 22*(6), 918-932. doi:https://doi.org/10.1111/j.1365-2117.2009.00446.x

Kley, J., Rossello, E. A., Monaldi, C. R., & Habighorst, B. (2005). Seismic and field evidence for selective inversion of Cretaceous normal faults, Salta rift, northwest Argentina. *Tectonophysics, 399*(1-4), 155-172. doi:https://doi.org/10.1016/j.tecto.2004.12.020

Kokkalas, S., & Doutsos, T. (2004). Kinematics and strain partitioning in the southeast Hellenides (Greece). *Geological Journal, 39*(2), 121-140. doi:https://doi.org/10.1002/gj.947

Koop, W. J., & Stoneley, R. (1982). Subsidence history of the Middle East Zagros basin, Permian to recent. *Philosophical Transactions of the Royal Society A Mathematical and Physical Sciences, 305*(1489), 149-168. doi:https://doi.org/10.1098/rsta.1982.0031

Kralik, M., Klima, K., & Riedmüller, G. (1987). Dating fault gouges. *Nature, 327*(6120), 315-317. doi:https://doi.org/10.1038/327315a0

Kuiper, Y. D. (2016). Development of the Norumbega fault system in mid-Paleozoic New England, USA: An integrated subducted oceanic ridge model. *Geology, 44*(6), 455-458. doi:https://doi.org/10.1130/G37599.1

Kuiper, Y. D., & Wakabayashi, J. (2018). A comparison between mid-Paleozoic New England, USA, and the modern western USA: Subduction of an oceanic ridge-transform fault system. *Tectonophysics, 745*, 278-292. doi:https://doi.org/10.1016/j.tecto.2018.08.020

Kwon, S., & Mitra, G. (2004). Strain distribution, strain history, and kinematic evolution associated with the formation of arcuate salients in fold-thrust belts: The example of the Provo salient, Sevier orogen, Utah. In A. J. Sussman & A. B. Weil (Eds.), *Orogenic Curvature: Integrating Paleomagnetic and Structural Analyses* (Vol. 383, pp. 205-223): Geological Society of America Special Paper.

Kwon, S., & Mitra, G. (2006). Three-dimensional kinematic history at an oblique ramp, Leamington zone, Sevier belt, Utah. *Journal of Structural Geology, 28*(3), 474-493. doi:https://doi.org/10.1016/j.jsg.2005.12.011

Lacombe, O., Mouthereau, F., Angelier, J., & Deffontaines, B. (2001). Structural, geodetic and seismological evidence for tectonic escape in SW Taiwan. *Tectonophysics, 333*(1-2), 323-345. doi:https://doi.org/10.1016/S0040-1951(00)00281-X

Lacombe, O., Mouthereau, F., Kargar, S., & Meyer, B. (2006). Late Cenozoic and modern stress fields in the western Fars (Iran): implications for the tectonic and kinematic evolution of central Zagros. *Tectonics, 25*(1), 1-27. doi:https://doi.org/10.1029/2005TC001831

Larson, K. P., Cottle, J.M. (2014). Midcrustal discontinuities and the assembly of the Himalayan midcrust. *Tectonics, 33*, 718-740. doi:https://doi.org/10.1002/2013TC003452

Larson, K. P., Price, R. A., & Archibald, D. A. (2006). Tectonic implications of 40Ar/39Ar muscovite dates from the Mt. Haley stock and Lussier River stock, near Fort Steele, British Columbia. *Canadian Journal of Earth Sciences, 43*(11), 1673-1684. doi:https://doi.org/10.1139/E06-048

Laubscher, H. P. (1971). Das Alpen-Dinariden-Problem und die Palinspastik der südlichen tethys. *Geologische rundschau, 60*(3), 813-833. doi:https://doi.org/10.1007/BF02046522

Laubscher, H. P. (1985). Large-scale, thin-skinned thrusting in the southern Alps: Kinematic models. *Geological Society of America Bulletin, 96*(6), 710-718. doi:https://doi.org/10.1130/0016-7606(1985)96<710:LTTITS>2.0.CO;2

Lawton, T. F., Sprinkel, D. A., Decelles, P. G., Mitra, G., Sussman, A. J., & Weiss, M. P. (1997). Stratigraphy and structure of the Sevier thrust belt and proximal foreland-basin system in central Utah: A transect from the Sevier Desert to the Wasatch Plateau. In K. P. Link & B. J. Kowallis (Eds.), *Brigham Young University Geology Studies Field Trip Guide Book, Part 2* (Vol. 42, pp. 33-68): Geological Society of America Annual Meeting.

Le Garzic, E., Vergés, J., Sapin, F., Saura, E., Meresse, F., & Ringenbach, J. (2019). Evolution of the NW Zagros Fold-and-Thrust Belt in Kurdistan Region of Iraq from balanced and restored crustal-scale sections and forward modeling. *Journal of Structural Geology, 124*, 51-69. doi:https://doi.org/10.1016/j.jsg.2019.04.006

Leier, A., McQuarrie, N., Garzione, C., & Eiler, J. (2013). Stable isotope evidence for multiple pulses of rapid surface uplift in the Central Andes, Bolivia. *Earth and Planetary Science Letters, 371*, 49-58. doi:https://doi.org/10.1016/j.epsl.2013.04.025

Lemieux, S., Ross, G. M., & Cook, F. A. (2000). Crustal geometry and tectonic evolution of the Archean crystalline basement beneath the southern Alberta Plains, from new seismic reflection and potential-field studies. *Canadian Journal of Earth Sciences, 37*(11), 1473-1491. doi:https://doi.org/10.1139/e00-065

Li, Z. X., Bogdanova, S. V., Collins, A. S., Davidson, A., De Waele, B., Ernst, R. E., Fitzsimons, I. C. W., Fuck, R. A., Gladkochub, D. P., Jacobs, J., Karlstrom, K. E., Lu, S., Natapov, L. M., Pease, V., Pisarevsky, S. A., Thrane, K., & Vernikovsky, V. (2008). Assembly, configuration, and break-up history of Rodinia: A synthesis. *Precambrian Research, 160*(1), 179-210. doi:https://doi.org/10.1016/j.precamres.2007.04.021

Likerman, J., Burlando, J. F., Cristallini, E. O., & Ghiglione, M. C. (2013). Along-strike structural variations in the Southern Patagonian Andes: insights from physical modeling. *Tectonophysics, 590*, 106-120. doi:https://doi.org/10.1016/j.tecto.2013.01.018

Lin, S., Staal, C. R. v., & Dubé, B. t. (1994). Promontory-promontory collision in the Canadian Appalachians. *Geology, 22*(10), 897-900. doi:https://doi.org/10.1130/0091-7613(1994)022<0897:PPCITC>2.3.CO;2

Linzer, H.-G., Ratschbacher, L., & Frisch, W. (1995). Transpressional collision structures in the upper crust: the fold-thrust belt of the Northern Calcareous Alps. *Tectonophysics, 242*(1-2), 41-61. doi:https://doi.org/10.1016/0040-1951(94)00152-Y

Llambías, E. J., Kleinman, L. E., & Salvarradi, J. A. (1993). El magmatismo Gondwánico. In V. Ramos (Ed.), *Rela- torio Geología y Recursos Naturales de Mendoza* (Vol. 1, pp. 53-64). Buenos Aires: Servicio Geológico Minero Argentino (SEGEMAR).

Long, S., McQuarrie, N., Tobgay, T., Grujic, D. (2011). Geometry and crustal shortening of the Himalayan fold-thrust belt, eastern and central Bhutan. *Geological Society of America Bulletin, 123*(7/8), 1427-1447. doi:https://doi.org/10.1130/B30203.1

Lupi, M., Trippanera, D., Gonzalez, D., D'amico, S., Acocella, V., Cabello, C., Stef, M. M., & Tassara, A. (2020). Transient tectonic regimes imposed by megathrust earthquakes and the growth of NW-trending volcanic systems in the Southern Andes. *Tectonophysics, 774*, 228204. doi:https://doi.org/10.1016/j.tecto.2019.228204

Mahoney, L., Hill, K., McLaren, S., & Hanani, A. (2017). Complex fold and thrust belt structural styles: Examples from the Greater Juha area of the Papuan Fold and Thrust Belt, Papua New Guinea. *Journal of Structural Geology, 100*, 98-119. doi:https://doi.org/10.1016/j.jsg.2017.05.010

Malekzade, Z., Bellier, O., Abbassi, M. R., Shabanian, E., & Authemayou, C. (2016). The effects of plate margin inhomogeneity on the deformation pattern within west-Central Zagros Fold-and-Thrust Belt. *Tectonophysics, 693*, 304-326. doi:http://dx.doi.org/10.1016/j.tecto.2016.01.030

Malusà, M. G. (2004). *Post-metamorphic evolution of the Western Alps: kinematic constraints from a multidisciplinary approach.* (PhD). University of Turin, Turin, Italy.

Mancktelow, N., Zwingmann, H., Campani, M., Fügenschuh, B., & Mulch, A. (2015). Timing and conditions of brittle faulting on the Silltal-Brenner fault zone, Eastern Alps (Austria). *Swiss Journal of Geosciences, 108*(2-3), 305-326. doi:https://doi.org/10.1007/s00015-015-0179-y

Mancktelow, N. S. (1992). Neogene lateral extension during convergence in the Central Alps: evidence from interrelated faulting and backfolding around the Simplonpass (Switzerland). *Tectonophysics, 215*(3-4), 295-317. doi:https://doi.org/10.1016/0040-1951(92)90358-D

Mancktelow, N. S., Stöckli, D. F., Grollimund, B., Müller, W., Fügenschuh, B., Viola, G., Seward, D., & Villa, I. M. (2001). The DAV and Periadriatic fault systems in the Eastern

Alps south of the Tauern window. *International Journal of Earth Sciences, 90*(3), 593-622. doi:https://doi.org/10.1007/s005310000190

Manea, V. C., Pérez-Gussinyé, M., & Manea, M. (2012). Chilean flat slab subduction controlled by overriding plate thickness and trench rollback. *Geology, 40*(1), 35-38. doi:10.1130/g32543.1

Marshak, S., & Wilkerson, M. S. (1992). Effect of overburden thickness on thrust belt geometry and development. *Tectonics, 11*(3), 560-566. doi:https://doi.org/10.1029/92TC00175

McGugan, A. (1987). "Horses" and transverse faults in the Lewis thrust sheet, Elk range, Kananaskis valley, Rocky mountain front ranges, Southwestern Alberta. *Bulletin of Canadian Petroleum Geology, 35*(3), 358-361. doi:https://doi.org/10.35767/gscpgbull.35.3.358

McMechan, M. (2001). Large-scale duplex structures in the McConnell thrust sheet, Rocky Mountains, Southwest Alberta. *Bulletin of Canadian Petroleum Geology, 49*(3), 408-425. doi:https://doi.org/10.2113/49.3.408

McMechan, M. (2007). Nature, origin and tectonic significance of anomalous transverse structures, southeastern Skeena Fold Belt, British Columbia. *Bulletin of Canadian Petroleum Geology, 55*(4), 262-274. doi:https://doi.org/10.2113/gscpgbull.55.4.262

McMechan, M. E. (2000). Walker Creek fault zone, central Rocky Mountains, British Columbia—southern continuation of the Northern Rocky Mountain Trench fault zone. *Canadian Journal of Earth Sciences, 37*(9), 1259-1273. doi:https://doi.org/10.1139/e00-038

McMechan, M. E. (2012). Deep transverse basement structural control of mineral systems in the southeastern Canadian Cordillera. *Canadian Journal of Earth Sciences, 49*(5), 693-708. doi:https://doi.org/10.1139/E2012-013

McMechan, M. E., & Price, R. A. (1982). Transverse folding and superposed deformation, Mount Fisher area, southern Canadian Rocky Mountain thrust and fold belt. *Canadian Journal of Earth Sciences, 19*(5), 1011-1024. doi:https://doi.org/10.1139/e82-084

McQuarrie, N. (2004). Crustal scale geometry of the Zagros fold–thrust belt, Iran. *Journal of Structural Geology, 26*(3), 519-535. doi:https://doi.org/10.1016/j.jsg.2003.08.009

McQuarrie, N., Stock, J. M., Verdel, C., & Wernicke, B. P. (2003). Cenozoic evolution of Neotethys and implications for the causes of plate motions. *Geophysical Research Letters, 30*(20). doi: https://doi.org/10.1029/2003GL017992

McQuarrie, N., & van Hinsbergen, D. J. J. (2013). Retrodeforming the Arabia-Eurasia collision zone: Age of collision versus magnitude of continental subduction. *Geology, 41*(3), 315-318. doi:https://doi.org/10.1130/G33591.1

McQuillan, H. (1991). The role of basement tectonics in the control of sedimentary facies, structural patterns and salt plug emplacements in the Zagros fold belt of southwest Iran. *Journal of Southeast Asian Earth Sciences, 5*(1-4), 453-463. doi:https://doi.org/10.1016/0743-9547(91)90061-2

Mendoza, M. M., Ghosh, A., Karplus, M.S., Klemperer, S.L., Sapkota, S.N., Adhikari, L.B., Velasco, A. (2019). Duplex in the Main Himalayan Thrust illuminated by aftershocks of the 2015 Mw 7.8 Gorkha earthquake. *Nature geoscience, 12*, 1018-1022. doi:https://doi.org/10.1038/s41561-019-0474-8

Mescua, J. F., & Giambiagi, L. B. (2012). Fault inversion vs. new thrust generation: a case study in the Malargüe fold-and-thrust belt, Andes of Argentina. *Journal of Structural Geology, 35*, 51-63. doi:https://doi.org/10.1016/j.jsg.2011.11.011

Mitra, S. (1988). Three-dimensional geometry and kinematic evolution of the Pine Mountain thrust system, southern Appalachians. *Geological Society of America Bulletin, 100*(1), 72-95. doi:https://doi.org/10.1130/0016-7606(1988)100<0072:TDGAKE>2.3.CO;2

Moffat, I. W., & Spang, J. H. (1984). Origin of transverse faulting, Rocky Mountain Front Ranges, Canmore, Alberta. *Bulletin of Canadian Petroleum Geology, 32*(2), 147-161. doi:https://doi.org/10.35767/gscpgbull.32.2.147

Mogk, D. W., Mueller, P. A., & Wooden, J. L. (1992). The nature of Archean terrane boundaries: an example from the northern Wyoming Province. *Precambrian Research, 55*(1-4), 155-168. doi:https://doi.org/10.1016/0301-9268(92)90020-O

Monod, B., Dhont, D., & Hervouët, Y. (2010). Orogenic float of the Venezuelan Andes. *Tectonophysics, 490*(1-2), 123-135. doi:https://doi.org/10.1016/j.tecto.2010.04.036

Mouthereau, F., Deffontaines, B., Lacombe, O., & Angelier, J. (2002). Variations along the strike of the Taiwan thrust belt: Basement control on structural style, wedge geometry, and kinematics. In T. Byrne & C.-S. Liu (Eds.), *Geology and Geophysics of an Arc-Continent collision, Taiwan, Republic of China* (Vol. 358, pp. 35-58). Boulder, Colorado: Geological Society of America Special Paper.

Mouthereau, F., & Lacombe, O. (2006). Inversion of the Paleogene Chinese continental margin and thick-skinned deformation in the Western Foreland of Taiwan. *Journal of Structural Geology, 28*(11), 1977-1993. doi:https://doi.org/10.1016/j.jsg.2006.08.007

Mouthereau, F., Lacombe, O., & Vergés, J. (2012). Building the Zagros collisional orogen: timing, strain distribution and the dynamics of Arabia/Eurasia plate convergence. *Tectonophysics, 532*, 27-60. doi:https://doi.org/10.1016/j.tecto.2012.01.022

Mpodozis, C., & Ramos, V. (1989). The Andes of Chile and Argentina. In G. Ericksen, M. Cañas, & J. Reinemund (Eds.), *Geology of the Andes and its Relation to Hydrocarbon* *and Mineral Resources* (Vol. 11, pp. 59-90): Circum-Pacific Council for Energy and Mineral Resources.

Mueller, P. A., Heatherington, A. L., Kelly, D. M., Wooden, J. L., & Mogk, D. W. (2002). Paleoproterozoic crust within the Great Falls tectonic zone: Implications for the assembly of southern Laurentia. *Geology, 30*(2), 127-130. doi:https://doi.org/10.1130/0091-7613(2002)030<0127:PCWTGF>2.0.CO;2

Mugnier, J. L., Jouanne, F., Bhattarai, R., Cortes-Aranda, J., Gajurel, A., Leturmy, P., Robert, X., Upreti, B., & Vassallo, R. (2017). Segmentation of the Himalayan megathrust around the Gorkha earthquake (25 April 2015) in Nepal. *Journal of Asian Earth Sciences, 141*, 236-252. doi:https://doi.org/10.1016/j.jseaes.2017.01.015

Mugnier, J. L., Leturmy, P., Mascle, G., Huyghe, P., Chalaron, E., Vidal, G., Husson, L., & Delcaillau, B. (1999). The Siwaliks of western Nepal 1: Geometry and kinematics. *Journal of Asian Earth Sciences, 17*, 629-642. doi:https://doi.org/10.1016/S1367-9120(99)00038-3

Mukherjee, S., Talbot, C. J., & Koyi, H. A. (2010). Viscosity estimates of salt in the Hormuz and Namakdan salt diapirs, Persian Gulf. *Geological Magazine, 147*(4), 497-507. doi:https://doi/org/10.1017/S001675680999077X

Mukul, M. (2010). First-order kinematics of wedge-scale active Himalayan deformation: insights from Darjiling-Sikkim-Tibet (DaSiT) wedge. *Journal of Asian Earth Sciences, 39*, 645-657. doi:https://doi.org/10.1016/j.jseaes.2010.04.029

Mukul, M., Jade, S., Ansari, K., Matin, A, Joshi, V. (2018). Structural insights from geodetic Global Positioning System measurements in the Darjiling-Sikkim Himalaya. *Journal of Structural Geology, 114*, 346-356. doi:https://doi.org/10.1016/j.jsg.2018.03.007

Müller, W., Mancktelow, N. S., & Meier, M. (2000). Rb–Sr microchrons of synkinematic mica in mylonites: an example from the DAV fault of the Eastern Alps. *Earth and Planetary Science Letters, 180*(3-4), 385-397. doi:https://doi.org/10.1016/S0012-821X(00)00167-9

Müller, W., Prosser, G., Mancktelow, N. S., Villa, I. M., Kelley, S. P., Viola, G., & Oberli, F. (2001). Geochronological constraints on the evolution of the Periadriatic Fault System (Alps). *International Journal of Earth Sciences, 90*(3), 623-653. doi:https://doi.org/10.1007/s005310000187

Murphy, J. B., & Keppie, J. D. (2005). The Acadian Orogeny in the Northern Appalachians. *International Geology Review, 47*(7), 663-687. doi:https://doi.org/10.2747/0020-6814.47.7.663

Murphy, J. B., Waldron, J. W., Kontak, D. J., Pe-Piper, G., & Piper, D. J. (2011). Minas Fault Zone: Late Paleozoic history of an intra-continental orogenic transform fault in the

Canadian Appalachians. *Journal of Structural Geology, 33*(3), 312-328. doi:https://doi.org/10.1016/j.jsg.2010.11.012

Nabelek, J., G. Hetenyi, J. Vergne, S. Sapkota, B. Kafle, M. Jiang, H. Su, J. Chen, and B.-S. Huang, and the Hi-CLIMB Team. (2009). Underplating in the Himalaya-Tibet collision zone revealed by the Hi-CL IMB experiment. *Science, 325,* 1371-1374. doi:https://doi.org/10.1126/science.1167719

Norris, D. (2001). Slickenlines and the kinematics of the Crowsnest Deflection in the southern Rocky Mountains of Canada. *Journal of Structural Geology, 23*(6-7), 1089-1102. doi:https://doi.org/10.1016/S0191-8141(00)00180-2

O'Brien, T. M., & van der Pluijm, B. A. (2012). Timing of Iapetus Ocean rifting from Ar geochronology of pseudotachylytes in the St. Lawrence rift system of southern Quebec. *Geology, 40*(5), 443-446. doi:10.1130/g32691.1

O'Neill, J. M., & Lopez, D. A. (1985). Character and regional significance of Great Falls tectonic zone, east-central Idaho and west-central Montana. *AAPG Bulletin, 69*(3), 437-447. doi:https://doi.org/10.1306/AD462506-16F7-11D7-8645000102C1865D

Oldham, R. D. (1917). Structure of the Himalayas and Indo-Gangetic plains. *Memoir of the Geological Survey of India, 156*.

Oldow, J. S., Bally, A. W., Lallemant, H. G. A., & Leeman, W. P. (1989). Phanerozoic evolution of the North American Cordillera, United States and Canada. In A. W. Bally & A. R. Palmer (Eds.), *The geology of North America: an overview* (Vol. A, pp. 139-232): Geological Society of America, The Geology of North America.

Oriolo, S., Japas, M. S., Cristallini, E. O., & Giménez, M. (2014). Cross-strike structures controlling magmatism emplacement in a flat-slab setting (Precordillera, Central Andes of Argentina). *Geological Society, London, Special Publications, 394*(1), 113-127. doi:https://doi.org/10.1144/sp394.6

Oswald, P., Ortner, H., & Gruber, A. (2019). Deformation around a detached half-graben shoulder during nappe stacking (Northern Calcareous Alps, Austria). *Swiss Journal of Geosciences, 112*(1), 23-37. doi:https://doi.org/10.1007/s00015-018-0333-4

Pantet, A., Epard, J.-L., & Masson, H. (2020). Mimicking Alpine thrusts by passive deformation of synsedimentary normal faults: a record of the Jurassic extension of the European margin (Mont Fort nappe, Pennine Alps). *Swiss Journal of Geosciences, 113*(1), 13. doi:10.1186/s00015-020-00366-2

Pash, R. R., Sarkarinejad, K., Ghoochaninejad, H. Z., Motamedi, H., & Yazdani, M. (2020). Accommodation of the different structural styles in the foreland fold-and-thrust belts: northern Dezful Embayment in the Zagros belt, Iran. *International Journal of Earth Sciences*, 1-12. doi:https://doi.org/10.1007/s00531-020-01844-6

Paul, H., Mitra, S., Bhattacharya, S.N., Suresh, G. (2015). Active transverse faulting within underthrust Indian crust beneath the Sikkim Himalaya. *Geophysics Journal International, 201*(2), 1070-1081. doi:https://doi.org/10.1093/gji/ggv058

Paulsen, T., & Marshak, S. (1997). Structure of the Mount Raymond transverse zone at the southern end of the Wyoming salient, Sevier fold-thrust belt, Utah. *Tectonophysics, 280*(3-4), 199-211. doi:https://doi.org/10.1016/S0040-1951(97)00205-9

Paulsen, T., & Marshak, S. (1998). Charleston transverse zone, Wasatch Mountains, Utah: Structure of the Provo salient's northern margin, Sevier fold-thrust belt. *Geological Society of America Bulletin, 110*(4), 512-522. doi:https://doi.org/10.1130/0016-7606(1998)110<0512:CTZWMU>2.3.CO;2

Paulsen, T., & Marshak, S. (1999). Origin of the Uinta recess, Sevier fold–thrust belt, Utah: influence of basin architecture on fold–thrust belt geometry. *Tectonophysics, 312*(2-4), 203-216. doi:https://doi.org/10.1016/S0040-1951(99)00182-1

Perello, P., Delle Piane, L., Piana, F., Morelli, M., Damiano, A., & Venturini, G. (2004). New constraints on late to post-Oligocene deformation history of the Western Alps: data from Middle Susa valley and High Maurienne valley. *Abstract, 32nd IGC—Firenze, 247*.

Perez-Estaun, A., Alvarez-Marron, J., Brown, D., Puchkov, V., Gorozhanina, Y., & Baryshev, V. (1997). Along-strike structural variations in the foreland thrust and fold belt of the southern Urals. *Tectonophysics, 276*(1-4), 265-280. doi:https://doi.org/10.1016/S0040-1951(97)00060-7

Pérez-Flores, P., Cembrano, J., Sánchez-Alfaro, P., Veloso, E., Arancibia, G., & Roquer, T. (2016). Tectonics, magmatism and paleo-fluid distribution in a strike-slip setting: Insights from the northern termination of the Liquiñe–Ofqui fault System, Chile. *Tectonophysics, 680*, 192-210. doi:http://dx.doi.org/10.1016/j.tecto.2016.05.016

Perrone, G., Cadoppi, P., Tallone, S., & Balestro, G. (2011). Post-collisional tectonics in the Northern Cottian Alps (Italian Western Alps). *International Journal of Earth Sciences, 100*(6), 1349-1373. doi:https://doi.org/10.1007/s00531-010-0534-1

Petrinovic, I., Riller, U., Brod, J., Alvarado, G., & Arnosio, M. (2006). Bimodal volcanism in a tectonic transfer zone: evidence for tectonically controlled magmatism in the southern Central Andes, NW Argentina. *Journal of Volcanology and Geothermal Research, 152*(3-4), 240-252. doi:https://doi.org/10.1016/j.jvolgeores.2005.10.008

Pfiffner, O. A. (2014). *Geology of the Alps*: John Wiley & Sons.

Picotti, V., Casolari, E., Castellarin, A., Mosconi, A., Cairo, E., Pessina, C., & Sella, M. (1997). Structural evolution of the eastern Lombardian Prealps: Alpine inversion of a Mesozoic rifted margin. *Agip SpA, San Donato Milanese, 102*.

Pilger, R. H. J. (1981). Plate reconstructions, aseismic ridges, and low-angle subduction beneath the Andes. *GSA bulletin, 92*(7), 448-456. doi:10.1130/0016-7606(1981)92<448:Praral>2.0.Co;2

Pilkington, M., Miles, W., Ross, G., & Roest, W. (2000). Potential-field signatures of buried Precambrian basement in the Western Canada Sedimentary Basin. *Canadian Journal of Earth Sciences, 37*(11), 1453-1471. doi:https://doi.org/10.1139/e00-020

Piquer, J., Rivera, O., Yañez, G., & Oyarzun, N. (2020). The Piuquencillo Fault System: a long-lived, Andean-transverse fault system and its relationship with magmatic and hydrothermal activity. *Solid Earth Discussions*, 1-34. doi:https://doi.org/10.5194/se-2020-142

Pizzi, A., & Galadini, F. (2009). Pre-existing cross-structures and active fault segmentation in the northern-central Apennines (Italy). *Tectonophysics, 476*(1-2), 304-319. doi:https://doi.org/10.1016/j.tecto.2009.03.018

Plint, H. E., & Jamieson, R. A. (1989). Microstructure, metamorphism and tectonics of the western Cape Breton Highlands, Nova Scotia. *Journal of Metamorphic Geology, 7*(4), 407-424. doi:https://doi.org/10.1111/j.1525-1314.1989.tb00606.x

Polinski, R. K., & Eisbacher, G. H. (1992). Deformation partitioning during polyphase oblique convergence in the Karawanken Mountains, southeastern Alps. *Journal of Structural Geology, 14*(10), 1203-1213. doi:https://doi.org/10.1016/0191-8141(92)90070-D

Pomella, H., Stipp, M., & Fügenschuh, B. (2012). Thermochronological record of thrusting and strike-slip faulting along the Giudicarie fault system (Alps, Northern Italy). *Tectonophysics, 579*, 118-130. doi:https://doi.org/10.1016/j.tecto.2012.04.015

Prey, S. (1989). Ein steilstehendes Störungssystem als Westbegrenzung des Tauernfensters. *Journal of Geologische Bundesanstalt, 132*(4), 745-749.

Price, R. A. (1981). The Cordilleran foreland thrust and fold belt in the southern Canadian Rocky Mountains. *Geological Society, London, Special Publications, 9*(1), 427-448. doi:https://doi.org/10.1144/GSL.SP.1981.009.01.39

Pride, K. R., Lecouteur, P. C., & Mawer, A. B. (1986). Geology and mineralogy of the Aley carbonatite, Ospika River area, British Columbia. *Canadian Institute of Mining Bulletin, 79*(891), 32-32.

Prosser, G. (1998). Strike-slip movements and thrusting along a transpressive fault zone: The North Giudicarie line (Insubric line, northern Italy). *Tectonics, 17*(6), 921-937. doi:https://doi.org/10.1029/1998TC900010

Raiverman, V., Kunte, S.V., and Mukherjea, A. (1983). Basin geometry, Cenozoic sedimentation and hydrocarbon in northwestern Himalaya and Indo-Gangetic plains. *Petroleum Geology of Asia Journal, 6*(4), 67-92.

Rajaure, S., Sapkota, S.N., Adhikari, L.B., Koirala, B., Bhattarai, M., Tiwari, D.R., Gautam, U., Shrestha, P., Maske, S., Avouac, J.P., Bollinger, L., Pandey, M.R. (2013). Double difference relocation of local earthquakes in the Nepal Himalaya. *Journal of the Nepal Geological Society, 46*, 133-142.

Ramos, V. A. (1988). The tectonics of the Central Andes (30°–33°S latitude). In S. Clark, D. Burchfiel, & D. Suppe (Eds.), *Processes in Continental Lithospheric Deformation* (Vol. 218, pp. 31-54): Geological Society of America Special Paper.

Ramos, V. A., Cristallini, E. O., & Pérez, D. J. (2002). The Pampean flat-slab of the Central Andes. *Journal of South American earth sciences, 15*(1), 59-78. doi:https://doi.org/10.1016/S0895-9811(02)00006-8

Ramos, V. A., & Folguera, A. (2009). Andean flat-slab subduction through time. *Geological Society, London, Special Publications, 327*(1), 31-54. doi:10.1144/sp327.3

Rankin, D. W. (1976). Appalachian salients and recesses: Late Precambrian continental breakup and the opening of the Iapetus Ocean. *Journal of Geophysical Research, 81*(32), 5605-5619. doi:https://doi.org/10.1029/JB081i032p05605

Rao, M. B. R. (1973). The subsurface geology of the Indo-Gangetic plains. *Journal of The Geological Society of India, 14*(3), 217-242.

Ratschbacher, L., Merle, O., Davy, P., & Cobbold, P. (1991). Lateral extrusion in the Eastern Alps, part 1: boundary conditions and experiments scaled for gravity. *Tectonics, 10*(2), 245-256. doi:https://doi.org/10.1029/90TC02622

Regard, V., Bellier, O., Thomas, J.-C., Bourles, D., Bonnet, S., Abbassi, M., Braucher, R., Mercier, J., Shabanian, E., & Soleymani, S. (2005). Cumulative right-lateral fault slip rate across the Zagros—Makran transfer zone: role of the Minab—Zendan fault system in accommodating Arabia—Eurasia convergence in southeast Iran. *Geophysical Journal International, 162*(1), 177-203. doi:https://doi.org/10.1111/j.1365-246X.2005.02558.x

Reiter, F., Freudenthaler, C., Hausmann, H., Ortner, H., Lenhardt, W., & Brandner, R. (2018). Active seismotectonic deformation in front of the Dolomites indenter, Eastern Alps. *Tectonics, 37*(12), 4625-4654. doi:https://doi.org/10.1029/2017TC004867

Reynolds, M. W. (1979). Character and Extent of Basin-Range Faultin, Western Montana and East-Central Idaho. In G. W. Newman & H. D. Goode (Eds.), *Basin and Range Symposium and Great Basin Field Conference* (pp. 185-193). Denver: Rocky Mountain Association of Geologists.

Ribes, C., Manatschal, G., Ghienne, J.-F., Karner, G. D., Johnson, C. A., Figueredo, P. H., Incerpi, N., & Epin, M.-E. (2019). The syn-rift stratigraphic record across a fossil hyper-extended rifted margin: the example of the northwestern Adriatic margin exposed in the Central Alps. *International Journal of Earth Sciences, 108*(6), 2071-2095. doi:10.1007/s00531-019-01750-6

Ring, U. (1994). The kinematics of the late Alpine Muretto fault and its relation to dextral transpression across the Periadriatic Line. *Eclogae Geologicae Helvetiae, 87*(3), 811-831.

Ring, U., & Gerdes, A. (2016). Kinematics of the Alpenrhein-Bodensee graben system in the Central Alps: Oligocene/Miocene transtension due to formation of the Western Alps arc. *Tectonics, 35*(6), 1367-1391. doi:https://doi.org/10.1002/2015TC004085

Rivers, T. (2008). Assembly and preservation of lower, mid, and upper orogenic crust in the Grenville Province—Implications for the evolution of large hot long-duration orogens. *Precambrian Research, 167*(3), 237-259. doi:https://doi.org/10.1016/j.precamres.2008.08.005

Rivers, T. (2012). Upper-crustal orogenic lid and mid-crustal core complexes: signature of a collapsed orogenic plateau in the hinterland of the Grenville Province 1This article is one of a series of papers published in CJES Special Issue: In honour of Ward Neale on the theme of Appalachian and Grenvillian geology. *Canadian Journal of Earth Sciences, 49*(1), 1-42. doi:https://doi.org/10.1139/e11-014

Rivers, T. (2015). Tectonic Setting and Evolution of the Grenville Orogen: An Assessment of Progress Over the Last 40 Years. *Geoscience Canada, 42*(1), 77-124. doi:10.12789/geocanj.2014.41.057

Robertson, A. H. F., Clift, P. D., Degnan, P. J., & Jones, G. (1991). Palaeogeographic and palaeotectonic evolution of the Eastern Mediterranean Neotethys. *Palaeogeography, Palaeoclimatology, Palaeoecology, 87*(1-4), 289-343. doi:https://doi.org/10.1016/0031-0182(91)90140-M

Robinson, D. P., Das, S., & Watts, A. B. (2006). Earthquake rupture stalled by a subducting fracture zone. *Science, 312*(5777), 1203-1205. doi:https://doi.org/10.1126/science.1125771

Robl, J., & Stüwe, K. (2005). Continental collision with finite indenter strength: 2. European Eastern Alps. *Tectonics, 24*(4). doi:https://doi.org/10.1029/2004TC001741

Rodgers, J. (1990). Fold-and-thrust belts in sedimentary rocks. Part 1: Typical examples. *American Journal of Science, 290*(4), 321-359. doi:https://doi.org/10.2475/ajs.290.4.321

Ronemus, C. B., Orme, D. A., Campbell, S., Black, S. R., & Cook, J. (2020). Mesoproterozoic−Early Cretaceous provenance and paleogeographic evolution of the

Northern Rocky Mountains: Insights from the detrital zircon record of the Bridger Range, Montana, USA. *GSA bulletin*. doi:10.1130/b35628.1

Root, K. G. (1987). *Geology of the Delphine Creek area, southeastern British Columbia: implications for the Proterozoic and Paleozoic development of the Cordilleran Divergent Margin.* (Ph.D.). University of Calgary, Calgary, Alberta.

Roquer, T., Arancibia, G., Rowland, J., Iturrieta, P., Morata, D., & Cembrano, J. (2017). Fault-controlled development of shallow hydrothermal systems: Structural and mineralogical insights from the Southern Andes. *Geothermics*, *66*, 156-173. doi:http://dx.doi.org/10.1016/j.geothermics.2016.12.003

Rosenberg, C. L., Brun, J.-P., & Gapais, D. (2004). Indentation model of the Eastern Alps and the origin of the Tauern Window. *Geology, 32*(11), 997-1000. doi:https://doi.org/10.1130/G20793.1

Rosenberg, C. L., & Garcia, S. (2011). Estimating displacement along the Brenner Fault and orogen-parallel extension in the Eastern Alps. *International Journal of Earth Sciences, 100*(5), 1129-1145. doi:https://doi.org/10.1007/s00531-011-0645-3

Ross, G., Parrish, R., Villeneuve, M., & Bowring, S. (1991). Geophysics and geochronology of the crystalline basement of the Alberta Basin, western Canada. *Canadian Journal of Earth Sciences*, *28*(4), 512-522. doi:https://doi.org/10.1139/e91-045

Royden, L., Horváth, F., Nagymarosy, A., & Stegena, L. (1983). Evolution of the Pannonian basin system: 2. Subsidence and thermal history. *Tectonics*, *2*(1), 91-137. doi:https://doi.org/10.1029/TC002i001p00091

Royden, L. H. (1993). Evolution of retreating subduction boundaries formed during continental collision. *Tectonics*, *12*(3), 629-638. doi:https://doi.org/10.1029/92TC02641

Sadeghi, S., & Yassaghi, A. (2016). Spatial evolution of Zagros collision zone in Kurdistan, NW Iran: Constraints on Arabia–Eurasia oblique convergence. *Solid Earth*, *7*(2), 659-659. doi:https://doi.org/10.5194/se-7-659-2016

Sahoo, P. K., Kumar, S., and Singh, R.P. (2000). Neotectonic study of Ganga and Yamuna tear faults, NW Himalaya, using remote sensing and GIS. *International Journal of Remote Sensing*, *21*(3), 499-518. doi:https://doi.org/10.1080/014311600210713

Saleeby, J. B. (2003). Segmentation of the Laramide slab—Evidence from the southern Sierra Nevada region. *Geological Society of America Bulletin, 115*(6), 655-668. doi:https://doi.org/10.1130/0016-7606(2003)115<0655:SOTLSF>2.0.CO;2

Saleeby, J. B., Busby-Spera, C., Oldow, J. S., Dunne, G. C., Wright, J. E., Cowan, D. S., Walker, R. W., & Alllmendinger, R. W. (1992). Early Mesozoic tectonic evolution of the western US Cordillera. In B. C. Burchfiel, W. Lipman, & M. L. Zoback (Eds.), *The Cordilleran*

Orogen, Conterminous U.S., The Geology of North America G3 (pp. 107-168): Geological Society of America.

Salfity, J. A., & Marquillas, R. A. (1994). Tectonic and sedimentary evolution of the Cretaceous-Eocene Salta Group basin, Argentina. In J. A. Salfity (Ed.), *Cretaceous tectonics of the Andes* (pp. 266-315): Vieweg+Teubner Verlag, Wiesbaden.

Sarkarinejad, K., Pash, R. R., Motamedi, H., & Yazdani, M. (2018). Deformation and kinematic evolution of the subsurface structures: Zagros foreland fold-and-thrust belt, northern Dezful Embayment, Iran. *International Journal of Earth Sciences, 107*(4), 1287-1304. doi:https://doi.org/10.1007/s00531-017-1532-3

Sastri, V. V., Bhandari, L.L., Raju, A.T.R., Datta, A.K. (1971). Tectonic framework and subsurface stratigraphy of the Ganga Basin. *Journal of The Geological Society of India, 12*(3), 222-233.

Satolli, S., Pace, P., Viandante, M. G., & Calamita, F. (2014). Lateral variations in tectonic style across cross-strike discontinuities: an example from the Central Apennines belt (Italy). *International Journal of Earth Sciences, 103*(8), 2301-2313. doi:https://doi.org/10.1007/s00531-014-1052-3

Schepers, G., Van Hinsbergen, D. J., Spakman, W., Kosters, M. E., Boschman, L. M., & McQuarrie, N. (2017). South-American plate advance and forced Andean trench retreat as drivers for transient flat subduction episodes. *Nature communications, 8*, 15249. doi:https://doi.org/10.1038/ncomms15249

Schmid, S. M., Aebli, H. R., Heller, F., & Zingg, A. (1989). The role of the Periadriatic Line in the tectonic evolution of the Alps. *Geological Society, London, Special Publications, 45*(1), 153-171. doi:https://doi.org/10.1144/gsl.Sp.1989.045.01.08

Schmid, S. M., Fügenschuh, B., Kissling, E., & Schuster, R. (2004). Tectonic map and overall architecture of the Alpine orogen. *Eclogae Geologicae Helvetiae, 97*(1), 93-117. doi:https://doi,org/10.1007/s00015-004-1113-x

Schmid, S. M., Pfiffner, O.-A., Froitzheim, N., Schönborn, G., & Kissling, E. (1996). Geophysical-geological transect and tectonic evolution of the Swiss-Italian Alps. *Tectonics, 15*(5), 1036-1064. doi: https://doi.org/10.1029/96TC00433

Schönborn, G. (1992). Kinematics of a transverse zone in the Southern Alps, Italy. In K. R. McClay (Ed.), *Thrust Tectonics* (pp. 299-310). Dordrecht: Springer Netherlands.

Schumacher, M. E. (1990). Alpine basement thrusts in the Eastern Seengebirge, Southern Alps (Italy Switzerland). *Eclogae Geologicae Helvetiae, 83*(3), 645-663.

Scrocca, D. (2006). Thrust front segmentation induced by differential slab retreat in the Apennines (Italy). *Terra nova, 18*(2), 154-161. doi: https://doi.org/10.1111/j.1365-3121.2006.00675.x

Searle, M. P., Simpson, R. L., Law, R. D., Parrish, R. R., & Waters, D. J. (2003). The structural geometry, metamorphic and magmatic evolution of the Everest massif, High Himalaya of Nepal–South Tibet. *Journal of the Geological Society*, *160*(3), 345-366. doi: https://doi.org/10.1144/0016-764902-126

Sears, J. W., Hendrix, M., Waddell, A., Webb, B., Nixon, B., King, T., Roberts, E., & Lerman, R. (2000). Structural and stratigraphic evolution of the Rocky Mountain foreland basin in central-western Montana. In S. Roberts & D. Winston (Eds.), *Geologic Field Trips, Western Montana and Adjacent Areas. Edited by S. Roberts and D. Winston. Rocky Mountain Section Geological Society of America Annual Meeting* (pp. 131-156). Missoula: University of Montana.

Sears, J. W., & Hendrix, M. S. (2004). Lewis and Clark line and the rotational origin of the Alberta and Helena salients, North American Cordillera. In A. Sussman & A. Weil (Eds.), *Orogenic Curvature: Integrating Paleomagnetic and Structural Analyses: Geological Society of America Special Paper* (Vol. 383, pp. 173-186).

Seifert, N. (2019). *Structural analysis of the Benkar Fault Zone, a cross structure in the higher Himalaya of the Khumbu Region, eastern Nepal.* (MS). Montana State University, Bozeman, Montana.

Séjourné, S., & Malo, M. (2007). Pre-, syn-, and post-imbrication deformation of carbonate slices along the southern Quebec Appalachian front—implications for hydrocarbon exploration. *Canadian Journal of Earth Sciences, 44*(4), 543-564. doi:https://doi.org/10.1139/E06-106

Selverstone, J. (1988). Evidence for east-west crustal extension in the Eastern Alps: Implications for the unroofing history of the Tauern Window. *Tectonics, 7*(1), 87-105. doi:https://doi.org/10.1029/TC007i001p00087

Sepehr, M., Cosgrove, J., & Moieni, M. (2006). The impact of cover rock rheology on the style of folding in the Zagros fold-thrust belt. *Tectonophysics, 427*(1-4), 265-281. doi:https://doi.org/10.1016/j.tecto.2006.05.021

Sepehr, M., & Cosgrove, J. W. (2004). Structural framework of the Zagros fold–thrust belt, Iran. *Marine and Petroleum Geology, 21*(7), 829-843. doi:https://doi.org/10.1016/j.marpetgeo.2003.07.006

Sielfeld, G., Ruz, J., Brogi, A., Cembrano, J., Stanton-Yonge, A., Pérez-Flores, P., & Iturrieta, P. (2019). Oblique-slip tectonics in an active volcanic chain: A case study from the Southern Andes. *Tectonophysics, 770*, 228221. doi:https://doi.org/10.1016/j.tecto.2019.228221

Silver, C. R. P., Murphy, M. A., Taylor, M. H., Gosse, J., & Baltz, T. (2015). Neotectonics of the Western Nepal Fault System: Implications for Himalayan strain partitioning. *Tectonics, 34*(12), 2494-2513. doi:https://doi.org/10.1002/2014TC003730

Simony, P. S., & Carr, S. D. (1997). Large lateral ramps in the Eocene Valkyr shear zone: extensional ductile faulting controlled by plutonism in southern British Columbia. *Journal of Structural Geology, 19*(6), 769-784. doi:https://doi.org/10.1016/S0191-8141(97)00011-4

Sims, P. K., Bankey, V., & Finn, C. (2001). *Preliminary Precambrian basement map of Colorado: A geologic interpretation of the aeromagnetic map*: U.S. Geological Survey.

Skourlis, K., & Doutsos, T. (2003). The Pindos Fold-and-thrust belt (Greece): inversion kinematics of a passive continental margin. *International Journal of Earth Sciences, 92*(6), 891-903. doi:https://doi.org/10.1007/s00531-003-0365-4

Sobornov, K. O. (1996). Lateral variations in structural styles of tectonic wedging in the northeastern Caucasus, Russia. *Bulletin of Canadian Petroleum Geology, 44*(2), 385-399.

Sorgi, C., Deffontaines, B., Hippolyte, J. C., & Cadet, J. P. (1998). An integrated analysis of transverse structures in the northern Apennines, Italy. *Geomorphology, 25*(3-4), 193-206. doi:https://doi.org/10.1016/S0169-555X(98)00041-5

Soucy La Roche, R., and Godin, L. (2019). Inherited cross-strike faults and Oligocene-early Miocene segmentation of the Main Himalayan Thrust, West Nepal. *Journal of Geophysical Research Solid Earth, 124*, 7429-7444. doi:https://doi.org/10.1029/2019JB017467

Southworth, C. S. (1986). Side-looking airborne radar image map showing cross-strike structural discontinuities and lineaments of the central Appalachians. In *Miscellaneous Field Studies Map. doi: https://doi.org/10.3133/mf1891*.

Sperner, B., Ratschbacher, L., & Nemčok, M. (2002). Interplay between subduction retreat and lateral extrusion: Tectonics of the Western Carpathians. *Tectonics, 21*(6), 1-1-1-24. doi:https://doi.org/10.1029/2001TC901028

Srivastava, V., Mukul, M., Barnes, J.B., Mukul, M. (2018). Geometry and kinematics of Main Frontal thrust-related fault propagation folding in the Mohand Range, northwest Himalaya. *Journal of Structural Geology, 115*, 1-18. doi:https://doi.org/10.1016/j.jsg.2018.06.022

Stampfli, G. M., & Borel, G. D. (2002). A plate tectonic model for the Paleozoic and Mesozoic constrained by dynamic plate boundaries and restored synthetic oceanic isochrons. *Earth and Planetary Science Letters, 196*(1), 17-33. doi:https://doi.org/10.1016/S0012-821X(01)00588-X

Stanton-Yonge, A., Griffith, W., Cembrano, J., St. Julien, R., & Iturrieta, P. (2016). Tectonic role of margin-parallel and margin-transverse faults during oblique subduction in the Southern Volcanic Zone of the Andes: Insights from Boundary Element Modeling. *Tectonics, 35*(9), 1990-2013. doi:https://doi.org/10.1002/2016TC004226

Steck, A. (2008). Tectonics of the Simplon massif and Lepontine gneiss dome: deformation structures due to collision between the underthrusting European plate and the Adriatic indenter. *Swiss Journal of Geosciences, 101*(2), 515-546. doi:https://doi.org//10.1007/s00015-008-1283-z

Stocklin, J. (1968). Structural history and tectonics of Iran: A review. *AAPG Bulletin, 52*(7), 1229-1258. doi:https://doi.org/10.1306/5D25C4A5-16C1-11D7-8645000102C1865D

Sue, C., & Tricart, P. (2003). Neogene to ongoing normal faulting in the inner western Alps: a major evolution of the late alpine tectonics. *Tectonics, 22*(5). doi:https://doi.org/10.1029/2002TC001426

Talbot, C. J., & Alavi, M. (1996). The past of a future syntaxis across the Zagros. *Geological Society, London, Special Publications, 100*(1), 89-109.

Tavarnelli, E., Butler, R. W. H., Decandia, F. A., Calamita, F., Grasso, M., Alvarez, W., Renda, P., Crescenti, U., & D'offizi, S. (2004). *Implications of fault reactivation and structural inheritance in the Cenozoic tectonic evolution of Italy*. Paper presented at the International Geological Congress 32.

Tchalenko, J., & Braud, J. (1974). Seismicity and structure of the Zagros (Iran): the Main Recent Fault between 33 and 35 N. *Philosophical Transactions of the Royal Society of London. Series A, Mathematical and Physical Sciences, 277*(1262), 1-25. doi:https://doi.org/10.1098/rsta.1974.0044

Thomas, W. A. (1977). Evolution of Appalachian-Ouachita salients and recesses from reentrants and promontories in the contineral margin. *American Journal of Science, 277*, 1233-1278. doi:http://dx.doi.org/10.2475/ajs.277.10.1233.

Thomas, W. A. (1990). Controls on locations of transverse zones in thrust belts. *Eclogae Geologicae Helvetiae, 83*(3), 727-744.

Thomas, W. A. (1991). The Appalachian-Ouachita rifted margin of southeastern North America. *Geological Society of America Bulletin, 103*(3), 415-431. doi:https://doi.org/10.1130/0016-7606(1991)103<0415:TAORMO>2.3.CO;2

Thomas, W. A. (2007). Role of the Birmingham basement fault in thin-skinned thrusting of the Birmingham anticlinorium, Appalachian thrust belt in Alabama. *American Journal of Science, 307*(1), 46-62. doi:https://doi.org/10.2475/01.2007.03

Thomas, W. A. (2014). A mechanism for tectonic inheritance at transform faults of the Iapetan margin of Laurentia. *Geoscience Canada*, 321-344. doi:http://dx.doi.org/10.12789/geocanj.2014.41.048

Thomas, W. A., & Bayona, G. (2002). Palinspastic restoration of the Anniston transverse zone in the Appalachian thrust belt, Alabama. *Journal of Structural Geology, 24*(4), 797-826. doi:https://doi.org/10.1016/S0191-8141(01)00117-1

Thompson, R. I. (1989). Stratigraphy, tectonic evolution and structural analysis of the Halfway River map area (94B), northern Rocky Mountains, British Columbia. *Geological Survey of Canada, 425*, 1-119.

Thomson, S. N. (2002). Late Cenozoic geomorphic and tectonic evolution of the Patagonian Andes between latitudes 42˚ S and 46˚ S: An appraisal based on fission-track results from the transpressional intra-arc Liquiñe-Ofqui fault zone. *Geological Society of America Bulletin, 114*(9), 1159-1173. doi:https://doi.org/10.1130/0016-7606(2002)114<1159:LCGATE>2.0.CO;2

Tricart, P. (1984). From passive margin to continental collision; a tectonic scenario for the Western Alps. *American Journal of Science, 284*(2), 97-120. doi:https://doi.org/10.2475/ajs.284.2.97

Tull, J. F., & Holm, C. S. (2005). Structural evolution of a major Appalachian salient-recess junction: Consequences of oblique collisional convergence across a continental margin transform fault. *Geological Society of America Bulletin, 117*(3-4), 482-499. doi:https://doi.org/10.1130/B25578.1

Urbanek, C., Frank, W., Grasemann, B., & Decker, K. (2002). Eoalpine versus Tertiary deformation: Dating of heterogeneously partitioned strain (Tauern Window, Austria). Pangeo Austria: Erdwissenschaften in€ Osterreich 28.-30.6. 2002 (Program and abstract). *Institute for geology and paleontology University of Salzburg*.

Valdiya, K. S. (1976). Himalayan transverse faults and folds and their parallelism with subsurface structures of North Indian plains. *Tectonophysics, 32*, 353-386. doi:https://doi.org/10.1016/0040-1951(76)90069-X

Valensise, G., & Pantosti, D. (2001). The investigation of potential earthquake sources in peninsular Italy: a review. *Journal of Seismology, 5*(3), 287-306. doi:https://doi.org/10.1023/A:1011463223440

van der Beek, P., Litty, C., Baudin, M., Mercier, J., Robert, X., Hardwick, E. (2016). Contrasting tectonically driven exhumation and incision patterns, western versus central Nepal Himalaya. *Geology, 44*(4), 327-330. doi:https://doi.org10.1130/G37579.1

van Staal, C. R., Whalen, J. B., McNicoll, V. J., Pehrsson, S., Lissenberg, C. J., Zagorevski, A., van Breemen, O., & Jenner, G. A. (2007). The Notre Dame arc and the Taconic orogeny in Newfoundland. In R. D. Hatcher, Jr., M. P. Carlson, J. H. McBride, & J. R. Martínez Catalán (Eds.), *4-D Framework of Continental Crust: Geological Society of America Memoir 200* (pp. 511-552).

Vargas, G., Rebolledo, S., Sepúlveda, S. A., Lahsen, A., Thiele, R., Townley, B., Padilla, C., Rauld, R., Herrera, M. J., & Lara, M. (2013). Submarine earthquake rupture, active faulting and volcanism along the major Liquiñe-Ofqui Fault Zone and implications for seismic hazard assessment in the Patagonian Andes. *Andean Geology, 40*(1), 141-171. doi:https://doi.org/10.5027/andgeoV40n1-a07

Vergani, G., Tankard, J., Belotti, J., & Welsink, J. (1995). Tectonic evolution and paleogeography of the Neuquén Basin, Argentina. In A. Tankard, R. Suárez, & H. Welsink (Eds.), *Petroleum Basins of South America* (Vol. 62): American Association of Petroleum Geologists.

Vernant, P., & Chéry, J. (2006). Mechanical modelling of oblique convergence in the Zagros, Iran. *Geophysical Journal International, 165*(3), 991-1002. doi:https://doi.org/10.1111/j.1365-246X.2006.02900.x

Vernant, P., Nilforoushan, F., Hatzfeld, D., Abbassi, M., Vigny, C., Masson, F., Nankali, H., Martinod, J., Ashtiani, A., & Bayer, R. (2004). Present-day crustal deformation and plate kinematics in the Middle East constrained by GPS measurements in Iran and northern Oman. *Geophysical Journal International, 157*(1), 381-398. doi:https://doi.org/10.1111/j.1365-246X.2004.02222.x

Viola, G., Mancktelow, N. S., & Seward, D. (2001). Late Oligocene-Neogene evolution of Europe-Adria collision: New structural and geochronological evidence from the Giudicarie fault system (Italian Eastern Alps). *Tectonics, 20*(6), 999-1020. doi:https://doi.org/10.1029/2001tc900021

Waldron, J. W., Barr, S. M., Park, A. F., White, C. E., & Hibbard, J. (2015). Late Paleozoic strike-slip faults in Maritime Canada and their role in the reconfiguration of the northern Appalachian orogen. *Tectonics, 34*(8), 1661-1684. doi:https://doi.org/10.1002/2015TC003882

Wallace, C. A., Lidke, D. J., & Schmidt, R. G. (1990). Faults of the central part of the Lewis and Clark line and fragmentation of the Late Cretaceous foreland basin in west-central Montana. *Geological Society of America Bulletin, 102*(8), 1021-1037. doi:https://doi.org/10.1130/0016-7606(1990)102<1021:FOTCPO>2.3.CO;2

Weil, A. B., Yonkee, A., & Schultz, M. (2016). Tectonic evolution of a Laramide transverse structural zone: Sweetwater Arch, south central Wyoming. *Tectonics, 35*(5), 1090-1120. doi:https://doi.org/10.1002/2016TC004122

Weinberg, R. F. (2016). Himalayan leucogranites and migmatites: nature, timing and duration of anatexis. *Journal of Metamorphic Geology, 34*(8), 821-843. doi:https://doi.org/10.1111/jmg.12204

West Jr, D. P., & Hubbard, M. S. (1997). Progressive localization of deformation during exhumation of a major strike-slip shear zone: Norumbega fault zone, south-central Maine, USA. *Tectonophysics, 273*(3-4), 185-201. doi:https://doi.org/10.1016/S0040-1951(96)00306-X

Wheeler, R. L. (1980). Cross-strike structural discontinuities: possible exploration tool for natural gas in Appalachian overthrust belt. *AAPG Bulletin, 64*(12), 2166-2178. doi:https://doi.org/10.1306/2F91975B-16CE-11D7-8645000102C1865D

Whisner, S. C., Schmidt, C. J., & Whisner, J. B. (2014). Structural analysis of the Lombard thrust sheet and adjacent areas in the Helena salient, southwest Montana, USA. *Journal of Structural Geology, 69*, 351-376. doi:http://dx.doi.org/10.1016/j.jsg.2014.08.006

Whitmeyer, S. J., & Karlstrom, K. E. (2007). Tectonic model for the Proterozoic growth of North America. *Geosphere, 3*(4), 220-259. doi:https://doi.org/10.1130/GES00055.1

Williams, H., & Cawood, P. (1986). Relationships along the eastern margin of the Humber Arm allochthon between Georges Lake and Corner Brook, Newfoundland. *Current Research, Part A. Geological Survey of Canada, Paper, 86*, 759-765.

Wooden, J., & Mueller, P. (1988). Pb, Sr, and Nd isotopic compositions of a suite of Late Archean, igneous rocks, eastern Beartooth Mountains: implications for crust-mantle evolution. *Earth and Planetary Science Letters, 87*(1-2), 59-72. doi:https://doi.org/10.1016/0012-821X(88)90064-7

Yeats, R. S., and Lillie, R.J. (1991). Contemporary tectonics of the Himalayan frontal fault system: folds, blind thrusts and the 1905 Kangra earthquake. *Journal of Structural Geology, 13*(2), 215-225.

Yonkee, W. A., & Weil, A. B. (2015). Tectonic evolution of the Sevier and Laramide belts within the North American Cordillera orogenic system. *Earth-Science Reviews, 150*, 531-593. doi:http://dx.doi.org/10.1016/j.earscirev.2015.08.001

Zanchetta, S., D'Adda, P., Zanchi, A., Barberini, V., & Villa, I. M. (2011). Cretaceous-Eocene compression in the central Southern Alps (N Italy) inferred from 40Ar/39Ar dating of pseudotachylytes along regional thrust faults. *Journal of Geodynamics, 51*(4), 245-263. doi:https://doi.org/10.1016/j.jog.2010.09.004

Zanchi, A., D'Adda, P., Zanchetta, S., & Berra, F. (2012). Syn-thrust deformation across a transverse zone: the Grem–Vedra fault system (central Southern Alps, N Italy). *Swiss Journal of Geosciences, 105*(1), 19-38. doi:https://doi.rog/10.1007/s00015-011-0089-6

Zerlauth, M., Ortner, H., Pomella, H., Pfiffner, O. A., & Fügenschuh, B. (2014). Inherited tectonic structures controlling the deformation style: an example from the Helvetic nappes of the Eastern Alps. *Swiss Journal of Geosciences*, *107*(2-3), 157-175. doi:https://doi.org/10.1007/s00015-014-0167-7

Zhao, W., K. D. Nelson, the Project INDEPTH Team. (1993). Deep seismic reflection evidence for continental underthrusting beneath southern Tibet. *Nature geoscience*, *366*, 557-559. doi:https://doi.org/10.1038/366557a0

CHAPTER THREE

THE BENKAR FAULT ZONE: AN OROGEN-SCALE CROSS FAULT IN THE EASTEN NEPAL HIMALAYA

Contribution of Authors and Co-Authors

Manuscript in Chapter 3

Author: Bibek Giri,
Contributions: Funds acquisition, Methodology, Investigation, Data analysis, Laboratory analysis, Writing – original draft and figures
Mary Hubbard: Conceptualization, Funds acquisition, Methodology, Investigation, Data analysis, Validation, Writing – review and editing
Christopher McDonald: Laboratory analysis, Writing – review and editing
Neil Seifert: Methodology, Writing – review and editing
Bishal KC: Methodology, Writing – review and editing

Manuscript Information

Bibek Giri[1], Mary Hubbard[1], Christopher McDonald[2], Neil Seifert[3], Bishal KC[4]

1 Montana State University
2 Arizona State University
3 Teck Resources Limited
4 Australian Institute of Management and Commerce

Status of Manuscript
__x_ Prepared for submission to a peer-reviewed journal
____ Officially submitted to a peer-reviewed journal
____ Accepted by a peer-reviewed journal
____ Published in a peer-reviewed journal

Abstract

The Benkar Fault Zone (BFZ) is a recently recognized, NNE-striking, ductile to semi-brittle, cross fault that cuts across the dominant, north-dipping metamorphic fabric of the Greater Himalayan Sequence (GHS) in the Everest region. $^{40}Ar/^{39}Ar$-muscovite cooling ages along a transect across the BFZ in the GHS indicate movement younger than 12 Ma. In order to understand the southern continuity, mode of genesis, and seismo-tectonic implications of the BFZ, we continued mapping this fault towards the south, across the Main Central Thrust, into the Lesser Himalayan Sequence (LHS), and the Greater Himalayan Klippe. We augment our mapping work with petrographic and kinematic analysis. We recognize a system of cross faults segments in the southern region, which we interpret as the continuation of the BFZ. The currently mapped section of the BFZ is > 100 km long and its width is up to 4 km in the LHS. Unlike in the GHS, the BFZ is brittle in the south and has been expressed as gouge zones, brecciated zones, sharp fault planes, and brittle deformation zones in a non-penetrative, segmented fashion. Our work did not continue into the Sub-Himalaya, but the BFZ may continue through this zone into the foreland as documented in other Himalayan cross faults. We also explore possible genetic models for the BFZ in reference to models proposed for other Himalayan cross faults. Cross faults have been interpreted as possible segment boundary along major, seismogenic thrusts. Therefore, it is important to recognize and develop a comprehensive understanding of cross faults such as the BFZ.

Introduction

A review of several convergent orogenic belts around the world reveals important lateral heterogeneities along the length of the mountain belts. Some of these heterogeneities are expressed as along-strike changes in deformation style, igneous activities, grade of metamorphism, surface processes and geomorphology, and seismic activities (Giri & Hubbard, 2023). In other cases, abrupt lateral transitions coincide with the spatial occurrence of cross faults/structures (faults/structures that strike at a high angle to the trend of the orogen). Previous authors have suggested a number of explanations for lateral variations such as changes in: 1) continental margin geometry (e.g.; Thomas, 2014); 2) basin geometry and sediment thickness (e.g.; Paulsen & Marshak, 1999; Bahroudi & Koyi, 2003); 3) plate kinematics and obliquity of plate convergence (e.g.; Ramos et al., 2002; Oriolo et al., 2014); 4) lithospheric strength (e.g.; Rosenberg & Garcia, 2011; Giambiagi et al., 2012; Malekzade et al., 2016); and 5) the presence of inherited basement structures (e.g.; Butler et al., 2006). In the Himalaya, Hubbard et al. (2021) has stressed the significance of cross faults as thrust segment boundaries, sometimes between adjacent zones of contrasting thrust geometries. While several cross faults have been recognized in the Himalayan orogen at multiple structural levels (Figure 3.1), their true extent, mode of genesis, and their impacts on the regional seismo-tectonics remains poorly understood. The Himalaya are the planet's most dynamic collisional orogenic system and researchers have found evidence that links cross faults with regional seismicity (e.g.; Drukpa et al., 2006b; Rajaure et al., 2013; Paul et al., 2015; Diehl, 2017; Mendoza et al., 2019; Tiwari et al., 2022), which makes it imperative to recognize and develop a comprehensive understanding of these structures. The Benkar Fault Zone (BFZ) is a recently recognized, NNE-striking, right lateral, normal cross fault that runs along and adjacent to the Dudh Koshi valley in the eastern Nepal Himalaya (Figure 3.2). Seifert (2019) mapped the BFZ in the Greater Himalayan Sequence of the Everest region but its southern continuity, its mode of formation, and timing of movement(s) were beyond the scope of that study. In this paper, we summarize the findings of Seifert (2019) and present new map data, from regions along the strike of the BFZ towards the south, within the Okhaldhunga Window and the Greater Himalayan Klippe. This new mapping data coupled with three $^{40}Ar/^{39}Ar$-muscovite cooling ages from the Greater Himalayan Sequence, and petrographic and kinematic analysis for samples collected from multiple levels supports the continuation of the BFZ southward cutting across different litho-tectonic units of the Himalaya. Finally, we explore possible modes of genesis of this structure.

Tectonic Setting

Tectono-stratigraphy of the Himalaya

The onset of continental collision along the Indian and Asian plate margins between 61-55 Ma (Decelles et al., 2014; Wu et al., 2014; Hu et al., 2015; Orme et al., 2015; Zhu et al., 2015; Ding et al., 2016; Kapp & DeCelles, 2019) was followed by thickening, shortening, and imbrication of the down-going Indian crustal rocks resulting in the formation of the dynamic Himalayan orogenic belt. The Himalaya has been viewed as a composite of four major, laterally continuous litho-tectonic units. From north to south they are the Tibetan Tethyan Series (TTS), the Greater Himalayan Sequence (GHS), the Lesser Himalayan Sequence (LHS), and the Sub-Himalaya. These units are each bounded by north-dipping faults: the South Tibetan Detachment System (STDS), the Main Central Thrust (MCT), the Main Boundary Thrust (MBT), and the Main Frontal Thrust (MFT) (Figure 3.1 & 3.2, Heim & Gansser, 1939; Gansser, 1964; Le Fort, 1975; Fuchs, 1982; Upreti, 1999; Hodges, 2000; Yin, 2006; Dhital, 2015; Goscombe et al., 2018; DeCelles et al., 2020).

The TTS has largely been defined as a Paleozoic and Mesozoic (Late Ordovician to Cretaceous; DeCelles et al., 2020) marine succession of siliciclastic and carbonate rocks deposited in the Tethys Sea (Baud et al., 1984; Colchen et al., 1986; Brookfield, 1993; Garzanti, 1999; Kellett & Godin, 2009). The STDS, active during ~23-28 Ma to 12 -16 Ma (see Goscombe et al., 2018), juxtaposes these very-low to low-grade (green-schist facies) metamorphic rocks of the TTS against the GHS along a system of low-angle, extensional, top-to-the-north, ductile shear zones and brittle faults (Burg et al., 1984; Burchfiel et al., 1992; Vannay & Hodges, 1996; Godin, 2003; Law et al., 2004; Searle, 2010; Kellett et al., 2019).

The GHS is the metamorphic core of the Himalaya and consists of Neo-Proterozoic to Ordovician (990 Ma to 520 Ma) rocks of the Indian continent (Parrish & Hodges, 1996; DeCelles et al., 2000; Hodges, 2000; Robinson et al., 2001; Cottle et al., 2009a; Wang et al., 2015; DeCelles et al., 2020). During the Cambrian Bhimphedian Orogeny, rocks of the GHS were deformed, metamorphosed, and intruded by granites ranging in age between 453 Ma to 581 Ma (Garzanti et al., 1986; Lombardo et al., 1993; Coleman, 1998; DeCelles et al., 2000; Godin et al., 2001; Robinson et al., 2001; Viskupic & Hodges, 2001; Gehrels et al., 2006; Gingele et al., 2007; Jessup et al., 2008; Cottle et al., 2009a). How these mid-crustal rocks exhumed remains an area of active research in the Himalaya (e.g.; Grujic et al., 1996; Nelson et al., 1996; Beaumont et al., 2001; DeCelles et al., 2001; Searle et al., 2003; Kohn, 2008; Webb et al., 2011). Carosi et al. (2018) has stressed the importance of in-sequence and out-of-sequence thrusts and shear zones within the GHS which in general has been mapped as one continuous tectonic unit.

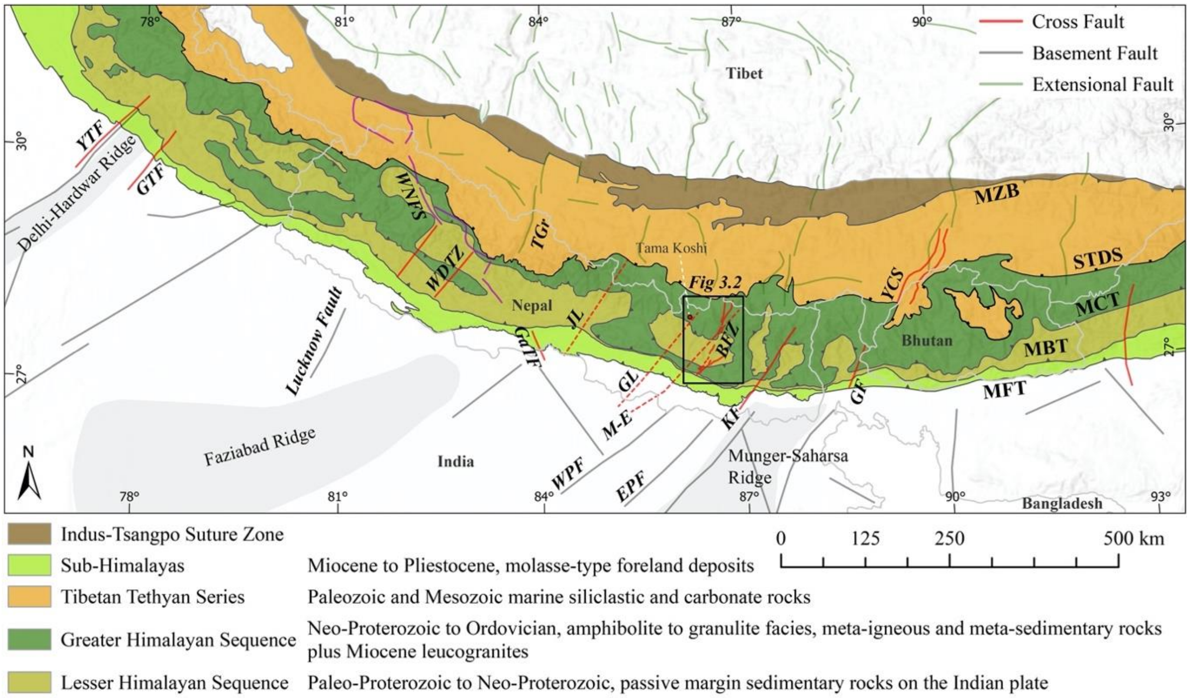

Figure 3.1: Simplified litho-tectonic map of the Himalaya. The red dashed and heavy lines indicate cross faults. Rectangle in the center shows extent of the area shown in Figure 3.2. Modified from Goscombe et al. (2018), Hubbard et al. (2021), and references therein. BFZ: Benkar Fault Zone; EPF: East Patna Fault; GaTF: Gadi Tear Fault; GF: Gish Fault; GL: Gaurishankar Lineament; GTF: Ganga Tear Fault; JL: Judi Lineament; KF: Kosi Fault; MBT: Main Boundary Thrust; MCT: Main Central Thrust; M-E: Motihari-Everest Lineament; MFT: Main Frontal Thrust; MZB: Main Zanskar Backthrust; STDS: South Tibetan Detachment System; TGr; Thak Khola Graben; WDTZ: Western Dang Transfer Zone; WNFS: Western Nepal Fault System; WPF: West Patna Fault; YCS: Yadong Cross Structure.

In the vicinity of the Everest region, the GHS consists of amphibolite to granulite facies, sillimanite-grade, metapelite, orthogneisses, calc-silicate, and amphibolite rock along with leucogranite intrusions (Bordet, 1961; Ishida, 1969; Ishida & Ohta, 1973; Hubbard, 1988; Schelling, 1992; Lombardo et al., 1993; Searle et al., 2003; Law et al., 2004; Searle et al., 2006; Cottle et al., 2009b). Following the India-Asia collision, these rocks experienced the prograde Barrovian Eohimalayan metamorphism under pressure-temperature conditions of 650 ˚C-680 ˚C, 7-8 kbar (kyanite ± sillimanite grade) between ~39 Ma to 30 Ma, which was followed by the sillimanite ± cordierite grade Neohimlayan metamorphism during 28 Ma to 16 Ma at 600 ˚C-750 ˚C, 3-5 kbar (Pognante & Benna, 1993; Simpson et al., 2000; Searle et al., 2003; Jessup et al., 2006; Jessup et al., 2008; Cottle et al., 2009b; Larson et al., 2011). Timing of voluminous melt injection and leucogranite crystallization within the GHS has been well constrained between 24 Ma-15 Ma (see Cottle et al., 2015). In the Everest region, the STDS is represented by the upper, brittle Qomolongoma Detachment, with the Ordovician Limestone in the hanging wall, and the lower, ductile Lhotse Shear Zone, with middle-to upper-greenschist facies schist and calc-silicate rock of the Everest Series in the hanging wall (Figure 3.2; Lombardo et al., 1993; Carosi et al., 1998; Carosi et al., 1999b; Searle, 1999). Movement along the Lhotse Shear Zone ceased prior to 16 Ma, while the Qomolongma Detachment was active until at least 13 Ma (Cottle et al., 2015; Schultz et al., 2017). Cessation of movement along the STDS has been interpreted as the end of tectonic exhumation of the GHS, which was followed by erosional exhumation that likely was accelerated in Pliocene (e.g.; Searle et al., 2003; Huntington et al., 2006; Clift et al., 2008; Wang et al., 2010; Schultz et al., 2017).

Apatite fission track ages within the GHS of the Everest and surrounding regions progressively increase with elevation from ~1 Ma near the MCT to ~ 3 Ma near the STDS (Streule et al., 2012). Zircon fission track ages range between ~4 Ma to ~16 Ma and $^{40}Ar/^{39}Ar$ muscovite cooling ages range between ~10 Ma and ~17 Ma and both systems show a systematic increase in ages with elevation (Hubbard & Harrison, 1989; Streule et al., 2012; Larson et al., 2019b).

The MCT is the southern boundary of the GHS and has been variously mapped as: 1) a lithological boundary between low-and high-grade metamorphic rocks (Heim & Gansser, 1939;

Brunel, 1986; Pêcher, 1989; Schelling, 1992; Daniel et al., 2003); 2) the kyanite isograd (Bordet, 1961; Le Fort, 1975; Colchen et al., 1986); 3) an abrupt change in U-Pb detrital zircon ages (Parrish & Hodges, 1996; Ahmad et al., 2000) and in Nd isotope compositions (Robinson et al., 2006; DeCelles et al., 2020); 4) a thick shear zone with or without an upper or lower fault (Arita, 1983; Hubbard, 1996); and 5) the base of a high strain zone (Searle et al., 2008). Above or within the MCT zone the metamorphism is inverted from chlorite- to sillimanite-grade towards the north (Heim & Gansser, 1939; Le Fort, 1975; Arita, 1983; Searle & Rex, 1989; Hubbard, 1996). The MCT has been interpreted to be coeval with the STDS between 22-19 Ma (Hubbard & Harrison, 1989; Searle & Rex, 1989; Hodges et al., 1992; Hodges et al., 1996; Kellett et al., 2019) along with localized Late Miocene to Pliocene movements (Harrison et al., 1997; Catlos et al., 2002; Montemagni et al., 2019).

Several researchers have mapped the MCT in the Dudh Koshi and the adjacent valleys and they have presented varying spatial locations and definitions of this structure. Ishida (1969) and Ishida and Ohta (1973) have mapped a system of thrusts that coincide with lithological changes. Hubbard (1989) mapped the MCT as a 3-5 km thick, north-dipping, ductile shear zone consisting of augen gneiss, pelitic schist, amphibolite, marble, calc-silicate, slate, and quartzite. Catlos et al. (2002) mapped the MCT as a discrete thrust that roughly passes along the top of the MCT zone of Hubbard (1989). The MCT has also been mapped further towards the south along the base of the Melung-Salleri Augen Gneiss zone (Goscombe et al., 2006; Jessup et al., 2006; Searle et al., 2006), which also corresponds to the Phaplu Thrust of Maruo and Kizaki (1981). Several other structural elements have also been mapped in the vicinity of the MCT. The base of the Melung-Salleri Augen Gneiss has been mapped as the MCT-I (Arita, 1983; Catlos et al., 2002), as a shear zone (Larson et al., 2017), and as the Midland Thrust (Ishida & Ohta, 1973). In the adjacent, Tama Koshi valley (Figure 3.1), the contact between the Lesser Himalayan metasediments and the Melung-Salleri Augen Gneiss has been mapped as the Upper Tamakoshi Thrust/Shear Zone (Larson, 2018; Larson et al., 2019b). Larson et al. (2022) interpreted an out of sequence movement along the Upper Tamakoshi Thrust during 11-8 Ma, which is in agreement with their previous $^{40}Ar/^{39}Ar$ cooling ages and quartz fabric work in the region (Larson et al., 2016; Larson, 2018; Larson et al., 2019b).

Like elsewhere in the Himalaya, the base of the MCT zone records pressure conditions of 7-8 kbar, which gradually decrease to 4-5 kbar towards the north (Hubbard, 1989; Searle et al., 2003). Peak temperature, however, sharply increases up section across the MCT from 450 ˚C to 670 ˚C (Hubbard & Harrison, 1989; Hubbard, 1996; Searle et al., 2003; Searle et al., 2006; Larson, 2012; From & Larson, 2014).

The LHS, footwall to the MCT, consists of Paleo-Proterozoic to Neo-Proterozoic, passive-margin sedimentary rocks on the Indian plate (Parrish & Hodges, 1996; Upreti, 1999; DeCelles et al., 2000; Hodges, 2000; Miller et al., 2000; DeCelles et al., 2001; Robinson et al., 2006; Martin, 2017). In places within the LHS an unconformity is exposed in imbricate slices near the MBT where Permian to Paleocene, siliciclastic, and fossiliferous deposits known as the Gondwana Sequence overlie the older Precambrian units (Bashyal, 1980; Sakai, 1983; DeCelles et al., 2001; DeCelles et al., 2020). The lower stratigraphic levels of the LHS host a gneissic body, which is referred to as the Ulleri Augen Gneiss in western and central Nepal (Le Fort & Raï, 1999; Upreti et al., 2003) and as the Melung-Salleri Augen Gneiss in eastern Nepal (Ishida, 1969; Schelling, 1992). Throughout the Himalaya, the age of this unit has been well-constrained between 1.75 Ga to 1.90 Ga (see Kohn et al., 2010; Larson et al., 2017; Larson et al., 2019a). Researchers have variously described this gneissic unit as a felsic extrusive rocks (Le Fort, 1975), a magmatic arc related rock in a convergent setting (Kohn et al., 2010), a rift-related rock (Sakai et al., 2013; Larson et al., 2019a), and a 'metasomized or tectonized' granitic basement rock (Arita, 1983). This unit consists of mylontized, quartz + alkali-feldspar + plagioclase + muscovite + biotite orthogneisses (Ishida, 1969; Schelling, 1992; Larson et al., 2019a), schistose gneiss, and assimilated fragments of the Lesser Himalayan metasedimentary rocks, which generally occur as chloritic schists. Hubbard (1989) noted garnets and k-feldspar augen with myrmekitic texture.

Within the LHS, rocks from the lower stratigraphic levels (Lower LHS) have been thrust over younger rocks (Upper LHS) along the Ramghar or Ramghar-Munsiari Thurst (RT) resulting in the structural culmination known as the Lesser Himalayan Duplex and/or the Midland Antiform/Anticlinorium (Figure 3.2; Frank & Fuchs, 1970; DeCelles et al., 1998; Pearson & DeCelles, 2005; Robinson et al., 2006; Kohn, 2008; Long et al., 2011; Bhattacharyya et al., 2015; Mandal et al., 2015; Mukhopadhyay et al., 2017; Long & Robinson, 2021). In the western Nepal Himalaya, major duplex growth occurred between 11 Ma - 5 Ma before the deformation propagated southward along the MBT (DeCelles et al., 2020). In eastern Nepal, Nakajima (2020) suggests that the Midland Anticlinorium developed during and/or after the cessation of the southward transport the Greater Himalayan thrust sheet at 12-10 Ma.

In our study area, the Lesser Himalayan rocks are well exposed within the Okhaldhunga Window, which, towards the south, is bounded by the Sun Koshi Thrust (SKT), the southern continuation of the MCT (Figure 3.2). Schelling (1992) has mapped this thrust as a north-dipping, out-of-sequence thrust. Previous mapping in the LHS of the Okhaldhunga Window and the surrounding region had been done by Ishida (1969), Ishida and Ohta (1973), Andrews (1985), Schelling (1992), Dhital (2015), and Baskota and Adhikari (2019). The earlier studies were aimed at building a regional tectonic-stratigraphic framework and more recent mapping work only covers parts of the Okhaldhunga Window. A detailed lithostratigraphic construction, well established in western Nepal (DeCelles et al., 2020) and in central Nepal (Stöcklin & Bhattarai, 1977; Stöcklin, 1980), is still lacking in this region.

Table 3.1: Litho-stratigraphic classification of the Kathmandu Complex rocks towards the south of the Okhaldhunga Window.

Stratigraphy the Kathmandu Complex		Lithologic descriptions of Dwivedi (1997)
Phulchauki Group	Tistung Formation	Biotite schists and phyllites in the lower section Slates and metasandstones in the upper section
Bhimphedi Group	Markhu Formation	Alternating sequence of quartzite, schist, and marble
	Kulikhani Formation	Psammitic schist, schistose phyllites, calcareous quartzites, and quartzites
	Chisapani Quartzite	Fine grained quartzites with thin pelitic partings
	Kalitar Formation	Mica schist, garnet-schist, and psammitic schist
	Bhainsedobhan Marble	Saccharoidal, micaceous marbles with schist partings and calc-silicate layers
	Raduwa Formation	Garnet–biotite–muscovite schists and quartzites

South of the SKT, the Greater Himalayan Klippe (GHK) rocks have been folded into an EW-trending Mahabharat Synclinorium (Figure 3.2). These rocks are generally interpreted as a klippe of the GHS above the LHS. Larson et al. (2022) constructed prograde (515 ˚C and 5.5 kbar to 575 ˚C and 7 kbar; 32.4±0.3 Ma) and subsequent retrograde (480 ˚C-515 ˚C and 6-7 kbar, until 17.5 Ma) metamorphic pathways for these klippe rocks. Equivalent rock units in central Nepal have been mapped as the Kathmandu Complex (Stöcklin & Bhattarai, 1977; Stöcklin, 1980), which underwent an earlier phase of metamorphism, deformation, and granitic and gneissic intrusion during the Bhimphedian Orogeny (Gehrels et al., 2006; Dhital, 2015). The GHK rocks in eastern Nepal were mapped by Ishida and Ohta (1973) and Schelling (1992) as the Mahabharat Crystallines. Subsequently, Dwivedi (1997) constructed a stratigraphic scheme, guided by that of Stöcklin and Bhattarai (1977), consisting of seven lithological units (Table 3.1).

The Sub-Himalaya, footwall to the MBT, consist of Miocene (Eocence; DeCelles et al., 2020) to Pleistocene, molasse-type foreland deposits which display an overall coarsening upward sequence correlating to the southward propagation of the Himalayan deformation front (Medlicott, 1864; Tokuoka, 1986; Nakayama & Ulak, 1999; Valdiya, 2002; Szulc et al., 2006; Ojha et al., 2009; Gautam et al., 2012; Chakraborty et al., 2020; Yoshida et al., 2021). The southern boundary of the Sub-Himalaya is the active and laterally continuous MFT, with a Holocene slip rate of 23 mm/year (Lavé & Avouac, 2000; Burgess et al., 2012). The MCT, MBT, and MFT have been interpreted to merge into a basal decollement known as the Main Himalayan Thrust (MHT) (Pandey et al., 1995; Pandey et al., 1999; Nábělek et al., 2009; Avouac et al., 2015; Elliott et al., 2016). Cumulative shortening along these faults varies laterally (e.g.; Long & Robinson, 2021) and accounts for about half of the convergence distance between the Indian and Asian Plates (DeCelles et al., 2020).

Himalayan Cross Faults

While the structural geology of the Himalaya is dominated by the major, orogen-parallel thrust fault traces, there is also evidence for structures that cut across the range and, in places, disrupt the lateral continuity of major thrust structures and litho-tectonic units. Maps produced in the last 40-50 years have noted fault segments orthogonal to the range, but these structures, referred to here as cross faults, have not been the focus of research until lately (e.g.; Mukul, 2010; Godin & Harris, 2014; Hubbard et al., 2018; Seifert, 2019). A number of explanations have been brought forward to explain cross faults, but the importance in their study lies in their potential link to both seismic and landslide hazards.

One on-going discussion about Himalayan cross faults is a possible link to structures in the Indian cratonic basement. In the Himalayan foreland, several basement ridges and faults, with high-angled orientation to the Himalayan front, have been recognized and mapped within the Indian plate (Figure 3.1: Burrard, 1915; Sastri et al., 1971; Rao, 1973; Valdiya, 1976; Dasgupta, 1987; Godin & Harris, 2014; Duvall et al., 2020). In the western Himalaya, introduction of the Delhi-Hardwar basement ridge underneath the evolving wedge spatially coincides with a visible offset of the deformation front, which is bounded by the Ganga and Yamuna Tear Faults (Sahoo et al., 2000; Srivastava et al., 2018). In western Nepal, between 82.5˚E and 81˚E, Harvey et al. (2015) demonstrated a bifurcation of a physiographic transition (east-west trending physiographic transition described by Hodges et al. (2001) divides the Himalaya into longitudinal belts of similar topography) and a widening of the regional micro-seismic trend. In the same region, Soucy La Roche and Godin (2019) interpret a NNE-striking lateral ramp in the MHT, formed in Oligocene, to explain along strike variations in peak temperatures, timing of peak metamorphism, and deformation pathways of two nearby Greater Himalayan thrust sheets. They attribute the genesis this lateral ramp to the Lucknow basement fault (Figure 3.1). This lateral ramp interpretation of Soucy La Roche and Godin (2019) is in agreement with conclusions of Harvey et al. (2015) and van der Beek (2016).

Towards the east, the West Dang transfer zone (WDTZ) has been described as an orthogonal structure in the Sub-Himalaya to account for abrupt changes in thrust sheet geometry (Mugnier et al., 1999a; Mugnier et al., 1999b). In central Nepal, the north-south trending, >70km long, asymmetric Thak Khola graben has been viewed as one of the many structures genetically related to the active east-west extension in Tibet (Bordet et al., 1971; Molnar & Tapponnier, 1975, 1978; Burchfiel et al., 1992; Hurtado et al., 2001). East of Kathmandu, the NE-striking Gaurishankar Lineament spatially coincides with an abrupt, NE-SW termination of the M_w 7.8 2015 Nepal Earthquake aftershocks (Mugnier et al., 2017; Hubbard et al., 2021 and references therein). In eastern Nepal and India, two cross faults, the Kosi Fault and the Gish Fault, have been mapped as recess-salient boundaries (Mukul, 2010; Srivastava et al., 2017; Mukul et al., 2018). The Kosi and the Gish Fault also align with the western and the eastern boundaries of the Munger-Saharsa basement ridge respectively (Figure 3.1). Clusters of micro-seismicity that follow the Kosi Fault serve to suggest that the Kosi Fault is an active structure (Pandey et al., 1999; Monsalve et al., 2006; De La Torre, 2007; Hubbard et al., 2021), which is not surprising given that this fault cuts the active MFT. The Gish Fault is along strike with the Yadong Cross Structure (YCS), which is a NNE-striking, left-lateral fault with apparent offset of the STDS of ~70 km (Wu et al., 1998). Wu et al. (1998) have interpreted the YCS as the surface manifestation of a lateral ramp in the MHT. In the eastern Himalaya, researchers have reported multiple small to moderate, strike-slip earthquake events that occurred at depths between 13-68 km on near-vertical fault planes oriented at high angle to the regional trend suggesting that Himalayan cross faults may pass below the MHT into the Indian plate basement below (Drukpa et al., 2006a; Paul et al., 2015; Diehl, 2017).

Benkar Fault Zone

One of the cross faults in eastern Nepal, the BFZ, was recently mapped in GHS rocks in the Everest area (Hubbard et al., 2018; Seifert, 2019). In earlier studies, fault segments and deformation zones, some interpreted as fold limbs in the Everest region, were recognized by Hubbard (1988), Carosi et al. (1999a), and Musumeci (2002) and were reinterpreted as cross fault and named the BFZ by Hubbard et al. (2018) (Figure 3.2 & 3.3). Seifert (2019) conducted field mapping, petrographic, structural and kinematic analysis including electron backscatter diffraction in quartz of the BFZ within the GHS and interpreted the structural and deformation style of this fault by considering existing geochronologic, thermochronologic, thermobarometric, and petrographic data. Hubbard et al. (2018) and Seifert (2019) interpret the BFZ in the GHS as a NNE-striking, SE-dipping zone of deformation with a dominant normal, right lateral sense of movement. A distinct topographic expression of the BFZ can be seen in proximity of Benkar village. Within the GHS, the zone of deformation widens northwards as it wraps around the increasing volume of leucogranite bodies. Around Gorakshep, the BFZ is ~11 km wide, with mean orientation of foliation 037˚/43˚SE, while about 30 km south of Gorakshep, the deformation zone narrows to 1-2 km, with a mean foliation orientation of 348˚/40˚NE. Mineral stretching lineations within the BFZ are represented by two groups of SW- and NE- plunging orientations. The BFZ deformation has been concentrated on anastomosing shear zones within sillimanite and mica rich domains in non-penetrative ductile to semi-brittle styles. Seifert (2019) has interpreted that the BFZ deformation occurred within upper greenschist to lower amphibolite facies conditions, during the regional retrograde metamorphism of the GHS. The deformation led to syndeformational growth of fibrolites and phyllosilicates within the shear planes. Seifert (2019) recognized that the BFZ likely continued to the south, but mapping in that direction was beyond the scope of his work. There is topographic evidence for a continuation of the BFZ southward and tracing it in that direction is important to determine cross cutting relationships with the major thrust fault systems. The goal of this study is to take the mapping and kinematic analysis southward and to collect data that might constrain the timing of movement.

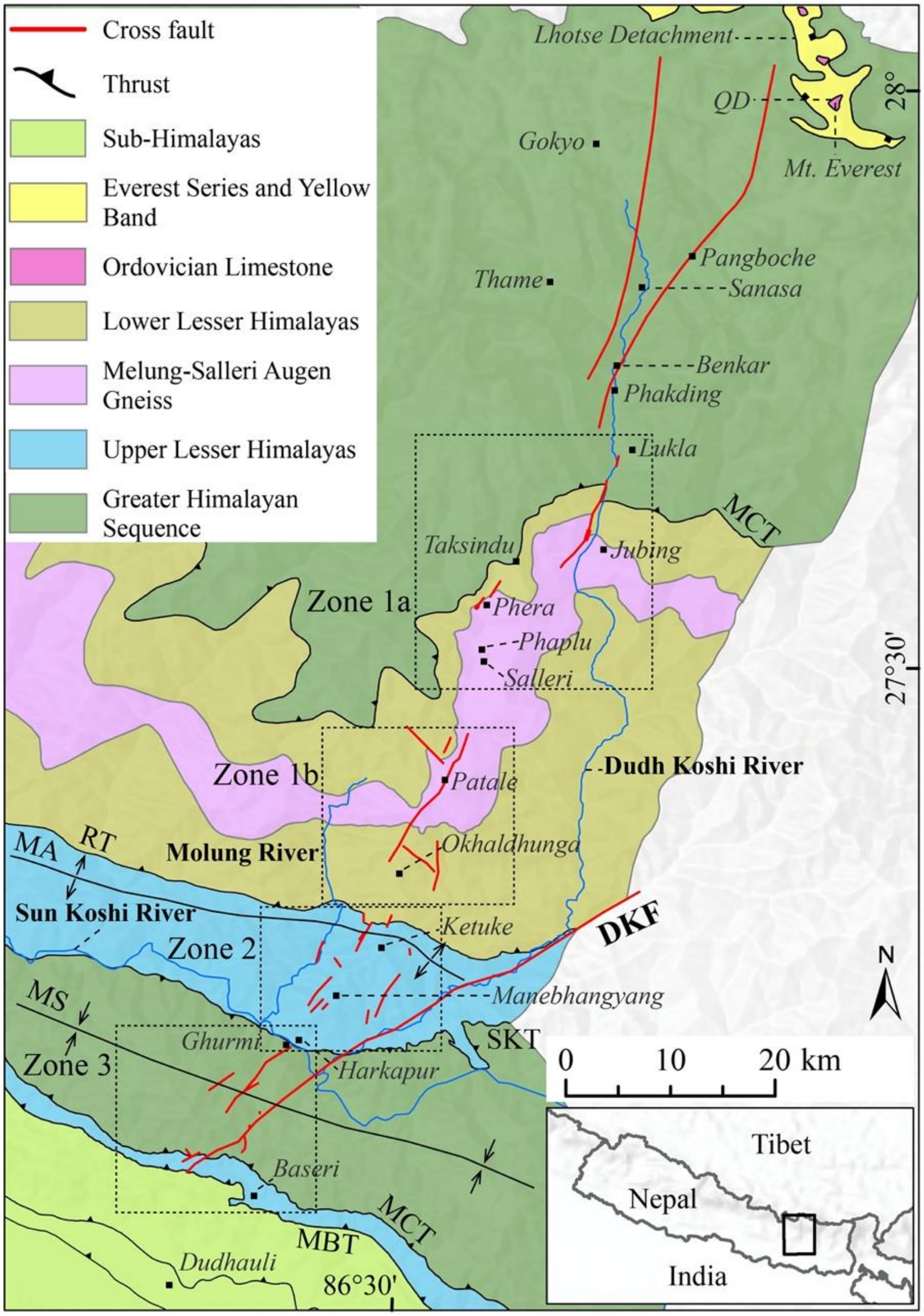

Figure 3.2: Litho-tectonic map of the study area showing the mapped extent of the Benkar Fault Zone. (source: Ishida & Ohta, 1973; Schelling, 1992; Searle et al., 2003; Dhital, 2015). DKF: Dudh Koshi Fault; MA: Midland Antiform; MBT: Main Boundary Thrust; MCT: Main Central Thrust; MS: Mahabharat Synclinorium; QD: Qomolongma Detachment; RT: Ramghar Thrust; SKT: Sun Koshi Thrust.

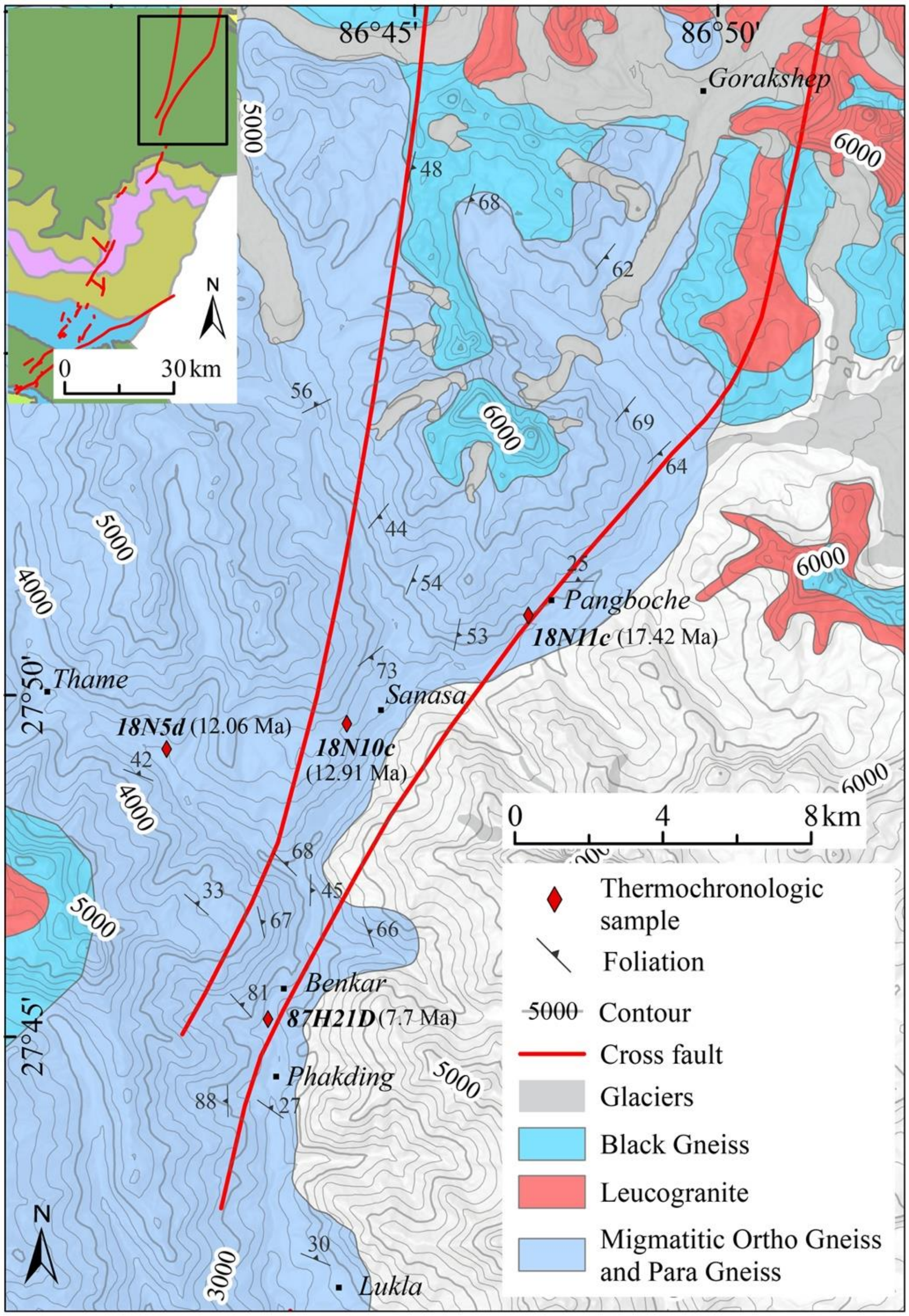

Figure 3.3: Map of the Benkar Fault Zone in the Everest region (source: Seifert (2019)). The inset map has been shown in detail in Figure 3.2. Contour values for all map figures are in meters.

Methods

Geologic Mapping

Our mapping work picks up at the southern limit of Seifert's map and was conducted along an 80 km-long swath between Jubing and Dudhauli and included several additional ~E-W transects within that zone (Figure 3.2). Our final geological maps include partial map data from Ishida and Ohta (1973), Hubbard (1988), Schelling (1992), Dwivedi (1997), Dhital (2015), and Baskota and Adhikari (2019). We have presented relevant structural data including the orientation of bedding and foliation in lower hemisphere, equal area projection by using 'Stereonet 11.5.1' of Rick Allmendinger.

During field work, we looked for evidence of shearing and/or faulting such as breccia, fault gouge, mylonitic rock, offsets markers, topographic lineaments, and deviations in rock fabric orientation. We used Google Earth to locate ~NNE- or ~NE-striking topographic lineament (Appendix A). Upon field investigation, we found out that most of these lineaments are zones with cross fault deformation. To develop a comprehensive understanding of cross faults, it is important to also recognize the regional rock fabric, the surrounding lithology, and the major structural elements. Therefore, we mapped the rocks units adjacent to and outside of cross fault segments wherever possible. Within the Okhaldunga Window, we have prepared a litho-stratigraphic classification for the LHS. This classification is primarily based on our lithological mapping along with previous work of Dhital (2015) and Baskota and Adhikari (2019) and has been guided by the classification scheme of DeCelles et al. (2020).

The biggest challenge in conducting geological mapping in the LHS, especially for cross faults, is the limited availability of rock exposures due to dense vegetation and human alteration of the landscape for agriculture. This situation limits our ability to precisely map contacts and trace cross fault segments along strike. We were able to find some excellent outcrops, however along newly cut road sections. Visual analysis of topographic features in Google Earth images helped to guide our field work.

Kinematic Analysis and Petrography

Oriented and non-oriented petrographic samples were collected from the LHS and the GHK. Standard thin sections were prepared and analyzed with a petrographic microscope. In the field, we measured strike and dip of shear fabric and the trend and plunge of linear features related to deformation such as slickenlines and stretched or aligned mineral lineations indicative of the most recent transport direction. Where possible we determined shear sense in the field or from thin section. Selected kinematic data have been presented on stereonets by using the Fault-Kin software package of Allmendinger. Our kinematic and petrographic analysis have largely been guided by Passchier and Trouw (2005).

$^{40}Ar/^{39}Ar$ Muscovite Thermochronology

In order to get a first order idea of the timing of deformation, we conducted $^{40}Ar/^{39}Ar$ analysis of muscovite in the GHS region to see whether cross fault deformation had enough of a vertical component of offset to place constraints on fault timing. Muscovite aliquots were hand separated from pulverized rock samples. Multiple crystals of muscovite were packed in Al foil, loaded into Al discs, and stacked in a flame-sealed glass vial for irradiation. Standards of FC EK (a recollection of FC-2; Morgan et al., 2014) with an age of 28.294 ± 0.036 Ma (Renne et al., 2011) were placed within wells adjacent to the samples and throughout the entire stack to permit detailed characterization of the irradiation flux both horizontally and vertically. Samples were irradiated in the Cd-lined (CLICIT) facility of the Oregon State University (USA) TRIGA reactor for 0.33 hours.

Ten to twelve grains samples were step-heated until fused with a Photon Machines 55W CO_2 laser. Isotope data were collected using a Nu Instrument's Nobelesse multi-collector mass spectrometer, run in single collector mode. Samples were heated for 5-10 seconds prior to 120 seconds clean-up. Extracted gases were cleaned using 2 GP50 SAES getters (one operated at 450°C and one at room temperature). The extraction, clean up, and data collection processes were entirely automated. Backgrounds ± standard deviations from all blank runs were used to correct isotope abundances. Air calibrations were collected after every six analyses to monitor mass discrimination. A $^{40}Ar/^{36}Ar$ value of 298.56 ± 0.31 was used to correct the data for mass discrimination (Lee et al., 2006). A power law function was used for the mass discrimination correction (Renne et al., 2009). Berkeley Geochronology Centre software 'mass spec' was used to regress and reduce age data using the decay constant of 5.5305×10^{-10} a^{-1} from Renne et al. (2011). The isotope data were corrected for blank, radioactive decay, mass discrimination and interfering reactions. Age uncertainties are reported to 2σ; uncertainties on the isotopic measurements are reported to 1σ.

Results

To best articulate our results, we have divided our study area in three litho-stratigraphic zones (Figure 3.2). Our northernmost zone, zone 1 consists of the Lower LHS between the MCT and the RT. This zone largely coincides with the northern limb of the Midland Anticlinorium. We have sub-divided this zone into zone 1a and 1b to show more detailed maps. We have marked the Upper LHS rocks between the RT and the SKT as zone 2, which forms the southern limb of the Midland Anticlinorium. The Mahabharat Synclinorium, between the SKT and the MBT, forms zone 3 and includes the GHK rocks and slivers of the Upper LHS.

For each zone, we first present brief lithologic and petrographic descriptions of the mapped units and when applicable, associated, major range-parallel structural elements. Subsequently, we present field evidence for the presence of the BFZ within the zone and where possible, augment our field observations with petrographic analysis.

Zone 1: The Lower Lesser Himalayan Sequence

Litho-stratigraphy and petrography Our litho-stratigraphic scheme of the Lower LHS consists of the Okhaldhunga Formation, the Melung-Salleri Augen Gneiss, the Phera Quartzite, and the Khare Formation (Table 3.2; Figure 3.4 & 3.5). We have further sub-divided the Okhaldhunga Formation into the Lower Okhaldhunga Formation, the Barnalu Quartzite, and the Upper Okhaldhunga Formation.

Table 3.2: Litho-stratigraphic classification of the Lesser Himalayan Sequence in Nepal.

<table>
<tr><th colspan="2">DeCelles et al. (2020) and approximate ages in Ma, Western Nepal</th><th>Stöcklin and Bhattarai (1977) ,Central Nepal</th><th colspan="2">This study</th><th>Lithologic description from this study</th></tr>
<tr><td rowspan="5">Upper Lesser Himalayan Sequence</td><td rowspan="4">Lakharpata Formation, 1500-1300 (?)</td><td>Robang Formation</td><td colspan="2" rowspan="2">Harkapur Formation</td><td rowspan="2">Dolomites and silicious carbonates interbedded with phyllites, calc-phyllites, and quartzites
Basic intrusions</td></tr>
<tr><td>Malekhu Limestone</td></tr>
<tr><td>Benighat Slates (with Jhiku Carbonate beds)</td><td colspan="2">Manebhangyang Formation</td><td>Dominated by dark/pitch black, carbonaceous slates along with siltstones, silty slates, quartzites, metasandstones, and silicious dolomites</td></tr>
<tr><td>Dhading Dolomite</td><td colspan="2">Halesi Dolomite*</td><td>Stromatolitic dolomite with black slate partings</td></tr>
<tr><td>Syangia Formation, 1760-1728</td><td>Nourpoul Formation</td><td colspan="2">Ketuke Formation</td><td>Thick to massive beds of arkose quartzites with variegated slaty partings and some granule to pebble-bearing conglomeratic beds</td></tr>
<tr><td rowspan="5">Lower Lesser Himalayan Sequence</td><td>Galyang Formation, <1760?</td><td>Dandagaon Phyllites</td><td colspan="2">Khare Formation</td><td>Phyllites, garnet-bearing graphitic schists, silicious carbonates, marble, staurolite-garnet schist, and amphibolite intrusions</td></tr>
<tr><td>Fagfog Formation, 1770-1760</td><td>Fagfog Quartzite</td><td colspan="2">Phera Quartzite</td><td>Medium to coarse grained quartzites with sub-ordinate amount of mica with thin interbeds phyllites/schists</td></tr>
<tr><td>Lesser Himalayan augen gneiss, 1890-1860</td><td rowspan="3">Kuncha Formation</td><td rowspan="3">Okhaldhunga Formation (OF) and Melung-Salleri Augen Gneiss</td><td>Upper OF</td><td>Phyllites, metasandstone, quartzites, psammitic schists, schistose phyllites, and graphitic schists</td></tr>
<tr><td>Kushma Formation, 1890-1840</td><td>Barnalu Quartzite</td><td>Medium to coarse grained micaceous quartzites with partings of lustrous phyllites</td></tr>
<tr><td>Kuncha/Ranimata Formations 1912-1840?</td><td>Lower OF</td><td>Gritty/silty slates and phyllites plus metasandstone/ metagraywackes
Granitic intrusions</td></tr>
</table>

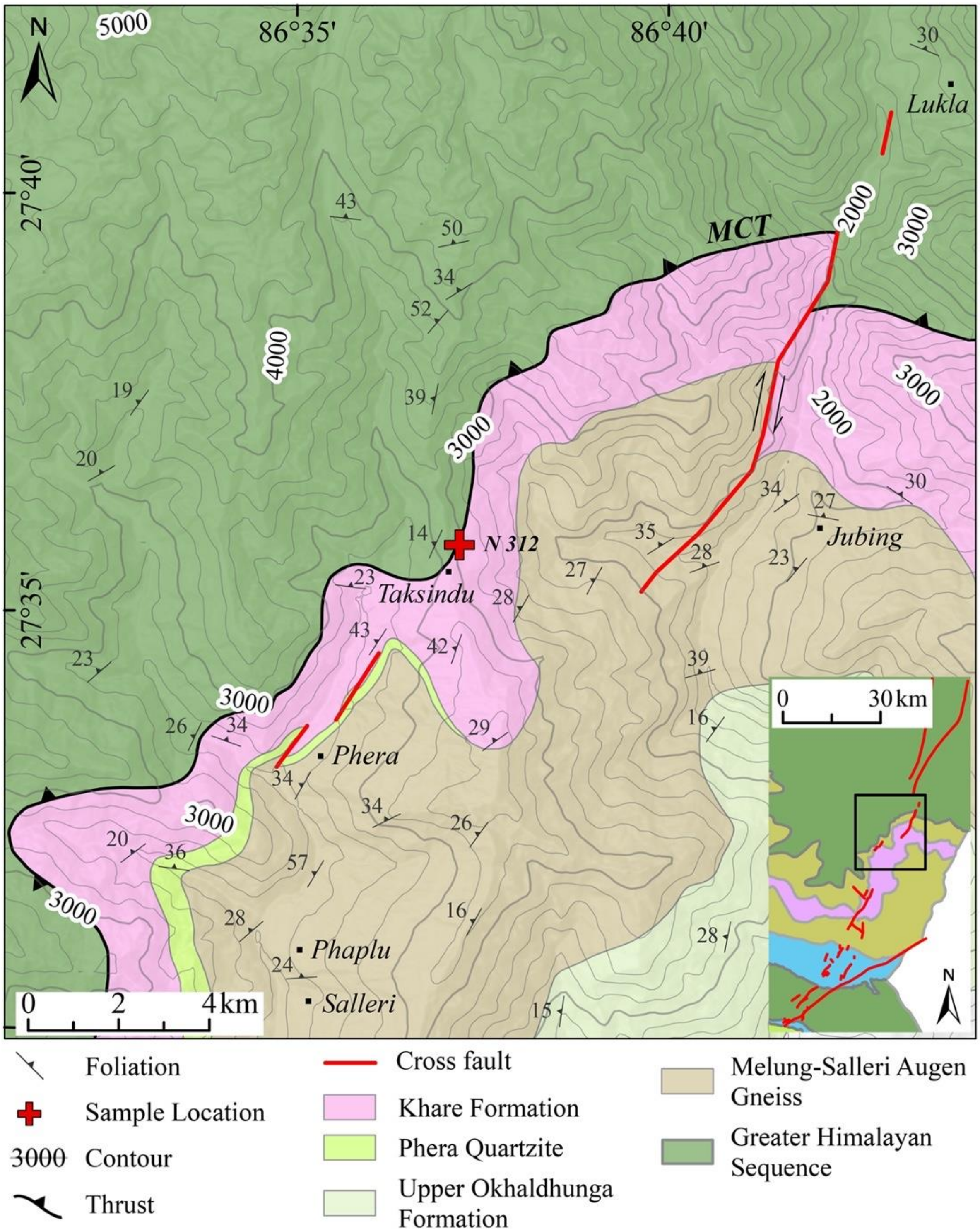

Figure 3.4: Geological map of Zone 1a. Red lines indicate segments of the Benkar Fault Zone. Trace of the MCT between Jubing-Lukla section from Hubbard (1988). MCT: Main Central Thrust. The inset map has been shown in detail in Figure 3.2.

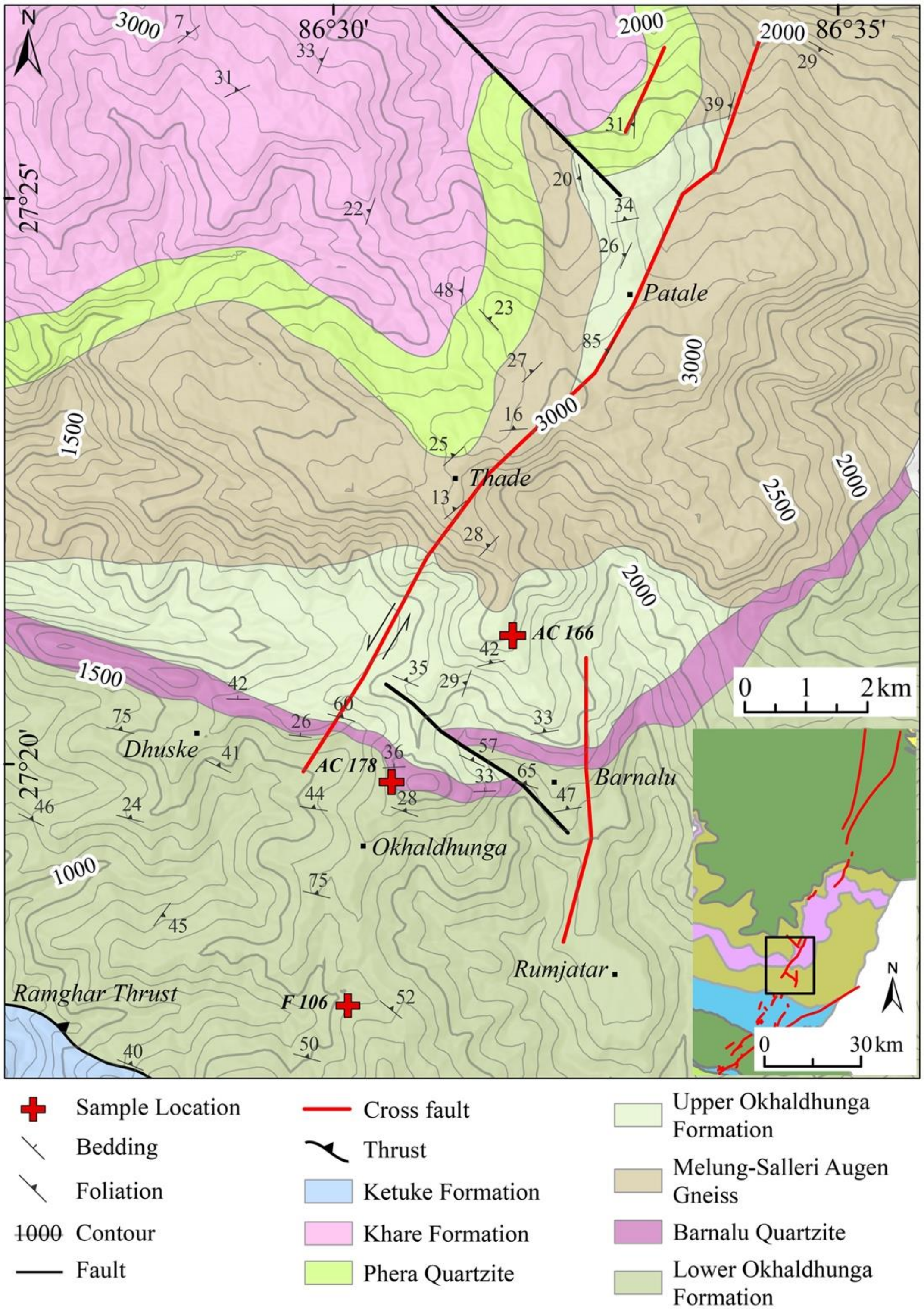

Figure 3.5: Geological map of Zone 1b. Red lines indicate segments of the Benkar Fault Zone. The inset map has been shown in detail in Figure 3.2.

The Lower Okhaldhunga Formation is dominated by gritty/sandy/silty slates and phyllites with frequent beds of metasandstone/metagraywackes. The overlying Barnalu Quartzite consists of micaceous quartzites with thin partings of lustrous phyllite. This unit is overlain by the Upper Okhaldhunga Formation, which is represented by slate, phyllite, metasandstone, quartzite, psammitic schist, schistose phyllite, and graphitic schist. Micaceous quartzite with interbeds of phyllite and schist belonging to the Phera Quartzite rest over the Upper Okhaldhunga Formation. The top-most unit of the Lower LHS is the Khare Formation, which we named after the comparable Khare Phyllite unit of Schelling (1992). The basal section of this unit consists of phyllite and graphitic schist. Laminated silicious carbonates and staurolite-garnet schist in the upper section of this unit have been intruded by amphibolite layers.

Within the Lower LHS, we collected four petrographic samples, one each from the Khare Formation (N312), the Melung-Salleri Augen Gneiss (AC166), the Barnalu Quartzite (AC178), and the Lower Okhaldhunga Formation (F106) (Figure 3.4, 3.5, & 3.6). All of these samples fall outside of the BFZ and reveal the regional, thrust-related, penetrative fabric. The Khare Formation sample (N312) is a garnet-schist (quartz, muscovite, chlorite, biotite, garnet, and plagioclase). This sample displays a strong S/C fabric (thrust-sense along 12˚/342˚ on 001˚/34˚NW foliation), spiral inclusion in garnet, deformation lamellae and chess board extinction in quartz, kinking in plagioclase, and retrograde reaction rims of chlorite on garnets (Figure 3.6a). We interpret this deformation to be related to the MCT. A strong degree of thrust-related shear deformation can also be found in samples from the Melung-Salleri Augen Gneiss (AC 166) and the Lower Okhaldhunga Formation (F106). Sample AC166 comes from an outcrop of granitic schist (quartz, plagioclase, muscovite, orthoclase, biotite, chlorite) (Figure 3.6b). In

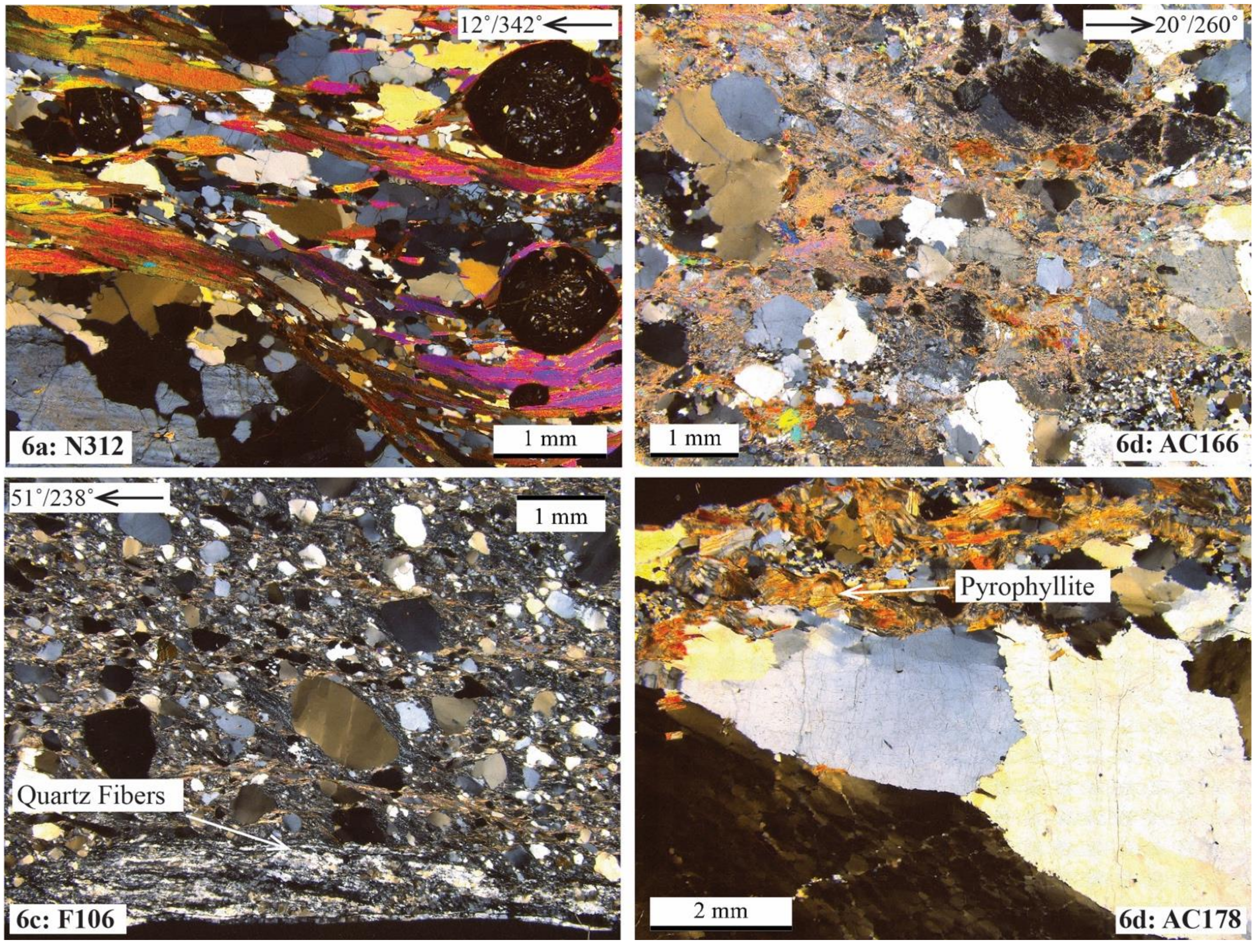

Figure 3.6 : Petrographic sections from Zone 1a). Khare Formation, b) Melung-Salleri Augen Gneiss, c) Lower Okhaldhunga Formation, and d) Barnalu Quartzite. Oriented sections are right way up. Arrows indicate downdip lineation direction.

thin section, we note undulose and sweeping extinction and sub-grains in quartz, several bulging grain boundaries, domains with strong grainsize reduction, and domains with relatively less intense deformation. Microstructures are consistent with an oblique thrust-sense movement along a plunge of 20° along an 260˚ trend on a 055˚/40˚NW foliation surface. The sample F016 thin section shows a fine-grained matrix of chlorite and muscovite surrounding coarser quartz clasts with tails, which suggests some degree of mylonitization and/or fluid involved deformation (Figure 3.6c). In an outcrop of the Barnalu Quarzite, we saw a small lens (a few centimeters long) of fibrous, lustrous, pale blue mineral, which we interpret to be pyrophyllite (AC178) (Figure 3.6d).

The Main Central Thrust and the Benkar Fault Zone The MCT is the northern fault boundary of zone 1. Understanding the cross-cutting relation between the BFZ and the MCT is crucial in defining the genesis of the BFZ because if the BFZ was to terminate at the MCT then the BFZ would most likely have been a tear fault related to the MCT. Since this work is aimed at mapping possible offset along the MCT, we follow the lithological boundary definition of the MCT, whereby the MCT follows the lithological contact between Khare Formation (see Table 3.2) of the LHS and ortho/para gneissic belonging to the GHS (Brunel & Kienast, 1986; Schelling, 1992; Pognante & Benna, 1993).

The regional fabric orientation in the vicinity of the MCT, west of the Dudh Koshi river, differs from the regional fabric orientation east of the Dudh Koshi river and from further towards the south (Figure 3.7). East of the Dudh Koshi river, fabric related to the MCT dip 30˚-60˚ towards N or NNE (Hubbard, 1988). Towards the west, the MCT makes a strong, counterclockwise bend and assumes a gentle, westward dip (Figure 3.7a) before switching back to a gentle northward dip further towards the west (Schelling, 1992). These changes in the structural grain of the MCT has been interpreted to reflect broad, NS-trending folds in the LHS (e.g.; Hubbard, 1988). East of the Dudh Koshi river, we have marked the MCT along the lithological boundary between the GHS and LHS of Hubbard (1989). West of the Dudh Koshi river, the corresponding lithological contact passes through just north of Taksindu, where garnet-schists, belonging to the Khare Formation, have been overlain by garnet bearing silicate gneiss and mica-schist. By utilizing a dark, graphitic schist unit that occurs in the basal levels of the

Khare Formation and extrapolating this basal contact based on observed dip domains, we infer a 2km right lateral offset in the MCT (Figure 3.4).

Evidence for the Benkar Fault Zone in Zone 1 Within zone 1, we were able to recognize and map several exposures of cross fault segments (Figure 3.8). A ~70m wide brecciated zone is exposed on a road cut section near the Phera village (Figure 3.4 & 3.8a). Within the breccia zone strongly deformed graphitic schists are juxtaposed against brecciated quartzites. Foliation orientation in the graphitic schist is 326˚/35˚NE, which differs from the regional thrust-related rock fabrics that are gently dipping towards the west (Figure 3.8a). Multiple shear planes within this zone display a NNE-strike (012˚/63˚SE).

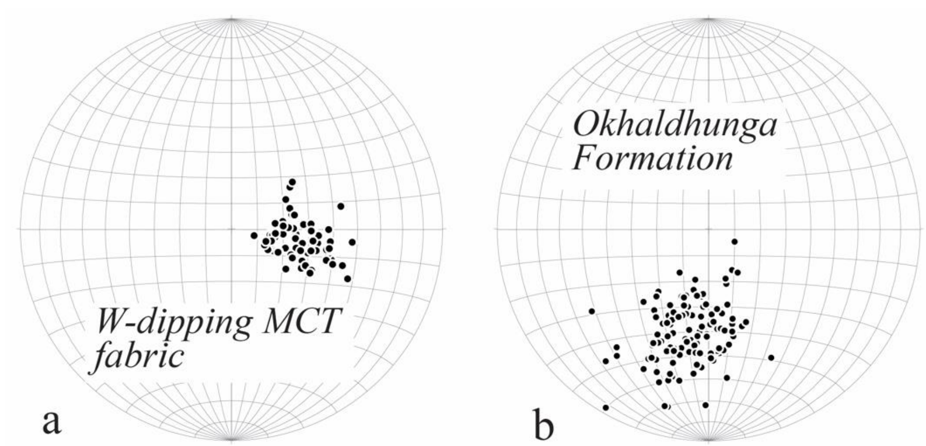

Figure 3.7: Poles to the regional foliation fabric in Zone 1.

About 2.5 km NNW from the town of Okhaldhunga, a nearly 250 m-wide, distinct topographic depression runs across an EW-trending quarzitic ridge. Within this zone, the north-dipping rocks of the Barnalu Quartzite have been sharply truncated by a >10 m thick gouge zone (Figure 3.8b). The contact between the gouge zone and the beds has an orientation of

210˚/70˚NW. Slip related lineations suggest movement along 19˚/217˚ in a dextral, thrust sense. While we did not observe a noticeable offset along this unit, we note that the unit becomes quite thin in the vicinity of this fault zone. Along the strike of this fault and towards the north, we document steep, W-dipping fault segments around Patale village (Figure 3.8c). A NNE-striking linear valley continues towards north from Patale to a west-flowing drainage, where the lineament truncates against a cliff. We interpret this lineament to be a topographic expression of a cross fault segment.

Towards the west from the aforementioned gouge zone, the Barnalu Quartzite is jointed but remains relatively undeformed. Towards the east, however, this unit has been sheared and jointed along multiple orientations across a distance of 600 m. The pyrophyllite bearing sample, AC178, was collected from an exposure within this sheared zone. Along the road section from Okhaldhunga to Rumjatar, this quartzite unit abruptly terminates against pelitic rocks belonging to the Lower Okhaldhunga Formation in a left lateral sense of shear with an offset of about 700 m (Figure 3.5). Based on the topographic expression, this fault most likely has a NW-SE trend. We did not find kinematic indictors related to this fault. However, we noted traces of this fault in the Upper Okhaldhunga Formation, which has been expressed as <1 m thick, sub-parallel, steep, brecciated zones (000˚/71E) that cut into the regional foliation. Just to the north of Rumjatar, we saw multiple exposures of cross faults that run into regional bedding/foliation planes (Figure 3.8d). These small-scale cross faults can be traced into the western, NS-striking boundary of the Rumjatar terrace. This terrace is an anomalous feature because the discharge of the accompanying stream is too small to create such a large terrace. It can be argued that the terrace is a tectonic feature and represents the footwall of a west-dipping normal fault.

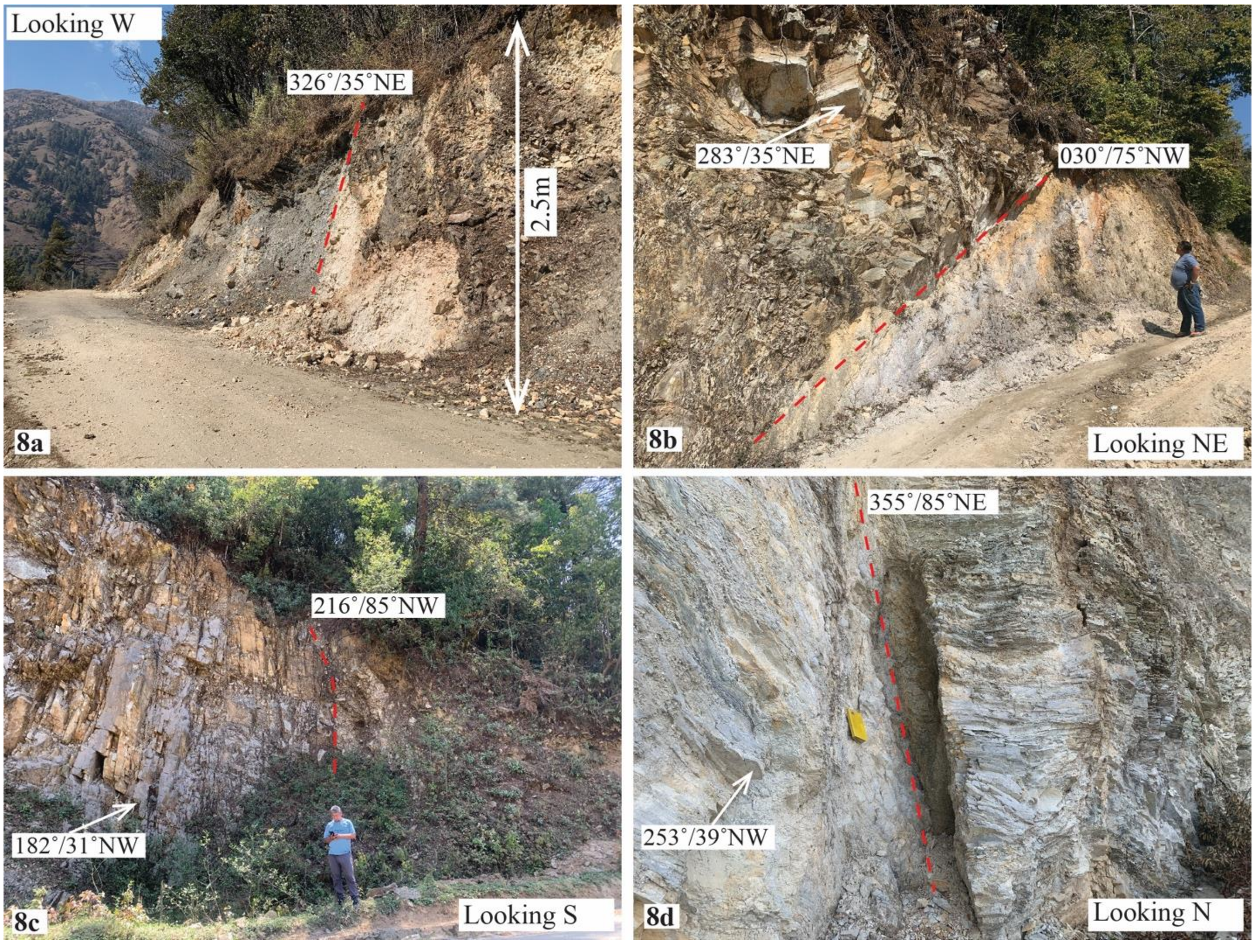

Figure 3.8: Exposures of cross faults in Zone 1. Red dashed lines indicate fault planes. a) Breccia zone near Phera, b) Gouge zone in the Barnalu Quartzite, c) Fault breccia in the Phera Quartzite, and d) Fault gouge in the Upper Okhaldhunga Formation.

Zone 2: The Upper Lesser Himalayan Sequence

Lithostratigraphy, Major EW-trending Faults, and Petrography The Upper LHS consists of the Harkapur Formation, the Halesi Dolomite, the Manebhangyang Formation, and the Ketuke Formation (Table 3.2; Figure 3.9). The Ketuke Formation is the oldest unit of the Upper LHS. This unit consists of thick to massive beds of multi-colored arkose quartzites interbedded with variegated slaty partings and a few granule to pebble-bearing conglomeratic beds. Around Ketuke, this unit is exposed along an east-west trending ridge with a gentle northern face and steep southern face. The Manebhangyang Formation overlies the Ketuke Formation along a transitional contact. The basal section of the formation consists of slates, siltstones, silty slates, quartzites, metasandstones, and silicious dolomites. Towards the upper section the succession is dominated by dark/pitch black, carbonaceous slates interbedded with slates and carbonates. The overlying Harkapur Formation consists of dolomites, silicious carbonates, calc-slates, phyllites, calc-phyllites, and quartzites along with frequent basic intrusions. Towards the east of zone 2, Dhital (2015) and Baskota and Adhikari (2019) have mapped the stromatolitic Halesi Dolomite between the Harkarpur Formation and the Manebhangyang Formation.

Regional rock fabric for zone 2 is presented in Figure 3.10. Both the Harkapur and Manebhangyang Formations are exposed in the south-dipping limb of the Midland Anticlinorium (Figure 3.10a). The Ketuke formation forms the core of the anticlinorium and has both north- and south-dipping limbs, in addition to NS-striking cross fault related domains (Figure 3.10b).

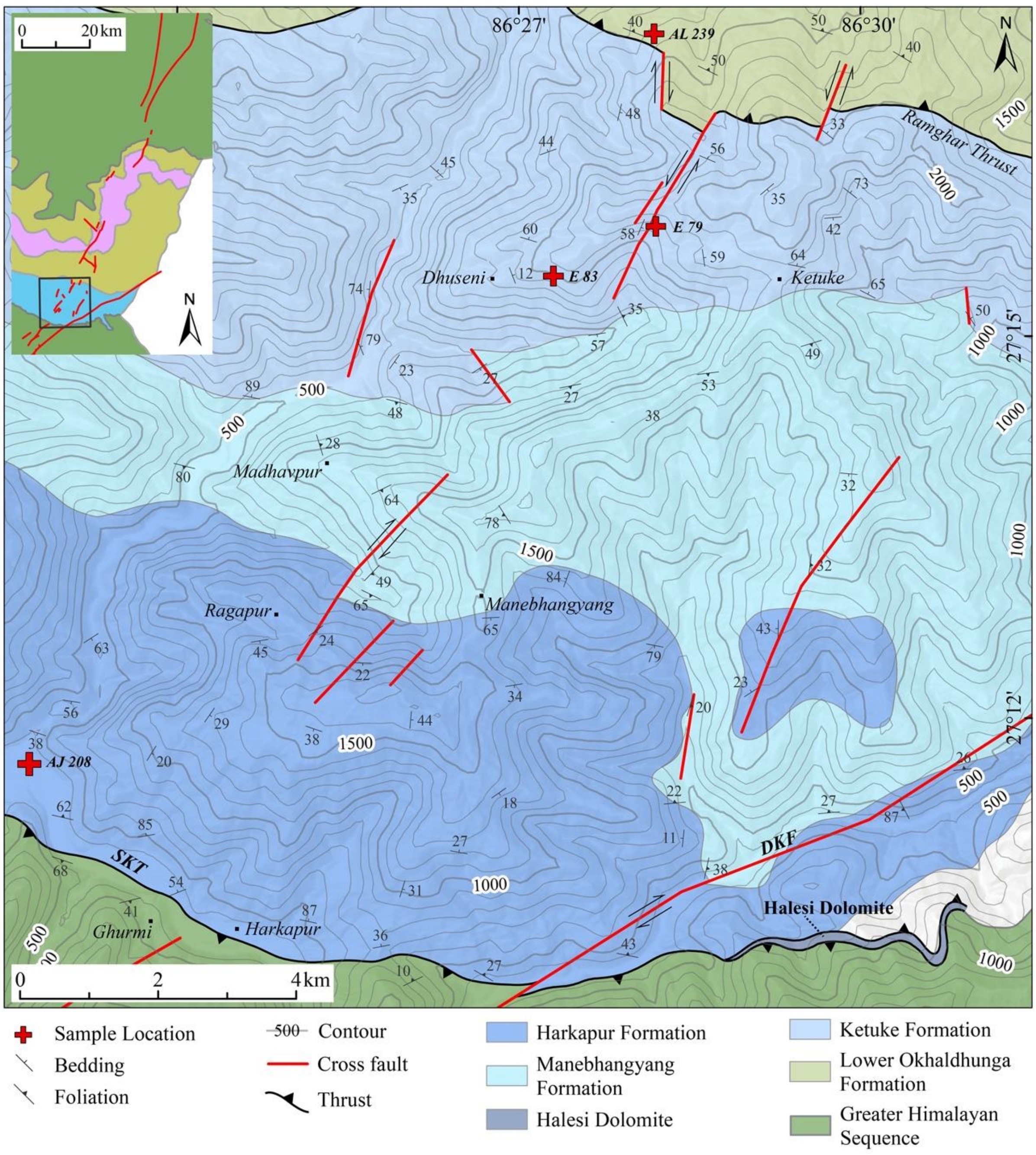

Figure 3.9: Geological map of zone 2. Red lines indicate segments of the Benkar Fault Zone and the Dudh Koshi Fault. Some map elements adopted from Ishida and Ohta (1973), Dhital (2015), and Baskota and Adhikari (2019). The inset map has been shown in detail in Figure 3.2. DKF: Dudh Koshi Fault; SKT: Sun Koshi Thrust.

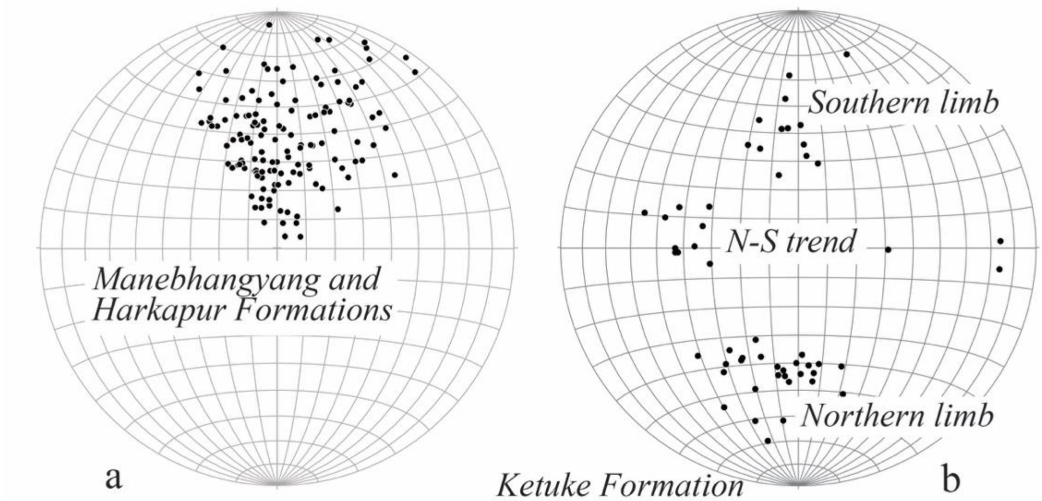

Figure 3.10: Poles to the regional foliation fabric in Zone 2.

The Ramghar Thrust (RT) within the Okhaldhunga window is a north-dipping fault that places the Lower Okhaldhunga Formation over the younger Ketuke Formation (Figure 3.9). While the RT accommodates the majority of shortening within the Lesser Himalayan fold and thrust belt, as demonstrated throughout the Himalaya, a significant component of shortening has also been taken up in shearing and folding at smaller, even microscopic, scales. The RT corresponds to the Taluwa Danda Thrust of Baskota and Adhikari (2019). The Taluwa Danda Thurst has been interpreted to fold over the Ketuke Formation and wedge into the contact the between the Ketuke Formation and the Madhavpur Slates. Because of the structural complexity and lack of field evidence related to this interpretation, we have not adapted this idea in our final map.

We have mapped the SKT as the south-dipping, southern continuation of the MCT and not as an out-of-sequence thrust as suggested by Schelling (1992). Immediately to the north of the SKT, the Harkapur Formation, footwall to the SKT, has been folded into a tight EW-trending synform. Mapping work of Dhital (2015) and Baskota and Adhikari (2019) indicate a juxtaposition of the Halesi Dolomite with the Harkapur Formation and the GHK rocks. These pieces of evidence could potentially support a presence of a north-dipping thrust that could have exhumed slivers of the Halesi Dolomite.

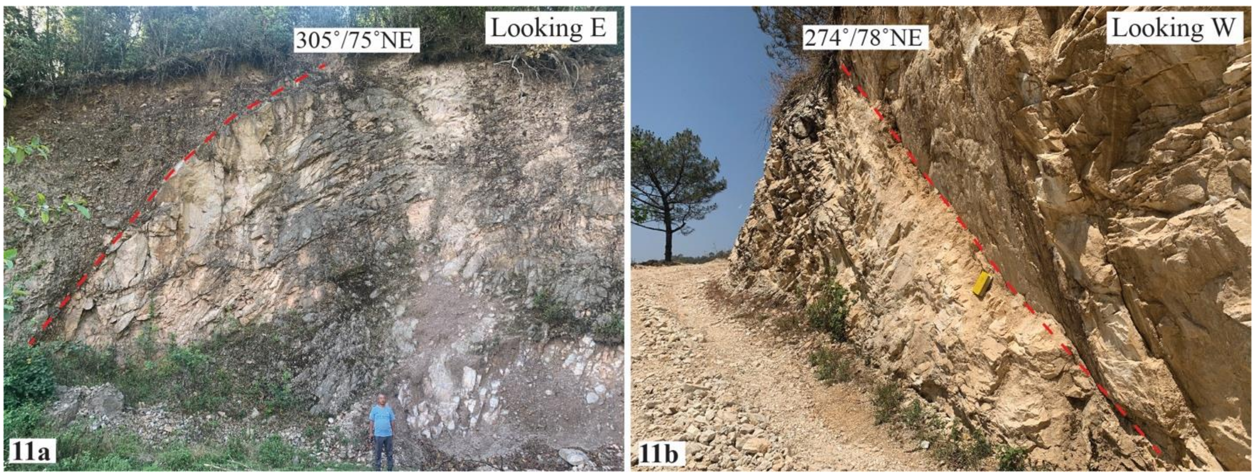

Figure 3.11: Exposure of normal faults within the Ketuke Formation, Zone 2. Red dashed lines indicate fault planes.

We also observed multiple exposures of normal faults within the Okhaldhunga Window (Figure 3.11). Just to the south of the Ramghar Thrust, a beautiful exposure of a normal fault (319˚/75˚ NE) can be seen within the Ketuke Formation. This normal fault has a dragging effect in the footwall rocks while the hanging wall rocks have been brecciated into pebble-cobble sized fragments (Figure 3.11a). Multiple segments of normal faults can also be seen in other locations within the Ketuke Formation (Figure 3.11b) and in the Lower Okhaldhunga Formation. The sample F106, from the Lower Okhaldhunga Formation, records deformation related to normal faulting in addition to thrust-related deformation. This sample was collected from a slickenside hosted by gritty phyllite. The penetrative regional, thrust-related fabric has been obliquely cut by quartz fibers, which show a sinistral-normal movement along 51˚/238˚ on 085˚/70˚SE slickenside.

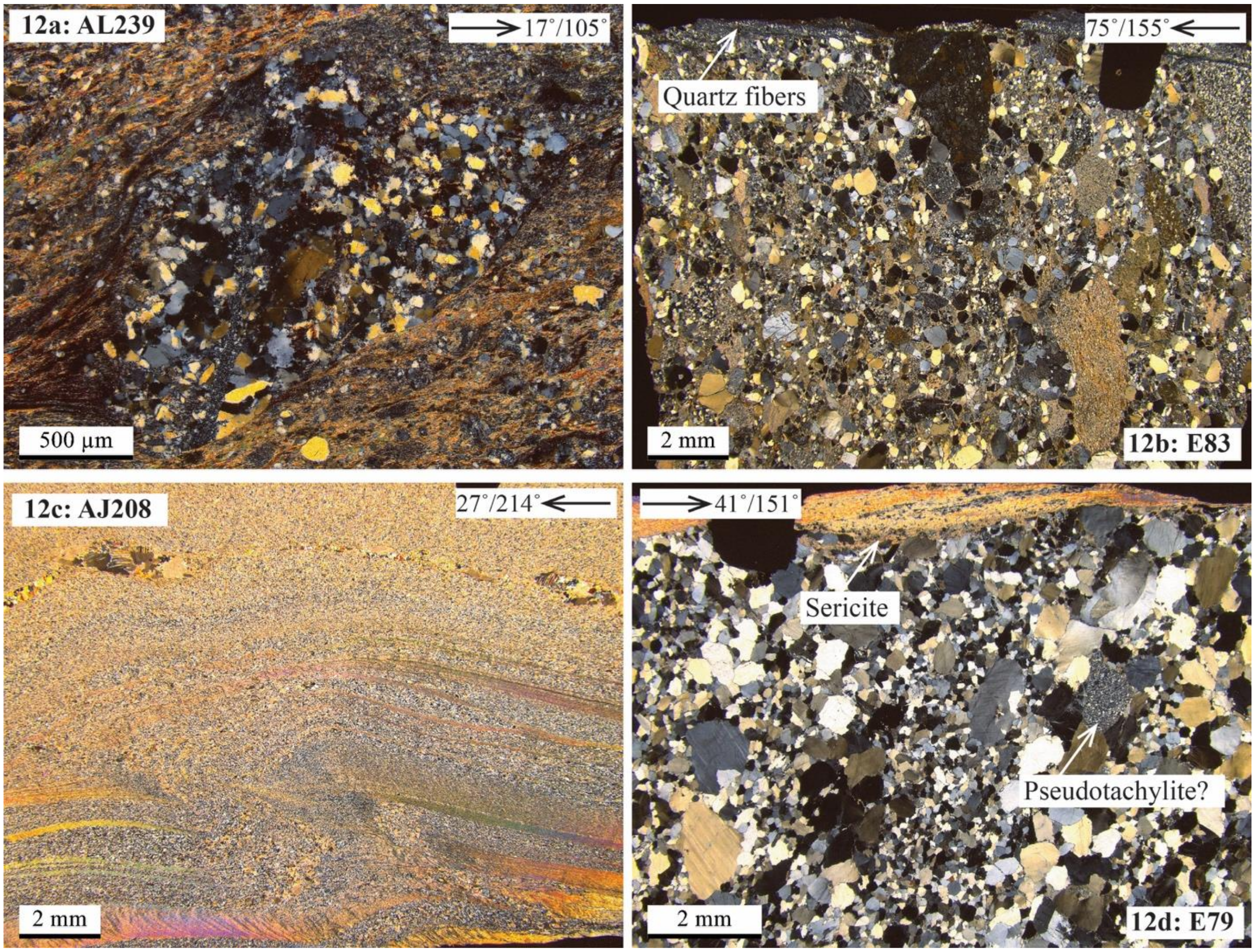

Figure 3.12: Petrographic sections from Zone 2. Sections shown in ‘a’, ‘b’, and ‘d’ are from the Ketuke Formation and shown in ‘c’ is from the Harkapur Formation. Oriented sections are right way up. Arrows indicate downdip lineation direction.

We collected three petrographic samples (E79, E83, AL239) from the Ketuke Formation and one sample (AJ210) from the Harkapur Formation (Figure 3.9 & 3.12). All samples, except E79, were collected from outside the BFZ. Sample AL239 was collected from strongly sheared granule-bearing slate from just to the south of the RT (Figure 3.12a). In thin section, this sample reveals multiple sigma clasts, within which grainsize has been strongly reduced. These sigma clasts suggest an extensional deformation along 17˚/105˚ on 140˚/28˚NE foliation, which is likely related some of the EW-striking normal faults described in the previous section. Sample E83 was collected near Dhuseni from an exposure of conglomeratic cataclasite containing an EW-striking slickenside (Figure 3.12b). This sample consists of quartz, plagioclase, and orthoclase in a glassy matrix and quartz fibers make up the slickenlines. In this sample, we interpret an earlier phase of grainsize reduction, pervasive deformation followed by a younger deformation phase. The latter occurred along 75˚/155˚ on 105˚/78SW in a normal sense of movement. The southernmost sample from zone 2 consists of quartz, calcite, and muscovite and displays an excellent fault propagation fold in thin section (Figure 3.12c). Petrography of sample E79 (Figure 3.12d) will be discussed in the next section in relation to cross faults.

<u>Evidence for the Benkar Fault Zone in Zone 2</u> Zone 2 also hosts excellent exposures of cross fault segments. Within the Ketuke to Dhuseni road cut, cross fault related deformation has been exposed in a ~500 m thick, NNE-striking, brittle zone. Within this zone, quartzite beds of the Ketuke Formation have been brecciated and gouged by ~NS- and NNE-striking deformation planes (Figure 3.13a & 3.13b). A prominent, NNE-striking gully is located within this zone, which we interpret to be a topographic lineament related to cross faulting. Several ~W-dipping slickensides indicate a normal, left-lateral motion towards ~SSW and ~E-dipping slickensides suggest a normal, right-lateral movement towards ~SSE (Figure 3.14a). Dip amount for these slickensides vary between 45˚-70˚ and the slickenlines plunge between 05˚-25˚. Slickenlines are made up of quartz and sericite mineral fibers as seen in the sample E79. A petrographic section of E79 reveals broken and diffused grain boundaries along with wavy and bent deformation

lamellae in quartz grains (Figure 3.12d). Anastomosing micro-faults run across quartz grains with a minor reverse-sense offset. The foliation, imparted by quartz grain size, has been cut by fibers of sericite, which in outcrop display a dextral, normal sense of movement along 41˚/151˚ on 034˚/45˚SE slickenside. Sericite mineralization has largely been localized within the slip surface, but some mineralization can be also noted within the nearby grain boundaries between quartz grains. We also note one anomalous grain with smaller grains, which is possibly a clast of pseudotachylite.

While cross fault related deformation dominates the Ketuke-Dhuseni road section, we also noted a few exposures of EW-trending, steep, outcrop-scale normal faults (Figure 3.11b). Kinematic indicators suggest stronger normal components on some faces and dominant strike-slip component on others (Figure 3.14b).

Towards the north, the cross fault deformation zone continues across the ridge and emerges on the other side, where we mapped ~300 m of left-lateral offset across a NNE-striking cross fault segment along the north-dipping thrust boundary between the Ketuke and the Lower Okhaldhunga Formations (the RT). Cross faulting in this region likely took place in a series of events with changing sense of movements. Similar offsets can also be noted in topography as the east-west-trending quarzitic ridge make abrupt clockwise as well as counter-clockwise bends. In the vicinity of these fault segments, rocks belonging to the Ketuke Formation have been rotated into NS-trending blocks (Figure 3.10b).

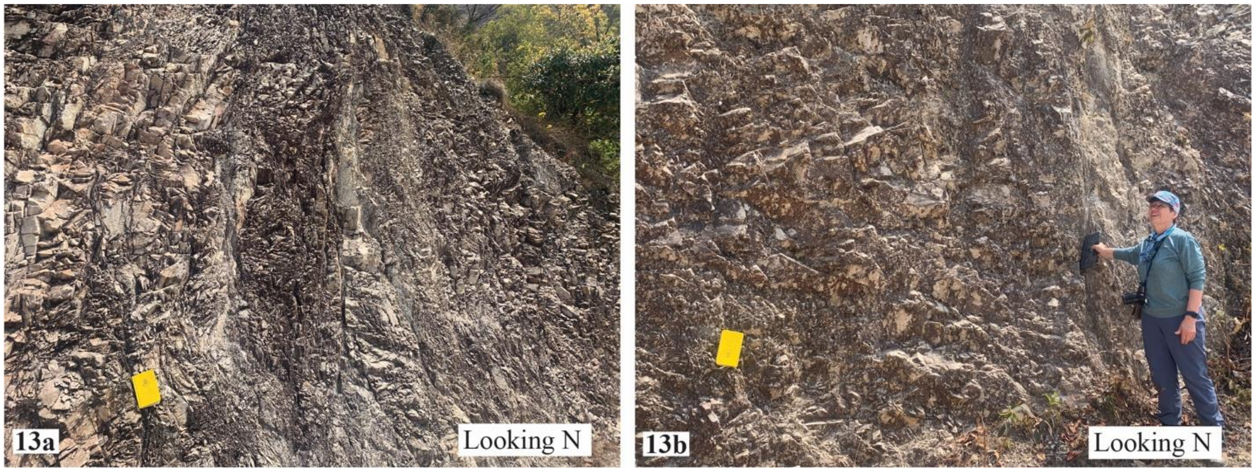

Figure 3.13: Exposures of cross fault zones in the Ketuke Formation.

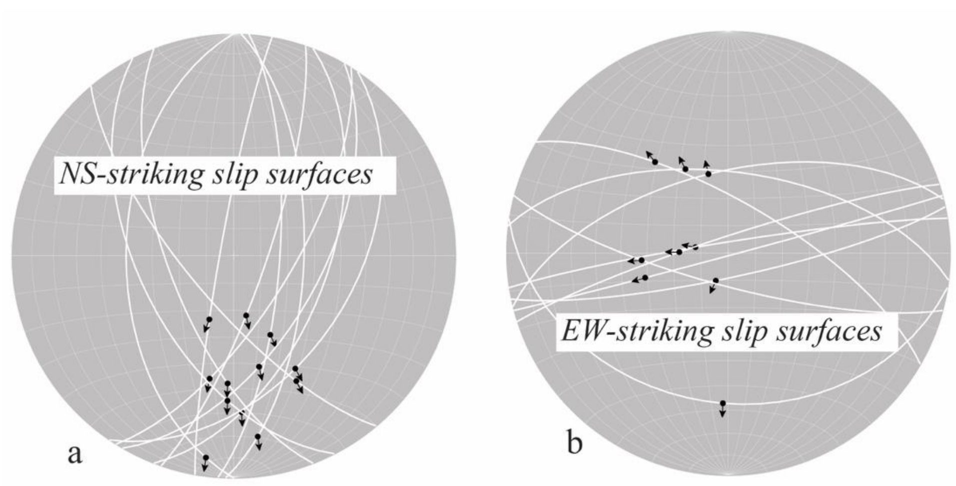

Figure 3.14: Kinematic data from the Ketuke Formation. White lines are slickenside planes and arrows indicate hanging wall movement direction.

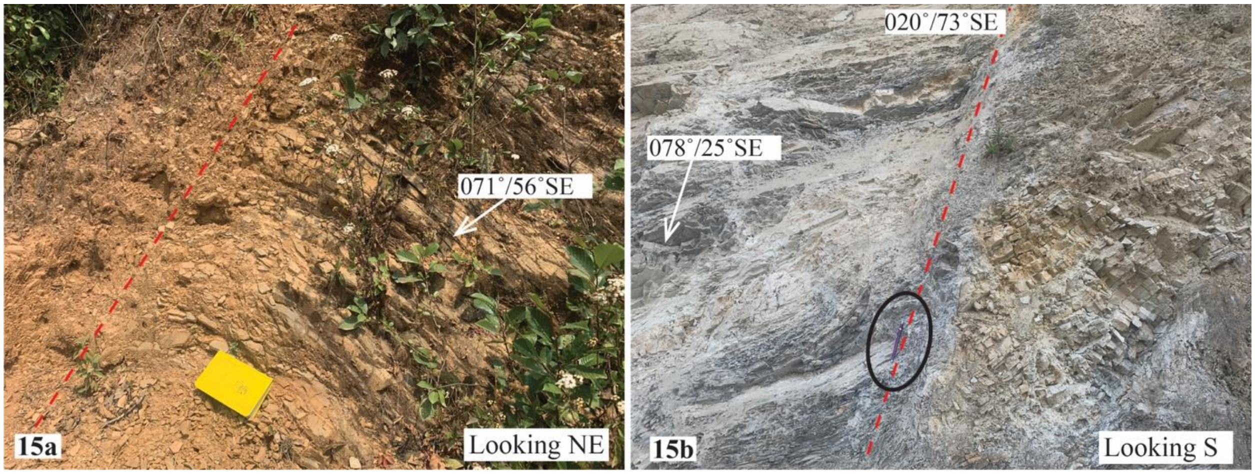

Figure 3.15: Exposures of cross faults in; a) Manebhangyang Formation and b) Harkapur Formation. Pencil for scale in '15b' is enclosed in an ellipse.

Cross fault related deformation can also be seen in the Manebhangyang and Harkapur Formations (Figure 3.15). Towards the south-east from Ketuke, we see multiple NNE-trending gullies in aerial images. Across some of these gullies, ridge crests abruptly change their trends. In an outcrop near one of such gullies, rock units (belonging to the Manebhangyang Formation) have been folded on the western side and abruptly terminate against a NNE-trending fault zone (Figure 3.15a). Based on this exposure, we interpret the other sub-parallel gully features to be fault-related. Towards the southwest from Ketuke, the Manebhangyang Formation shows a higher degree of shear deformation and quartz vein intrusions in the road section west of Manebhangyang (towards Madhavpur) than we saw to the east. Along this section rock units show a NNE-striking foliation, while the same unit shows an EW-trend along both the Molung Khola and the Dudh Koshi river transects. Across an EW-trending river valley towards the south, exposures of cross faults cut into the foliation planes of carbonate rocks belonging to the Harkapur Formation along a 1500 m road section between Ragapur and Manebhangyang. These faults appear as ≤ 1m-thick gouge zones and can display both normal and reverse sense of shear with up to a meter of offset (Figure 3.15b). Our mapping suggests a possibility of up to 500 m of right lateral offset along the contact between Manebhangyang and Harkapur Formations.

Zone 3: The Greater Himalayan Klippe

Lithostratigraphy and Petrography While we recognize the difficulties in establishing a stratigraphy in a high-grade metamorphic zone, we are adopting the classification scheme of Dwivedi (1997) to better visualize possible offsets along cross faults and to outline the structural framework of the GHK (Table 3.1, Figure 3.16). Regional foliation within the GHK has been presented in Figure 3.17. Figures 3.17a and 3.17b represent foliation data from the northern and southern limb of the Mahabharat synclinorium respectively.

Like in central Nepal, the GHK in our study area consists of the Kathmandu Complex rocks as well as injection gneisses and granites. Figure 3.18 shows representative petrographic sections from zone 3. Around the town of Ghurmi, a peculiar augen gneiss (quartz, muscovite, chlorite, orthoclase, plagioclase, and garnet) is seen, which has also been exposed in the southern flank of the synclinorium. From a distance this unit appears to be massive beds of quartzite and only upon close inspection reveals gneissic fabric along with quartz and feldspar augens. In petrographic section, this gneissic unit (sample AT333, Figure 3.18a) shows quartz delta clasts, strong grain size reduction, elongation of quartz grains parallel to foliation, and sub-grains formed along boundaries of larger quartz and orthoclase grains. The northern flank of the synclinorium is dominated by banded gneiss, paragneiss, and silicate gneiss. Garnets, often in pelitic lenses, lenses of biotite rich pods, and up to 5mm wide muscovite flakes are typical in the lower levels. Gneissic fabric along with parallel and oblique quartz veins, some >1 m in thickness, have been folded into isoclines with the axial plane parallel to the regional foliation. A sample, C57, collected from just to the south of SKT consists of clinopyroxene (plus quartz, plagioclase, and biotite, Figure 3.18b), which indicates that there are a few basic layers within these generally felsic rocks. The core of the Mahabharat synclinorium is dominated by augen gneiss, granite, and granitic gneiss along with minor occurrences of schist and calc-silicate gneiss and pegmatite intrusions and leucocratic lenses. Clasts in the augen-gneiss, some up to 4 cm in diameter, are dominantly of quartz and feldspar and can have stretched tails.

A petrographic sample, AR306, was collected from the Chisapani Quartzite of the Bhimphedi Group from the southern limb of the synclinorium. Microscopic section of this strongly sheared sample shows grain shape preferred foliation along with some bulging grain boundaries and pinning of quartz grains by muscovite (Figure 3.18c). Garnet-bearing silicate gneiss, biotite-paragneiss, and granite are common in the vicinity of the southern strand of the MCT. Up to 1 cm wide garnets can be seen in gneissic rocks around Jinakhu. These garnets, as seen in sample A26, consist of voluminous inclusions of quartz and biotite indicating a rapid growth (Figure 3.18d). Delta clast garnets and dominant S/C fabric seen in petrographic section of A26 suggests an extensional deformation along 55˚/347˚ on 125˚/65˚NE foliation.

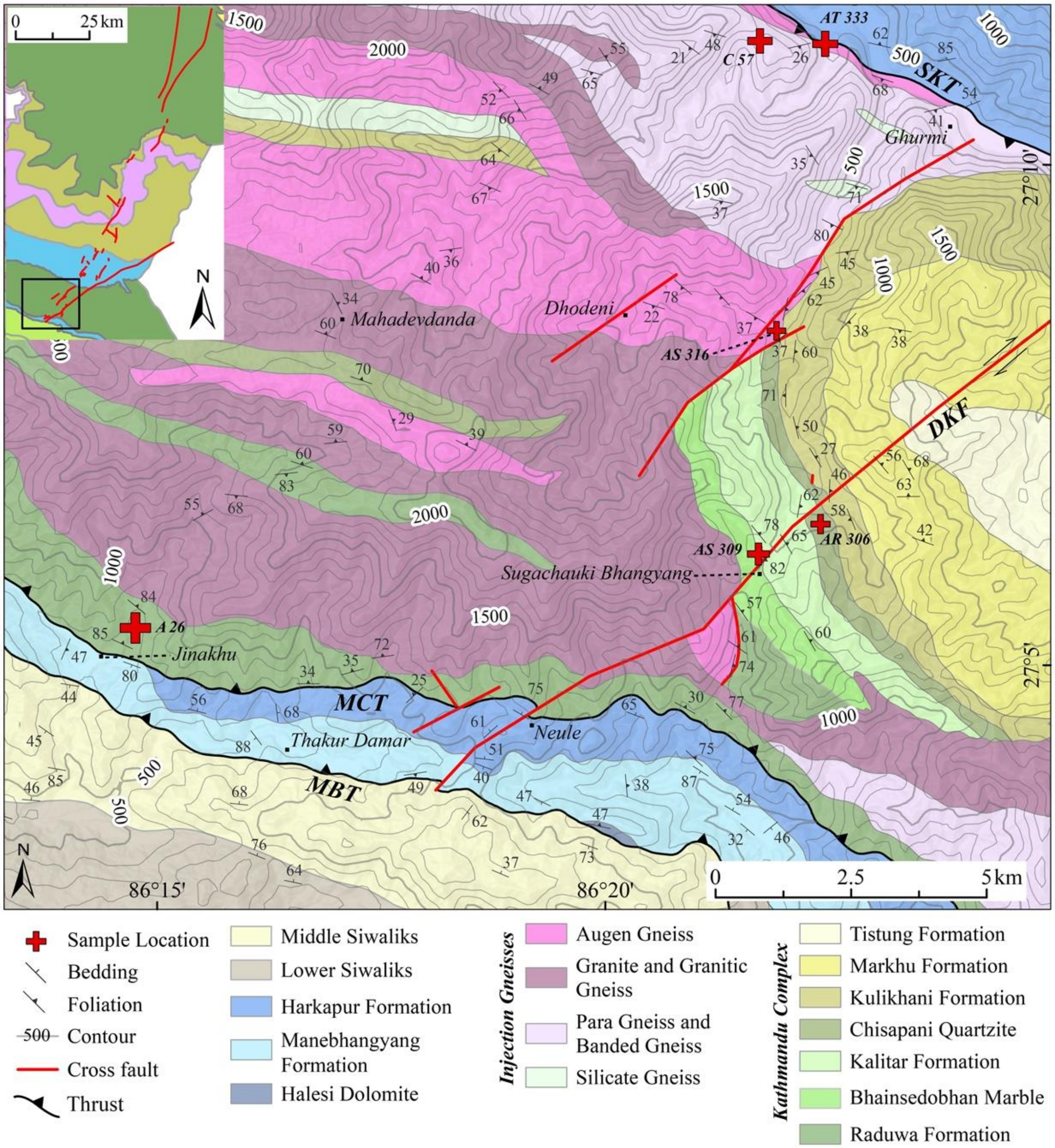

Figure 3.16: Geological map of Zone 3. Red lines indicate segments of the Benkar Fault Zone and the Dudh Koshi Fault. (source: Ishida & Ohta, 1973; Schelling, 1992; Dwivedi, 1997; Dhital, 2015). The inset map has been shown in detail in Figure 3.2.DKF: Dudh Koshi Fault; MBT: Main Boundary Thrust; MCT: Main Central Thrust; SKT: Sun Koshi Thrust.

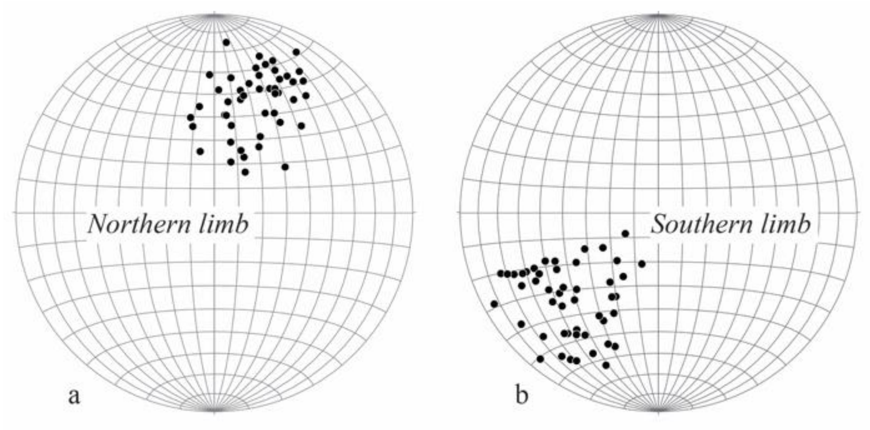

Figure 3.17: Poles to the regional foliation fabric in zone 3.

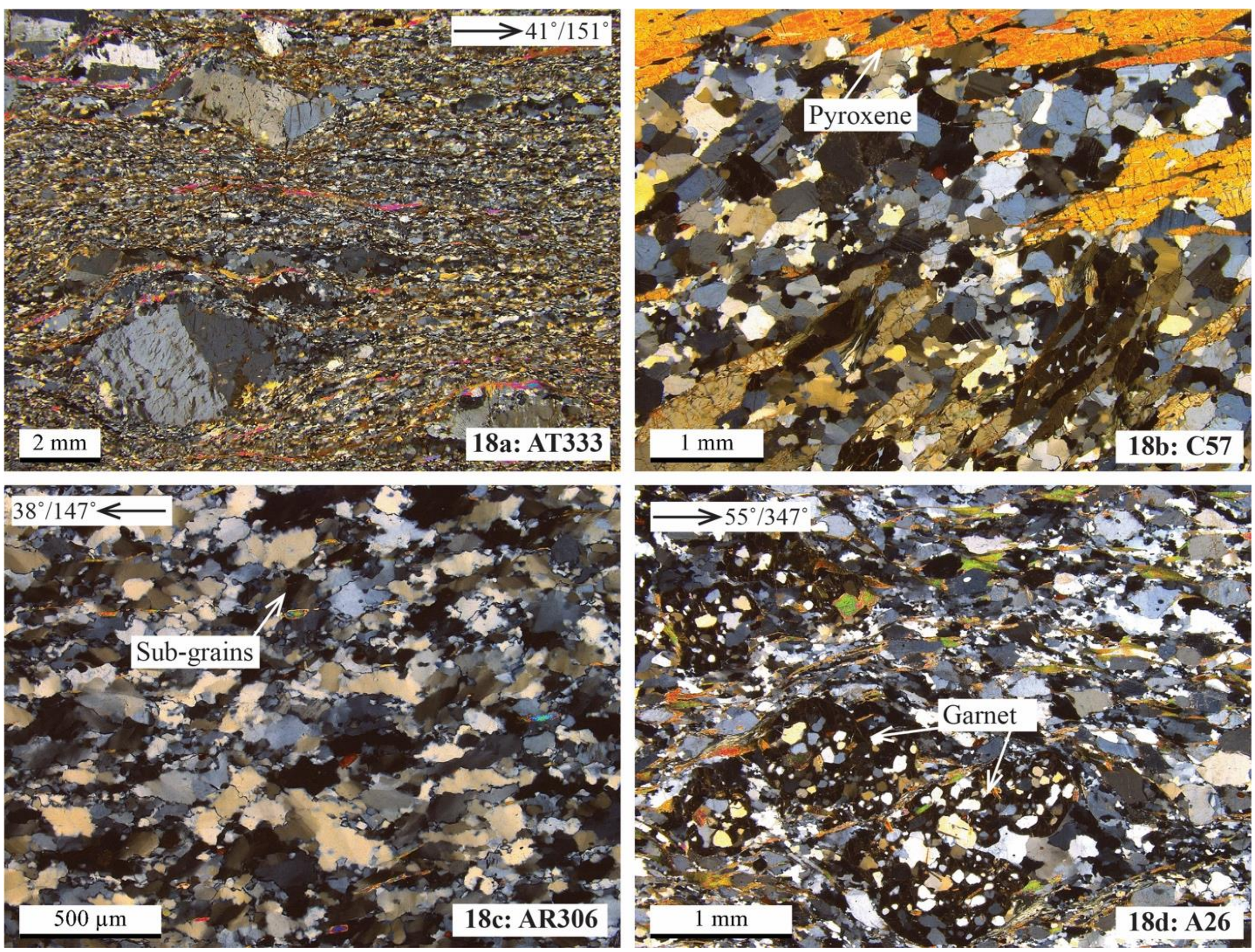

Figure 3.18: Petrographic sections from the Greater Himalayan Klippe rocks. Sections shown in 'a' and 'b' were collected from Injection Gneisses near Ghurmi, shown in 'c' from the Chisapani

Quartzite, and shown in 'd' from Jinakhu. Oriented sections are right way up. Arrows indicate the downdip lineation direction.

Figure 3.19: Exposures of cross faults in Zone 3. Red dashed lines indicate cross faults. a) Sharp fault plane places orthogneiss against the Kulikhani Formation, b) Para gneiss near Ghurmi showing a small-scale cross fault, c) Exposure of the Dudh Koshi Fault at Sugachauki Bhangyang, and d) Gouge zone in the Lesser Himalayan Sequence south of the Main Central Thrust. Hammer for scale in '19d' is enclosed in an ellipse.

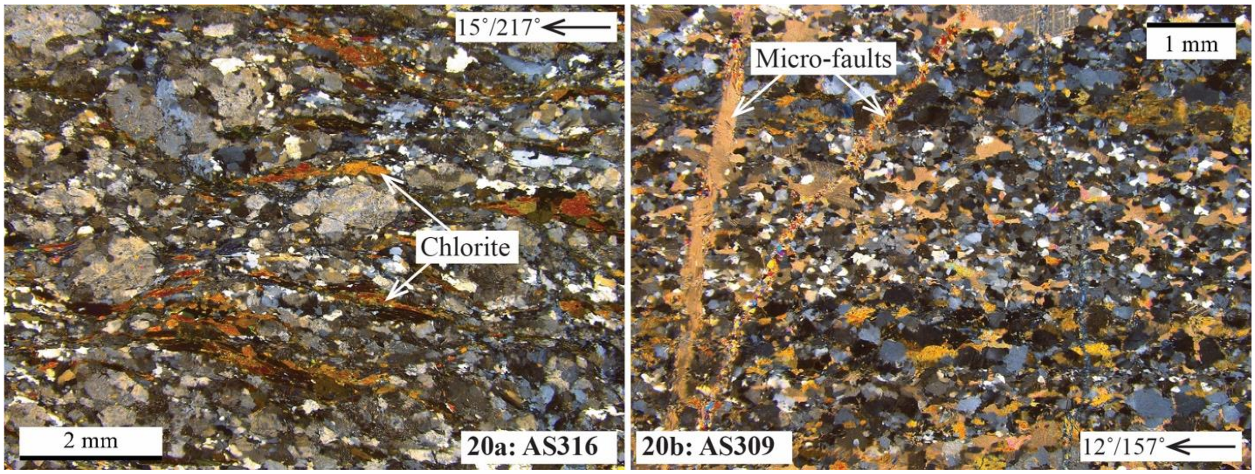

Figure 3.20: Petrographic sections from rocks within cross fault segments in Zone 3.a) chlorite-bearing augen gneiss and b) calc-silicate gneiss. Thin sections are right way up. Arrows indicate the downdip lineation direction.

Evidence for the Benkar Fault Zone in Zone 3 Like within the Okhaldhunga Window, we saw several exposures of cross faults towards the south of the SKT (Figure 3.19). Deformation related to these fault segments can also be noted in petrographic samples (Figure 3.20). An excellent exposure of a cross fault can be seen south of Ghurmi, at the confluence between two small drainages. This west-dipping (214˚/65˚NW,) sharp fault plane places sheared orthogneiss on top of quartzites belonging to the Kulikhani Formation (Figure 3.19a). A peculiar chloritic augen gneiss occurs in the vicinity of this fault, from which the sample AS316 was collected. It can be seen, in thin section, that plagioclase grains have been highly altered, and chlorite dominates the mineralogy, which is not a feature that we commonly see in these klippe rocks (Figure 3.20a). Shear fabric from this sample indicates a dextral extensional deformation along 15˚/217˚ on 050˚/50˚SE foliation. This foliation is sub-parallel to the mapped fault. It is, therefore, likely that these alterations in the sample are related to the faulting event. A nearly 8 km long, distinct topographic lineament trends with an orientation similar to that of the fault.

Several small-scale, in the order of few centimeters, shear planes are frequently seen along the strike of this fault within the injection gneiss and granites (Figure 3.19b). The Dudh Koshi Fault (DKF) of Ishida and Ohta (1973) may merge with the BFZ at this point. We found an excellent exposure of the DKF along roadcuts in Sugachauki Bhangyang (Figure 3.19c). At this location, the DKF is a ~100 m wide, NE-striking, steeply dipping, semi-brittle zone of deformation with a right lateral sense of movement. Rock units on the western side of this fault show strong drag folding into the fault. The rocks on the eastern side, however, do not display such folding. A petrographic sample, AS309, from a deformation zone related to the DKF reveals multiple micro-scale faults that cut the foliation plane (160˚/75˚NE) (Figure 3.20b). These brittle micro-faults run through larger grains and have minor right-lateral offsets. Based on the adjacent Chisapani Quartzite unit, we interpret at least 400m of right-lateral, strike slip displacement along this fault. The structural trend of the DKF has been mimicked by several topographic lineaments, which suggests that the DKF played a role in shaping the geomorphology of this region.

Towards the south, the DKF can be traced into the thin slivers of the LHS rocks that have been exposed between the MCT and the folded and imbricated MBT. These LHS rocks have been mapped by Adhikari (2013a), Adhikari (2013b), and Dhital (2015, Chapter 11). As indicated by lineaments in aerial images, the southern continuation of the DKF most likely passes in proximity of a large-scale landslide around Neule. There are several exposures of outcrop-scale cross faults that are cutting the LHS units. One such fault is a >1 m thick, pitch-black, gouge zone with an orientation of 247˚/73˚NW with a normal sense displacement (Figure 3.19d).

$^{40}Ar/^{39}Ar$ Muscovite Thermochronology in the Greater Himalayan Sequence

Three samples (18N5d, 18N10c, and 18N11c) were collected along a transect across the BFZ in the GHS in the Everest region and were analyzed for $^{40}Ar/^{39}Ar$-muscovite cooling ages. Our western most sample, 18N5d (quartz + muscovite + biotite + albite + orthoclase + sillimanite), was collected from the eastern edge of the Thame village (3,443 m). The second sample, 18N10c, was collected near Sanasa (3,663 m) from an outcrop of quartzofeldspathic gneiss (quartz, biotite, muscovite, orthoclase, sillimanite, garnet). The easternmost sample, 18N11c, is a biotite gneiss (quartz, biotite, muscovite, orthoclase, sillimanite, garnet, hornblende, albite) from near Pangboche (4,017 m).

The sample west of the BFZ (18N5d) yielded a plateau age of 12.06±0.42 Ma, within the zone sample18N10c yielded an age of 12.91±0.37 Ma, and to the east of the BFZ, sample 18N11c yielded a plateau age of 17.42±0.30 Ma (Figure 3.21 and Appendix B). Steps with high values of uncertainties in the right-hand side of the release spectra correlate with the final stages of the step heating experiments.

In general, cooling ages increase towards north within the GHS, while they laterally remain comparable (e.g.; Streule et al., 2012; Larson et al., 2019b). It is noted that there is an elevation difference of ~600 m between the youngest and oldest samples. However, at 1 mm/yr exhumation rate (Hubbard et al., 1991; Streule et al., 2012), this elevation difference can only account for a cooling difference of ~1 Ma. Therefore, the juxtaposition of 12 Ma rocks and 17 Ma rocks can represent: 1) a dominant-component of right lateral movement along the BFZ; 2) a dominant-component of normal movement on the BFZ; or 3) oblique right lateral movement. In any scenario, this age pattern suggests movement(s) on the BFZ younger than 12 Ma. The interpretation of oblique right lateral movement is consistent with the field and thin section kinematic interpretation. Given that researchers have constrained an erosional exhumation rate of ~1 mm/yr (Hubbard et al., 1991; Streule et al., 2012), a difference of 5 Ma across a fault could indicate a displacement of a few kilometers. Just to the south of this transect, Hubbard and Harrison (1989) got a rather young $^{40}Ar/^{39}Ar$-muscovite age of 7.7±0.4 Ma from a 'sheared pegmatite' (sample 87H21D, Figure 3.3). This age could potentially represent mica growth at 7.5 Ma, which could indicate an even younger movement along the BFZ.

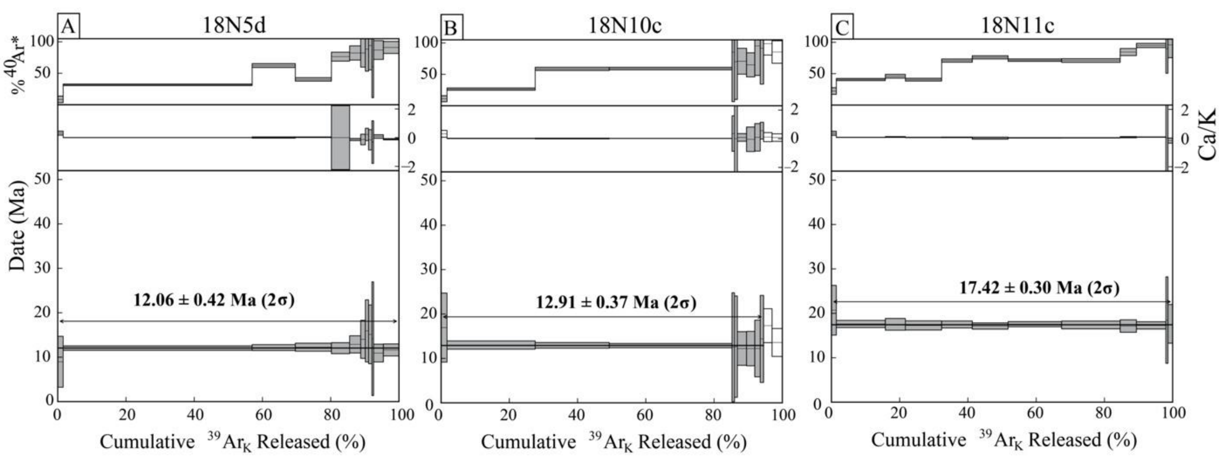

Figure 3.21: $^{40}Ar/^{39}Ar$-muscovite cooling ages of three samples from the Greater Himalayan Sequence. Sample locations are shown in Figure 3.3.

Discussions and Conclusions

Nature, Geometry, and Extent of the Benkar Fault Zone to the South of the Main Central Thrust

We mapped several segments of NNE- to NE-striking brittle deformation zones aligned from Jubing to Dudhauli in the LHS, the GHK, and in the slivers of the LHS just north of the MBT. Based on the dominance of NE-striking zones, we interpret these to be cross fault segments and to be the southern continuation of the BFZ. The length of the currently mapped BFZ is > 100 km and it spans the GHS, LHS, and GHK and cuts across their regional, boundary thrusts. Unlike in the GHS, where the BFZ is ductile to semi-brittle, the BFZ is brittle within both the LHS and the GHK. Within the Okhaldhunga Window, the BFZ has been expressed as gouge zones, brecciated zones, and brittle deformation zones in a non-penetrative, segmented fashion. In the GHK, the BFZ occurs as sharp fault planes, fractures, and as micro shear zones as seen in Figure 3.19b. The width of the BFZ in the Okhaldhunga Window is up to 4 km. Some of these segments within this zone are east dipping while others are dipping towards the west. The sense of movement (dextral vs sinistral) also varies across segments. We interpret that the BFZ is a culmination of a series of cross faulting events that may have had a changing sense of shear through time. In general, cross fault segments are more pronounced in more competent units rich in quartz and carbonate such as the Phera quartzite, the Barnalu Quartzite, Ketuke Formation, and the Harkapur Formation. Within pelitic rocks, deformation is most likely accommodated through shearing and folding. We were able to map up to 300 m of offset across some of the fault segments. Poor exposure and laterally variable thickness of the LHS rocks made it challenging to precisely constrain offsets and segment lengths. The BFZ does not have a significant amount of slip compared to the major thrust faults, but this fault might serve as a seismic segment boundary and thereby influence seismic hazards. The weakened fault zone rocks are often striking parallel to the valley walls on which they are exposed, which also may enhance the landslide hazard in that area.

As shown by Nakajima et al. (2020), zircon fission track (ZFT) ages (closure temperature 205˚±18 ˚C, Bernet, 2009) within the Okhaldhunga Window gradually decrease towards the north and range between 11 Ma and 2.4 Ma. Similarly, ZFT ages in the GHK range between 13Ma to 10.8Ma and also show a general, northward younging trend (Nakajima et al., 2020). Just towards the west of our study area, Larson et al. (2019b) constrained the $^{40}Ar/^{39}Ar$-muscovite cooling ages of the GHK rocks between 27.5 Ma and 17.3 Ma. The brittle nature of cross fault exposures within the Okhaldhunga Window and the GHK suggest that movements along these segments occurred well below 280˚±30 ˚C, at which a transition from mylonite to cataclasite occurs (Stipp et al., 2002). Thus, it can be inferred that cross fault segments in the Okhaldhunga Window have had movements synchronous to or younger than the ZFT ages. This interpretation is in line with the observation in the GHS, where the BFZ had activity younger than 12 Ma.

While our work did not continue into the Sub-Himalaya, we cannot rule out the possibility that the BFZ continues towards the south into the foreland as seen with other cross faults in the Himalaya (e.g.; Sahoo et al., 2000; Mukul, 2010). We saw multiple exposures of cross faults in the LHS just to the north of the MBT. It is possible that some of these BFZ- and/or the DKF-related segments continue as offset and/or segmented faults across the MFT.

Genesis of the Benkar Fault Zone and its Implications

Researchers have interpreted the genesis of Himalayan cross faults through one of three models (Hubbard et al., 2021); transport accommodation structures within the orogenic belt, Tibetan-extension related structures, and surface expression of the basement structures in the down-going Indian plate. Tectonic transport of the Himalayan belt occurs along a vector perpendicular to the range front (e.g.; Styron et al., 2011; Ader et al., 2012; Stevens & Avouac, 2016). Because of the arcuate shape of the Himalaya, this vector gradually changes from SE-directed in the eastern part of Himalaya to SW-directed in the western part of the Himalaya. This changing direction of the transport vector requires NS-striking, extensional, accommodation structures as the adjacent thrust sheets diverge away. Such cross fault segments would be confined within the deforming wedge and would have a strong extensional component that gradually decreases away from the deformation front. The eastward directed extension in the Tibetan plate has been interpreted as a causal mechanism for most of the extensional cross faults mapped in the Tethyan Sequence such as the Thak Khola graben. To date there is no documentation of such cross faults cutting across the STDS and into the GHS. Most of the previously mapped Himalayan cross faults have been described as the Indian cratonic basement related structures. Inherited basement structures in the Indian plate include basement ridges and basement faults. Basement ridges obstruct the propagation of thrust-sheets and may create tear-faults such as the Ganga and Yamuna Tear Faults (Sahoo et al., 2000). Basement faults can serve as lateral ramps or can get reactivated and thereby induce cross faults. The Lukhnow Basement Fault has been interpreted to be responsible for abrupt lateral changes in metamorphic pathways of thrust sheets and in the topography (Harvey et al., 2015; Soucy La Roche & Godin, 2019). This model would require the relative plate motion vector of the Indian Plate with respect to the Asian Plate to be parallel to the basement ridges, which currently this is not the case. This lack of alignment would mean that the ridges are subducting obliquely under the Himalaya. Such oblique subduction of ridges could still be responsible for lateral ramps and other cross structures, but might suggest a lateral migration of cross structures with time. At this point there is no documentation of such lateral migration of cross fault systems. At this point, we cannot confidently choose between one of these three models for the BFZ.

We stress the importance of recognizing and understanding cross faults because of their impacts in regional seismicity and in landslide-related hazards. We note that the West Patna Basement Fault and the Motihari-Everest Lineament are in close proximity of the BFZ (Figure 3.1). These structures may or may not be genetically related to the BFZ. The West Patna Fault is a NE-striking, active, fault within the Indian basement and is roughly on strike with the BFZ (GSI, 2000; Jain & Sinha, 2005). Based on interpretation of satellite images and seismic data, Dasgupta (1987) identified the Motihari-Everest Lineament as one of the many cross faults that originate in the Indian basement and span across the Himalayan orogen. Some of these structures are seismically active and most of them display strike-slip fault plane solutions. Tiwari et al. (2022) concludes, “the Motihari-Everest fault area is in critical strain (mechanically locked) conditions, as indicated by the stepwise energy release pattern”. Tiwari et al. (2022) further suggest that cross faults have an impact on the release of strain energy along regional thrusts during or after a seismic event. To the west, Mendoza et al. (2019) reported an abrupt termination of aftershocks of the Gorkha Earthquake along a SE-dipping plane, the surface projection of which coincides with the Gaurishankar Lineament. In parts of eastern Nepal, regional micro-seismic data also show multiple clusters of micro-seismicity concentrated along NNE-trends, some of which have strike-slip sense (Figure 6 of Hubbard et al., 2021 and references therein). Based on these two observations, we believe that cross faults potentially play a role in limiting lateral propagation of thrust rupture, and furthermore they also have the potential to generate their own seismicity. Cross faults also tend to be co-located with major river valleys and dip slopes of fault fabric on valley walls may increase the landslide hazard.

Gaining a better understanding of the location and structural nature of cross faults is therefore important to the study of natural hazards in the Himalaya.

Conclusions

We continued mapping the BFZ towards the south from Lukla, in the regions between Jubing and Dudhauli, and corroborated our mapping results with kinematic and petrographic analysis. The BFZ is a large-scale cross fault that cuts across the GHS, LHS, GHK, and their regional thrust boundaries. Currently, mapped length of this fault is at least 100 km in length and it is possible that the BFZ continues further towards the south into the foreland. Within the LHS and the GKS, the BFZ is expressed as brittle, non-penetrative, offset fault segments with varying sense of shear. In general, these fault segments have a ~NS- or NNE-strike but the dip-direction and sense of movement varies between segments, which might indicate multiple deformational events along this fault. $^{40}Ar/^{39}Ar$-muscovite thermochronology from a transect in the GHS indicates that movement(s) along the BFZ is younger than 12 Ma. Timing of the BFZ is likely to be even younger in the LHS and the GHK as indicated by the brittle nature of this fault towards the south. Cross faults, such as the BFZ, can pose seismic and/or landslide-related hazards and it is, therefore, important to recognize and understand these structures.

References

Ader, T., Avouac, J.-P., Liu-Zeng, J., Lyon-Caen, H., Bollinger, L., Galetzka, J., Genrich, J., Thomas, M., Chanard, K., Sapkota, S. N., Rajaure, S., Shrestha, P., Ding, L., & Flouzat, M. (2012). Convergence rate across the Nepal Himalaya and interseismic coupling on the Main Himalayan Thrust: Implications for seismic hazard. *Journal of Geophysical Research: Solid Earth*, *117*(B4). doi:https://doi.org/10.1029/2011JB009071

Adhikari, N. (2013a). *Lithology and stratigraphy of the Pre-Siwalik rocks around Katari–Patana Bhanjyang area, Udayapur district, eastern Nepal.* (MSc). Tribhuvan University, Kritipur.

Adhikari, S. (2013b). *Geology of Katari–Patana Bhanjyang area, eastern Nepal, with special reference to petrography of Pre-Siwalik rocks.* (MSc). Tribhuvan University, Kritipur.

Ahmad, T., Harris, N., Bickle, M., Chapman, H., Bunbury, J., & Prince, C. (2000). Isotopic constraints on the structural relationships between the Lesser Himalayan Series and the High Himalayan Crystalline Series, Garhwal Himalaya. *GSA bulletin, 112*(3), 467-477. doi:10.1130/0016-7606(2000)112<467:Icotsr>2.0.Co;2

Andrews, E. (1985). Stratigraphy of the Sabhaya khola region, Sankhuha Sabha district, Eastern Nepal. *Journal of Nepal Geological Society, 2*(2), 12–35. doi:10.3126/jngs.v2i2.32531

Arita, K. (1983). Origin of the inverted metamorphism of the lower Himalayas, Central Nepal. *Tectonophysics, 95*(1), 43-60. doi:https://doi.org/10.1016/0040-1951(83)90258-5

Avouac, J. P., Meng, L., Wei, S., Wang, T., & Ampuero, J. P. (2015). Lower edge of locked Main Himalayan Thrust unzipped by the 2015 Gorkha earthquake. *Nature geoscience, 8*(9), 708-711. doi:10.1038/ngeo2518

Bahroudi, A., & Koyi, H. A. (2003). Effect of spatial distribution of Hormuz salt on deformation style in the Zagros fold and thrust belt: an analogue modelling approach. *Journal of the Geological Society, 160*(5), 719-733. doi:https://doi.org/10.1144/0016-764902-135

Bashyal, R. P. (1980). Gondwana Type of formation with Phosphatic Rocks in S.E. Nepal. *Journal of Geological Society of India, 21*(10), 489-491. Retrieved from https://samvad.sibmpune.edu.in/index.php/jgsi/article/view/64779

Baskota, S. K., & Adhikari, S. (2019). *Geological map of parts of Solukhumbu, Okhaldhunga, Khotang and Udayapur Districts*. Retrieved from Lainchaur:

Baud, A., Gaetani, M., Garzanti, E., Fors, E., Nicora, A., & Tintori, A. (1984). Geological observations in southeastern Zanskar and adjacent Lahul area (northwestern Himalaya). *Eclogae Geologicae Helvetiae, 77*(1), 171-199. doi:https://www.e-periodica.ch/digbib/voltoc?lang=en&pid=egh-001%3A1984%3A77#3

Beaumont, C., Jamieson, R. A., Nguyen, M. H., & Lee, B. (2001). Himalayan tectonics explained by extrusion of a low-viscosity crustal channel coupled to focused surface denudation. *Nature, 414*(6865), 738-742. doi:10.1038/414738a

Bernet, M. (2009). A field-based estimate of the zircon fission-track closure temperature. *Chemical Geology, 259*(3), 181-189. doi:https://doi.org/10.1016/j.chemgeo.2008.10.043

Bhattacharyya, K., Mitra, G., & Kwon, S. (2015). Geometry and kinematics of the Darjeeling–Sikkim Himalaya, India: Implications for the evolution of the Himalayan fold-thrust belt. *Journal of Asian Earth Sciences, 113*, 778-796. doi:https://doi.org/10.1016/j.jseaes.2015.09.008

Bordet, P. (1961). *Recherches géologiques dans l'Himalaya du Népal, région du Makalu, Expéditions Françaises a l'Himalaya 1954– 1955 (with geological maps in colors)*. Paris: Paris Editions du Centre National de la Recherche Scientifique.

Bordet, P., Colchen, M., Krummenacher, D., Le Fort, P., Mouterde, R., & Remy, M. (1971). *Recherches Géologiques dans l'Himalaya du Népal, Région de la Thakkhola*. Paris: Paris Édition du Centre National de la Recherche Scientifique.

Brookfield, M. E. (1993). The Himalayan passive margin from Precambrian to Cretaceous times. *Sedimentary Geology, 84*(1), 1-35. doi:https://doi.org/10.1016/0037-0738(93)90042-4

Brunel, M. (1986). Ductile thrusting in the Himalayas: Shear sense criteria and stretching lineations. *Tectonics, 5*(2), 247-265. doi:https://doi.org/10.1029/TC005i002p00247

Brunel, M., & Kienast, J.-R. (1986). Étude pétro-structurale des chevauchements ductiles himalayens sur la transversale de l'Everest–Makalu (Népal oriental). *Canadian Journal of Earth Sciences, 23*(8), 117-1137. doi:https://doi.org/10.1139/e86-111

Burchfiel, B. C., Zhiliang, C., Hodges, K. V., Yuping, L., Royden, L. H., Changrong, D., Jiene, X., Burchfiel, B. C., Zhiliang, C., Hodges, K. V., Yuping, L., Royden, L. H., Changrong, D., & Xu, J. (1992). *The South Tibetan Detachment System, Himalayan Orogen: Extension Contemporaneous With and Parallel to Shortening in a Collisional Mountain Belt* (Vol. 269): Geological Society of America Special Papers.

Burg, J. P., Brunel, M., Gapais, D., Chen, G. M., & Liu, G. H. (1984). Deformation of leucogranites of the crystalline Main Central Sheet in southern Tibet (China). *Journal of Structural Geology, 6*(5), 535-542. doi:https://doi.org/10.1016/0191-8141(84)90063-4

Burgess, P. W., Yin, A., Dubey, C. S., Shen, Z.-K., & Kelty, T. K. (2012). Holocene shortening across the Main Frontal Thrust zone in the eastern Himalaya. *Earth and Planetary Science Letters, 357-358*, 152-167. doi:https://doi.org/10.1016/j.epsl.2012.09.040

Burrard, S. G. (1915). On the origin of the Indo-Gangetic trough, commonly called the Himalayan foredeep. *Proceedings of the Royal Society of London. Series A, Containing Papers of a Mathematical and Physical Character, 91*(628), 220-238. doi:doi:10.1098/rspa.1915.0014

Butler, R. W. H., Tavarnelli, E., & Grasso, M. (2006). Structural inheritance in mountain belts: an Alpine–Apennine perspective. *Journal of Structural Geology, 28*(11), 1893-1908. doi:https://doi.org/10.1016/j.jsg.2006.09.006

Carosi, R., Lombardo, B., Molli, G., Musumeci, G., & Pertusati, P. C. (1998). The south Tibetan detachment system in the Rongbuk valley, Everest region. Deformation features and geological implications. *Journal of Asian Earth Sciences, 16*(2), 299-311. doi:https://doi.org/10.1016/S0743-9547(98)00014-2

Carosi, R., Lombardo, B., Musumeci, G., & Pertusati, P. C. (1999a). Geology of the Higher Himalayan Crystallines in Khumbu Himal (Eastern Nepal). *Journal of Asian Earth Sciences, 17*(5), 785-803. doi:https://doi.org/10.1016/S1367-9120(99)00014-0

Carosi, R., Montomoli, C., & Iaccarino, S. (2018). 20years of geological mapping of the metamorphic core across Central and Eastern Himalayas. *Earth-Science Reviews, 177*, 124-138. doi:https://doi.org/10.1016/j.earscirev.2017.11.006

Carosi, R., Musumeci, G., & Pertusati, P. C. (1999b). Extensional tectonics in the higher Himalayan crystallines of Khumbu Himal, eastern Nepal. *Geological Society of America Special Paper, 328*, 211-223.

Catlos, E. J., Harrison, T. M., Manning, C. E., Grove, M., Rai, S. M., Hubbard, M. S., & Upreti, B. N. (2002). Records of the evolution of the Himalayan orogen from in situ Th–Pb ion microprobe dating of monazite: Eastern Nepal and western Garhwal. *Journal of Asian Earth Sciences, 20*(5), 459-479. doi:https://doi.org/10.1016/S1367-9120(01)00039-6

Chakraborty, T., Taral, S., More, S., & Bera, S. (2020). Cenozoic Himalayan Foreland Basin: An Overview and Regional Perspective of the Evolving Sedimentary Succession. In N. Gupta & S. K. Tandon (Eds.), *Geodynamics of the Indian Plate: Evolutionary Perspectives* (pp. 395-437). Cham: Springer International Publishing.

Clift, P. D., Hodges, K. V., Heslop, D., Hannigan, R., Van Long, H., & Calves, G. (2008). Correlation of Himalayan exhumation rates and Asian monsoon intensity. *Nature geoscience, 1*(12), 875-880. doi:10.1038/ngeo351

Colchen, M., Le Fort, P., & Pêcher, A. (1986). *Annapurna, Manaslu, Ganesh, Himal: notice de la carte géologique au 1/200,000 e*. Paris: Centre National de la Recherches Scientifique, Special Publication.

Coleman, M. E. (1998). U-Pb constraints on Oligocene-Miocene deformation and anatexis within the central Himalaya, Marsyandi Valley, Nepal. *American Journal of Science, 298*(7), 553-571. doi:10.2475/ajs.298.7.553

Cottle, J. M., Jessup, M. J., Newell, D. L., Horstwood, M. S. A., Noble, S. R., Parrish, R. R., Waters, D. J., & Searle, M. P. (2009a). Geochronology of granulitized eclogite from the Ama Drime Massif: Implications for the tectonic evolution of the South Tibetan Himalaya. *Tectonics, 28*(1). doi:https://doi.org/10.1029/2008TC002256

Cottle, John M., Searle, Michael P., Horstwood, Matthew S. A., & Waters, David J. (2009b). Timing of Midcrustal Metamorphism, Melting, and Deformation in the Mount Everest

Region of Southern Tibet Revealed by U(-Th)-Pb Geochronology. *The Journal of Geology, 117*(6), 643-664. doi:https://doi.org/10.1086/605994

Cottle, J. M., Searle, M. P., Jessup, M. J., Crowley, J. L., & Law, R. D. (2015). Rongbuk re-visited: Geochronology of leucogranites in the footwall of the South Tibetan Detachment System, Everest Region, Southern Tibet. *Lithos, 227*, 94-106. doi:https://doi.org/10.1016/j.lithos.2015.03.019

Daniel, C. G., Hollister, L. S., Parrish, R. R., & Grujic, D. (2003). Exhumation of the Main Central Thrust from Lower Crustal Depths, Eastern Bhutan Himalaya. *Journal of Metamorphic Geology, 21*(4), 317-334. doi:https://doi.org/10.1046/j.1525-1314.2003.00445.x

Dasgupta, S., Mukhopadhyay, M., Nandy, D.R. (1987). Active transverse features in the central portion of the Himalaya. *Tectonophysics, 136*, 255-264.

De La Torre, T. L., Monsalve, G., Sheehan, A.F., Sapkota, S., and Wu, F. (2007). Earthquake processes of the Himalayan collision zone in eastern Nepal and the southern Tibetan Plateau. *Geophysical Journal International, 171*, 718-738.

DeCelles, P. G., Carrapa, B., Ojha, T. P., Gehrels, G. E., & Collins, D. (2020). Structural and thermal evolution of the Himalayan thrust belt in midwestern Nepal. *Geological Society of America Special Paper, 547*, 1-77. doi:https://doi.org/10.1130/2020.2547(01)

DeCelles, P. G., Gehrels, G. E., Quade, J., LaReau, B., & Spurlin, M. (2000). Tectonic Implications of U-Pb Zircon Ages of the Himalayan Orogenic Belt in Nepal. *Science, 288*(5465), 497-499. doi:doi:10.1126/science.288.5465.497

DeCelles, P. G., Gehrels, G. E., Quade, J., Ojha, T. P., Kapp, P. A., & Upreti, B. N. (1998). Neogene foreland basin deposits, erosional unroofing, and the kinematic history of the Himalayan fold-thrust belt, western Nepal. *GSA bulletin, 110*(1), 2-21. doi:10.1130/0016-7606(1998)110<0002:Nfbdeu>2.3.Co;2

Decelles, P. G., Kapp, P., Gehrels, G. E., & Ding, L. J. T. (2014). Paleocene-Eocene foreland basin evolution in the Himalaya of southern Tibet and Nepal: Implications for the age of initial India-Asia collision. *33*(5), 824-849.

DeCelles , P. G., Robinson, D. M., Quade, J., Ojha, T. P., Garzione, C. N., Copeland, P., & N., U. B. (2001). Stratigraphy, structure, and tectonic evolution of the Himalayan fold-thrust belt in western Nepal. *Tectonics, 20*, 487-509. doi:https://doi.org/10.1029/2000TC001226

Dhital, M. R. (2015). *Geology of the Nepal Himalaya: regional perspective of the classic collided orogen*: Springer.

Diehl, T., Singer, J., Hetényi, G., Grujic, D., Clinton, J., Giardini, D., Kissling,E., GANSSER Working Group. (2017). Seismotectonics of Bhutan: Evidence for segmentation of the

Eastern Himalayas and link to foreland deformation. *Earth and Planetary Science Letters, 471*, 54-65. doi:https://doi.org/10.1016/j.epsl.2017.04.038

Ding, L., Qasim, M., Jadoon, I. A. K., Khan, M. A., Xu, Q., Cai, F., Wang, H., Baral, U., & Yue, Y. (2016). The India–Asia collision in north Pakistan: Insight from the U–Pb detrital zircon provenance of Cenozoic foreland basin. *Earth and Planetary Science Letters, 455*, 49-61. doi:https://doi.org/10.1016/j.epsl.2016.09.003

Drukpa, D., Velasco, A. A., & Doser, D. I. (2006a). Seismicity in the Kingdom of Bhutan (1937–2003): Evidence for crustal transcurrent deformation. *Journal of Geophysical Research, 111*, B06301. doi:https://doi/org/10.1029/2004JB003087

Drukpa, D., Velasco, A. A., & Doser, D. I. (2006b). Seismicity in the Kingdom of Bhutan (1937–2003): Evidence for crustal transcurrent deformation. *Journal of Geophysical Research: Solid Earth, 111*(B6). doi:https://doi.org/10.1029/2004JB003087

Duvall, M. J., Waldron, J. W. F., Godin, L., & Najman, Y. (2020). Active strike-slip faults and an outer frontal thrust in the Himalayan foreland basin. *Proceedings of the National Academy of Sciences, 117*(30), 17615-17621. doi:doi:10.1073/pnas.2001979117

Dwivedi, S. K. (1997). *Geology of the area between the Sunkoshi River and the Kakaru Khola, Udayapur District, Eastern Nepal.* (M.Sc.). Tribhuvan University,

Elliott, J. R., Jolivet, R., González, P. J., Avouac, J. P., Hollingsworth, J., Searle, M. P., & Stevens, V. L. (2016). Himalayan megathrust geometry and relation to topography revealed by the Gorkha earthquake. *Nature geoscience, 9*(2), 174-180. doi:10.1038/ngeo2623

Frank, W., & Fuchs, G. (1970). Geological investigations in west Nepal and their significance for the geology of the Himalayas. *Geologische rundschau, 59*, 552-580.

From, R., & Larson, K. (2014). Tectonostratigraphy, deformation, and metamorphism of the Himalayan mid-crust exposed in the Likhu Khola region, east-central Nepal. *Geosphere, 10*(2), 292-307. doi:10.1130/ges00938.1

Fuchs, G. (1982). *Geologic-Tectonic Map of the Himalaya*. Vienna: Geologische Bundesanstalt/Geological Survey of Austria, scale 1:2,000,000.

Gansser, A. (1964). *Geology of the Himalayas*. London: Wiley Interscience.

Garzanti, E. (1999). Stratigraphy and sedimentary history of the Nepal Tethys Himalaya passive margin. *Journal of Asian Earth Sciences, 17*(5), 805-827. doi:https://doi.org/10.1016/S1367-9120(99)00017-6

Garzanti, E., Casnedi, R., & Jadoul, F. (1986). Sedimentary evidence of a Cambro-Ordovician orogenic event in the northwestern Himalaya. *Sedimentary Geology, 48*(3), 237-265. doi:https://doi.org/10.1016/0037-0738(86)90032-1

Gautam, P., Ulak, P. D., Paudayal, K. N., Gyawali, B. R., & Bhandari, S. (2012). Magnetostratigraphic dating of the prime-time sedimentary record of Himalayan tectonics and climate: new age constraints (13–10 Ma) from the Siwaliks of the Tinau Khola north section, Nepal. *Geophysical Journal International, 190*(3), 1378-1392. doi:https://doi.org/10.1111/j.1365-246X.2012.05568.x

Gehrels, G. E., DeCelles, P. G., Ojha, T. P., & Upreti, B. N. (2006). Geologic and U-Th-Pb geochronologic evidence for early Paleozoic tectonism in the Kathmandu thrust sheet, central Nepal Himalaya. *GSA bulletin, 118*(1-2), 185-198. doi:10.1130/b25753.1

Giambiagi, L., Mescua, J., Bechis, F., Tassara, A., & Hoke, G. (2012). Thrust belts of the southern Central Andes: Along-strike variations in shortening, topography, crustal geometry, and denudation. *Bulletin, 124*(7-8), 1339-1351. doi:https://doi.org/10.1130/B30609.1

Gingele, F., De Deckker, P., & Norman, M. (2007). Late Pleistocene and Holocene climate of SE Australia reconstructed from dust and river loads deposited offshore the River Murray Mouth. *Earth and Planetary Science Letters, 255*(3), 257-272. doi:https://doi.org/10.1016/j.epsl.2006.12.019

Giri, B., & Hubbard, M. (2023). Lateral Heterogeneity in Compressional Mountain Belt Settings. In E. J. Catlos & I. Cemen (Eds.), *Compressional Tectonics: Plate Convergence to Mountain Building* (Vol. 1, pp. 47-86): AGU Books.

Godin, L. (2003). Structural evolution of the Tethyan sedimentary sequence in the Annapurna area, central Nepal Himalaya. *Journal of Asian Earth Sciences, 22*(4), 307-328. doi:https://doi.org/10.1016/S1367-9120(03)00066-X

Godin, L., & Harris, L. B. (2014). Tracking basement cross-strike discontinuities in the Indian crust beneath the Himalayan orogen using gravity data – relationship to upper crustal faults. *Geophysical Journal International, 198*(1), 198-215. doi:10.1093/gji/ggu131

Godin, L., Parrish, R. R., Brown, R. L., & Hodges, K. V. (2001). Crustal thickening leading to exhumation of the Himalayan Metamorphic core of central Nepal: Insight from U-Pb Geochronology and 40Ar/39Ar Thermochronology. *Tectonics, 20*(5), 729-747. doi:https://doi.org/10.1029/2000TC001204

Goscombe, B., Gray, D., & Foster, D. A. (2018). Metamorphic response to collision in the Central Himalayan Orogen. *Gondwana Research, 57*, 191-265. doi:https://doi.org/10.1016/j.gr.2018.02.002

Goscombe, B., Gray, D., & Hand, M. (2006). Crustal architecture of the Himalayan metamorphic front in eastern Nepal. *Gondwana Research, 10*(3), 232-255. doi:https://doi.org/10.1016/j.gr.2006.05.003

Grujic, D., Casey, M., Davidson, C., Hollister, L. S., Kündig, R., Pavlis, T., & Schmid, S. (1996). Ductile extrusion of the Higher Himalayan Crystalline in Bhutan: evidence from quartz microfabrics. *Tectonophysics, 260*(1), 21-43. doi:https://doi.org/10.1016/0040-1951(96)00074-1

GSI. (2000). Eastern Nepal Himalaya and Indo-Gangetic Plains of Bihar. In P. L. Narula, S. K. Acharyya, & J. Banerjee (Eds.), *Seismotectonics Atlas of India and Its Environs* (pp. 26-27): Geological Survey of India (GSI).

Harrison, T. M., Ryerson, F. J., Le Fort, P., Yin, A., Lovera, O. M., & Catlos, E. J. (1997). A Late Miocene-Pliocene origin for the Central Himalayan inverted metamorphism. *Earth and Planetary Science Letters, 146*(1), E1-E7. doi:https://doi.org/10.1016/S0012-821X(96)00215-4

Harvey, J. E., Burbank, D. W., & Bookhagen, B. (2015). Along-strike changes in Himalayan thrust geometry: Topographic and tectonic discontinuities in western Nepal. *Lithosphere, 7*(5), 511-518. doi:10.1130/l444.1

Heim, A., & Gansser, A. (1939). *Central Himalaya: Geological Observations of the Swiss expedition 1936 (with geological maps in colors, sections, and plates).* (Vol. 73): Memoires de la Societe Helvetique des Sciences Naturelles.

Hodges, K. V. (2000). Tectonics of the Himalaya and southern Tibet from two perspectives. *Geological Society of America Bulletin, 112*(3), 324-350. doi:https://doi.org/10.1130/0016-7606(2000)112<324:TOTHAS>2.0.CO;2

Hodges, K. V., Hurtado, J. M., & Whipple, K. X. (2001). Southward extrusion of Tibetan crust and its effect on Himalayan tectonics. *Tectonics, 20*(6), 799-809. doi:https://doi.org/10.1029/2001TC001281

Hodges, K. V., Parrish, R. R., Housh, T. B., Lux, D. R., Burchfiel, B. C., Royden, L. H., & Chen, Z. (1992). Simultaneous Miocene Extension and Shortening in the Himalayan Orogen. *Science, 258*(5087), 1466-1470. doi:doi:10.1126/science.258.5087.1466

Hodges, K. V., Parrish, R. R., & Searle, M. P. (1996). Tectonic evolution of the central Annapurna Range, Nepalese Himalayas. *Tectonics, 15*(6), 1264-1291. doi:https://doi.org/10.1029/96TC01791

Hu, X., Garzanti, E., Moore, T., & Raffi, I. (2015). Direct stratigraphic dating of India-Asia collision onset at the Selandian (middle Paleocene, 59 ± 1 Ma). *Geology, 43*(10), 859-862. doi:10.1130/g36872.1

Hubbard, M., Gajurel, A. P., Mukul, M., & Seifert, N. (2018). *Cross faults and their role in Himalayan Structural Evolution*. Paper presented at the Geological Society of America Abstracts with Programs.

Hubbard, M., Mukul, M., Gajurel, A. P., Ghosh, A., Srivastava, V., Giri, B., Seifert, N., & Mendoza, M. M. (2021). Orogenic Segmentation and Its Role in Himalayan Mountain Building. *Frontiers in Earth Science*, *9*(259). doi:https://doi.org/10.3389/feart.2021.641666

Hubbard, M., Royden, L., & Hodges, K. (1991). Constraints on unroofing rates in the High Himalaya, eastern Nepal. *Tectonics*, *10*(2), 287-298. doi:https://doi.org/10.1029/90TC02777

Hubbard, M. S. (1988). *Thermobarometry, 40Ar/39Ar geochronology, and structure of the Main Central Thrust zone and Tibetan Slab, eastern Nepal Himalaya.* (Doctoral Dissertation). Massachusetts Institute of Technology

Hubbard, M. S. (1989). Thermobarometric constraints on the thermal history of the Main Central Thrust Zone and Tibetan Slab, eastern Nepal Himalaya. *Journal of Metamorphic Geology, 7*(1), 19-30. doi:https://doi.org/10.1111/j.1525-1314.1989.tb00572.x

Hubbard, M. S. (1996). Ductile Shear as a Cause of Inverted Metamorphism: Example from the Nepal Himalaya. *The Journal of Geology, 104*(4), 493-499. doi:10.1086/629842

Hubbard, M. S., & Harrison, M. T. (1989). 40Ar/39Ar age constraints on deformation and metamorphism in the main central thrust zone and Tibetan slab, eastern Nepal Himalaya. *Tectonics, 8*(4), 865-880. doi:https://doi.org/10.1029/TC008i004p00865

Huntington, K. W., Blythe, A. E., & Hodges, K. V. (2006). Climate change and Late Pliocene acceleration of erosion in the Himalaya. *Earth and Planetary Science Letters, 252*(1), 107-118. doi:https://doi.org/10.1016/j.epsl.2006.09.031

Hurtado, J. M., Jr, Hodges, K. V., & Whipple, K. X. (2001). Neotectonics of the Thakkhola graben and implications for recent activity on the South Tibetan fault system in the central Nepal Himalaya. *GSA bulletin*, *113*(2), 222-240. doi:10.1130/0016-7606(2001)113<0222:Nottga>2.0.Co;2

Ishida, T. (1969). Petrography and structure of the area between the Dudh Kosi and the Tamba Kosi, East Nepal. *Journal of Geological society of Japan, 75*, 115-125.

Ishida, T., & Ohta, Y. (1973). Ramechhap-Okhaldhunga Region. In S. Hashimoto, O. Y, & A. C (Eds.), *Geology of the Nepal Himalayas* (pp. 35-68). Japan: Himalayan Committee of Hokkaido University.

Jain, V., & Sinha, R. (2005). Response of active tectonics on the alluvial Baghmati River, Himalayan foreland basin, eastern India. *Geomorphology, 70*(3), 339-356. doi:https://doi.org/10.1016/j.geomorph.2005.02.012

Jessup, M. J., Cottle, J. M., Searle, M. P., Law, R. D., Newell, D. L., Tracy, R. J., & Waters, D. J. (2008). P–T–t–D paths of Everest Series schist, Nepal. *Journal of Metamorphic Geology, 26*(7), 717-739. doi:https://doi.org/10.1111/j.1525-1314.2008.00784.x

Jessup, M. J., Law, R. D., Searle, M. P., & Hubbard, M. S. (2006). Structural evolution and vorticity of flow during extrusion and exhumation of the Greater Himalayan Slab, Mount Everest Massif, Tibet/Nepal: implications for orogen-scale flow partitioning. *Geological Society, London, Special Publications, 268*(1), 379-413. doi:doi:10.1144/GSL.SP.2006.268.01.18

Kapp, P., & DeCelles, P. G. (2019). Mesozoic–Cenozoic geological evolution of the Himalayan-Tibetan orogen and working tectonic hypotheses. *American Journal of Science, 319*(3), 159. doi:10.2475/03.2019.01

Kellett, D. A., Cottle, J. M., & Larson, K. P. (2019). The South Tibetan detachment system: History, advances, definition and future directions. In P. J. Treloar & M. P. Searle (Eds.), *Himalayan Tectonics: A Modern Synthesis* (Vol. 483, pp. 377-400). London: Geological Society, Special Publication.

Kellett, D. A., & Godin, L. (2009). Pre-Miocene deformation of the Himalayan superstructure, Hidden valley, central Nepal. *Journal of the Geological Society, 166*(2), 261-275. doi:doi:10.1144/0016-76492008-097

Kohn, M. J. (2008). P-T-t data from central Nepal support critical taper and repudiate large-scale channel flow of the Greater Himalayan Sequence. *GSA bulletin, 120*(3-4), 259-273. doi:10.1130/b26252.1

Kohn, M. J., Paul, S. K., & Corrie, S. L. (2010). The lower Lesser Himalayan sequence: A Paleoproterozoic arc on the northern margin of the Indian plate. *GSA bulletin, 122*(3-4), 323-335. doi:10.1130/b26587.1

Larson, K., Cottle, J., Lederer, G., & Rai, S. M. (2017). Defining shear zone boundaries using fabric intensity gradients: An example from the east-central Nepal Himalaya. *Geosphere, 13*(3), 771-781. doi:10.1130/ges01373.1

Larson, K., Piercey, S., & Cottle, J. (2019a). Preservation of a Paleoproterozoic rifted margin in the Himalaya: Insight from the Ulleri-Phaplu-Melung orthogneiss. *Geoscience Frontiers, 10*(3), 873-883. doi:https://doi.org/10.1016/j.gsf.2017.05.010

Larson, K. P. (2012). The geology of the Tama Kosi and Rolwaling valley region, East-Central Nepal. *Geosphere, 8*(2), 507-517. doi:10.1130/ges00711.1

Larson, K. P. (2018). Refining the structural framework of the Khimti Khola region, east-central Nepal Himalaya, using quartz textures and c-axis fabrics. *Journal of Structural Geology, 107*, 142-152. doi:https://doi.org/10.1016/j.jsg.2017.12.014

Larson, K. P., Camacho, A., Kumar, K. C., & Shrestha, S. (2019b). Kinematic implications of regional 40Ar/39Ar ages, east-central Nepal. *Journal of Asian Earth Sciences, 172*, 383-392. doi:https://doi.org/10.1016/j.jseaes.2018.09.023

Larson, K. P., Cottle, J. M., & Godin, L. (2011). Petrochronologic record of metamorphism and melting in the upper Greater Himalayan sequence, Manaslu–Himal Chuli Himalaya, west-central Nepal. *Lithosphere, 3*(6), 379-392. doi:10.1130/l149.1

Larson, K. P., Kellett, D. A., Cottle, J. M., King, J., Lederer, G., & Rai, S. M. (2016). Anatexis, cooling, and kinematics during orogenesis: Miocene development of the Himalayan metamorphic core, east-central Nepal. *Geosphere, 12*(5), 1575-1593. doi:10.1130/ges01293.1

Larson, K. P., Shrestha, S., Soret, M., & Smit, M. (2022). The P-T-t-D evolution of the Mahabharat, east-central Nepal: The out-of-sequence development of the Himalaya. *Geoscience Frontiers, 13*(2), 101057. doi:https://doi.org/10.1016/j.gsf.2020.08.001

Lavé, J., & Avouac, J. P. (2000). Active folding of fluvial terraces across the Siwaliks Hills, Himalayas of central Nepal. *Journal of Geophysical Research: Solid Earth, 105*(B3), 5735-5770. doi:https://doi.org/10.1029/1999JB900292

Law, R. D., Searle, M. P., & Simpson, R. L. (2004). Strain, deformation temperatures and vorticity of flow at the top of the Greater Himalayan Slab, Everest Massif, Tibet. *Journal of the Geological Society, 161*(2), 305-320. doi:10.1144/0016-764903-047

Le Fort, P. (1975). Himalayas:Collided range:Present knowledge of continental arc. *American Journal of Science, 275 (A)*, 1-44.

Le Fort, P., & Raï, S. M. (1999). Pre-Tertiary felsic magmatism of the Nepal Himalaya: recycling of continental crust. *Journal of Asian Earth Sciences, 17*(5), 607-628. doi:https://doi.org/10.1016/S1367-9120(99)00015-2

Lee, J.-Y., Marti, K., Severinghaus, J. P., Kawamura, K., Yoo, H.-S., Lee, J. B., & Kim, J. S. (2006). A redetermination of the isotopic abundances of atmospheric Ar. *Geochimica et Cosmochimica Acta, 70*(17), 4507-4512. doi:https://doi.org/10.1016/j.gca.2006.06.1563

Lombardo, B., Pertusati, P., & Borghi, S. (1993). Geology and tectonomagmatic evolution of the eastern Himalaya along the Chomolungma-Makalu transect. In P. J. Treloar & M. P. Searle (Eds.), *Himalayan Tectonics* (Vol. 74, pp. 341-355): Geological Society, London, Special Publications.

Long, S., McQuarrie, N., Tobgay, T., & Grujic, D. (2011). Geometry and crustal shortening of the Himalayan fold-thrust belt, eastern and central Bhutan. *GSA bulletin, 123*(7-8), 1427-1447. doi:10.1130/b30203.1

Long, S. P., & Robinson, D. M. (2021). Construction of the Lesser Himalayan–Subhimalayan thrust belt: The primary driver of thickening, exhumation, and high elevations in the Himalayan orogen since the middle Miocene. *Geology, 49*(11), 1283-1288. doi:10.1130/g48967.1

Malekzade, Z., Bellier, O., Abbassi, M. R., Shabanian, E., & Authemayou, C. (2016). The effects of plate margin inhomogeneity on the deformation pattern within west-Central Zagros Fold-and-Thrust Belt. *Tectonophysics, 693*, 304-326. doi:http://dx.doi.org/10.1016/j.tecto.2016.01.030

Mandal, S., Robinson, D. M., Khanal, S., & Das, O. (2015). Redefining the tectonostratigraphic and structural architecture of the Almora klippe and the Ramgarh–Munsiari thrust sheet in NW India. *Geological Society, London, Special Publications, 412*(1), 247-269. doi:doi:10.1144/SP412.6

Martin, A. J. (2017). A review of Himalayan stratigraphy, magmatism, and structure. *Gondwana Research, 49*, 42-80. doi:https://doi.org/10.1016/j.gr.2017.04.031

Maruo, Y., & Kizaki, K. (1981). Structure and metamorphism in eastern Nepal. In P. S. Saklani (Ed.), *Metamorphic Tectonites of the Himalaya* (pp. 175-230). New Delhi: Today and Tomorrow's Printers and Publishers.

Medlicott, H. B. (1864). *On the geological Structure and relations of the Himalayan ranges, between the rivers Ganges and Ravee*. Retrieved from

Mendoza, M. M., Ghosh, A., Karplus, M. S., Klemperer, S. L., Sapkota, S. N., Adhikari, L. B., & Velasco, A. (2019). Duplex in the Main Himalayan Thrust illuminated by aftershocks of the 2015 Mw 7.8 Gorkha earthquake. *Nature geoscience, 12*(12), 1018-1022. doi:10.1038/s41561-019-0474-8

Miller, C., Klötzli, U., Frank, W., Thöni, M., & Grasemann, B. (2000). Proterozoic crustal evolution in the NW Himalaya (India) as recorded by circa 1.80 Ga mafic and 1.84 Ga granitic magmatism. *Precambrian Research, 103*(3), 191-206. doi:https://doi.org/10.1016/S0301-9268(00)00091-7

Molnar, P., & Tapponnier, P. (1975). Cenozoic Tectonics of Asia: Effects of a Continental Collision. *Science, 189*(4201), 419-426. doi:doi:10.1126/science.189.4201.419

Molnar, P., & Tapponnier, P. (1978). Active tectonics of Tibet. *Journal of Geophysical Research: Solid Earth, 83*(B11), 5361-5375. doi:https://doi.org/10.1029/JB083iB11p05361

Monsalve, G., Sheehan, A., Schulte-Pelkum, V., Rajaure, S., Pandey, M. R., & Wu, F. (2006). Seismicity and one-dimensional velocity structure of the Himalayan collision zone: Earthquakes in the crust and upper mantle. *Journal of Geophysical Research: Solid Earth, 111*(B10). doi:https://doi.org/10.1029/2005JB004062

Montemagni, C., Montomoli, C., Iaccarino, S., Carosi, R., Jain, A. K., Massonne, H.-J., & Villa, I. M. (2019). Dating protracted fault activities: microstructures, microchemistry and geochronology of the Vaikrita Thrust, Main Central Thrust zone, Garhwal Himalaya, NW India. In R. Sharma, I. M. Villa, & S. Kumar (Eds.), *Crustal Architecture and Evolution of the Himalaya–Karakoram–Tibet Orogen* (Vol. 481): The Geological Society of London.

Morgan, L. E., Mark, D. F., Imlach, J., Barfod, D., & Dymock, R. (2014). FCs-EK: a new sampling of the Fish Canyon Tuff 40Ar/39Ar neutron flux monitor. In F. Jourdan, D. F. Mark, & C. Verati (Eds.), *Advances in 40Ar/39Ar Dating: from Archaeology to Planetary Sciences* (Vol. 378, pp. 63-67): Geological Society of London, Special Publications.

Mugnier, J. L., Jouanne, F., Bhattarai, R., Cortes-Aranda, J., Gajurel, A., Leturmy, P., Robert, X., Upreti, B., & Vassallo, R. (2017). Segmentation of the Himalayan megathrust around the Gorkha earthquake (25 April 2015) in Nepal. *Journal of Asian Earth Sciences, 141*, 236-252. doi:https://doi.org/10.1016/j.jseaes.2017.01.015

Mugnier, J. L., Leturmy, P., Huyghe, P., & Chalaron, E. (1999a). The Siwaliks of western Nepal: II. Mechanics of the thrust wedge. *Journal of Asian Earth Sciences, 17*(5), 643-657. doi:https://doi.org/10.1016/S1367-9120(99)00039-5

Mugnier, J. L., Leturmy, P., Mascle, G., Huyghe, P., Chalaron, E., Vidal, G., Husson, L., & Delcaillau, B. (1999b). The Siwaliks of western Nepal 1: Geometry and kinematics. *Journal of Asian Earth Sciences, 17*, 629-642. doi:https://doi.org/10.1016/S1367-9120(99)00038-3

Mukhopadhyay, D. K., Chakraborty, S., Trepmann, C., Rubatto, D., Anczkiewicz, R., Gaidies, F., Dasgupta, S., & Chowdhury, P. (2017). The nature and evolution of the Main Central Thrust: Structural and geochronological constraints from the Sikkim Himalaya, NE India. *Lithos, 282-283*, 447-463. doi:https://doi.org/10.1016/j.lithos.2017.01.015

Mukul, M. (2010). First-order kinematics of wedge-scale active Himalayan deformation: Insights from Darjiling–Sikkim–Tibet (DaSiT) wedge. *Journal of Asian Earth Sciences, 39*(6), 645-657. doi:https://doi.org/10.1016/j.jseaes.2010.04.029

Mukul, M., Jade, S., Ansari, K., Matin, A., & Joshi, V. (2018). Structural insights from geodetic Global Positioning System measurements in the Darjiling-Sikkim Himalaya. *Journal of Structural Geology, 114*, 346-356. doi:https://doi.org/10.1016/j.jsg.2018.03.007

Musumeci, G. (2002). Sillimanite-bearing shear zones in syntectonic leucogranite: fluid-assisted brittle–ductile deformation under amphibolite facies conditions. *Journal of Structural Geology, 24*(9), 1491-1505. doi:https://doi.org/10.1016/S0191-8141(01)00153-5

Nábělek, J., Hetényi, G., Vergne, J., Sapkota, S., Kafle, B., Jiang, M., Su, H., Chen, J., Huang, B.-S., & Team, t. H.-C. (2009). Underplating in the Himalaya-Tibet Collision Zone Revealed by the Hi-CLIMB Experiment. *Science, 325*(5946), 1371-1374. doi:doi:10.1126/science.1167719

Nakajima, T., Sakai, H., Iwano, H., Danhara, T., & Hirata, T. (2020). Northward younging zircon fission-track ages from 13 to 2 Ma in the eastern extension of the Kathmandu nappe and underlying Lesser Himalayan sediments distributed to the south of Mt. Everest. *Island Arc, 29*(1), e12352. doi:https://doi.org/10.1111/iar.12352

Nakayama, K., & Ulak, P. D. (1999). Evolution of fluvial style in the Siwalik Group in the foothills of the Nepal Himalaya. *Sedimentary Geology, 125*(3), 205-224. doi:https://doi.org/10.1016/S0037-0738(99)00012-3

Nelson, K. D., Zhao, W., Brown, L. D., Kuo, J., Che, J., Liu, X., Klemperer, S. L., Makovsky, Y., Meissner, R., Mechie, J., Kind, R., Wenzel, F., Ni, J., Nabelek, J., Leshou, C., Tan, H., Wei, W., Jones, A. G., Booker, J., Unsworth, M., Kidd, W. S. F., Hauck, M., Alsdorf, D., Ross, A., Cogan, M., Wu, C., Sandvol, E., & Edwards, M. (1996). Partially Molten Middle Crust Beneath Southern Tibet: Synthesis of Project INDEPTH Results. *Science, 274*(5293), 1684-1688. doi:doi:10.1126/science.274.5293.1684

Ojha, T. P., Butler, R. F., DeCelles, P. G., & Quade, J. (2009). Magnetic polarity stratigraphy of the Neogene foreland basin deposits of Nepal. *Basin Research, 21*(1), 61-90. doi:https://doi.org/10.1111/j.1365-2117.2008.00374.x

Oriolo, S., Japas, M. S., Cristallini, E. O., & Giménez, M. (2014). Cross-strike structures controlling magmatism emplacement in a flat-slab setting (Precordillera, Central Andes of Argentina). *Geological Society, London, Special Publications, 394*(1), 113-127. doi:https://doi.org/10.1144/sp394.6

Orme, D. A., Carrapa, B., & Kapp, P. (2015). Sedimentology, provenance and geochronology of the upper Cretaceous–lower Eocene western Xigaze forearc basin, southern Tibet. *Basin Research, 27*(4), 387-411. doi:https://doi.org/10.1111/bre.12080

Pandey, M. R., Tandukar, R. P., Avouac, J. P., Lavé, J., & Massot, J. P. (1995). Interseismic strain accumulation on the Himalayan crustal ramp (Nepal). *Geophysical Research Letters, 22*(7), 751-754. doi:https://doi.org/10.1029/94GL02971

Pandey, M. R., Tandukar, R. P., Avouac, J. P., Vergne, J., & Héritier, T. (1999). Seismotectonics of the Nepal Himalaya from a local seismic network. *Journal of Asian Earth Sciences, 17*(5), 703-712. doi:https://doi.org/10.1016/S1367-9120(99)00034-6

Parrish, R. R., & Hodges, V. (1996). Isotopic constraints on the age and provenance of the Lesser and Greater Himalayan sequences, Nepalese Himalaya. *GSA bulletin, 108*(7), 904-911. doi:10.1130/0016-7606(1996)108<0904:Icotaa>2.3.Co;2

Passchier, C. W., & Trouw, R. A. (2005). *Micro-tectonics*: Springer.

Paul, H., Mitra, S., Bhattacharya, S. N., & Suresh, G. (2015). Active transverse faulting within underthrust Indian crust beneath the Sikkim Himalaya. *Geophysics Journal International, 201*(2), 1070-1081. doi:https://doi.org/10.1093/gji/ggv058

Paulsen, T., & Marshak, S. (1999). Origin of the Uinta recess, Sevier fold–thrust belt, Utah: influence of basin architecture on fold–thrust belt geometry. *Tectonophysics, 312*(2-4), 203-216. doi:https://doi.org/10.1016/S0040-1951(99)00182-1

Pearson, O. N., & DeCelles, P. G. (2005). Structural geology and regional tectonic significance of the Ramgarh thrust, Himalayan fold-thrust belt of Nepal. *Tectonics, 24*(4). doi:https://doi.org/10.1029/2003TC001617

Pêcher, A. (1989). The metamorphism in the Central Himalaya. *Journal of Metamorphic Geology, 7*(1), 31-41. doi:https://doi.org/10.1111/j.1525-1314.1989.tb00573.x

Pognante, U., & Benna, P. (1993). Metamorphic zonation, migmatization and leucogranites along the Everest transect of Eastern Nepal and Tibet: record of an exhumation history. *Geological Society, London, Special Publications, 74*(1), 323-340. doi:doi:10.1144/GSL.SP.1993.074.01.22

Rajaure, S., Sapkota, S. N., Adhikari, L. B., Koirala, B., Bhattarai, M., Tiwari, D. R., Gautam, U. G., Shrestha, P., Maske, S., Avouac, J. P., Bollinger, L., & Pandey, M. R. (2013). Double difference relocation of local earthquakes in the Nepal Himalaya. *Journal of Nepal Geological Society, 46*(0), 133–142. doi:10.3126/jngs.v46i0.31590

Ramos, V. A., Cristallini, E. O., & Pérez, D. J. (2002). The Pampean flat-slab of the Central Andes. *Journal of South American earth sciences, 15*(1), 59-78. doi:https://doi.org/10.1016/S0895-9811(02)00006-8

Rao, M. B. R. (1973). The subsurface geology of the Indo-Gangetic plains. *Journal of The Geological Society of India, 14*(3), 217-242.

Renne, P. R., Balco, G., Ludwig, K. R., Mundil, R., & Min, K. (2011). Response to the comment by W. H. Schwarz et al. on “Joint determination of 40K decay constants and the 40Ar*/40K for the Fish Canyon sanidine, and improved accuracy for 40Ar/39Ar geochronology” by P.R. Renne et al. (2010). *Geochimica et Cosmochimica Acta, 75*, 5097-5100.

Renne, P. R., Cassata, W. S., & Morgan, L. E. (2009). The isotopic composition of atmospheric argon and 40Ar/39Ar geochronology: Time for a change? *Quaternary Geochronology, 4*(4), 288-298. doi:https://doi.org/10.1016/j.quageo.2009.02.015

Robinson, D. M., DeCelles, P. G., & Copeland, P. (2006). Tectonic evolution of the Himalayan thrust belt in western Nepal: Implications for channel flow models. *GSA bulletin, 118*(7-8), 865-885. doi:10.1130/b25911.1

Robinson, D. M., DeCelles, P. G., Patchett, P. J., & Garzione, C. N. (2001). The kinematic evolution of the Nepalese Himalaya interpreted from Nd isotopes. *Earth and Planetary Science Letters, 192*(4), 507-521. doi:https://doi.org/10.1016/S0012-821X(01)00451-4

Rosenberg, C. L., & Garcia, S. (2011). Estimating displacement along the Brenner Fault and orogen-parallel extension in the Eastern Alps. *International Journal of Earth Sciences, 100*(5), 1129-1145. doi:https://doi.org/10.1007/s00531-011-0645-3

Sahoo, P. K., Kumar, S., & Singh, R. P. (2000). Neotectonic study of Ganga and Yamuna tear faults, NW Himalaya, using remote sensing and GIS. *International Journal of Remote Sensing, 21*(3), 499-518. doi:10.1080/014311600210713

Sakai, H. (1983). Geology of the Tansen Group of the Lesser Himalaya in Nepal. *Memoirs of the Faculty of Science, Kyūsyū University. Series D, Geology, 23*, 27-74. doi:https://doi.org/10.5109/1546083

Sakai, H., Iwano, H., Danhara, T., Takigami, Y., Rai, S. M., Upreti, B. N., & Hirata, T. (2013). Rift-related origin of the Paleoproterozoic Kuncha Formation, and cooling history of the Kuncha nappe and Taplejung granites, eastern Nepal Lesser Himalaya: a multichronological approach. *Island Arc, 22*(3), 338-360. doi:https://doi.org/10.1111/iar.12021

Sastri, V. V., Bhandari, L. L., Raju, A. T. R., & Datta, A. K. (1971). *Tectonic Framework and Subsurface Stratigraphy of the Ganga Basin*.

Schelling, D. (1992). The tectonostratigraphy and structure of the eastern Nepal Himalaya. *Tectonics, 11*(5), 925-943. doi:https://doi.org/10.1029/92TC00213

Schultz, M. H., Hodges, K. V., Ehlers, T. A., van Soest, M., & Wartho, J.-A. (2017). Thermochronologic constraints on the slip history of the South Tibetan detachment system in the Everest region, southern Tibet. *Earth and Planetary Science Letters, 459*, 105-117. doi:https://doi.org/10.1016/j.epsl.2016.11.022

Searle, M. P. (1999). Extensional and compressional faults in the Everest–Lhotse massif, Khumbu Himalaya, Nepal. *Journal of the Geological Society, 156*(2), 227-240. doi:https://doi.org/10.1144/gsjgs.156.2.0227

Searle, M. P. (2010). Low-angle normal faults in the compressional Himalayan orogen; Evidence from the Annapurna–Dhaulagiri Himalaya, Nepal. *Geosphere, 6*(4), 296-315. doi:10.1130/ges00549.1

Searle, M. P., Law, R. D., Godin, L., Larson, K. P., Streule, M. J., Cottle, J. M., & Jessup, M. J. (2008). Defining the Himalayan Main Central Thrust in Nepal. *Journal of the Geological Society, 165*(2), 523-534. doi:10.1144/0016-76492007-081

Searle, M. P., Law, R. D., & Jessup, M. J. (2006). Crustal structure, restoration and evolution of the Greater Himalaya in Nepal-South Tibet: implications for channel flow and ductile extrusion of the middle crust. *Geological Society, London, Special Publications, 268*(1), 355-378. doi:doi:10.1144/GSL.SP.2006.268.01.17

Searle, M. P., & Rex, A. J. (1989). Thermal model for the Zanskar Himalaya. *Journal of Metamorphic Geology, 7*(1), 127-134. doi:https://doi.org/10.1111/j.1525-1314.1989.tb00579.x

Searle, M. P., Simpson, R. L., Law, R. D., Parrish, R. R., & Waters, D. J. (2003). The structural geometry, metamorphic and magmatic evolution of the Everest massif, High Himalaya of Nepal–South Tibet. *Journal of the Geological Society, 160*(3), 345-366. doi:doi:10.1144/0016-764902-126

Seifert, N. (2019). *Structural analysis of the Benkar Fault Zone, a cross structure in the Higher Himalaya of the Khumbu Region, eastern Nepal.* (MS). Montana State University, Bozeman, Montana.

Simpson, R. L., Parrish, R. R., Searle, M. P., & Waters, D. J. (2000). Two episodes of monazite crystallization during metamorphism and crustal melting in the Everest region of the Nepalese Himalaya. *Geology, 28*(5), 403-406. doi:10.1130/0091-7613(2000)28<403:Teomcd>2.0.Co;2

Soucy La Roche, R., & Godin, L. (2019). Inherited Cross-Strike Faults and Oligocene-Early Miocene Segmentation of the Main Himalayan Thrust, West Nepal. *Journal of Geophysical Research: Solid Earth, 124*(7), 7429-7444. doi:https://doi.org/10.1029/2019JB017467

Srivastava, V., Mukul, M., Barnes, J. B., & Mukul, M. (2018). Geometry and kinematics of Main Frontal thrust-related fault propagation folding in the Mohand Range, northwest Himalaya. *Journal of Structural Geology, 115*, 1-18. doi:https://doi.org/10.1016/j.jsg.2018.06.022

Srivastava, V., Mukul, M., & Mukul, M. (2017). Quaternary deformation in the Gorubathan recess: Insights on the structural and landscape evolution in the frontal Darjiling Himalaya. *Quaternary International, 462*, 138-161. doi:https://doi.org/10.1016/j.quaint.2017.05.004

Stevens, V. L., & Avouac, J.-P. (2016). Millenary Mw > 9.0 earthquakes required by geodetic strain in the Himalaya. *Geophysical Research Letters, 43*(3), 1118-1123. doi:https://doi.org/10.1002/2015GL067336

Stipp, M., Stünitz, H., Heilbronner, R., & Schmid, S. M. (2002). The eastern Tonale fault zone: a 'natural laboratory' for crystal plastic deformation of quartz over a temperature range from 250 to 700°C. *Journal of Structural Geology*, *24*(12), 1861-1884. doi:https://doi.org/10.1016/S0191-8141(02)00035-4

Stöcklin, J. (1980). Geology of Nepal and its regional frame. *Journal of the Geological Society, 137*(1), 1-34. doi:doi:10.1144/gsjgs.137.1.0001

Stöcklin, J., & Bhattarai, K. D. (1977). *Geology of the Kathmandu area and central Mahabharat range, Nepal Himalaya*. Retrieved from

Streule, M. J., Carter, A., Searle, M. P., & Cottle, J. M. (2012). Constraints on brittle field exhumation of the Everest-Makalu section of the Greater Himalayan Sequence: Implications for models of crustal flow. *Tectonics, 31*(3). doi:https://doi.org/10.1029/2011TC003062

Styron, R. H., Taylor, M. H., & Murphy, M. A. (2011). Oblique convergence, arc-parallel extension, and the role of strike-slip faulting in the High Himalaya. *Geosphere, 7*(2), 582-596. doi:10.1130/ges00606.1

Szulc, A. G., Najman, Y., Sinclair, H. D., Pringle, M., Bickle, M., Chapman, H., Garzanti, E., Andò, S., Huyghe, P., Mugnier, J. L., Ojha, T., & DeCelles, P. (2006). Tectonic evolution of the Himalaya constrained by detrital 40Ar–39Ar, Sm–Nd and petrographic data from the Siwalik foreland basin succession, SW Nepal. *Basin Research, 18*(4), 375-391. doi:https://doi.org/10.1111/j.1365-2117.2006.00307.x

Thomas, W. A. (2014). A mechanism for tectonic inheritance at transform faults of the Iapetan margin of Laurentia. *Geoscience Canada*, 321-344. doi:http://dx.doi.org/10.12789/geocanj.2014.41.048

Tiwari, R. K., Paudyal, H., & Shanker, D. (2022). On the spatio-temporal variation in b-value after 25 April 2015 Gorkha, Nepal earthquake. *Geodesy and Geodynamics, 13*(5), 525-533. doi:https://doi.org/10.1016/j.geog.2022.01.006

Tokuoka, T. (1986). The Churia (Siwalik) Group of the Arung Khola, West Central Nepal. *Memoir of the Faculty of Science, Shimane University, 20*, 135-210. Retrieved from https://cir.nii.ac.jp/crid/1573668925765389184

Upreti, B. N. (1999). An overview of the stratigraphy and tectonics of the Nepal Himalaya. *Journal of Asian Earth Sciences, 17*(5), 577-606. doi:https://doi.org/10.1016/S1367-9120(99)00047-4

Upreti, B. N., Rai, S. M., Sakai, H., Koirala, D. R., & Takigam, Y. (2003). Early Proterozoic granite of the Taplejung Window, far eastern Lesser Nepal Himalaya. *Journal of Nepal Geological Society*, *28*(0), 9–18. doi:10.3126/jngs.v28i0.31720

Valdiya, K. S. (1976). Himalayan transverse faults and folds and their parallelism with subsurface structures of North Indian plains. *Tectonophysics, 32*, 353-386. doi:https://doi.org/10.1016/0040-1951(76)90069-X

Valdiya, K. S. (2002). Emergence and evolution of Himalaya: reconstructing history in the light of recent studies. *Progress in Physical Geography: Earth and Environment*, *26*(3), 360-399. doi:10.1191/0309133302pp342ra

van der Beek, P., Litty, C., Baudin, M., Mercier, J., Robert, X., Hardwick, E. (2016). Contrasting tectonically driven exhumation and incision patterns, western versus central Nepal Himalaya. *Geology*, *44*(4), 327-330. doi:https://doi.org10.1130/G37579.1

Vannay, J. C., & Hodges, K. V. (1996). Tectonometamorphic evolution of the Himalayan metamorphic core between the Annapurna and Dhaulagiri, central Nepal. *Journal of Metamorphic Geology, 14*(5), 635-656. doi:https://doi.org/10.1046/j.1525-1314.1996.00426.x

Viskupic, K., & Hodges, K. V. (2001). Monazite–xenotime thermochronometry: methodology and an example from the Nepalese Himalaya. *Contributions to Mineralogy and Petrology, 141*(2), 233-247. doi:10.1007/s004100100239

Wang, A., Garver, J. I., Wang, G., Smith, J. A., & Zhang, K. (2010). Episodic exhumation of the Greater Himalayan Sequence since the Miocene constrained by fission track thermochronology in Nyalam, central Himalaya. *Tectonophysics, 495*(3-4), 315-323.

Wang, J.-M., Rubatto, D., & Zhang, J.-J. (2015). Timing of Partial Melting and Cooling across the Greater Himalayan Crystalline Complex (Nyalam, Central Himalaya): In-sequence Thrusting and its Implications. *Journal of Petrology, 56*(9), 1677-1702. doi:10.1093/petrology/egv050

Webb, A. A. G., Schmitt, A. K., He, D., & Weigand, E. L. (2011). Structural and geochronological evidence for the leading edge of the Greater Himalayan Crystalline complex in the central Nepal Himalaya. *Earth and Planetary Science Letters, 304*(3), 483-495. doi:https://doi.org/10.1016/j.epsl.2011.02.024

Wu, C., Nelson, K. D., Wortman, G., Samson, S. D., Yue, Y., Li, J., Kidd, W. S. F., & Edwards, M. A. (1998). Yadong cross structure and South Tibetan Detachment in the east central Himalaya (89°–90°E). *Tectonics, 17*(1), 28-45. doi:https://doi.org/10.1029/97TC03386

Wu, F.-Y., Ji, W.-Q., Wang, J.-G., Liu, C.-Z., Chung, S.-L., & Clift, P. D. (2014). Zircon U–Pb and Hf isotopic constraints on the onset time of India-Asia collision. *American Journal of Science, 314*(2), 548. doi:10.2475/02.2014.04

Yin, A. (2006). Cenozoic tectonic evolution of the Himalayan orogen as constrained by along-strike variation of structural geometry, exhumation history, and foreland sedimentation. *Earth-Science Reviews, 76*(1), 1-131. doi:https://doi.org/10.1016/j.earscirev.2005.05.004

Yoshida, K., Nakajima, T., Matsumoto, Y., Osaki, A., Rai, L. K., Cruz, J. W., & Sakai, H. (2021). Miocene provenance change in Himalayan foreland basin and Bengal Fan sediments, with special reference to detrital garnet chemistry. *Island Arc*, *30*(1), e12408. doi:https://doi.org/10.1111/iar.12408

Zhu, D.-C., Wang, Q., Zhao, Z.-D., Chung, S.-L., Cawood, P. A., Niu, Y., Liu, S.-A., Wu, F.-Y., & Mo, X.-X. (2015). Magmatic record of India-Asia collision. *Scientific reports, 5*(1), 14289. doi:10.1038/srep14289

CHAPTER FOUR

GEOMORPHIC IMPLICATIONS OF LATE PLIESTOCENCE SURFICIAL SAND DEPOSITS IN THE LOWER KHUMBU REGION, NEPAL

Contribution of Authors and Co-Authors

Manuscript in Chapter 4

Bibek Giri: Methodology, Investigation, Data analysis, Writing – original draft and figures
Mary Hubbard: Conceptualization, Funds acquisition, Methodology, Investigation, Data analysis, Writing – review and editing, Validation
Ananta Prasad Gajurel: Conceptualization, Writing – review and editing
Michelle Nelson: Laboratory analysis, Writing – review and editing

Manuscript Information

Bibek Giri[1], Mary Hubbard[1], Ananta Prasad Gajurel[2], and Michelle Nelson[3]
1 Montana State University
2 Trichandra Multiple Campus
3 Utah State University

The Nature of Geomorphological Hazards in the Nepal Himalaya

Status of Manuscript
____ Prepared for submission to a peer-reviewed journal
__x_ Officially submitted to a peer-reviewed journal
____ Accepted by a peer-reviewed journal
____ Published in a peer-reviewed journal

Submitted: November 2022

Abstract

In the Lower Khumbu of eastern Nepal, a number of well-bedded, sandy/silty deposits are perched high on hillslopes with no obvious connection to a depositional setting. In this study we utilize infrared stimulated luminescence analysis (IRSL) to determine the age of deposition of six of these deposits as a first step in understanding the environment in which they formed. This area of the high Himalaya has experienced multiple glaciations as well as large and small landslide events. From field mapping and literature review we propose several possibilities for how these deposits fit into the regional Quaternary history. The data suggest that strath terrace of Phortse was carved during a glacial advance around 42 ka. Towards the south, the Khumjung Rockslide Complex occurred before 26 ka and was probably triggered by a paleo, mega-earthquake. Smaller landslide events cut the Khumjung Rockslide to create the amphitheater that hosts the village of Namche Bazar. These smaller events post-date 26 ka. This post-26 ka time also aligns with deposits near the ridge of the Tyangboche monastery. Seismic events could have been responsible for triggering a number of events at 24-26 ka.

Keywords: Khumbu region, Infrared stimulated luminescence (IRSL) dating, Landslides, Lake deposits, River incision, Himalaya

Introduction

In the Khumbu region of eastern Nepal, like all of the high mountains of the Himalaya, the landscape was shaped by a combination of tectonic and earth surface processes. Erosion through a combination of landslides, glaciation, and rivers has left deep valleys surrounded by high mountain peaks. In a lower area of the Khumbu, where three major valleys come together (Figure 4.1), there are anomalous exposures of fine-grained, thinly bedded, unconsolidated sediment perched 600 meters above the modern rivers that are not easily associated with any landscape feature (pond, lake, or stream) that might have been linked to their deposition. Upstream from this area of river confluence in the Upper Khumbu, the geomorphology of the extreme-altitude regions (>4,000 m) is primarily defined by spectacular rock exposures of high-grade metamorphic rocks, which has continuously been modified by alpine glacier processes. It is not surprising that much of the work to date around the area has been focused on hard rock geology (e.g., Hubbard, 1989; Carosi et al., 1999; Searle, 1999; Jessup et al., 2006; Cottle et al., 2009; Carrapa et al., 2016), glaciology (e.g., Wessels et al., 2002; Kang et al., 2004; Owen et al., 2009; Quincey et al., 2009; Bolch et al., 2011; Sherpa et al., 2017), and glacial geomorphology (e.g., Benedict, 1976; Iwata, 1976; Fushimi, 1977; Muller, 1980; Aoki & Imamura, 1999; Richards et al., 2000; Finkel et al., 2003; Barnard et al., 2006). Towards the south in the Lower Khumbu (<4,000 m), the influence of glacial processes on the tectonic landscape gradually diminishes, while landslide and fluvial processes become the more dominant surficial processes (Weidinger & Korup, 2009; Götz et al., 2015). A peculiar geological feature in the Khumbu region is the Benkar Fault Zone (BFZ) that cuts the north-dipping metamorphic fabric of high-grade metamorphic rocks (Seifert, 2019; Hubbard et al., 2021). This NNE-striking, normal fault runs along the Dudh Koshi valley (Seifert, 2019) and may have created the zone of weakness that has influence the location of the river valley and the fault may have facilitated mass wasting processes on the valley walls.

Generally, erosion outpaces deposition at these extreme topographies. Terraces along river valleys, however, offer preservation potential, where glacial, landslide, aeolian, fluvial, and debris flow deposits have been preserved. In the Lower Khumbu region, a number of well-bedded, sandy/silty deposits are perched high on hillslopes with no obvious connection to a depositional setting. This study has been aimed at understanding the possible depositional environments for these stranded deposits, constraining their depositional ages, and exploring possible connections between the depositional setting and the contemporaneous geomorphic processes. We examined and sampled six deposits for infrared stimulated luminescence (IRSL) analysis on feldspar sand grains, to constrain their respective depositional ages. The dating results have been integrated with the glacial chronology and landslide events for these valleys that is presented in the literature, and which has enabled us to constrain the timing for a few paleo-geomorphic events and partially reconstruct the Quaternary geomorphic history of the Lower Khumbu region.

Background

Two of the large modern glacial systems in the Khumbu region are the Ngozumpa glacier, within the Gokyo valley, which is the headwaters of the Dudh Koshi river, and the Khumbu glacier in the Khumbu valley, a side valley to the Imja river (Figure 4.1). The Ngozumpa glacier begins in the cirque below the peaks of Cho Oyu (8,153m) and Gyachung Kang (7,122 m) and flows past the settlement of Gokyo. To the east, the Khumbu glacier emerges from the south facing slopes of Mt. Everest. Early radiocarbon dating of organic material from within the glacial deposits in the Khumbu region revealed multiple pulses of glaciation (Benedict, 1976; Fushimi, 1977; Muller, 1980; Röthlisberger & Geyh, 1985), including the most recent, late Holocene, moraines (Richards et al., 2000) (Table 4. 1). Iwata (1976) mapped moraines in the Dudh Koshi and the Imja river valleys and identified four stages of glacial advance; the Thyangboche Stage (~40-50 ka), the Periche Stage (~20 ka), the Thuklha Stage (< 5 ka), and the Lobuche Stage (Late Holocence). The study suggested that the asynchronous Lobuche and Thukhla stages represent a culmination of advances between a few hundred to several thousand years ago, corresponding to the Neoglacial readvances in Europe and North America. The Periche and Thyangboche stages possibly represent the Late Glacial and Last Glacial Maximum advances respectively. Fushimi (1977) studied U-shaped glacial valleys and identified the Thukhla Series (<5 ka, Late Holocene), Periche Stage (ca 20 ka), and the U-1, U-2 and U-3 valleys (>150 ka). Richards et al. (2000) pointed out the shortcoming of using relative ages in their chronologies based on the degree of weathering of surface boulders, vegetation cover, modifications, and correlation with the marine oxygen isotope stages and pioneered numerical dating of the glacial landforms. Richards et al. (2000) identified 3 stages of glacier advance in the Khumbu region based on optically stimulated luminescence (OSL) ages on moraines , namely; Pheriche Glacial Stage (ca 18-25 ka); the Chukung Glacial Stage or Early Holocene Advance (ca. 10 ka); the Lobuche Stage or Late Holocene advance (ca. 1-2 ka). Using cosmogenic nuclides surface exposure dating of moraine boulders, Finkel et al. (2003) constructed a glacial chronology for the Dudh Koshi Valley consisting of eight glacial advances,

Figure 4.1: Map of the Everest region showing rivers, glaciers, major peaks, settlements, and extent of the Benkar Cross Fault Zone (modified from Hubbard et al. (2021). The rectangles show the extent of detailed maps in the Figures 4.2 and 4.3. Map frame location shown in the inset map.

Table 4.1: Tentative correlations, relative chronologies, and age constraints for glacial history in the Everest region, eastern Nepal.

Iwata (1976)	Fushimi (1977)	Williams (1983)	Muller (1980), Benedict (1976), Fushimi (1978)	Richards et al. (2000)	Finkel et al. (2003)	Owen et al. (2009)
			Outer moraine (Pumore) (~410–550 ^{14}C yr B.P.)		Historical (<500 yr B.P.)	Historical (<500 yr B.P.)
Lobuche I–III (late Holocene*)	Thuklha 3–4 (late Holocene*)	Yykugikcga I–III (late Holocene*)	Outer moraine (Tsola) (~1150–1200 ^{14}C yr B.P.)	Lobuche (~ 1–2 ka: OSL)	Lobuche (~ 1 ka)	Lobuche (~1.1 ± 0.4 ka)
Thuklha (<5 ka*)	Thuklha 1 (<5 ka*)	Tamba (<5 ka*)	Dhugla I and II		Thuklha (3.6 ± 0.3 ka)	Thuklha (3.5 ± 0.3 ka)
				Chhukung (~10 ka: OSL)	Chhukung (9.2 ± 0.2)	Chhukung (10.1 ± 0.4)
Periche (~20 ka*)	Periche (~20 ka*)	Lhaog (~20 ka*)		Periche (18–25 ka: OSL	Periche II (16 ± 2 ka)	Periche II (17.0 ± 1.7 ka)
					Periche I (23 ± 3 ka)	Periche I (23.9 ± 2.5 ka)
Thyangboche (~40–50 ka*)					Thyangboche II (35 ± 3 ka)	Thyangboche II (40.0 ± 5.0 ka)
					Thyangboche I (86 ±6 ka)	Thyangboche I (68.1 ± 34.6 ka)
Platform (>150 ka*)	U1					
	U2–3					

The asterisked ages are estimations of the moraine ages based on relative-weathering criteria and tentative correlation with glacial successions elsewhere in the world. OSL: optically stimulated luminescence.

which include the Thyangboche Stage I (86 ± 6 ka), Thyangboche Stage II (35±3 ka), Pheriche Stage I (23±3 ka), Pheriche Stage II (16±2 ka), Chhukhung (9.2±0.2 ka), Thuklha (3.6 ± 0.3 ka), Lobuche (ca 1 ka) and Historical (<0.5 ka). Owen et al. (2009) have further refined the glacial chronology of the Everest region using optically stimulated luminescence and 10^{Be} terrestrial cosmogenic nuclide dating (Table 4.1).

Geomorphic Setting

Namche Bazaar-Sanasa

The settlement of Namche Bazaar is located within a SSW-facing, landslide scarp, which is about 470 m long and 370 m wide. Nearby to the east, but separated by a ridge, is another similar, south facing scarp with a 30 m high hillock in the middle part of the depression (Figure 4.2). Looking at the remnant topography and the topographic curvature of the scarps, both of these slides seem to be rotational in nature. Within the western slide, referred to as the ‘Namche amphitheater’, materials were fully detached from the sliding surface and subsequently removed, leaving the bowl- shaped topography in which the modern village has been built. The topographic depression east of the Namche village that has a hillock in its center likely formed in a similar manner as the Namche amphitheater, yet the hill may represent remnants of the landslide material.

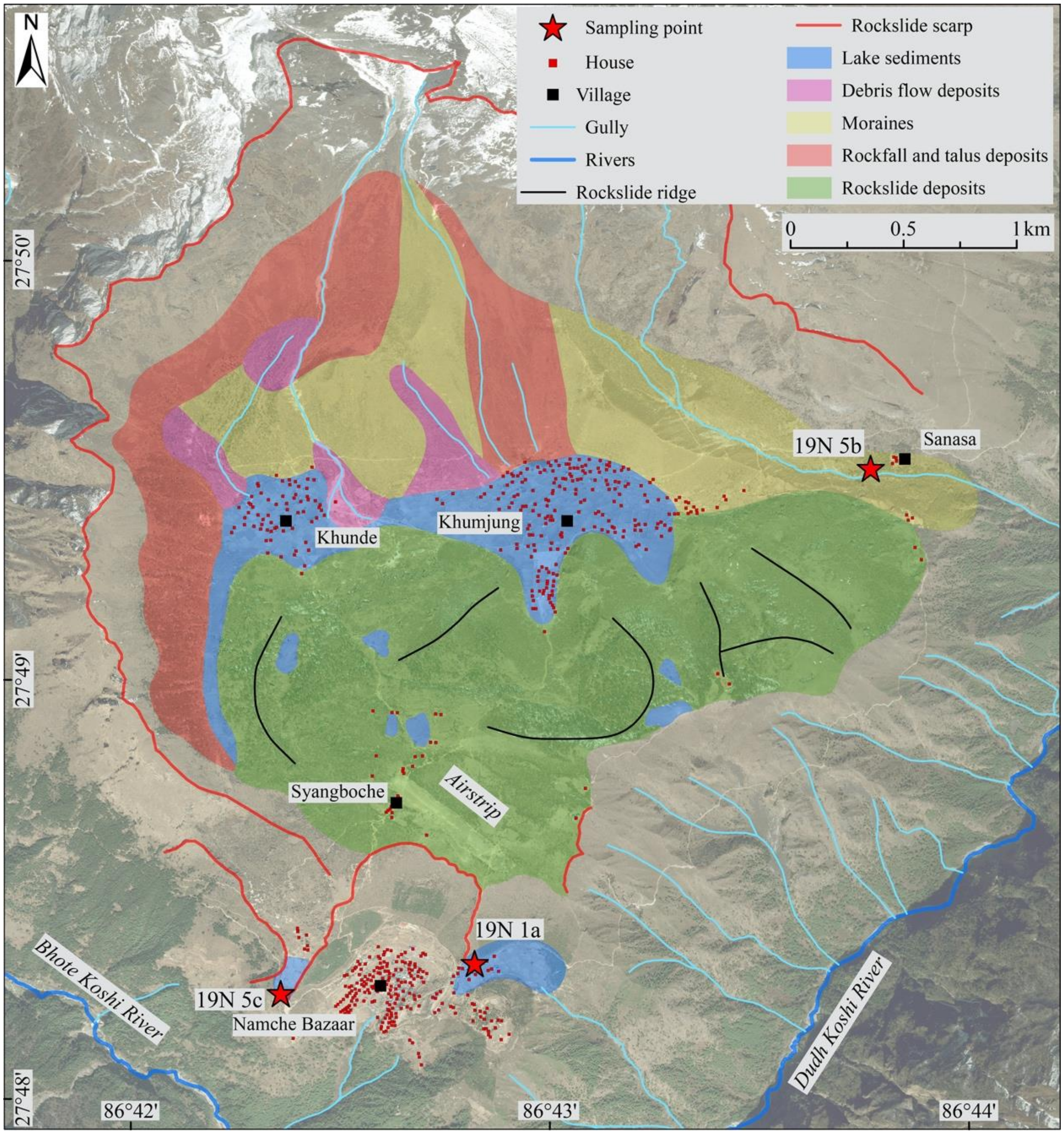

Figure 4.2: Simplified geomorphological map of the Khumjung-Namche region showing the extent of the Khumbu Rockslide Complex and Namche slides, different landforms, and sampled locations (modified from Götz et al. (2015)). The satellite image was downloaded from SAS planet application (May 25, 2020).

About 500 m west of Namche Bazaar is another scarp similar to the Namche amphitheater except much smaller and planar, which gives an indication that topography-forming, landslides are common in these high mountains.

The scarps in and adjacent to Namche Bazar cut into a broad and somewhat terrace-like topography, on the southern edge of which the settlement of Syangboche and the Syangboche Airstrip are located. A low ridge separates Syangboche from the villages of Khunde and Khumjung to the north, which are located on lacustrine and alluvial deposits (Heuberger, 1986) (Figure 4.2). This ridge consists mostly of angular fragments and massive boulders, within which ‘ponor-like sinkholes, ridge features, lacustrine deposits, and hummocky structures’ can be observed (Götz et al., 2015). To the north of these settlements is a 5761 m tall peak, known as Khumbi Yul Lha. Moraine ridges, originated from Khumbu Yul Lha (Figure 4.1) and reworked in places by debris flows, can be traced in both the eastern and western edges of these settlements. The geomorphologic system around this region is bounded by a semi-circular, arcuate shaped scarp of a mega rockslide: the Khumjung Rockslide Complex (KRC), whose deposits dominate the ridge south of Khunde and Khumjung and have been cut by the Namche landslides and multiple other smaller landslides (Figure 4.2). Following the Rockslide event, moraine deposits from Khumbi Yul La likely dammed the eastern and the only outlet of the elongated landslide depression, leading to the formation of a paleolake. Heuberger (1956) first recognized these landslide features and later he (Heuberger (1986) hypothesized that the landslide of Khumjung came from the Thamsherku peak, which is located towards the south-east, across the Dudh Koshi river. Different researchers (Korup & Weidinger, 2011; Götz et al., 2015; Posch et al., 2015) have described the Rockslide Complex in detail and inferred that it originated from Khumbu Yul Lha and the adjacent ridges. Based on an average rate of bedrock incision of the Imja River, Posch et al. (2015) estimated the maximum age of the rockslide to be about 50 ka. As Götz et al. (2015) pointed out, it will be difficult to determine the volume of material transported and the extent to which the material travelled during this event, primarily because much of the debris would have been removed by the Dudh Koshi river.

Bedrock in the headwall region of Khumbi Yul Lha is dipping towards the southeast, and assuming this is the source of the Khumjung Rockslide, it is likely that slip occurred along the foliation surfaces, possibly triggered by a paleo-earthquake event. These foliation surfaces are the slip planes of the BFZ suggesting that the tectonic history has influenced the location of surface process events.

The settlement of Sanasa is at the eastern end of the KRC where the modern drainage from the Khumjung area approaches the Dudh Koshi river. There is a sand deposit that on the edge of the broad terrace area of the KRC. This deposit does not appear to be associated with a smaller landslide setting but likely post-dates the KRC.

Phortse

The village of Phortse sits on a northeast-trending, almost rectangular terrace, which is about 700 m in length and 400 m wide (Figure 4.3 and 4.4). The edges of this terrace facing the adjacent Dudh Koshi and Imja rivers are all concave in shape, suggesting that landslides have been the erosional agent shaping the boundaries of this landform. The Phortse terrace is a strath terrace with bedrock just ~4 m below the current terrace surface (Figure 4.4). The Dudh Koshi and the Imja rivers merge just south of Phortse. A peculiar feature around the southeastern edge of Phortse is the presence of an arc-shaped, partially vegetated ridge (the Phortse ridge) of unconsolidated fine sand/silt capped by an angular boulder diamict. The south-eastern edge of this ridge has likely eroded into the Imja river below. The ridge, itself is roughly 10-15 m high with respect to the terrace surface and the sandy matrix in the cap supports boulders, which range in size from several 10's of centimeters to several meters in diameter. The fact that the boulders are sand supported suggests that it is not a moraine but more likely is related to a landslide or rockfall into the sand-dominated deposit.

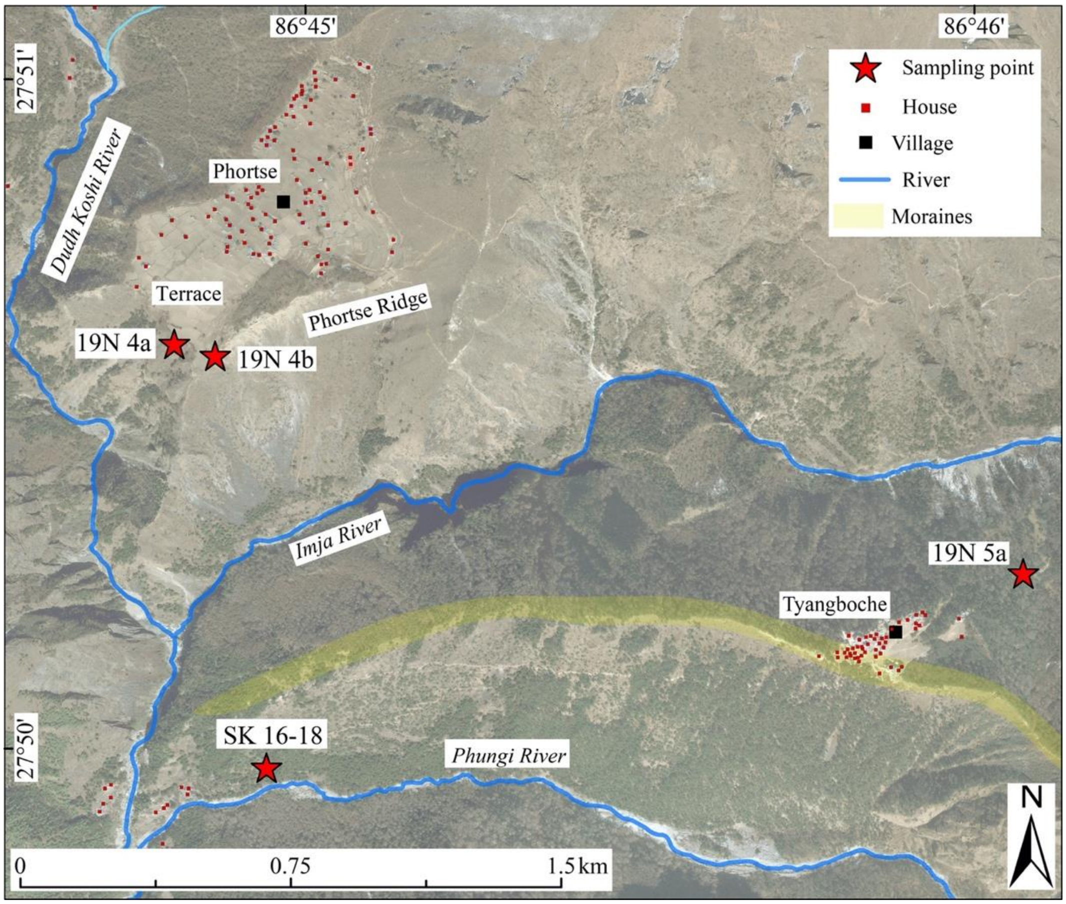

Figure 4.3: Geomorphological map of the Phortse-Thyangboche region showing the Phortse terrace, Phortse ridge, Thyangboche moraine ridge, and sampled locations. The satellite image was downloaded from SAS planet application (May 25, 2020).

Figure 4.4: Strath terrace of Phortse village. The view is looking northeast towards Phortse with the peak of Ama Dablam in the background. The dotted line shows the contact between bedrock and the overlying fine-grained sediments. The “X”s represent the sample locations. While much of the village is on a terrace of fine-grained sediment, the Phortse Ridge is an anamolous feature on the southeast side of the terrace and it contains large blocks of gneissic rock in addition to the fine-grained sediment. (Photograph by Mary Hubbard; Peter Molnar and student in the foreground).

<u>Thyangboche</u>

The village of Thyangboche sits on an east-west trending ridge between the Imja river to the north and the Phungi river to the south (Figure 4.3). Moraine deposits can be traced along the ridge, which generally has covered the bedrock. Richards et al. (2000) identified and constrained the depositional ages (21-25 ka) of lake deposits on the south side of the ridge (Figure 4.3). The Imja valley broadens upstream towards the east, where it retains the U-shape from its glacial history, though valley walls are modified by coalescing alluvial and rockfall deposits.

Site Descriptions and Luminescence Sampling

A total of six sandy/silty deposits have been sampled for infrared stimulated luminescence (IRSL) analysis on feldspar sand grains. Two of the studied deposits are located around Namche Bazar, two near Phortse village, and one each near Sanasa and Tyangboche. The sedimentology of these deposits and their loci within the broader geomorphic setting have been integrated to interpret their depositional environments.

Namche Bazar-Sanasa

The areas surrounding the settlement of Namche Bazaar are generally draped with fine grained sediments, which are, in places, overlain by boulders. Around the Namche Helipad, at the western edge of the town, a 3-4 m-thick stratigraphic section has been exposed, which in its lower section consists of a meter-thick unit with alternating bands of lighter and darker sand layers, each about 20 cm thick. These layers are dominated by fine to very fine sand with a minor silt component. The lighter units also locally contain angular cobbles/pebbles. Within the sampled section, 2 dark layers and 2 lighter layers have been delineated (Figure 4.5a and 4.6a). Sample 19N5c was collected from the lighter layer within the lower part of the exposed sequence. The sampled section is overlain by a 5-8 cm-thick layer, which consists of coarse sand as well as angular cobble/pebble-sized clasts. A 2-3 m-thick boulder diamict overlies the layered sequence. The gneissic boulders in this diamict unit are mostly angular, and some of them are massive, greater than 4 m across. The sedimentology of this succession indicates that the deposit most likely represents re-worked materials of the KRC. The stratigraphically lower fine sand sequence could either be slope colluvium deposit or pond deposit, which was formed within the landslide debris. The overlying unit, thin layers of angular boulders, were likely deposited during a later rockfall event.

At the eastern side of Namche Bazaar at the top of the amphitheater scarp, there is a 3 m-thick exposure of well-bedded sand (Figure 4.5b and 4.6b). Similar to the section at the western edge of Namche above the helipad, this sequence consists of alternating darker and lighter sand layers, where both types of layers consist mostly of fine to medium grained sand and are 2-3 cm-thick. Unlike the Helipad sequence, where only a couple of layers could be traced, here multiple beds can be identified, but the overlying conglomeratic layer is absent. Locally, minor deformation disrupts the otherwise continuous bedding (Figure 4.6b). Sample 19N1a was collected from the middle part of the section. This succession is devoid of any sedimentary structures normally associated with water currents or eolian processes, which led us to interpret these beds to have been deposited in still water. The possibility of these deposits instead being laminated slope colluvium (Mücher et al., 2018) has also been considered, but has been dismissed because of lack of evidence for the deposits following paleoslopes.

Figure 4.5: Field photographs of the six sampled exposures. a: Namche Helipad; b: Namche Bazar; c: Sanasa; d: Phortse Ridge; e: Phortse Bench; and f: Thyangboche. (Photographs by Mary Hubbard).

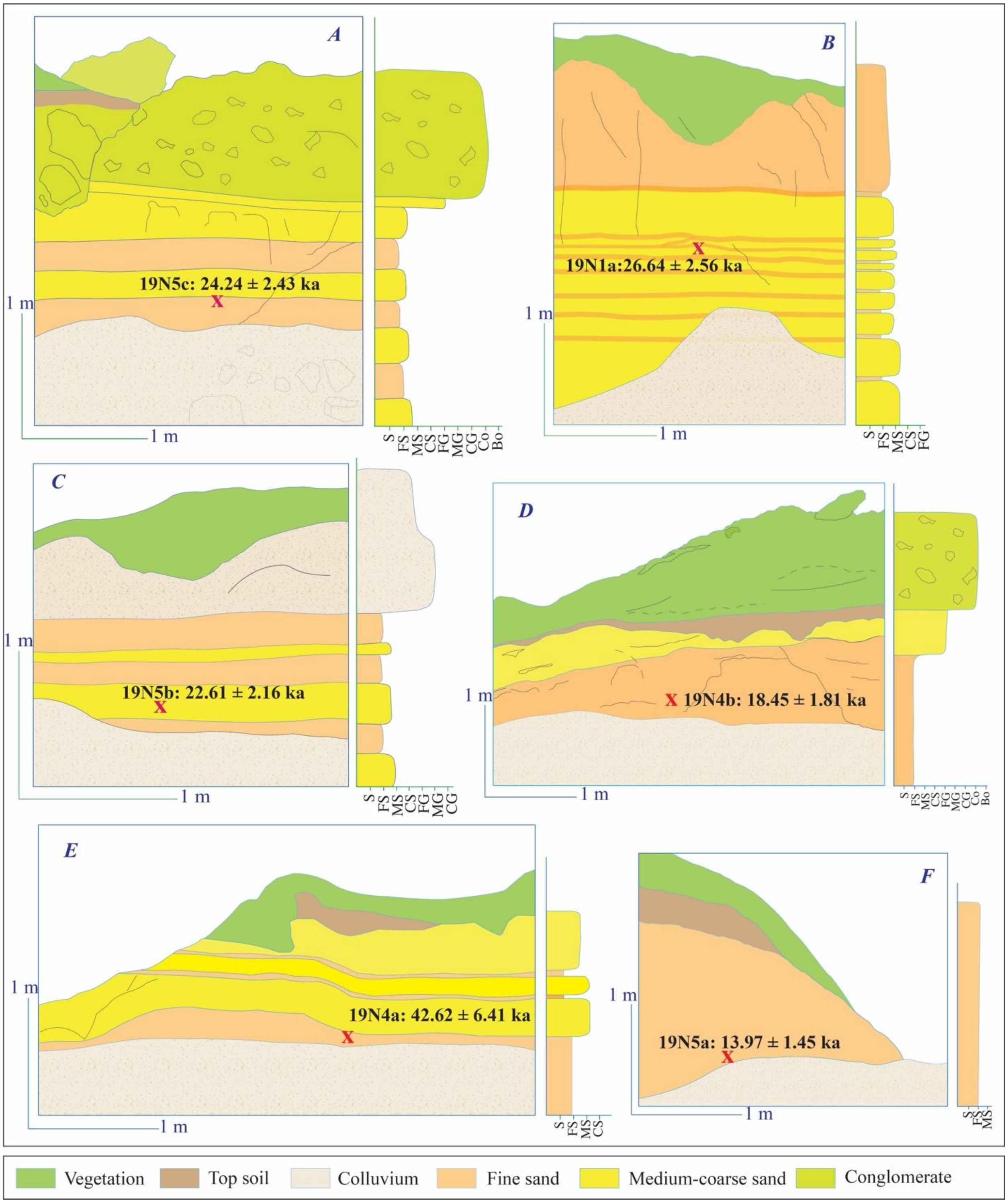

Figure 4.6: Schematic sections, and graphic sedimentary logs of the six sampled exposures shown in Figure 4.5. a: Namche Helipad; b: Namche Bazar; c: Sanasa; d: Phortse Ridge; e: Phortse Bench; and f: Thyangboche. Particle sizes are indicated on the graphic sedimentary logs

(S: silt; FS: fine sand; MS: medium sand; CS: coarse sand; FG: fine gravel; MG: medium gravel; Co: cobbles; Bo: boulders and/or conglomerates). Sampling points are shown as (x).

Around the eastern edge of the KRC, a meter-thick section exposed along the main trail, just west of Sanasa, displays well bedded, thinly laminated, light and dark sandy/silty layers (Figure 4.5c and 4.6c). The fine layering of the deposit serves as an indication of a calm depositional environment. Ample sediment supply from the moraine terminus, from Khumbi Yul La, was the likely source for the deposit near Sanasa. Entrapment of this sediment by moraine material or a landslide deposit suggests a comparable setting to the modern glacial lakes in the Gokyo and Imja valleys. Coring of modern lakes in the Khumbu region shows that ages of the lake sediment are more than 2-3 ka (Gajurel et al., 2021), indicating prolonged persistence of such lakes. The exposure near Sanasa is located close to the stream gully, so that the original lateral extent of this exposure and the size of the depositional pond is impossible to determine. Sample 19N5b was collected from the basal part of this section.

Phortse

A ~1.5 m-thick sequence of the fine-grained sediments can be traced along the base of the Phortse ridge (Figure 4.5d and 4.6d). An exposed section at the southern end of the ridge consists of a 70-cm-thick bed of muddy, fine sand, which gradually transitions into a thinner silt unit that contains numerous, angular cobbles and pebbles. This silt unit together with some of the embedded platy lithic fragments defines a bed dipping ~10° to the northwest. Sample 19N4b was collected from the basal, fine sand layer. The depositional environment of the Phortse ridge sediments is enigmatic due to its location around the edge of a terrace and its sedimentary profile.

Sample 19N4a was collected from a meter-thick section in the sequence, which covers the bedrock strath and forms the surface of the Phortse terrace (Figure 4.5e and 4.6e). In this section, a basal silty to fine sand layer transitions to a 15 cm-thick, pebble-granule sand unit, which is overlain by a unit of similar thickness, consisting of medium to fine sand. To a certain degree, both of these sandy units are fining upward sequences and are capped by a very fine layer of silt rich unit, altogether defining faint horizontal bedding. This alternating succession is overlain by a much thicker sequence of fine sand. These sandy units very closely resemble the stratigraphy of the samples SK16-18 of Richards et al. (2000), which were collected from south of the Imja river (Figure 4.3). Richards et al. (2000) interpreted those successions to have been deposited in a still-water environment. The Phortse ridge could represent a hyperconcentrated flow fan deposit (two phase flow of sediment and water) as suggested by Barnard et al. (2006) for multiple terrace deposits in the upstream region of the Imja river, around Pheriche. Barnard et al. (2006) suggested that hyperconcentrated flow deposits could consist of inversely graded, poorly sorted, massive beds with thicknesses ranging from 2-85 m, similar to the sediment of the Phortse ridge.

Tyangboche

The southern valley wall of the Imja river just east of Thyangboche is covered with meters of thick fine to very fine-grained sediments that support dense vegetation. Sample 19N5a was collected from a section along the trail east of Thyangboche. This section consists of a meter-thick massive, fine-grained sand, which is slightly dipping towards the Imja river and is capped by ca 20cm-thick topsoil (Figure 4.5f and 4.6f). The deposit lacks internal bedding or other sedimentologic structures, and therefore the depositional environment is unconstrained. This sequence could be a pond deposit, flood-deposit, eolian deposit, or slope colluvium deposit.

Materials and Methods

Field

Based on past observations and Google Earth imagery, sedimentary exposures described above were selected for IRSL sampling. Within each of the deposits, suitable dating targets were chosen such that any sampling point was within a sandy layer and had at least 1.5m of overlying sediment and/or soil. After the sampling location was selected, the outer 2-3cm of materials were scraped off within a 50x50cm^2 area. The metal sampling tube was 10cm long with an inner diameter of 3cm. Opaque rubber caps were used to eliminate light exposure and secure the sediment within the light-proof tube to prevent mixing. Additional sample material was collected from around the tube-collection area in order to calculate the dose rate.

Luminescence Dating

Infrared Stimulated Luminescence dating (IRSL) is a Quaternary dating technique applied to quartz and feldspar minerals in the sand and silt grain size range to date the last time sediment was exposed to sunlight or high temperatures (Aitken, 1998). Through exposure to naturally occurring radioactive decay from minerals within the sediment, a dose is gained in the mineral structure that over time saturates as the finite number of available charge traps fill up (i.e. Brown, 2020). Luminescence-derived burial ages are the quotient of the equivalent dose (D_E), that is the radiation dose the sample received following removal from sunlight, and the dose rate (D_R) supplied by the surrounding sediments which is related primarily to sediment chemistry, water content, and burial depth (Huntley et al., 1985).

Sample Processing Six sediment samples were processed and analyzed at the Utah State University Luminescence Laboratory in North Logan, Utah for infrared stimulated luminescence (IRSL) dating of feldspar sand (Wintle, 1997). D_E samples from tubes were opened under dim amber light (~590nm) and wet sieved to a target grain size range of 90-150 or 150-250µm. Target grain size ranges were treated with 10% hydrochloric acid and bleach to dissolve carbonates and organic material, respectively. Feldspar grains were twice separated in high density water-based liquid to isolate them from heavy minerals and quartz using sodium polytungstate at 2.7g/cm^3 and 2.58g/cm^3, respectively. After the second density separation, feldspar targets were dried at room temperature (Wintle, 1997).

Dose Rate Processing and Calculation Sediment for D_R samples was uniformly collected within 15cm of the OSL tube. Representative subsamples (~30 grams) of bulk sediment were analyzed for radioelemental concentrations of K, Rb, Th, and U using ICP-MS and ICP-AES analyses (i.e. Bailey et al., 2003). In-situ gravimetric moisture content was measured on all samples and used in the dose rate calculations. Few exceptions include USU-3124, USU-3127, and USU-3128, which were expected to be wetter than average conditions during the sampling event (Table 4. 2).

D_R calculations include concentration conversion factors from Aitken (1998) and Guérin et al. (2011), for alpha, beta, and gamma radiation, the influence of water attenuation, cosmic contribution by using sample depth, elevation, and longitude/latitude following Prescott and Hutton[51], and uncertainty in elemental measurements. Internal beta D_R from K was added to the dose rate calculation, assuming a mineral composition of 12.5% K on feldspar grains (following Huntley & Baril, 1997), and attenuated to water content and grain size using factors outlined by Mejdahl (1979) and (Aitken, 1985). For the internal Rb content, we assumed 400ppm following Huntley and Lamothe (2001) and attenuated the internal beta D_R to water content. Finally, due to the lack of etched edges on the feldspar grains, an alpha effectiveness value ('a-value') is used to correct the saturated nature of traps along highly ionizing alpha tracks (Aitken, 1985). We assume an alpha efficiency of 0.09±0.01 following Rees-Jones (1995) in the alpha D_R calculation.

Table 4.2: Dose rate information.

Sample Id.	USU num.	Depth (m)	In-situ H_2O (%)	Grain size (µm)	K (%)[1]	Rb (ppm)[1]	Th (ppm) [1]	U (ppm)[1]	Cosmic (Gy/ka)
19N1a	USU-3124	2	21.8[2]	90-150	3.63±0.09	284.0±11.4	45.1±4.1	5.6±0.4	0.23±0.02
19N4a	USU-3125	2	6.0	150-250	2.89±0.07	186.0±7.4	16.4±1.5	7.1±0.5	0.26±0.03
19N4b	USU-3126	2	9.1	90-150	2.39±0.06	205.0±8.2	27.9±2.5	7.1±0.5	0.26±0.03
19N5a	USU-3127	2	22.7[2]	90-150	2.11±0.05	206.0±8.2	29.3±2.6	6.2±0.4	0.26±0.03
19N5b	USU-3128	2	4.8	150-250	2.97±0.07	209.0±8.4	21.2±1.9	6.1±0.4	0.25±0.02
19N5c	USU-3129	2	33.0[2]	90-150	2.82±0.07	231.0±9.2	37.3±3.4	7.6±0.5	0.25±0.02

[1]Radioelemental concentrations determined using ICP-MS and ICP-AES techniques; dose rate is derived from concentrations by conversion factors from Guérin et al. (2011). Grain-size based internal beta dose rate determined assuming 12.5% K and 400ppm Rb using Mejdahl (1979). Alpha contribution to dose rate determined using an efficiency factor, or 'a-value', of 0.09±0.01 after Rees-Jones (1995).
[2]Assumed 16±5% for moisture content over burial history.
USU: Utah State University

Infrared Luminescence Measurements Luminescence measurements were performed on Risø TL/OSL Model DA-20 readers with infrared light-emitting diodes (LEDs) (870±40nm) and reader dose rates of 0.10 Gy/sec from a decaying ^{90}Sr beta radiation source (Bøtter-Jensen et al., 2003) at the USU Luminescence Laboratory. The Single-Aliquot Regenerative (SAR) protocol of Wallinga et al. (2000) was followed for IRSL dating of K-rich feldspathic sand (90-150 or 150-250 µm) loaded onto 1-mm aliquots (~5-10 grains per aliquot) (Table 4. 3). Temperature (preheat) conditions were held constant at 250 °C for 60 seconds prior to the natural, regenerative and test dose infrared measurements (Blair et al., 2005). The luminescence signal was measured through a blue filter pack of 2-mm and 4-mm thick filters (BG-39 and Corning 7-39, respectively) over 100 seconds (250 channels) at 50 °C with LED diodes at 85% power (~120 mW/cm^2). The resultant signal was calculated by subtracting the average of the last 10 seconds (background signal) from the first 0.8 seconds (2 channels) of the signal decay curve. Dose response curves were fit within saturating-exponential or saturating-exponential plus linear fits to calculate equivalent dose (D_E) values (Figure 4.7).

Table 4.3: Infrared stimulated luminescence protocol of Wallinga et al. (2000).

Step	Procedure
1	Start with Step 2; Dose
2	Preheat, 250°C for 60 s
3	IRSL, 50°C for 100s (Lx)
4	Test Dose (beta)
5	Preheat, 250°C for 60 s
6	IRSL, 50°C for 100s (Tx)
7	Return to step 1, repeat for 5 regenerative doses (lower than, at, and above natural, no dose, and repeat first dose)

Equivalent Dose (D_E) and Age Calculation The IRSL age is calculated by correcting individual D_E measurements for fading (athermal loss of signal with time) in g_{2days} %/decade using the method of Auclair et al. (2003) and the age correction model of Huntley and Lamothe (2001). Cumulative D_E and IRSL age values were calculated using the Central Age Model (CAM) of Galbraith and Roberts (2012) of at least 12 accepted aliquots (Table 4. 4, Figure 4.7). One out of 82 total aliquots analyzed across all six samples was rejected because the natural D_E was two times the dose of the highest regenerative dose given. Thus, the natural dose for that aliquot could not be fit along the dose-response curve (Figure 4.7). Errors in D_E and age estimates are reported at 2-sigma and include errors related to instrument calibration, and dose rate and equivalent dose calculations and were calculated in quadrature using the methods of Aitken and Alldred (1972) and Guérin et al. (2011).

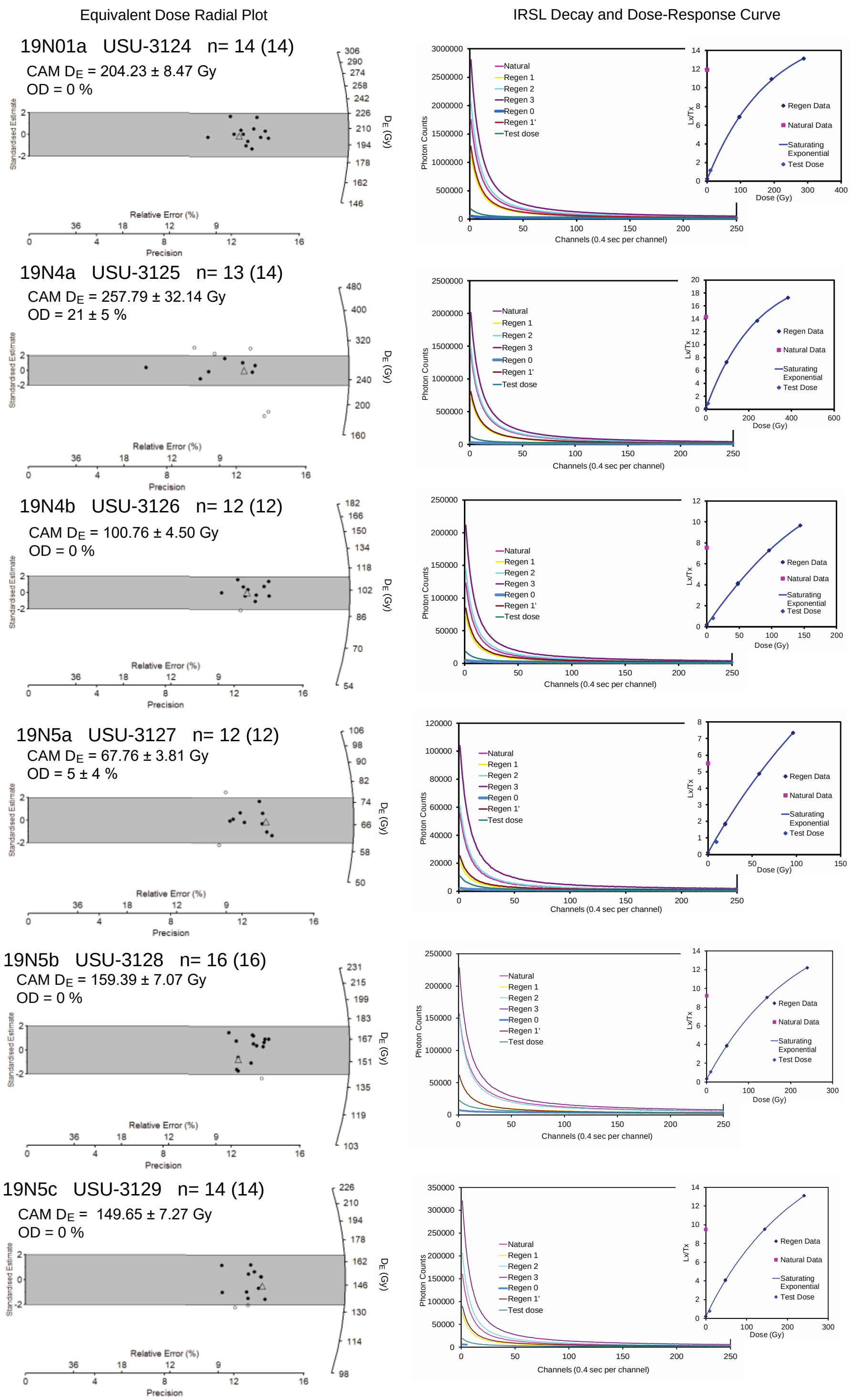

Figure 4.7: Radial plots, IRSL decay, and dose-response curve. Left: Radial plots of equivalent dose (DE) distributions. Right: IRSL decay (Channels vs Photon Counts) and dose-response

curve (Channels vs Lx/Tx) for aliquot represented as a triangle in the radial plot. Lx = luminescence signal from natural and regenerative doses, Tx = luminescence signal from test dose (Table 4. 4).

Table 4.4: Infrared stimulated luminescence age information.

Sample Id.	USU num.	Num. of aliquots[1]	Dose rate (Gy/ka)	Fading Rate g_{2days} (%/decade)	Equivalent Dose[2] ± 2σ (Gy)	IRSL age[3] ± 2σ (ka)
19N1a	USU-3124	14 (14)	10.97 ± 0.56	3.9 ± 0.3	204.23 ± 8.47	**26.64 ± 2.56**
19N4a	USU-3125	13 (14)	8.67± 0.41	3.8 ± 0.3	257.79 ± 32.14	**42.61 ± 6.41**
19N4b	USU-3126	12 (12)	9.28 ± 0.48	5.5 ± 0.7	100.76 ± 4.50	**18.45 ± 1.81**
19N5a	USU-3127	12 (12)	8.19 ± 0.43	5.5 ± 0.6	67.76 ± 3.81	**13.97 ± 1.45**
19N5b	USU-3128	16 (16)	9.01 ± 0.43	2.7 ± 0.5	159.39 ± 7.07	**22.61 ± 2.16**
19N5c	USU-3129	14 (14)	10.22 ± 0.54	5.2 ± 0.4	149.65 ± 7.27	**24.24 ± 2.43**

[1] Age analysis using the single-aliquot regenerative-dose procedure of Wallinga et al. (2000) on 1-mm small-aliquots of feldspar sand at 50°C IRSL. Number of aliquots used in age calculation and number of aliquots analyzed in parentheses.
[2] Equivalent dose (D_E) and IRSL ages calculated using the Central Age Model (CAM) of Galbraith and Roberts (2012).
[3] IRSL age on each aliquot corrected for fading following the method by Auclair et al. (2003) and correction model of Huntley and Lamothe (2001).

Results

Depositional ages of the six sedimentary sequences have been constrained by utilizing IRSL technique on feldspathic sand (Table 4. 4). Initially the samples were collected to be analyzed with the quartz OSL technique, but due to the high contamination of the quartz with K-rich feldspar, IRSL dating was pursued. Feldspars can be prone to athermal loss of signal (fading), which results in an underestimation of the age if unaccounted for (Huntley & Lamothe, 2001; Auclair et al., 2003). Given the well-constrained D_Es from individual measurements and minimum scatter on the laboratory-calculated fading rates (2.7-5.5 g2days %/decade; Table 4. 4), we do not expect inheritance from a previous depositional cycle (partial bleaching) or significant fading to have affected the outcome of the age results. From their study in the nearby Kanchenjunga Himal, Tsukamoto et al. (2002) concluded that most of the supra-glacier tills/lakes deposits around the region are likely to have been completely bleached prior to their deposition and therefore the quartz and feldspar luminescence dating could prove to be a valuable tool in reconstruction of glacial history throughout the Himalayas. Coupling the conclusion of Tsukamoto et al. (2002) with the nicely clustered feldspar IRSL results obtained in this study, it can be understood that feldspar IRSL ages provide a good constraint on timing of the Quaternary deposits in these regions. We interpret our feldspar IRSL ages as representing the timing of deposition within their respective sections (Table 4. 4).

Luminescence samples from the Namche Bazaar area include one from the western edge of the landslide scarp (19N5c) and one from the eastern edge of this scarp (19N1a). The western sample is slightly, but indistinguishably, younger at 24.24±2.43ka than the eastern sample at 26.64±2.56ka, and elevations are 3529m and 3513m, respectively. The luminescence sample from Sanasa (19N5b) came from a small area of pond deposit at 3784m and about 2.7km up the Dudh Koshi Valley from Namche Bazaar. The IRSL age for this sample is 22.61±2.16 ka. This site is higher than the two Namche Bazaar samples and is ~2 ka years younger than the western Namche sample. The older sample (19N4a) at Phortse was sampled ~2 m above the glacial bedrock strath at an elevation of 3700 m and has an IRSL age of 42.62±6.41 ka. The younger sample from this area was part of the Phortse ridge at an elevation of 3730 m and it has an IRSL age of 18.45±1.81 ka (19N4b). The sample from Thyangboche came from an exposure about 300 m east of the village. The IRSL age of 13.97±1.45 ka is the youngest age of any of the deposits and the sample site elevation of 3800 m is higher than any of our other sites. Richards et al. (2000) sampled stratified deposits on the south side of the Thyangboche ridge at an elevation of 3830 m, which yielded OSL ages of ~21-25 ka (Figure 4.5).

Ages Interpretation and Discussion

The IRSL ages obtained for the sampled deposits represent their respective depositional ages, at least for that sampled layer within the deposit, if not for the entire succession. Because these deposits likely came from within a localized depositional locus, the IRSL ages have generally been interpreted separately. By coupling these depositional ages with respective depositional and geomorphic setting, the relative timing of a few geomorphic processes around the lower Khumbu region has been constrained.

Namche Bazaar

While both successions are within the extent of the KRC, the eastern Namche deposit (26.64±2.56 ka) sits within the Namche scarp, whereas, the Helipad deposits (24.24±2.43 ka) is just outside of the Namche amphitheater. This locus of the eastern deposit led us to interpret that the Namche slide occurred in at least two phases. The older slide event cut into the KRC material, thus forming the Namche amphitheatre. On the eastern side, however, there is a small bedrock hill that may have limited the size of a second slide event. The shape of the smaller slide may have included a small pond. Subsequent sliding events have now exposed the pond deposits which we sampled. For such a depositional environment, the obtained IRSL age of the deposit is sandwiched between the first and subsequent phase of Namche sliding. Because the

Namche slide is younger than the KRC, it can be concluded that the KRC is older than 26 ka, which is further supported by the 24.24±2.43 ka age of the Helipad deposit.

A couple of other depositional environments have also been considered for the Namche deposits. In all these scenarios, however, the implications of IRSL ages on age of the KRC remains the same. It is possible that both these stratified sections are laminated colluvium deposits (Mücher et al., 2018) rather than still-water, pond deposits. Smaller pockets of potential depositional centers could exist within a large and scalloped landslide deposit, such as the deposit of the KRC (Posch et al., 2015). Subsequent rainfall events would wash the unconsolidated, fine sediment from the unstable diamicton in steep upslope regions. The slope wash transports the fines and then redeposits the fines in those pockets as laterally and vertically sorted slope colluvium deposits (Mücher et al., 2018). Each rainfall event would further winnow the sediment at the upper part of the scar and produce a fining upward stratum. A vertical accretion of multiple slope wash deposits could produce a stratified succession, which resembles a typical, near-shore, still-water deposit. This alternative explanation does not require the existence of a pond, and the deposits would likely be in multiple, isolated, and smaller patches.

The least likely scenario is that both of these sections are peripheral deposits of a large lake. Similar ages of deposition and elevation does support the idea of both sequences being a part of the same depositional system. Lake formation would have been most likely due to damming of the Dudh Koshi river by another mega-landslide downstream, which occurred prior to 26 ka. The regional exhumation rate of 1 mm/yr (Hubbard et al., 1991; Streule et al., 2012) suggests that the paleo-elevation of the river valley would have been only about 26m higher than at present. To have a damming effect 100s of meters deep, it would require a very large landslide. Around Lukla (~12 km south of Namche Bazaar), there was a massive rockslide around ~22 ka (Götz et al., 2015; Posch et al., 2015), but this would have been too young and at an elevation too low to create a lake at Namche Bazaar. Furthermore, our dates coincide most closely with the Pheriche glacial stage (16-23 ka) of Finkel et al. (2003), suggesting that the glacial termini were significantly up-valley (~15 km) and influence of glacial processes on these deposits can be ruled out.

<u>Sanasa</u>

The luminescence sample from Sanasa (19N5b, Figure 4.2) came from a small area of pond sediments at 3784 m and about 2.7 km from Namche Bazaar, on the west side of the Dudh Koshi Valley towards the eastern extent of the KRC. The IRSL age for this sample is 22.61±2.16 ka. The Sanasa deposit could have been deposited in a small, localized pond setting within materials derived from the terminal moraines of the side-valley glacier coming from Khumbi Yul Lha. This deposit overlies the KRC deposits and the obtained IRSL age of this deposit requires the age of KRC to be older than 22ka.

<u>Phortse</u>

The older sample (19N4a) at Phortse, taken ~2 m above the glacial bedrock strath at an elevation of 3700 m, has an IRSL age of 42.62±6.41 ka. The younger sample from this area was part of the Phortse ridge at an elevation of 3730 m and it has an IRSL age of 18.45±1.81 ka (19N4b).

The arcuate morphology of the strath terrace indicates that the terrace floor may have been shaped by an advancing valley glacier. Looking at the established glacial chronology of the region, the Thyangboche II glacial stage (lower bound 40.0±5.0 ka, (Owen et al., 2009)) could have been responsible for this carving. The terrace sediments were most likely deposited within a pond or lake environment created around the glacial terminus as suggested by Richards et al. (2000) for their samples (Figure 4.3). The Phortse ridge sediments unconformably overlie the terrace sediments. Although, the sedimentology of the ridge does match the 'hyper-concentrated' flow deposit of Barnard et al. (2006), the young age of this sequence contradicts this idea. Considering the 3.9 mm/yr regional erosion rate constrained by Barnard et al. (2006), at around 18 ka, the Imja river valley would only have been about 70 m above the modern day river floor (~200 m lower than the terrace), which makes the terrace an unlikely depositional locus. We interpret that the basal finer succession of the ridge to be an aeolian deposit, which was overlain by subsequent rockfall deposit. Perhaps the overlying, coarser deposits "armored" the basal fine deposits and played a significant role in the preservation of those fines. The orientation of the ridge and the abundance of fine material make it an unlikely candidate for a moraine deposit.

Thyangboche

The sample from Thyangboche came from an exposure about 300 m east of the village. The exposure shows little bedding or other internal structure. The IRSL age of 13.97±1.45 ka is the youngest age of any of the deposits. The elevation of this sample site is 3800 m which is higher than any of the other sites. As mentioned earlier, Richards et al. (2000) sampled a layered deposit on the south side of the Thyangboche ridge at an elevation of 3830m and obtained the OSL ages of 21.3±2.7 ka for the sample SK16 and 25.3±6.9 ka for the sample SK18 (Figure 4.3). Their sampled deposit has been interpreted as: "the product of low-density underflows (turbidites) deposited in a pond or small lake formed against the Tyangboche ridge by glacier ice". The deposit examined in this study lacks any internal structure and is significantly younger than Richards et al. (2000)'s samples. It is difficult to establish if this is an eolian deposit, colluvial re-working of older deposits, or a pond deposit.

Conclusions

A part of the dynamic Pleistocene geomorphologic history of the lower Khumbu region has been constructed by integrating the sedimentology, geomorphic loci, and feldspar IRSL ages of six anomalous sandy/silty deposits. The strath terrace of Phortse was carved during a glacial advance at around 42 ka. Towards the south, the Khumjung Rockslide Complex occurred before 26 ka and was probably triggered by a paleo, mega-earthquake. The rockslide complex hosts multiple topographic features including the paleo-lake around Khunde and Khumjung, the Namche amphitheater, and elevated ridge deposits towards the north of Syangboche.

Data Availability

All data and the relevant information about the experimental procedures can be found within the main text.

Acknowledgements

The field work for this study was conducted as an integral part of the 2019 National Geographic Mt. Everest Science Expedition, with approval from all relevant agencies of the Government of Nepal. The authors are extremely grateful to the National Geographic Society (Life at the Extremes initiative team) and Rolex for supporting the entirety of the field trip and laboratory analysis. We would also like to extend our gratitude to the Shangri-La Trek and locals of the Khumbu region for their support and hospitality. We further thank MSc students Bal

Krishna Shrestha, Anil Ghimire, and Sanjeet Maka from Tri-Chandra Multiple Campus of Tribhuvan University for their assistance in sample collection in the field. This work benefited from discussions in the field and following data collection with Dr. Aaron Putnam, Laura Mattas, and Peter Strand from the University of Maine.

References

Aitken, M. J. (1985). *Thermoluminescence dating*. London: Academic Press.

Aitken, M. J. (1998). *Introduction to optical dating: the dating of Quaternary sediments by the use of photon-stimulated luminescence*: Oxford University Press.

Aitken, M. J., & Alldred, J. C. (1972). The assessment of error limits in thermoluminescent dating. *Archaeometry, 14*(2), 257-267. doi:https://doi.org/10.1111/j.1475-4754.1972.tb00068.x

Aoki, T., & Imamura, M. (1999). *Reconstructing the glacial chronology based on the 10Be exposure age in the Khumbu glacier, eastern Nepal Himalayas-a problem on the production rate of in-situ cosmogenic radionuclides.* Paper presented at the Proc. the Korea-Japan/Japan-Korea Geomorphological Conference.

Auclair, M., Lamothe, M., & Huot, S. (2003). Measurement of anomalous fading for feldspar IRSL using SAR. *Radiation measurements, 37*(4), 487-492. doi:https://doi.org/10.1016/S1350-4487(03)00018-0

Bailey, R., Stokes, S., & Bray, H. (2003). Inductively-coupled plasma mass spectrometry (ICP-MS) for dose rate determination: some guidelines for sample preparation and analysis. *Ancient TL, 21*(1), 11-15.

Barnard, P. L., Owen, L. A., & Finkel, R. C. (2006). Quaternary fans and terraces in the Khumbu Himal south of Mount Everest: their characteristics, age and formation. *Journal of the Geological Society, 163*(2), 383-399. doi:https://doi.org/10.1144/0016-764904-157

Benedict, J. (1976). Khumbu glacier series, Nepal. *Radiocarbon, 18*(2), 117-178.

Blair, M. W., Yukihara, E. G., & McKeever, S. W. S. (2005). Experiences with single-aliquot OSL procedures using coarse-grain feldspars. *Radiation measurements, 39*(4), 361-374. doi:https://doi.org/10.1016/j.radmeas.2004.05.008

Bolch, T., Pieczonka, T., & Benn, D. I. (2011). Multi-decadal mass loss of glaciers in the Everest area (Nepal Himalaya) derived from stereo imagery. *The Cryosphere, 5*(2), 349-358. doi:https://doi.org/10.5194/tc-5-349-2011

Bøtter-Jensen, L., Andersen, C. E., Duller, G. A. T., & Murray, A. S. (2003). Developments in radiation, stimulation and observation facilities in luminescence measurements. *Radiation measurements, 37*(4), 535-541. doi:https://doi.org/10.1016/S1350-4487(03)00020-9

Brown, N. D. (2020). Which geomorphic processes can be informed by luminescence measurements? *Geomorphology, 367*, 107296. doi:https://doi.org/10.1016/j.geomorph.2020.107296

Carosi, R., Musumeci, G., & Pertusati, P. C. (1999). Extensional tectonics in the higher Himalayan crystallines of Khumbu Himal, eastern Nepal. *Geological Society of America Special Paper, 328*, 211-223.

Carrapa, B., Robert, X., DeCelles, P. G., Orme, D. A., Thomson, S. N., & Schoenbohm, L. M. (2016). Asymmetric exhumation of the Mount Everest region: Implications for the tectono-topographic evolution of the Himalaya. *Geology, 44*(8), 611-614. doi:https://doi.org/10.1130/g37756.1

Cottle, John M., Searle, Michael P., Horstwood, Matthew S. A., & Waters, David J. (2009). Timing of Midcrustal Metamorphism, Melting, and Deformation in the Mount Everest Region of Southern Tibet Revealed by U(-Th)-Pb Geochronology. *The Journal of Geology, 117*(6), 643-664. doi:https://doi.org/10.1086/605994

Finkel, R. C., Owen, L. A., Barnard, P. L., & Caffee, M. W. (2003). Beryllium-10 dating of Mount Everest moraines indicates a strong monsoon influence and glacial synchroneity throughout the Himalaya. *Geology, 31*(6), 561-564. doi:https://doi.org/10.1130/0091-7613(2003)031<0561:Bdomem>2.0.Co;2

Fushimi, H. (1977). Glaciations in the Khumbu Himal (1) Glaciological Expedition of Nepal, Contribution No. 41. *Journal of the Japanese Society of Snow and Ice, 39*(Special), 60-67. doi:https://doi.org/10.5331/seppyo.39.Special_60

Gajurel, A. P., Hubbard, M. S., Giri, B., Elmore, A. C., Maka, S., Rafter, P. A., Putnam, A. E., Elvin, S., Tait, A., & Mayewski, P. A. (2021). Climatic and tectonic significance of Taboche Lake, Khumbu Region, Nepal. *iScience, 24*(5), 102418. doi:https://doi.org/10.1016/j.isci.2021.102418

Galbraith, R. F., & Roberts, R. G. (2012). Statistical aspects of equivalent dose and error calculation and display in OSL dating: An overview and some recommendations. *Quaternary Geochronology, 11*, 1-27. doi:https://doi.org/10.1016/j.quageo.2012.04.020

Götz, J., Weidinger, J. T., Kraxberger, S., Hennecke, A.-L., Buckel, J., & Adhikari, B. R. (2015). Geomorphologic and hydrogeologic characteristics of populated rockslide deposits

(Sagarmatha National Park, Khumbu Himal, Nepal). *Journal of Water Resource and Protection*, *7*(13), 11. doi:https://doi.org/10.4236/jwarp.2015.713085

Guérin, G., Mercier, N., & Adamiec, G. (2011). Dose-rate conversion factors: update. *Ancient TL*, *29*(1), 5-8.

Heuberger, H. (1956). Beobachtungen uber die heutige und eiszeitliche Vergletscherung in Ost Nepal. *Zeitschrift für Gletscherkunde und Glazialgeologie, 3(3),* 349-363.

Heuberger, H. (1986). Der Bergsturz von Khumdschung, Mount-Everest-Gebiet, Nepal. *Material und Technik*, *3*, 175-181.

Hubbard, M., Mukul, M., Gajurel, A. P., Ghosh, A., Srivastava, V., Giri, B., Seifert, N., & Mendoza, M. M. (2021). Orogenic Segmentation and Its Role in Himalayan Mountain Building. *Frontiers in Earth Science*, *9*(259). doi:https://doi.org/10.3389/feart.2021.641666

Hubbard, M., Royden, L., & Hodges, K. (1991). Constraints on unroofing rates in the High Himalaya, eastern Nepal. *Tectonics*, *10*(2), 287-298. doi:https://doi.org/10.1029/90TC02777

Hubbard, M. S. (1989). Thermobarometric constraints on the thermal history of the Main Central Thrust Zone and Tibetan Slab, eastern Nepal Himalaya. *Journal of Metamorphic Geology*, *7*(1), 19-30. doi:https://doi.org/10.1111/j.1525-1314.1989.tb00572.x

Huntley, D., & Lamothe, M. (2001). Ubiquity of anomalous fading in K-feldspars and the measurement and correction for it in optical dating. *Canadian Journal of Earth Sciences*, *38*(7), 1093-1106. doi:https://doi.org/10.1139/e01-013

Huntley, D. J., & Baril, M. (1997). The K content of the K-feldspars being measured in optical dating or in thermoluminescence dating. *Ancient TL*, *15*(1), 11-13.

Huntley, D. J., Godfrey-Smith, D. I., & Thewalt, M. L. W. (1985). Optical dating of sediments. *Nature*, *313*(5998), 105-107. doi:https://doi.org/10.1038/313105a0

Iwata, S. (1976). Late Pleistocene and Holocene Moraines in the Sagarmatha (Everest) Region, Khumbu Himal

Glaciological Expedition to Nepal, Contribution No. 23. *Journal of the Japanese Society of Snow and Ice*, *38*(Special), 109-114. doi:https://doi.org/10.5331/seppyo.38.Special_109

Jessup, M. J., Law, R. D., Searle, M. P., & Hubbard, M. S. (2006). Structural evolution and vorticity of flow during extrusion and exhumation of the Greater Himalayan Slab, Mount Everest Massif, Tibet/Nepal: implications for orogen-scale flow partitioning. *Geological Society, London, Special Publications*, *268*(1), 379-413. doi:10.1144/gsl.Sp.2006.268.01.18

Kang, S., Mayewski, P. A., Qin, D., Sneed, S. A., Ren, J., & Zhang, D. (2004). Seasonal differences in snow chemistry from the vicinity of Mt. Everest, central Himalayas. *Atmospheric Environment*, *38*(18), 2819-2829. doi:https://doi.org/10.1016/j.atmosenv.2004.02.043

Korup, O., & Weidinger, J. T. (2011). Rock type, precipitation, and the steepness of Himalayan threshold hillslopes. *Geological Society, London, Special Publications*, *353*(1), 235-249. doi:https://doi.org/10.1144/sp353.12

Mejdahl, V. (1979). Thermoluminescence dating: beta-dose attenuation in quartz grains. *Archaeometry, 21*(pt1), 61-72. Retrieved from http://inis.iaea.org/search/search.aspx?orig_q=RN:10451974

Mücher, H., van Steijn, H., & Kwaad, F. (2018). Chapter 2 - Colluvial and Mass Wasting Deposits. In G. Stoops, V. Marcelino, & F. Mees (Eds.), *Interpretation of Micromorphological Features of Soils and Regoliths (Second Edition)* (pp. 21-36): Elsevier.

Muller, F. (1980). *Present and late Pleistocene equilibrium line altitudes in the Mt. Everest region-An application of the glacier inventory.* Paper presented at the Proceedings of the Riederalp Workshop.

Owen, L. A., Robinson, R., Benn, D. I., Finkel, R. C., Davis, N. K., Yi, C., Putkonen, J., Li, D., & Murray, A. S. (2009). Quaternary glaciation of Mount Everest. *Quaternary Science Reviews, 28*(15), 1412-1433. doi:https://doi.org/10.1016/j.quascirev.2009.02.010

Posch, E., Bell, R., Weidinger, J. T., & Glade, T. (2015). Geomorphic Processes, Rock Quality and Solid Waste Management—Examples from the Mt. Everest Region of Nepal. *Journal of Water Resource and Protection, 7*(16), 18. doi:https://doi.org/10.4236/jwarp.2015.716105

Quincey, D. J., Luckman, A., & Benn, D. (2009). Quantification of Everest region glacier velocities between 1992 and 2002, using satellite radar interferometry and feature tracking. *Journal of Glaciology, 55*(192), 596-606. doi:https://doi.org/10.3189/002214309789470987

Rees-Jones, J. (1995). Optical dating of young sediments using fine-grain quartz. *Ancient TL, 13*(2), 9-14.

Richards, B. W. M., Benn, D. I., Owen, L. A., Rhodes, E. J., & Spencer, J. Q. (2000). Timing of late Quaternary glaciations south of Mount Everest in the Khumbu Himal, Nepal. *GSA bulletin, 112*(10), 1621-1632. doi:https://doi.org/10.1130/0016-7606(2000)112<1621:Tolqgs>2.0.Co;2

Röthlisberger, F., & Geyh, M. A. (1985). Glacier variations in Himalayas and Karakorum. *Zeitschrift für Gletscherkunde und Glazialgeologie, 21*, 237-249.

Searle, M. P. (1999). Extensional and compressional faults in the Everest–Lhotse massif, Khumbu Himalaya, Nepal. *Journal of the Geological Society, 156*(2), 227-240. doi:https://doi.org/10.1144/gsjgs.156.2.0227

Seifert, N. (2019). *Structural analysis of the Benkar Fault Zone, a cross structure in the Higher Himalaya of the Khumbu Region, eastern Nepal.* (MS). Montana State University, Bozeman, Montana.

Sherpa, S. F., Wagnon, P., Brun, F., Berthier, E., Vincent, C., Lejeune, Y., Arnaud, Y., Kayastha, R. B., & Sinisalo, A. (2017). Contrasted surface mass balances of debris-free glaciers observed between the southern and the inner parts of the Everest region (2007–15). *Journal of Glaciology, 63*(240), 637-651. doi:https://doi.org/10.1017/jog.2017.30

Streule, M. J., Carter, A., Searle, M. P., & Cottle, J. M. (2012). Constraints on brittle field exhumation of the Everest-Makalu section of the Greater Himalayan Sequence: Implications for models of crustal flow. *Tectonics, 31*(3). doi:https://doi.org/10.1029/2011TC003062

Tsukamoto, S., Asahi, K., Watanabe, T., & Rink, W. J. (2002). Timing of past glaciations in Kanchenjunga Himal, Nepal by optically stimulated luminescence dating of tills. *Quaternary International, 97-98*, 57-67. doi:https://doi.org/10.1016/S1040-6182(02)00051-4

Wallinga, J., Murray, A., & Wintle, A. (2000). The single-aliquot regenerative-dose (SAR) protocol applied to coarse-grain feldspar. *Radiation measurements, 32*(5), 529-533. doi:https://doi.org/10.1016/S1350-4487(00)00091-3

Weidinger, J. T., & Korup, O. (2009). Frictionite as evidence for a large Late Quaternary rockslide near Kanchenjunga, Sikkim Himalayas, India — Implications for extreme events in mountain relief destruction. *Geomorphology, 103*(1), 57-65. doi:https://doi.org/10.1016/j.geomorph.2007.10.021

Wessels, R. L., Kargel, J. S., & Kieffer, H. H. (2002). ASTER measurement of supraglacial lakes in the Mount Everest region of the Himalaya. *Annals of Glaciology, 34*, 399-408. doi:https://doi.org/10.3189/172756402781817545

Wintle, A. G. (1997). Luminescence dating: laboratory procedures and protocols. *Radiation measurements, 27*(5), 769-817. doi:https://doi.org/10.1016/S1350-4487(97)00220-5

CHAPTER FIVE

DISCUSSIONS AND CONCLUSIONS

The Himalayas are an active collisional orogen that has resulted in geologic features that have hazard implications. These features range in scope from faults in the bedrock to surficial deposits created from glacial or fluvial processes. My dissertation addresses a fault zone that is orthogonal to the orogen, yet may have had recent movement and a set of sandy deposits in the higher Himalaya that may have formed from paleo lakes behind former landslides. Specifically, my dissertation work focused on examining the Benkar Fault Zone (BFZ), and on investigating well-bedded, sandy deposits in the Khumbu region of eastern Nepal. To gain an in-depth understanding of the structural nature, genesis, and implications of cross faults, I also conducted a comprehensive review of cross faults in other mountain belts around the world.

My second chapter discusses the ubiquitous occurrence of cross faults and lateral heterogeneities in several mountain belts including the Alps, the Andes, the Appalachians, the North American Cordilleras, and the Zagros. In general, convergent mountain belts are composites of spatially and temporally continuous orogen-parallel rock packages. Geological and geophysical data from these mountain belts, however, also reveal various forms of lateral heterogeneity, often marked by cross faults/structures. These lateral heterogeneities are manifested as: 1) along-strike changes in deformation style; 2) variation in igneous activity or metamorphic grade; 3) variation in seismic activity; 4) changes in topography and geomorphology; and 5) abrupt lateral stratigraphic changes. Common drivers behind these lateral heterogeneities include the geometry of the continental margin, inherited basement structures, lateral variation in stratigraphy of deforming sedimentary sequences, variation in crustal rheology, along-strike changes in plate tectonic setting, physiography of the lower plate, and obliquity of plate convergence. In most settings, these factors are interrelated and simultaneously influence the morpho-tectonic evolution of an orogen. Apart from their influence on foreland sedimentation and orogenic evolution, lateral heterogeneity and cross structures can have an impact on patterns of seismicity, natural resource occurrence, and natural hazards.

In the third chapter, I have documented the southern continuity of the BFZ. I conducted field mapping towards the south from Lukla and corroborated the mapping results with kinematic and petrographic analysis. This chapter establishes the BFZ as a large-scale, young (<12 Ma), cross fault that spans across almost the width of the eastern Nepal Himalaya. It is possible that the BFZ continues further towards the south into the foreland. Currently, the mapped length of this fault is at least 100 km. Based on my mapping data, I interpret the BFZ to be a culmination of a series of cross faulting events. I have also outlined possible genetic models for the BFZ. More mapping and/or geophysical data will be required to confidently choose between these genetic models. Cross faults, such as the BFZ, can serve as a seismic segment boundary and thereby have an impact on regional seismicity. Cross faults can also enhance landslide-related hazards by creating zones of weaknesses, especially on river valley walls. It is, therefore, important to recognize and understand cross faults.

In the fourth chapter, I have reconstructed a part of the dynamic Pleistocene geomorphologic history of the lower Everest/Khumbu region. I constrained the depositional ages of six sandy/silty deposits by utilizing infrared stimulated luminescence analysis (IRSL) dating. By integrating the IRSL ages with the sedimentology and geomorphic setting of these deposits, I interpret that they were likely deposited in localized pond settings. In high-altitude regions, like the Everest region, such ponds and/or lake deposits play an important role in creating land parcels suitable for agricultural use and for settlements, where the rugged landscapes are constantly carved by glaciers, large-scale landslides, and rivers.

REFERENCES CITED

Ader, T., Avouac, J.-P., Liu-Zeng, J., Lyon-Caen, H., Bollinger, L., Galetzka, J., Genrich, J., Thomas, M., Chanard, K., Sapkota, S. N., Rajaure, S., Shrestha, P., Ding, L., & Flouzat, M. (2012). Convergence rate across the Nepal Himalaya and interseismic coupling on the Main Himalayan Thrust: Implications for seismic hazard. *Journal of Geophysical Research: Solid Earth, 117*(B4). doi:https://doi.org/10.1029/2011JB009071

Adhikari, N. (2013a). *Lithology and stratigraphy of the Pre-Siwalik rocks around Katari–Patana Bhanjyang area, Udayapur district, eastern Nepal.* (MSc). Tribhuvan University, Kritipur.

Adhikari, S. (2013b). *Geology of Katari–Patana Bhanjyang area, eastern Nepal, with special reference to petrography of Pre-Siwalik rocks.* (MSc). Tribhuvan University, Kritipur.

Ahmad, T., Harris, N., Bickle, M., Chapman, H., Bunbury, J., & Prince, C. (2000). Isotopic constraints on the structural relationships between the Lesser Himalayan Series and the High Himalayan Crystalline Series, Garhwal Himalaya. *GSA bulletin, 112*(3), 467-477. doi:10.1130/0016-7606(2000)112<467:Icotsr>2.0.Co;2

Aitken, M. J. (1985). *Thermoluminescence dating*. London: Academic Press.

Aitken, M. J. (1998). *Introduction to optical dating: the dating of Quaternary sediments by the use of photon-stimulated luminescence*: Oxford University Press.

Aitken, M. J., & Alldred, J. C. (1972). The assessment of error limits in thermoluminescent dating. *Archaeometry*, *14*(2), 257-267. doi:https://doi.org/10.1111/j.1475-4754.1972.tb00068.x

Aleinikoff, J. N., Zartman, R. E., Walter, M., Rankin, D. W., Lyttle, P. T., & Burton, W. C. (1995). U-Pb ages of metarhyolites of the Catoctin and Mount Rogers Formations, central and southern Appalachians: Evidence for two pulses of Iapetan rifting. *American Journal of Science*, *295*(4), 428-454. doi:https://doi.org/10.2475/ajs.295.4.428

Allen, M. B., & Armstrong, H. A. (2008). Arabia–Eurasia collision and the forcing of mid-Cenozoic global cooling. *Palaeogeography, Palaeoclimatology, Palaeoecology, 265*(1-2), 52-58. doi:https://doi.org/10.1016/j.palaeo.2008.04.021

Allmendinger, R. W., Jordan, T. E., Kay, S. M., & Isacks, B. L. (1997). The evolution of the Altiplano-Puna plateau of the Central Andes. *Annual Review of Earth and Planetary Sciences*, *25*(1), 139-174. doi:https://doi.org/10.1146/annurev.earth.25.1.139

Anderson, H. E., & Davis, D. W. (1995). U–Pb geochronology of the Moyie sills, Purcell Supergroup, southeastern British Columbia: implications for the Mesoproterozoic geological history of the Purcell (Belt) basin. *Canadian Journal of Earth Sciences*, *32*(8), 1180-1193. doi:https://doi.org/10.1139/e95-097

Andrews, E. (1985). Stratigraphy of the Sabhaya khola region, Sankhuha Sabha district, Eastern Nepal. *Journal of Nepal Geological Society, 2*(2), 12–35. doi:10.3126/jngs.v2i2.32531

Angermann, D., Klotz, J., & Reigber, C. (1999). Space-geodetic estimation of the Nazca-South America Euler vector. *Earth and Planetary Science Letters, 171*(3), 329-334. doi:https://doi.org/10.1016/S0012-821X(99)00173-9

Aoki, T., & Imamura, M. (1999). *Reconstructing the glacial chronology based on the 10Be exposure age in the Khumbu glacier, eastern Nepal Himalayas-a problem on the production rate of in-situ cosmogenic radionuclides.* Paper presented at the Proc. the Korea-Japan/Japan-Korea Geomorphological Conference.

Arita, K. (1983). Origin of the inverted metamorphism of the lower Himalayas, Central Nepal. *Tectonophysics, 95*(1), 43-60. doi:https://doi.org/10.1016/0040-1951(83)90258-5

Arriagada, C., Roperch, P., Mpodozis, C., & Cobbold, P. (2008). Paleogene building of the Bolivian Orocline: Tectonic restoration of the central Andes in 2-D map view. *Tectonics, 27*(6). doi:https://doi.org/10.1029/2008TC002269

Auclair, M., Lamothe, M., & Huot, S. (2003). Measurement of anomalous fading for feldspar IRSL using SAR. *Radiation measurements, 37*(4), 487-492. doi:https://doi.org/10.1016/S1350-4487(03)00018-0

Audemard, F. A. (2009). Key issues on the post-Mesozoic southern Caribbean plate boundary. In K. James, M. Lorente, & J. Pindell (Eds.), *Origin and Evolution of the Caribbean Plate* (Vol. 328, pp. 569-586). London: Geological Society, Special Publications.

Audemard, F. A., Romero, G., Rendon, H., & Cano, V. (2005). Quaternary fault kinematics and stress tensors along the southern Caribbean from fault-slip data and focal mechanism solutions. *Earth-Science Reviews, 69*(3-4), 181-233. doi:https://doi.org/10.1016/j.earscirev.2004.08.001

Authemayou, C., Chardon, D., Bellier, O., Malekzadeh, Z., Shabanian, E., & Abbassi, M. R. (2006). Late Cenozoic partitioning of oblique plate convergence in the Zagros fold-and-thrust belt (Iran). *Tectonics, 25*(3). doi:https://doi.org/10.1029/2005TC001860

Avouac, J.-P. (2003). Mountain building, erosion, and the seismic cycle in the Nepal Himalaya. *Advances in geophysics, 46*, 1-80. doi:https://doi.org/10.1016/S0065-2687(03)46001-9

Avouac, J. P., Meng, L., Wei, S., Wang, T., & Ampuero, J. P. (2015). Lower edge of locked Main Himalayan Thrust unzipped by the 2015 Gorkha earthquake. *Nature geoscience, 8*(9), 708-711. doi:10.1038/ngeo2518

Bader, J. W. (2008). Structural and tectonic evolution of the Cherokee Ridge arch, south-central Wyoming: implications for recurring strike-slip along the Cheyenne Belt suture zone. *Rocky Mountain Geology, 43*(1), 23-40. doi:https://doi.org/10.2113/gsrocky.43.1.23

Bader, J. W. (2009). Structural and tectonic evolution of the Douglas Creek arch, the Douglas Creek fault zone, and environs, northwestern Colorado and northeastern Utah Implications for petroleum accumulation in the Piceance and Uinta basins. *Rocky Mountain Geology, 44*(2), 121-145. doi:https://doi.org/10.2113/gsrocky.44.2.121

Bahroudi, A., & Koyi, H. A. (2003). Effect of spatial distribution of Hormuz salt on deformation style in the Zagros fold and thrust belt: an analogue modelling approach. *Journal of the Geological Society, 160*(5), 719-733. doi:https://doi.org/10.1144/0016-764902-135

Bailey, R., Stokes, S., & Bray, H. (2003). Inductively-coupled plasma mass spectrometry (ICP-MS) for dose rate determination: some guidelines for sample preparation and analysis. *Ancient TL, 21*(1), 11-15.

Barnard, P. L., Owen, L. A., & Finkel, R. C. (2006). Quaternary fans and terraces in the Khumbu Himal south of Mount Everest: their characteristics, age and formation. *Journal of the Geological Society*, *163*(2), 383-399. doi:https://doi.org/10.1144/0016-764904-157

Bartosch, T., Stüwe, K., & Robl, J. (2017). Topographic evolution of the Eastern Alps: The influence of strike-slip faulting activity. *Lithosphere*, *9*(3), 384-398. doi:https://doi.org/10.1130/L594.1

Bashyal, R. P. (1980). Gondwana Type of formation with Phosphatic Rocks in S.E. Nepal. *Journal of Geological Society of India*, *21*(10), 489-491. Retrieved from https://samvad.sibmpune.edu.in/index.php/jgsi/article/view/64779

Baskota, S. K., & Adhikari, S. (2019). *Geological map of parts of Solukhumbu, Okhaldhunga, Khotang and Udayapur Districts*. Retrieved from Lainchaur:

Baud, A., Gaetani, M., Garzanti, E., Fors, E., Nicora, A., & Tintori, A. (1984). Geological observations in southeastern Zanskar and adjacent Lahul area (northwestern Himalaya). *Eclogae Geologicae Helvetiae, 77*(1), 171-199. doi:https://www.e-periodica.ch/digbib/voltoc?lang=en&pid=egh-001%3A1984%3A77#3

Bayona, G., Thomas, W. A., & Van der Voo, R. (2003). Kinematics of thrust sheets within transverse zones: a structural and paleomagnetic investigation in the Appalachian thrust belt of Georgia and Alabama. *Journal of Structural Geology, 25*(8), 1193-1212. doi:https://doi.org/10.1016/S0191-8141(02)00162-1

Beaumont, C., Jamieson, R. A., Nguyen, M. H., & Lee, B. (2001). Himalayan tectonics explained by extrusion of a low-viscosity crustal channel coupled to focused surface denudation. *Nature, 414*(6865), 738-742. doi:10.1038/414738a

Beck, R. A., Vondra, C. F., Filkins, J. E., & Olander, J. D. (1988). Syntectonic sedimentation and Laramide basement thrusting, Cordilleran foreland; timing of deformation. In C. J. Schmidt Jr & W. J. Perry (Eds.), *Interaction of the Rocky Mountain Foreland and the Cordilleran Thrust Belt* (Vol. 171, pp. 465-488): Geological Society of America Memoir.

Behrmann, J. H. (1988). Crustal-scale extension in a convergent orogen: the Sterzing-Steinach mylomte zone in the Eastern Alps. *Geodinamica Acta*, *2*(2), 63-73. doi:https://doi.org/10.1080/09853111.1988.11105157

Benedict, J. (1976). Khumbu glacier series, Nepal. *Radiocarbon, 18*(2), 117-178.

Benvenuto, G. L., & Price, R. A. (1979). Structural evolution of the Hosmer thrust sheet, southeastern British Columbia. *Bulletin of Canadian Petroleum Geology, 27*(3), 360-394.

Berberian, M. (1995). Master "blind" thrust faults hidden under the Zagros folds: active basement tectonics and surface morphotectonics. *Tectonophysics, 241*(3-4), 193-224. doi:https://doi.org/10.1016/0040-1951(94)00185-C

Berberian, M., & King, G. C. P. (1981). Towards a paleogeography and tectonic evolution of Iran. *Canadian Journal of Earth Sciences, 18*(2), 210-265. doi:https://doi.org/10.1139/e81-019

Berger, Z., Boast, M., & Mushayandebvu, M. (2008). The contribution of integrated HRAM studies to exploration and exploitation of unconventional plays in North America. *Reservoir*, *Canadian Society of Petroleum Geologist*, *35*(10), 42-48.

Bernet, M. (2009). A field-based estimate of the zircon fission-track closure temperature. *Chemical Geology, 259*(3), 181-189. doi:https://doi.org/10.1016/j.chemgeo.2008.10.043

Bernoulli, D. (2007). The pre-Alpine geodynamic evolution of the Southern Alps: a short summary. *Bulletin für angewandte Geologie, 12*(2), 3-10.

Berra, F., & Carminati, E. (2010). Subsidence history from a backstripping analysis of the Permo-Mesozoic succession of the Central Southern Alps (Northern Italy). *Basin Research*, *22*(6), 952-975. doi:https://doi.org/10.1111/j.1365-2117.2009.00453.x

Bertotti, G., Picotti, V., Bernoulli, D., & Castellarin, A. (1993). From rifting to drifting: tectonic evolution of the South-Alpine upper crust from the Triassic to the Early Cretaceous. *Sedimentary Geology, 86*(1-2), 53-76. doi:https://doi.org/10.1016/0037-0738(93)90133-P

Bhattacharyya, K., Mitra, G., & Kwon, S. (2015). Geometry and kinematics of the Darjeeling–Sikkim Himalaya, India: Implications for the evolution of the Himalayan fold-thrust belt. *Journal of Asian Earth Sciences*, *113*, 778-796. doi:https://doi.org/10.1016/j.jseaes.2015.09.008

Bianchi, M., Heit, B., Jakovlev, A., Yuan, X., Kay, S., Sandvol, E., Alonso, R. N., Coira, B., Brown, L., & Kind, R. (2013). Teleseismic tomography of the southern Puna plateau in Argentina and adjacent regions. *Tectonophysics, 586*, 65-83. doi:http://dx.doi.org/10.1016/j.tecto.2012.11.016

Bielenstein, H. U. (1969). *The Rundle thrust sheet, Banff, Alberta—a structural analysis.* (Ph.D.). Queen's University, Kingston, Ontario.

Bigi, S., Carminati, E., Aldega, L., Trippetta, F., & Kavoosi, M. A. (2018). Zagros fold and thrust belt in the Fars province (Iran) I: Control of thickness/rheology of sediments and pre-thrusting tectonics on structural style and shortening. *Marine and Petroleum Geology, 91*, 211-224. doi:https://doi.org/10.1016/j.marpetgeo.2018.01.005

Bilham, R. (2019). Himalayan earthquakes: a review of historical seismicity and early 21st century slip potential. In P. J. Treloar & M. P. Searle (Eds.), *Himalayan Tectonics: a Modern Synthesis* (Vol. 483, pp. 423-482). London: Geological Society of London Special Publication.

Bilham, R., Gaur, V. K., & Molnar, P. (2001). Himalayan seismic hazard. *Science, 293*. doi:https://doi.org/10.1126/science.1062584

Blair, M. W., Yukihara, E. G., & McKeever, S. W. S. (2005). Experiences with single-aliquot OSL procedures using coarse-grain feldspars. *Radiation measurements, 39*(4), 361-374. doi:https://doi.org/10.1016/j.radmeas.2004.05.008

Bolch, T., Pieczonka, T., & Benn, D. (2011a). Multi-decadal mass loss of glaciers in the Everest area (Nepal Himalaya) derived from stereo imagery. *The Cryosphere, 5*(2), 349-358.

Bolch, T., Pieczonka, T., & Benn, D. I. (2011b). Multi-decadal mass loss of glaciers in the Everest area (Nepal Himalaya) derived from stereo imagery. *The Cryosphere, 5*(2), 349-358. doi:https://doi.org/10.5194/tc-5-349-2011

Bordet, P. (1961). *Recherches géologiques dans l'Himalaya du Népal, région du Makalu, Expéditions Françaises a l'Himalaya 1954– 1955 (with geological maps in colors)*. Paris: Paris Editions du Centre National de la Recherche Scientifique.

Bordet, P., Colchen, M., Krummenacher, D., Le Fort, P., Mouterde, R., & Remy, M. (1971). *Recherches Géologiques dans l'Himalaya du Népal, Région de la Thakkhola*. Paris: Paris Édition du Centre National de la Recherche Scientifique.

Bøtter-Jensen, L., Andersen, C. E., Duller, G. A. T., & Murray, A. S. (2003). Developments in radiation, stimulation and observation facilities in luminescence measurements. *Radiation measurements, 37*(4), 535-541. doi:https://doi.org/10.1016/S1350-4487(03)00020-9

Boyer, S. E. (1995). Sedimentary basin taper as a factor controlling the geometry and advance of thrust belts. *American Journal of Science, 295*(10), 1220-1254. doi:https://doi.org/0.2475/ajs.295.10.1220

Boyer, S. E., & Elliott, D. (1982). Thrust systems. *AAPG Bulletin, 66*(9), 1196-1230. doi:https://doi.org/10.1306/03B5A77D-16D1-11D7-8645000102C1865D

Brack, P. (1981). Structures in the southwestern border of the Adamello intrusion (Alpi Bresciane, Italy). *Schweizerische Mineralogische und Petrographische Mitteilungen, 61(1)*, 37-50. doi:http://pascal-francis.inist.fr/vibad/index.php?action=getRecordDetail&idt=PASCALGEODEBRGM8220070062

Brewer, M. C. (2004). *Geometric and Kinematic Evolution of the Bessemer Transverse Zone, Alabama Alleghanian Thrust Belt.* (Ph.D.). University of Kentucky,

Brookfield, M. E. (1993). The Himalayan passive margin from Precambrian to Cretaceous times. *Sedimentary Geology, 84*(1), 1-35. doi:https://doi.org/10.1016/0037-0738(93)90042-4

Brown, D., Alvarez-Marrón, J., Perez-Estaun, A., Gorozhanina, Y., Baryshev, V., & Puchkov, V. (1997). Geometric and kinematic evolution of the foreland thrust and fold belt in the southern Urals. *Tectonics, 16*(3), 551-562. doi:https://doi.org/10.1029/97TC00815

Brown, N. D. (2020). Which geomorphic processes can be informed by luminescence measurements? *Geomorphology, 367*, 107296. doi:https://doi.org/10.1016/j.geomorph.2020.107296

Brunel, M. (1986). Ductile thrusting in the Himalayas: Shear sense criteria and stretching lineations. *Tectonics, 5*(2), 247-265. doi:https://doi.org/10.1029/TC005i002p00247

Brunel, M., & Kienast, J.-R. (1986). Étude pétro-structurale des chevauchements ductiles himalayens sur la transversale de l'Everest–Makalu (Népal oriental). *Canadian Journal of Earth Sciences*, *23*(8), 117-1137. doi:https://doi.org/10.1139/e86-111

Burchfiel, B. C., Cowan, D. S., & Davis, G. A. (1992a). Tectonic overview of the Cordilleran orogen in the western United States. In B. C. Burchfiel, W. Lipman, & M. L. Zoback (Eds.), *The Cordilleran Orogen: Conterminous US* (Vol. G3, pp. 107-168): Geoogical Society of America.

Burchfiel, B. C., Zhiliang, C., Hodges, K. V., Yuping, L., Royden, L. H., Changrong, D., Jiene, X., Burchfiel, B. C., Zhiliang, C., Hodges, K. V., Yuping, L., Royden, L. H., Changrong, D., & Xu, J. (1992b). *The South Tibetan Detachment System, Himalayan Orogen: Extension Contemporaneous With and Parallel to Shortening in a Collisional Mountain Belt* (Vol. 269): Geological Society of America Special Papers.

Burg, J. P., Brunel, M., Gapais, D., Chen, G. M., & Liu, G. H. (1984). Deformation of leucogranites of the crystalline Main Central Sheet in southern Tibet (China). *Journal of Structural Geology, 6*(5), 535-542. doi:https://doi.org/10.1016/0191-8141(84)90063-4

Burgess, P. W., Yin, A., Dubey, C. S., Shen, Z.-K., & Kelty, T. K. (2012). Holocene shortening across the Main Frontal Thrust zone in the eastern Himalaya. *Earth and Planetary Science Letters, 357-358*, 152-167. doi:https://doi.org/10.1016/j.epsl.2012.09.040

Burrard, S. G. (1915a). On the origin of the Indo-Gangetic trough, commonly called the Himalayan foredeep. *Proceedings of the Royal Society of London. Series A, Containing Papers of a Mathematical and Physical Character, 91*(628), 220-238. doi:doi:10.1098/rspa.1915.0014

Burrard, S. G. (1915b). Origin of the Indo-Gangetic trough, commonly called Himalayan foredeep. *Proceedings of the Royal Society of Londong, 91A*, 220-238. doi:https://doi.org/10.1098/rspa.1915.0014

Butler, R. W. H., Tavarnelli, E., & Grasso, M. (2006). Structural inheritance in mountain belts: an Alpine–Apennine perspective. *Journal of Structural Geology, 28*(11), 1893-1908. doi:https://doi.org/10.1016/j.jsg.2006.09.006

Calais, E., Nocquet, J.-M., Jouanne, F., & Tardy, M. (2002). Current strain regime in the Western Alps from continuous Global Positioning System measurements, 1996–2001. *Geology, 30*(7), 651-654. doi:https://doi.org/10.1130/0091-7613(2002)030<0651:CSRITW>2.0.CO;2

Campani, M., Mancktelow, N., Seward, D., Rolland, Y., Müller, W., & Guerra, I. (2010). Geochronological evidence for continuous exhumation through the ductile-brittle transition along a crustal-scale low-angle normal fault: Simplon Fault Zone, central Alps. *Tectonics, 29*(3). doi:https://doi.org/10.1029/2009TC002582

Canavan, R. R., Carrapa, B., Clementz, M. T., Quade, J., DeCelles, P. G., & Schoenbohm, L. M. (2014). Early Cenozoic uplift of the Puna Plateau, Central Andes, based on stable isotope paleoaltimetry of hydrated volcanic glass. *Geology, 42*(5), 447-450. doi:https://doi.org/101130/G35239.1

Carosi, R., Lombardo, B., Molli, G., Musumeci, G., & Pertusati, P. C. (1998). The south Tibetan detachment system in the Rongbuk valley, Everest region. Deformation features and geological implications. *Journal of Asian Earth Sciences, 16*(2), 299-311. doi:https://doi.org/10.1016/S0743-9547(98)00014-2

Carosi, R., Lombardo, B., Musumeci, G., & Pertusati, P. C. (1999a). Geology of the Higher Himalayan Crystallines in Khumbu Himal (Eastern Nepal). *Journal of Asian Earth Sciences, 17*(5), 785-803. doi:https://doi.org/10.1016/S1367-9120(99)00014-0

Carosi, R., Montomoli, C., & Iaccarino, S. (2018). 20years of geological mapping of the metamorphic core across Central and Eastern Himalayas. *Earth-Science Reviews, 177*, 124-138. doi:https://doi.org/10.1016/j.earscirev.2017.11.006

Carosi, R., Montomoli, C., Rubatto, D., Visoná, D. (2010). Late Oligocene high-temperature shear zones in the core of the Higher Himalayan Crystallines (lower Dolpo, Western Nepal). *Tectonics, 29*. doi:https://doi.org/10.1029/2008TC002400

Carosi, R., Musumeci, G., & Pertusati, P. C. (1999b). Extensional tectonics in the higher Himalayan crystallines of Khumbu Himal, eastern Nepal. *Geological Society of America Special Paper, 328*, 211-223.

Carrapa, B., Robert, X., DeCelles, P. G., Orme, D., Thomson, S., & Schoenbohm, L. (2016a). Asymmetric exhumation of the Mount Everest region: Implications for the tectono-topographic evolution of the Himalaya. *Geology*, *44*(8), 611-614.

Carrapa, B., Robert, X., DeCelles, P. G., Orme, D. A., Thomson, S. N., & Schoenbohm, L. M. (2016b). Asymmetric exhumation of the Mount Everest region: Implications for the tectono-topographic evolution of the Himalaya. *Geology*, *44*(8), 611-614. doi:https://doi.org/10.1130/g37756.1

Castellarin, A., & Cantelli, L. (2000). Neo-Alpine evolution of the southern Eastern Alps. *Journal of Geodynamics*, *30*(1-2), 251-274. doi:https://doi.org/10.1016/j.tecto.2005.10.019

Castellarin, A., Vai, G. B., & Cantelli, L. (2006). The Alpine evolution of the Southern Alps around the Giudicarie faults: A Late Cretaceous to Early Eocene transfer zone. *Tectonophysics*, *414*(1), 203-223. doi:https://doi.org/10.1016/j.tecto.2005.10.019

Catlos, E. J., Harrison, T. M., Manning, C. E., Grove, M., Rai, S. M., Hubbard, M. S., & Upreti, B. N. (2002). Records of the evolution of the Himalayan orogen from in situ Th–Pb ion microprobe dating of monazite: Eastern Nepal and western Garhwal. *Journal of Asian Earth Sciences*, *20*(5), 459-479. doi:https://doi.org/10.1016/S1367-9120(01)00039-6

Cawood, P. A., & Botsford, J. W. (1991). Facies and structural contrasts across Bonne Bay cross-strike discontinuity, western Newfoundland. *American Journal of Science*, *291*(8), 737-759. doi:https://doi.org/10.2475/ajs.291.8.737

Cembrano, J., Hervé, F., & Lavenu, A. (1996). The Liquiñe Ofqui fault zone: a long-lived intra-arc fault system in southern Chile. *Tectonophysics*, *259*(1-3), 55-66. doi:https://doi.org/10.1016/0040-1951(95)00066-6

Chakraborty, T., Taral, S., More, S., & Bera, S. (2020). Cenozoic Himalayan Foreland Basin: An Overview and Regional Perspective of the Evolving Sedimentary Succession. In N. Gupta & S. K. Tandon (Eds.), *Geodynamics of the Indian Plate: Evolutionary Perspectives* (pp. 395-437). Cham: Springer International Publishing.

Chapin, C. E. (2012). Origin of the Colorado mineral belt. *Geosphere*, *8*(1), 28-43. doi:https://doi.org/10.1130/GES00694.1

Chapple, W. M. (1978). Mechanics of thin-skinned fold-and-thrust belts. *Geological Society of America Bulletin*, *89*(8), 1189-1198. doi:https://doi.org/10.1130/0016-7606(1978)89<1189:MOTFB>2.0.CO;2

Chatzaras, V., Xypolias, P., Kokkalas, S., & Koukouvelas, I. (2013). Tectonic evolution of a crustal-scale oblique ramp, Hellenides thrust belt, Greece. *Journal of Structural Geology, 57*, 16-37. doi:https://doi.org/10.1016/j.jsg.2013.10.003

Chauvet, A., Onézime, J., Charvet, J., & Barbanson, L. (2004). Syn-to late-tectonic stockwork emplacement within the spanish section of the iberian pyrite belt: Structural, textural, and mineralogical constraints in the tharsis and la zarza areas. *Economic Geology, 99*(8), 1781-1792. doi:https://doi.org/10.2113/gsecongeo.99.8.1781

Chen, Y.-W., Wu, J., & Suppe, J. (2019). Southward propagation of Nazca subduction along the Andes. *Nature, 565*(7740), 441-447. doi:https://doi.org/10.1038/s41586-018-0860-1

Ching, K.-E., Johnson, K. M., Rau, R.-J., Chuang, R. Y., Kuo, L.-C., & Leu, P.-L. (2011). Inferred fault geometry and slip distribution of the 2010 Jiashian, Taiwan, earthquake is consistent with a thick-skinned deformation model. *Earth and Planetary Science Letters, 301*(1-2), 78-86. doi:https://doi.org/10.1016/j.epsl.2010.10.021

Ching, K.-E., Rau, R.-J., Lee, J.-C., & Hu, J.-C. (2007). Contemporary deformation of tectonic escape in SW Taiwan from GPS observations, 1995–2005. *Earth and Planetary Science Letters, 262*(3-4), 601-619. doi:https://doi.org/10.1016/j.epsl.2007.08.017

Clift, P. D., Hodges, K. V., Heslop, D., Hannigan, R., Van Long, H., & Calves, G. (2008). Correlation of Himalayan exhumation rates and Asian monsoon intensity. *Nature geoscience, 1*(12), 875-880. doi:10.1038/ngeo351

Colchen, M., Le Fort, P., & Pêcher, A. (1986). *Annapurna, Manaslu, Ganesh, Himal: notice de la carte géologique au 1/200,000 e*. Paris: Centre National de la Recherches Scientifique, Special Publication.

Coleman, M. E. (1998). U-Pb constraints on Oligocene-Miocene deformation and anatexis within the central Himalaya, Marsyandi Valley, Nepal. *American Journal of Science, 298*(7), 553-571. doi:10.2475/ajs.298.7.553

Colman-Sadd, S. P. (1978). Fold development in Zagros simply folded belt, Southwest Iran. *AAPG Bulletin, 62*(6), 984-1003. doi:https://doi.org/10.1306/C1EA4F81-16C9-11D7-8645000102C1865D

Colman-Sadd, S. P., Cawood, P. A., Dunning, G. R., Hall, J. M., Kean, B. F., O'Brien, B. H., & O'Brien, S. J. (1992). *Lithoprobe East in Newfoundland (Burgeo Transect): A cross-section through the southwest New- foundland Appalachians* (Vol. 92-A7).

Coltorti, M., Farabollini, P., Gentili, B., & Pambianchi, G. (1996). Geomorphological evidence for anti-Apennine faults in the Umbro-Marchean Apennines and in the peri-Adriatic basin, Italy. *Geomorphology, 15*(1), 33-45. doi:https://doi.org/10.1016/0169-555X(95)00117-N

Coney, P. J., & Reynolds, S. J. (1977). Cordilleran benioff zones. *Nature, 270*(5636), 403-406. doi:https://doi.org/10.1038/270403a0

Constenius, K. N. (1996). Late Paleogene extensional collapse of the Cordilleran foreland fold and thrust belt. *Geological Society of America Bulletin, 108*(1), 20-39. doi:https://doi.org/10.1130/0016-7606(1996)108<0020:LPECOT>2.3.CO;2

Cook, B. S., & Thomas, W. A. (2009). Superposed lateral ramps in the Pell City thrust sheet, Appalachian thrust belt, Alabama. *Journal of Structural Geology, 31*(9), 941-949. doi:https://doi.org/10.1016/j.jsg.2009.06.001

Cooley, M. A., Price, R. A., Dixon, J. M., & Kyser, T. K. (2011). Along-strike variations and internal details of chevron-style, flexural-slip thrust-propagation folds within the southern Livingstone Range anticlinorium, a paleohydrocarbon reservoir in southern Alberta Foothills, Canada. *AAPG Bulletin, 95*(11), 1821-1849. doi:https://doi.org/10.1306/01271107097

Corbett, G. J. (1994). *Regional structural control of selected Cu/Au occurrences in Papua New Guinea.* Paper presented at the Proceedings of the Papua New Guinea Geology, Exploration and Mining Conference, Melbourne.

Cottle, J. M., Jessup, M. J., Newell, D. L., Horstwood, M. S. A., Noble, S. R., Parrish, R. R., Waters, D. J., & Searle, M. P. (2009a). Geochronology of granulitized eclogite from the Ama Drime Massif: Implications for the tectonic evolution of the South Tibetan Himalaya. *Tectonics, 28*(1). doi:https://doi.org/10.1029/2008TC002256

Cottle, J. M., Searle, M. P., Horstwood, M. S., & Waters, D. J. (2009b). Timing of midcrustal metamorphism, melting, and deformation in the Mount Everest region of southern Tibet revealed by U (-Th)-Pb geochronology. *The Journal of Geology, 117*(6), 643-664.

Cottle, John M., Searle, Michael P., Horstwood, Matthew S. A., & Waters, David J. (2009c). Timing of Midcrustal Metamorphism, Melting, and Deformation in the Mount Everest Region of Southern Tibet Revealed by U(-Th)-Pb Geochronology. *The Journal of Geology, 117*(6), 643-664. doi:https://doi.org/10.1086/605994

Cottle, J. M., Searle, M. P., Jessup, M. J., Crowley, J. L., & Law, R. D. (2015). Rongbuk re-visited: Geochronology of leucogranites in the footwall of the South Tibetan Detachment System, Everest Region, Southern Tibet. *Lithos, 227*, 94-106. doi:https://doi.org/10.1016/j.lithos.2015.03.019

Cotton, J. T., & Koyi, H. A. (2000). Modeling of thrust fronts above ductile and frictional detachments: Application to structures in the Salt Range and Potwar Plateau, Pakistan. *Geological Society of America Bulletin, 112*(3), 351-363. doi:https://doi.org/10.1130/0016-7606(2000)112<351:MOTFAD>2.0.CO;2

Coutand, I., Cobbold, P. R., de Urreiztieta, M., Gautier, P., Chauvin, A., Gapais, D., Rossello, E. A., & López-Gamundí, O. (2001). Style and history of Andean deformation, Puna plateau, northwestern Argentina. *Tectonics, 20*(2), 210-234. doi:https://doi.org/10.1029/2000TC900031

Dahl, P. S., Holm, D. K., Gardner, E. T., Hubacher, F. A., & Foland, K. A. (1999). New constraints on the timing of Early Proterozoic tectonism in the Black Hills (South Dakota), with implications for docking of the Wyoming province with Laurentia. *Geological Society of America Bulletin, 111*(9), 1335-1349. doi:https://doi.org/10.1130/0016-7606(1999)111<1335:NCOTTO>2.3.CO;2

Dahlen, F. A. (1990). Critical taper model of fold-and-thrust belts and accretionary wedges. *Annual Review of Earth and Planetary Sciences, 18*(1), 55-99. doi:https://doi.org/10.1146/annurev.ea.18.050190.000415

Daniel, C. G., Hollister, L. S., Parrish, R. R., & Grujic, D. (2003). Exhumation of the Main Central Thrust from Lower Crustal Depths, Eastern Bhutan Himalaya. *Journal of Metamorphic Geology, 21*(4), 317-334. doi:https://doi.org/10.1046/j.1525-1314.2003.00445.x

Dasgupta, S., Mukhopadhyay, M., Nandy, D.R. (1987). Active transverse features in the central portion of the Himalaya. *Tectonophysics, 136*, 255-264.

Davies, H. L. (1991). *Regional geologic setting of some mineral deposits of the New Guinea Orogen.* Paper presented at the Papua New Guinea Geology, Exploration and Mining Conference; Rabaul, Papua New Guinea, 1991.

De La Torre, T. L., Monsalve, G., Sheehan, A.F., Sapkota, S., and Wu, F. (2007). Earthquake processes of the Himalayan collision zone in eastern Nepal and the southern Tibetan Plateau. *Geophysical Journal International, 171*, 718-738.

DeCelles, P. G. (2004). Late Jurassic to Eocene evolution of the Cordilleran thrust belt and foreland basin system, western USA. *American Journal of Science, 304*(2), 105-168. doi:https://doi.org/10.2475/ajs.304.2.105

DeCelles, P. G., Carrapa, B., Ojha, T. P., Gehrels, G. E., & Collins, D. (2020). Structural and thermal evolution of the Himalayan thrust belt in midwestern Nepal. *Geological Society of America Special Paper, 547*, 1-77. doi:https://doi.org/10.1130/2020.2547(01)

DeCelles, P. G., Gehrels, G. E., Quade, J., LaReau, B., & Spurlin, M. (2000). Tectonic Implications of U-Pb Zircon Ages of the Himalayan Orogenic Belt in Nepal. *Science, 288*(5465), 497-499. doi:doi:10.1126/science.288.5465.497

DeCelles, P. G., Gehrels, G. E., Quade, J., Ojha, T. P., Kapp, P. A., & Upreti, B. N. (1998). Neogene foreland basin deposits, erosional unroofing, and the kinematic history of the

Himalayan fold-thrust belt, western Nepal. *GSA bulletin, 110*(1), 2-21. doi:10.1130/0016-7606(1998)110<0002:Nfbdeu>2.3.Co;2

Decelles, P. G., Gray, M., Ridgway, K., Cole, R., Pivnik, D., Pequera, N., & Srivastava, P. (1991). Controls on synorogenic alluvial-fan architecture, Beartooth Conglomerate (Palaeocene), Wyoming and Montana. *Sedimentology, 38*(4), 567-590. doi:https://doi.org/10.1111/j.1365-3091.1991.tb01009.x

Decelles, P. G., Kapp, P., Gehrels, G. E., & Ding, L. J. T. (2014). Paleocene-Eocene foreland basin evolution in the Himalaya of southern Tibet and Nepal: Implications for the age of initial India-Asia collision. *33*(5), 824-849.

DeCelles , P. G., Robinson, D. M., Quade, J., Ojha, T. P., Garzione, C. N., Copeland, P., & N., U. B. (2001). Stratigraphy, structure, and tectonic evolution of the Himalayan fold-thrust belt in western Nepal. *Tectonics, 20*, 487-509. doi:https://doi.org/10.1029/2000TC001226

Deffontaines, B., Lacombe, O., Angelier, J., Chu, H., Mouthereau, F., Lee, C., Deramond, J., Lee, J., Yu, M., & Liew, P. (1997). Quaternary transfer faulting in the Taiwan Foothills: evidence from a multisource approach. *Tectonophysics, 274*(1-3), 61-82. doi:https://doi.org/10.1016/S0040-1951(96)00298-3

Dewey, J. F., & Bird, J. M. (1970). Mountain belts and the new global tectonics. *Journal of Geophysical Research, 75*(14), 2625-2647. doi:https://doi.org/10.1029/JB075i014p02625

Dewey, J. F., Holdsworth, R. E., & Strachan, R. A. (1998). Transpression and transtension zones. In R. E. Holdworth, R. A. Strachan, & J. F. Dewey (Eds.), *Continental Transpressional and Transtensional Tectonics* (Vol. 135, pp. 1-14): Geological Society, London, Special Publications.

Dhital, M. R. (2015). *Geology of the Nepal Himalaya: regional perspective of the classic collided orogen*: Springer.

Dickinson, W. R. (2004). Evolution of the North American cordillera. *Annual Reviwe of Earth and Planetary Sciences, 32*, 13-45. doi:https://doi.org/10.1146/annurev.earth.32.101802.120257

Dickinson, W. R., & Snyder, W. S. (1978). Plate tectonics of the Laramide orogeny. In V. W. Matthews (Ed.), *Laramide folding associated with block faulting in the Western United States* (Vol. 151, pp. 355-366): Geoloical Society of America Memoir.

Diehl, T., Singer, J., Hetényi, G., Grujic, D., Clinton, J., Giardini, D., Kissling,E., GANSSER Working Group. (2017). Seismotectonics of Bhutan: Evidence for segmentation of the Eastern Himalayas and link to foreland deformation. *Earth and Planetary Science Letters, 471*, 54-65. doi:https://doi.org/10.1016/j.epsl.2017.04.038

Ding, L., Qasim, M., Jadoon, I. A. K., Khan, M. A., Xu, Q., Cai, F., Wang, H., Baral, U., & Yue, Y. (2016). The India–Asia collision in north Pakistan: Insight from the U–Pb detrital zircon provenance of Cenozoic foreland basin. *Earth and Planetary Science Letters, 455*, 49-61. doi:https://doi.org/10.1016/j.epsl.2016.09.003

Dini, A., Westerman, D., Innocenti, F., & Rocchi, S. (2008). Magma emplacement in a transfer zone: the Miocene mafic Orano dyke swarm of Elba Island, Tuscany, Italy. *Geological Society, London, Special Publications, 302*(1), 131-148. doi:https://doi.org/10.1144/SP302.10

Divyadarshini, A. a. S., Vi. (2019). Investigating topographic metrics to decipher structural model and morphotectonic evolution of the Frontal Siwalik Ranges, Central Himalaya, Nepal. *Geomorphology, 337*, 31-52. doi:10.1016/j.geomorph.2019.03.028

Domeier, M. (2016). A plate tectonic scenario for the Iapetus and Rheic oceans. *Gondwana Research, 36*, 275-295. doi:https://doi.org/10.1016/j.gr.2015.08.003

Doutsos, T., Koukouvelas, I., & Xypolias, P. (2006). A new orogenic model for the External Hellenides. In A. H. F. Robertson & D. Mountrakis (Eds.), *Tectonic development of the Eastern Mediterranean Region* (Vol. 260, pp. 507-520): Geological Society, London, Special Publications.

Drahovzal, J. A., & Thomas, W. A. (1976). *Cross-strike structural discontinuities in the Appalachians of Alabama: Geological Society of America Abstracts with Programs* (Vol. 8).

Drake, A. A. J., Sinha, A. K., Larid, J., & Guy, R. E. (1989). The Taconian Orogen. In R. D. Hatcher Jr, W. A. Thomas, & G. W. Viele (Eds.), *The Appalachian-Ouachita Orogen in the United States, The Geology of North America* (Vol. F-2, pp. 101-177): Geological Society of America.

Drukpa, D., Velasco, A. A., & Doser, D. I. (2006a). Seismicity in the Kingdom of Bhutan (1937–2003): Evidence for crustal transcurrent deformation. *Journal of Geophysical Research: Solid Earth, 111*(B6). doi:https://doi.org/10.1029/2004JB003087

Drukpa, D., Velasco, A. A., & Doser, D. I. (2006b). Seismicity in the Kingdom of Bhutan (1937–2003): Evidence for crustal transcurrent deformation. *Journal of Geophysical Research, 111*, B06301. doi:https://doi/org/10.1029/2004JB003087

Drukpa, D., Velasco, A.A., Doser, D. (2006). Seismicity in the Kingdom of Bhutan (1937–2003): Evidence for crustal transcurrent deformation. *Journal of Geophysical Research, 111*, B06301. doi:https://doi/org/10.1029/2004JB003087

Dubey, A. K., Mishra, R and Bhakuni, S.S. (2001). Erratic shortening from balanced cross sections of the western Himalayan foreland basin causes and implications for basin evolution. *Journal of Asian Earth Sciences*, *19*, 765-777. doi:https://doi.org/10.1016/S1367-9120(01)00010-4

Duncan, C., Masek, J., & Fielding, E. (2003). How steep are the Himalaya? Characteristics and implications of along-strike topographic variations. *Geology, 31*(1), 75-78. doi:https://doi.org/10.1130/0091-7613(2003)031<0075:HSATHC>2.0.CO;2

Dunkl, I., Kuhlemann, J., Reinecker, J., & Frisch, W. (2005). Cenozoic relief evolution of the Eastern Alps—constraints from apatite fission track age-provenance of Neogene intramontane sediments. *Austrian Journal of Earth Sciences, 98*, 92-105.

Duvall, M. J., Waldron, J. W. F., Godin, L., & Najman, Y. (2020). Active strike-slip faults and an outer frontal thrust in the Himalayan foreland basin. *Proceedings of the National Academy of Sciences, 117*(30), 17615-17621. doi:doi:10.1073/pnas.2001979117

Duvall, M. J., Waldron, J.W.F., Godin, L., Najman, Y. (2020). Active strike-slip faults and an outer frontal thrust in the Himalayan foreland basin. *Proceedings of the National Academy of Sciences, 117*(30), 17615-17621. doi:https://doi.org/10.1073/pnas.2001979117

Dwivedi, S. K. (1997). *Geology of the area between the Sunkoshi River and the Kakaru Khola, Udayapur District, Eastern Nepal.* (M.Sc.). Tribhuvan University,

Edey, A., Allen, M., & Nilfouroushan, F. (2020). Kinematic variation within the Fars Arc, eastern Zagros, and the development of fold-and-thrust belt curvature. *Tectonics, 39*(8), e2019TC005941. doi:https://doi.org/10.1029/2019TC005941

Egbue, O., & Kellogg, J. (2010). Pleistocene to present North Andean “escape”. *Tectonophysics, 489*(1-4), 248-257. doi:https://doi.org/10.1016/j.tecto.2010.04.021

Elliott, D. (1976). The motion of thrust sheets. *Journal of Geophysical Research, 81*(5), 949-963. doi:https://doi.org/10.1029/JB081i005p00949

Elliott, J. R., Jolivet, R., González, P. J., Avouac, J. P., Hollingsworth, J., Searle, M. P., & Stevens, V. L. (2016). Himalayan megathrust geometry and relation to topography revealed by the Gorkha earthquake. *Nature geoscience, 9*(2), 174-180. doi:10.1038/ngeo2623

Elter, F. M., Piero, E., Claudio, E., Elena, E., Katharina, K. R., Matteo, P., & Stefano, S. (2011). Strike-slip geometry inferred from the seismicity of the Northern-Central Apennines (Italy). *Journal of Geodynamics, 52*(5), 379-388. doi:https://doi.org/10.1016/j.jog.2011.03.003

Eugster, P., Thiede, R.C., Scherler, D., Stubner, K., Sobel, E.R., Strecker, M.R. (2018). Segmentation of the Main Himalayan Thrust Revealed by Low-Temperature

Thermochronometry in the Western Indian Himalaya. *Tectonics*, *37*, 2710-2726. doi:https://doi.org/10.1029/2017TC004752

Fakhari, M. D., Axen, G. J., Horton, B. K., Hassanzadeh, J., & Amini, A. (2008). Revised age of proximal deposits in the Zagros foreland basin and implications for Cenozoic evolution of the High Zagros. *Tectonophysics, 451*(1-4), 170-185. doi:https://doi.org/10.1016/j.tecto.2007.11.064

Falcon, N. L. (1974). Southern Iran: Zagros Mountains. *Geological Society, London, Special Publications*, *4*(1), 199-211. doi:https://doi.org/10.1144/GSL.SP.2005.004.01.11

Farzipour-Saein, A., Nilfouroushan, F., & Koyi, H. (2013). The effect of basement step/topography on the geometry of the Zagros fold and thrust belt (SW Iran): an analog modeling approach. *International Journal of Earth Sciences, 102*(8), 2117-2135. doi:https://doi.org/10.1007/s00531-013-0921-5

Fermor, P. (1999). Aspects of the three-dimensional structure of the Alberta Foothills and Front Ranges. *GSA bulletin, 111*(3), 317-346. doi:https://doi.org/10.1130/0016-7606(1999)111<0317:AOTTDS>2.3.CO;2

Festa, A., Balestro, G., Borghi, A., De Caroli, S., & Succo, A. (2020). The role of structural inheritance in continental break-up and exhumation of Alpine Tethyan mantle (Canavese Zone, Western Alps). *Geoscience Frontiers*, *11*(1), 167-188. doi:https://doi.org/10.1016/j.gsf.2018.11.007

Fiigenschuh, B., Seward, D., & Mancktelow, N. (1997). Exhumation in a convergent orogen: the western Tauern window. *Terra nova*, *9*(5-6), 213-217. doi:https://doi.org/10.1111/j.1365-3121.1997.tb00015.x

Finkel, R. C., Owen, L. A., Barnard, P. L., & Caffee, M. W. (2003). Beryllium-10 dating of Mount Everest moraines indicates a strong monsoon influence and glacial synchroneity throughout the Himalaya. *Geology, 31*(6), 561-564.

Folguera, A., Ramos, V. A., Hermanns, R. L., & Naranjo, J. (2004). Neotectonics in the foothills of the southernmost central Andes (37–38 S): Evidence of strike-slip displacement along the Antiñir-Copahue fault zone. *Tectonics, 23*(5). doi:https://doi.org/10.1029/2003TC001533

Fondriest, M., Aretusini, S., Di Toro, G., & Smith, S. A. (2015). Fracturing and rock pulverization along an exhumed seismogenic fault zone in dolostones: The Foiana Fault Zone (Southern Alps, Italy). *Tectonophysics, 654*, 56-74. doi:http://dx.doi.org/10.1016/j.tecto.2015.04.015

Foo, W. K. (1979). *Evolution of transverse structures linking the Purcell Anticlinorium to the western Rocky Mountains near Canal Flats, British Columbia.* (MSc). Queen's University, Kingston, Foster, D. A., Doughty, P. T., Kalakay, T. J., Fanning, C. M., Coyner, S., Grice, W. C., & Vogl, J. (2007). Kinematics and timing of exhumation of metamorphic core complexes along the Lewis and Clark fault zone, northern Rocky Mountains, USA. *Special Papers-Geological Society of America, 434*, 207. doi:https://doi.org/10.1130/2007.2434(10)

Foster, D. A., Mueller, P. A., Mogk, D. W., Wooden, J. L., & Vogl, J. J. (2006). Proterozoic evolution of the western margin of the Wyoming craton: Implications for the tectonic and magmatic evolution of the northern Rocky Mountains. *Canadian Journal of Earth Sciences, 43*(10), 1601-1619. doi:https://doi.org/10.1139/E06-052

Frank, W., & Fuchs, G. (1970). Geological investigations in west Nepal and their significance for the geology of the Himalayas. *Geologische rundschau, 59*, 552-580.

Frisch, W., Kuhlemann, J., Dunkl, I., & Brügel, A. (1998). Palinspastic reconstruction and topographic evolution of the Eastern Alps during late Tertiary tectonic extrusion. *Tectonophysics, 297*(1-4), 1-15. doi:https://doi.org/10.1016/S0040-1951(98)00160-7

From, R., & Larson, K. (2014). Tectonostratigraphy, deformation, and metamorphism of the Himalayan mid-crust exposed in the Likhu Khola region, east-central Nepal. *Geosphere, 10*(2), 292-307. doi:10.1130/ges00938.1

Fuchs, G. (1982). *Geologic-Tectonic Map of the Himalaya*. Vienna: Geologische Bundesanstalt/Geological Survey of Austria, scale 1:2,000,000.

Fushimi, H. (1977). Glaciations in the Khumbu Himal (1) Glaciological Expedition of Nepal, Contribution No. 41. *Journal of the Japanese Society of Snow and Ice, 39*(Special), 60-67. doi:https://doi.org/10.5331/seppyo.39.Special_60

Fushimi, H. (1978). Glaciations in the Khumbu Himal (2). *Journal of the Japanese Society of Snow and Ice, 40*(Special), 71-77.

Gaetani, M., Gianotti, R., Jadoul, F., Ciarapica, G., & Cirilli, S. (1986). Carbonifero superiore, Permiano et Triassico nell'area Lariana. *Memorie della Società Geologica Italiana, 32*, 5-48. doi:http://pascal-francis.inist.fr/vibad/index.php?action=getRecordDetail&idt=7204188

Gajurel, A. P., Hubbard, M. S., Giri, B., Elmore, A. C., Maka, S., Rafter, P. A., Putnam, A. E., Elvin, S., Tait, A., & Mayewski, P. A. (2021). Climatic and tectonic significance of Taboche Lake, Khumbu Region, Nepal. *iScience, 24*(5), 102418. doi:https://doi.org/10.1016/j.isci.2021.102418

Galbraith, R. F., & Roberts, R. G. (2012). Statistical aspects of equivalent dose and error calculation and display in OSL dating: An overview and some recommendations. *Quaternary Geochronology, 11*, 1-27. doi:https://doi.org/10.1016/j.quageo.2012.04.020

Galliski, M., & Viramonte, J. (1988). The Cretaceous paleorift in northwestern Argentina: a petrologic approach. *Journal of South American earth sciences, 1*(4), 329-342. doi:https://doi.org/10.1016/0895-9811(88)90021-1

Gansser, A. (1964a). *Geology of the Himalayas*. London: Wiley Interscience.

Gansser, A. (1964b). *Geology of the Himalayas*. New York: Wiley Interscience.

Garzanti, E. (1999). Stratigraphy and sedimentary history of the Nepal Tethys Himalaya passive margin. *Journal of Asian Earth Sciences, 17*(5), 805-827. doi:https://doi.org/10.1016/S1367-9120(99)00017-6

Garzanti, E., Casnedi, R., & Jadoul, F. (1986). Sedimentary evidence of a Cambro-Ordovician orogenic event in the northwestern Himalaya. *Sedimentary Geology, 48*(3), 237-265. doi:https://doi.org/10.1016/0037-0738(86)90032-1

Gaupp, R., & Batten, D. (1983). Depositional setting of middle to Upper Cretaceous sediments in the Northern Calcareous Alps from palynological evidence. *Neues Jahrbuch für Geologie und Paläontologie-Monatshefte*, 585-600. doi:https://doi.org/10.1127/njgpm/1983/1983/585

Gautam, P., Ulak, P. D., Paudayal, K. N., Gyawali, B. R., & Bhandari, S. (2012). Magnetostratigraphic dating of the prime-time sedimentary record of Himalayan tectonics and climate: new age constraints (13–10 Ma) from the Siwaliks of the Tinau Khola north section, Nepal. *Geophysical Journal International*, *190*(3), 1378-1392. doi:https://doi.org/10.1111/j.1365-246X.2012.05568.x

Gehrels, G. E., DeCelles, P. G., Ojha, T. P., & Upreti, B. N. (2006). Geologic and U-Th-Pb geochronologic evidence for early Paleozoic tectonism in the Kathmandu thrust sheet, central Nepal Himalaya. *GSA bulletin, 118*(1-2), 185-198. doi:10.1130/b25753.1

Ghiglione, M. C., Suarez, F., Ambrosio, A., Da Poian, G., Cristallini, E. O., Pizzio, M. F., & Reinoso, R. M. (2009). Structure and evolution of the Austral Basin fold-thrust belt, southern Patagonian Andes. *Revista de la Asociación Geológica Argentina, 65*(1), 215-226.

Giambiagi, L., Mescua, J., Bechis, F., Tassara, A., & Hoke, G. (2012). Thrust belts of the southern Central Andes: Along-strike variations in shortening, topography, crustal geometry, and denudation. *Bulletin, 124*(7-8), 1339-1351. doi:https://doi.org/10.1130/B30609.1

Gifford, J. N., Mueller, P. A., Foster, D. A., & Mogk, D. W. (2014). Precambrian crustal evolution in the Great Falls tectonic zone: Insights from xenoliths from the Montana Alkali Province. *The Journal of Geology, 122*(5), 531-548. doi:https://doi.org/10.1086/677262

Gillis, R. J., Horton, B. K., & Grove, M. (2006). Thermochronology, geochronology, and upper crustal structure of the Cordillera Real: Implications for Cenozoic exhumation of the central Andean plateau. *Tectonics, 25*(6). doi:https://doi.org/10.1029/2005TC001887

Gingele, F., De Deckker, P., & Norman, M. (2007). Late Pleistocene and Holocene climate of SE Australia reconstructed from dust and river loads deposited offshore the River Murray Mouth. *Earth and Planetary Science Letters*, *255*(3), 257-272. doi:https://doi.org/10.1016/j.epsl.2006.12.019

Giri, B., & Hubbard, M. (2023). Lateral Heterogeneity in Compressional Mountain Belt Settings. In E. J. Catlos & I. Cemen (Eds.), *Compressional Tectonics: Plate Convergence to Mountain Building* (Vol. 1, pp. 47-86): AGU Books.

Godin, L. (2003). Structural evolution of the Tethyan sedimentary sequence in the Annapurna area, central Nepal Himalaya. *Journal of Asian Earth Sciences, 22*(4), 307-328. doi:https://doi.org/10.1016/S1367-9120(03)00066-X

Godin, L., & Harris, L. B. (2014a). Tracking basement cross-strike discontinuities in the Indian crust beneath the Himalayan orogen using gravity data – relationship to upper crustal faults. *Geophysical Journal International*, *198*(1), 198-215. doi:10.1093/gji/ggu131

Godin, L., & Harris, L. B. (2014b). Tracking basement cross-strike discontinuities in the Indian crust beneath the Himalayan orogen using gravity data – relationship to upper crustal faults. *Geophysical Journal International, 198*, 198-215. doi:https://doi.org/10.1093/gji/ggu131

Godin, L., Parrish, R. R., Brown, R. L., & Hodges, K. V. (2001). Crustal thickening leading to exhumation of the Himalayan Metamorphic core of central Nepal: Insight from U-Pb Geochronology and 40Ar/39Ar Thermochronology. *Tectonics*, *20*(5), 729-747. doi:https://doi.org/10.1029/2000TC001204

Goldfinger, C., Kulm, L.D., Yeats, R.S., McNeill, L., and Hummon, C. (1997). Oblique strike-slip faulting of the central Cascadia submarine forearc. *Journal of Geophysical Research, 102*(B4), 8217-8243. doi:https://doi.org/10.1029/96JB02655

Goscombe, B., Gray, D., & Foster, D. A. (2018). Metamorphic response to collision in the Central Himalayan Orogen. *Gondwana Research*, *57*, 191-265. doi:https://doi.org/10.1016/j.gr.2018.02.002

Goscombe, B., Gray, D., & Hand, M. (2006). Crustal architecture of the Himalayan metamorphic front in eastern Nepal. *Gondwana Research*, *10*(3), 232-255. doi:https://doi.org/10.1016/j.gr.2006.05.003

Götz, J., Weidinger, J. T., Kraxberger, S., Hennecke, A.-L., Buckel, J., & Adhikari, B. R. (2015). Geomorphologic and hydrogeologic characteristics of populated rockslide deposits

(Sagarmatha National Park, Khumbu Himal, Nepal). *Journal of Water Resource and Protection, 7*(13), 11. doi:https://doi.org/10.4236/jwarp.2015.713085

Graindorge, D., Klingelhoefer, F., Sibuiet, J.C., McNeill, L., Henstock, T., Dean, S., Gutscher, M., Dessa, J.X., Permana, H., and 15 others. (2008). Impact of lower plate structure on upper plate deformation at the NW Sumatran convergent margin from seafloor morphology. *Earth and Planetary Science Letters*, *275*, 201-210. doi:https://doi.org/10.1016/j.epsl.2008.04.053

Grosjean, G., Sue, C., & Burkhard, M. (2004). Late Neogene extension in the vicinity of the Simplon fault zone (central Alps, Switzerland). *Eclogae Geologicae Helvetiae, 97*(1), 33-46. doi:https://doi.org/10.1007/s00015-004-1114-9

Grujic, D., Casey, M., Davidson, C., Hollister, L. S., Kündig, R., Pavlis, T., & Schmid, S. (1996). Ductile extrusion of the Higher Himalayan Crystalline in Bhutan: evidence from quartz microfabrics. *Tectonophysics*, *260*(1), 21-43. doi:https://doi.org/10.1016/0040-1951(96)00074-1

Grujic, D., Hollister, L.S., and Parrish, R.P. (2002). Himalayan metamorphic sequence as an orogenic channel: Insight from Bhutan. *Earth and Planetary Science Letters, 198*, 177-191. doi:https://doi.org/10.1016S0012-821X(02)00482-X.

GSI. (2000). Eastern Nepal Himalaya and Indo-Gangetic Plains of Bihar. In P. L. Narula, S. K. Acharyya, & J. Banerjee (Eds.), *Seismotectonics Atlas of India and Its Environs* (pp. 26-27): Geological Survey of India (GSI).

Guérin, G., Mercier, N., & Adamiec, G. (2011). Dose-rate conversion factors: update. *Ancient TL, 29*(1), 5-8.

Guillot, S., Mahéo, G., De Sigoyer, J., Hattori, K., & Pecher, A. (2008). Tethyan and Indian subduction viewed from the Himalayan high-to ultrahigh-pressure metamorphic rocks. *Tectonophysics*, *451*(1-4), 225-241. doi:https://doi.org/10.1016/j.tecto.2007.11.059

Gutscher, M. A., Spakman, W., Bijwaard, H., & Engdahl, E. R. (2000). Geodynamics of flat subduction: Seismicity and tomographic constraints from the Andean margin. *Tectonics, 19*(5), 814-833. doi:https://doi.org/10.1029/1999TC001152

Handy, M. R., Schmid, S. M., Bousquet, R., Kissling, E., & Bernoulli, D. (2010). Reconciling plate-tectonic reconstructions of Alpine Tethys with the geological–geophysical record of spreading and subduction in the Alps. *Earth-Science Reviews*, *102*(3-4), 121-158. doi:https://doi.org/10.1007/s00531-014-1060-3

Harrison, J., & Bally, A. (1988). Cross-sections of the Parry Islands fold belt on Melville Island, Canadian Arctic Islands: Implications for the timing and kinematic history of some thin-skinned decollement systems. *Bulletin of Canadian Petroleum Geology*, *36*(3), 311-332.

Harrison, J. E., Griggs, A. B., & Wells, J. D. (1974). *Tectonic features of the Precambrian Belt basin and their influcence on post-Belt structures* (Vol. 886): United States Geological Survey Professional Paper.

Harrison, T. M., Ryerson, F. J., Le Fort, P., Yin, A., Lovera, O. M., & Catlos, E. J. (1997). A Late Miocene-Pliocene origin for the Central Himalayan inverted metamorphism. *Earth and Planetary Science Letters, 146*(1), E1-E7. doi:https://doi.org/10.1016/S0012-821X(96)00215-4

Harvey, J. E., Burbank, D. W., & Bookhagen, B. (2015). Along-strike changes in Himalayan thrust geometry: Topographic and tectonic discontinuities in western Nepal. *Lithosphere, 7*(5), 511-518. doi:10.1130/l444.1

Harvey, J. E., Burbank, D.W., Bookhagen, B. (2015). Along-strike changes in Himalayan thrust geometry: Topographic and tectonic discontinuities in western Nepal. *Lithosphere, 7*(5), 511-518. doi:https://doi.org/10.1130/L444.1

Hatcher, J. R. D. (1972). Developmental model for the southern Appalachians. *Geological Society of America Bulletin, 83*(9), 2735-2760.

Hatcher, J. R. D. (2010). The Appalachian orogen: A brief summary. In R. P. Tollo, M. J. Bartholomew, J. P. Hibbard, & P. M. Karabinos (Eds.), *From Rodinia to Pangea: The Lithotectonic Record of the Appalachian Region: Geological Society of America Memoir 206* (pp. 1-19).

Hatcher, J. R. D., Thomas, W. A., Geiser, P. A., Snoke, A. W., Mosher, S., & Wiltschko, D. V. (1989). Alleghanian orogen. In R. D. Hatcher Jr, W. A. Thomas, & G. W. Viele (Eds.), *The Appalachian-Ouachita Orogen in the United States, The Geology of North America* (Vol. F-2, pp. 233-319): Geological Society of America.

Hauck, M. L., Nelson, K.D., Brown, L.D., Wenjin, Z., and Ross, A.R. (1998). Crustal structure of the Himalayan orogen at ~90° east longitude from Project INDEPTH deep reflection profiles. *Tectonics, 17*, 481-500. doi:https://doi.org/10.1029/98TC01314

Haynes, S. J., & McQuillan, H. (1974). Evolution of the Zagros suture zone, southern Iran. *Geological Society of America Bulletin, 85*(5), 739-744. doi:https://doi.org/10.1130/0016-7606(1974)85<739:EOTZSZ>2.0.CO;2

Haynes, S. J., & Reynolds, P. (1980). Early development of Tethys and Jurassic ophiolite displacement. *Nature, 283*(5747), 561-563. doi:https://doi.org/10.1038/283561a0

Heim, A., & Gansser, A. (1939). *Central Himalaya: Geological Observations of the Swiss expedition 1936 (with geological maps in colors, sections, and plates).* (Vol. 73): Memoires de la Societe Helvetique des Sciences Naturelles.

Hessami, K., Koyi, H. A., & Talbot, C. J. (2001). The significance of strike-slip faulting in the basement of the Zagros fold and thrust belt. *Journal of petroleum Geology, 24*(1), 5-28. doi:https://doi.org/10.1111/j.1747-5457.2001.tb00659.x

Heuberger, H. (1956). Beobachtungen uber die heutige und eiszeitliche Vergletscherung in Ost Nepal. *Zeitschrift für Gletscherkunde und Glazialgeologie, 3(3)*, 349-363.

Heuberger, H. (1986). Der Bergsturz von Khumdschung, Mount-Everest-Gebiet, Nepal. *Material und Technik, 3*, 175-181.

Hibbard, J. P., van Staal, C. R., Rankin, D. W., & Williams, H. (2006). *Lithotectonic map of the Appalachian orogen, Canada–United States of America, Geological Survey of Canada, Map 2096A, scale 1:1,500,000.*

Hill, K. C., Kendrick, R. D., Crowhurst, P. V., & Gow, P. A. (2002). Copper-gold mineralisation in New Guinea: Tectonics, lineaments, thermochronology and structure. *Australian Journal of Earth Sciences, 49*(4), 737-752. doi:https://doi.org/10.1046/j.1440-0952.2002.00944.x

Hodges, K. V. (2000). Tectonics of the Himalaya and southern Tibet from two perspectives. *Geological Society of America Bulletin, 112*(3), 324-350. doi:https://doi.org/10.1130/0016-7606(2000)112<324:TOTHAS>2.0.CO;2

Hodges, K. V., Hurtado, J. M., & Whipple, K. X. (2001). Southward extrusion of Tibetan crust and its effect on Himalayan tectonics. *Tectonics, 20*(6), 799-809. doi:https://doi.org/10.1029/2001TC001281

Hodges, K. V., Parrish, R. R., Housh, T. B., Lux, D. R., Burchfiel, B. C., Royden, L. H., & Chen, Z. (1992). Simultaneous Miocene Extension and Shortening in the Himalayan Orogen. *Science, 258*(5087), 1466-1470. doi:doi:10.1126/science.258.5087.1466

Hodges, K. V., Parrish, R. R., & Searle, M. P. (1996). Tectonic evolution of the central Annapurna Range, Nepalese Himalayas. *Tectonics, 15*(6), 1264-1291. doi:https://doi.org/10.1029/96TC01791

Hoffman, P. F. (1988). Early Proterozoic Assembly. *Annual Review of Earth and Planetary Sciences, 6*, 543-603. doi:https://doi.org/10.1146/annurev.ea.16.050188.002551

Hofmann, F., Schlatter, R., & Weh, M. (2000). Erläuterungen zu Blatt 97: Beggingen (LK 1011) des Geologischen Atlas der Schweiz 1: 25,000. *Bundesamt für Wasser und Geologie, Bern*, 113.

Hogan, J. P., & Gilbert, M. C. (1998). The Southern Oklahoma aulacogen: A Cambrian analog for Mid-Proterozoic AMCG (anorthosite-mangerite-charnockite-granite) complexes? In H. J.P. & G. M.C (Eds.), *Basement tectonics 12. Proceedings of the International Conferences on Basement Tectonics* (Vol. 6, pp. 39-78): Springer.

Hope, J., & Eaton, D. (2002). Crustal structure beneath the Western Canada Sedimentary Basin: constraints from gravity and magnetic modelling. *Canadian Journal of Earth Sciences, 39*(3), 291-312. doi:https://doi.org/10.1139/e01-060

Horváth, F., & Cloetingh, S. A. P. L. (1996). Stress-induced late stage subsidence anomalies in the Pannonian Basin. *Tectonophysics, 266*, 287-300.

Höy, T., & Heyden, P. v. d. (1988). Geochemistry, geochronology, and tectonic implications of two quartz monzonite intrusions, Purcell Mountains, southeastern British Columbia. *Canadian Journal of Earth Sciences, 25*(1), 106-115. doi:https://doi.org/10.1139/e88-011

Hu, X., Garzanti, E., Moore, T., & Raffi, I. (2015). Direct stratigraphic dating of India-Asia collision onset at the Selandian (middle Paleocene, 59 ± 1 Ma). *Geology, 43*(10), 859-862. doi:10.1130/g36872.1

Hubbard, J., Almeida, R., Foster, A., Sapkota, S. N., Burgi, P., & Tapponnier, P. (2016). Structural segmentation controlled the 2015 MW 7.8 Gorkha earthquake rupture in Nepal. *Geology, 44*(8), 639-642. doi:https://doi.org/10.1130/G38077.1

Hubbard, M., Gajurel, A. P., Mukul, M., & Seifert, N. (2018). *Cross faults and their role in Himalayan Structural Evolution*. Paper presented at the Geological Society of America Abstracts with Programs.

Hubbard, M., Mukul, M., Gajurel, A. P., Ghosh, A., Srivastava, V., Giri, B., Seifert, N., & Mendoza, M. M. (2021). Orogenic Segmentation and Its Role in Himalayan Mountain Building. *Frontiers in Earth Science*, *9*(259). doi:https://doi.org/10.3389/feart.2021.641666

Hubbard, M., Royden, L., & Hodges, K. (1991). Constraints on unroofing rates in the High Himalaya, eastern Nepal. *Tectonics*, *10*(2), 287-298. doi:https://doi.org/10.1029/90TC02777

Hubbard, M. S. (1988). *Thermobarometry, 40Ar/39Ar geochronology, and structure of the Main Central Thrust zone and Tibetan Slab, eastern Nepal Himalaya.* (Doctoral Dissertation). Massachusetts Institute of Technology

Hubbard, M. S. (1989). Thermobarometric constraints on the thermal history of the Main Central Thrust Zone and Tibetan Slab, eastern Nepal Himalaya. *Journal of Metamorphic Geology, 7*(1), 19-30.

Hubbard, M. S. (1996). Ductile Shear as a Cause of Inverted Metamorphism: Example from the Nepal Himalaya. *The Journal of Geology, 104*(4), 493-499. doi:10.1086/629842

Hubbard, M. S. (1999). Norumbega fault zone: part of an orogen-parallel strike-slip system, northern Appalachians. In A. Ludman & D. P. J. West (Eds.), *Normumberga Fault*

System of the Northern Appalachians (Vol. 331, pp. 155-166). Boulder, Colorado: Geological Society of America Special Paper.

Hubbard, M. S., & Harrison, M. T. (1989). 40Ar/39Ar age constraints on deformation and metamorphism in the main central thrust zone and Tibetan slab, eastern Nepal Himalaya. *Tectonics, 8*(4), 865-880. doi:https://doi.org/10.1029/TC008i004p00865

Hubbard, M. S., & Mancktelow, N. S. (1992). Lateral displacement during Neogene convergence in the western and central Alps. *Geology, 20*(10), 943-946. doi:https://doi.org/10.1130/0091-7613(1992)020<0943:LDDNCI>2.3.CO;2

Huntington, K. W., Blythe, A. E., & Hodges, K. V. (2006). Climate change and Late Pliocene acceleration of erosion in the Himalaya. *Earth and Planetary Science Letters, 252*(1), 107-118. doi:https://doi.org/10.1016/j.epsl.2006.09.031

Huntley, D., & Lamothe, M. (2001). Ubiquity of anomalous fading in K-feldspars and the measurement and correction for it in optical dating. *Canadian Journal of Earth Sciences, 38*(7), 1093-1106. doi:https://doi.org/10.1139/e01-013

Huntley, D. J., & Baril, M. (1997). The K content of the K-feldspars being measured in optical dating or in thermoluminescence dating. *Ancient TL, 15*(1), 11-13.

Huntley, D. J., Godfrey-Smith, D. I., & Thewalt, M. L. W. (1985). Optical dating of sediments. *Nature, 313*(5998), 105-107. doi:https://doi.org/10.1038/313105a0

Hunziker, J. C., Frey, M., Clauer, N., Dallmeyer, R. D., Friedrichsen, H., Flehmig, W., Hochstrasser, K., Roggwiler, P. T., & Schwander, H. (1986). The evolution of illite to muscovite: mineralogical and isotopic data from the Glarus Alps, Switzerland. *Contributions to Mineralogy and Petrology, 92*(2), 157-180. doi:https://doi.org/10.1007/BF00375291

Hurtado, J. M., Jr, Hodges, K. V., & Whipple, K. X. (2001). Neotectonics of the Thakkhola graben and implications for recent activity on the South Tibetan fault system in the central Nepal Himalaya. *GSA bulletin, 113*(2), 222-240. doi:10.1130/0016-7606(2001)113<0222:Nottga>2.0.Co;2

Husseini, M. I. (1988). The Arabian infracambrian extensional system. *Tectonophysics, 148*(1-2), 93-103. doi:https://doi.org/10.1016/0040-1951(88)90163-1

Hyndman, D. W., Alt, D., & Sears, J. W. (1988). Post-Archean metamorphic and tectonic evolution of western Montana and northern Idaho. In W. G. Ernst (Ed.), *Metamorphism and crustal evolution of the western United States* (Vol. 7, pp. 332-361). Englewood Cliffs, New Jersey: Prentice Hall.

Hynes, A., & Rivers, T. (2010). Protracted continental collision—Evidence from the Grenville orogen. *Canadian Journal of Earth Sciences, 47*(5), 591-620. doi:https://doi.org/10.1139/E10-003

Isacks, B. L. (1988). Uplift of the central Andean plateau and bending of the Bolivian orocline. *Journal of Geophysical Research: Solid Earth, 93*(B4), 3211-3231. doi:https://doi.org/10.1029/ JB093iB04p03211

Ishida, T. (1969). Petrography and structure of the area between the Dudh Kosi and the Tamba Kosi, East Nepal. *Journal of Geological society of Japan, 75*, 115-125.

Ishida, T., & Ohta, Y. (1973). Ramechhap-Okhaldhunga Region. In S. Hashimoto, O. Y, & A. C (Eds.), *Geology of the Nepal Himalayas* (pp. 35-68). Japan: Himalayan Committee of Hokkaido University.

Iwata, S. (1976a). Late pleistocene and holocene moraines in the Sagarmatha (Everest) Region, Khumbu Himal. *Journal of the Japanese Society of Snow and Ice, 38*(Special), 109-114.

Iwata, S. (1976b). Late Pleistocene and Holocene Moraines in the Sagarmatha (Everest) Region, Khumbu Himal
Glaciological Expedition to Nepal, Contribution No. 23. *Journal of the Japanese Society of Snow and Ice, 38*(Special), 109-114. doi:https://doi.org/10.5331/seppyo.38.Special_109

Jackson, J. A. (1980). Reactivation of basement faults and crustal shortening in orogenic belts. *Nature, 283*(5745), 343-346. doi:https://doi.org/10.1038/283343a0

Jadoon, I. A. K., Lawrence, R. D., & Lillie, R. J. (1994). Seismic data, geometry, evolution, and shortening in the active Sulaiman fold-and-thrust belt of Pakistan, southwest of the Himalayas. *AAPG Bulletin, 78*(5), 758-774. doi:https://doi.org/10.1306/A25FE3AB-171B-11D7-8645000102C1865D

Jain, V., & Sinha, R. (2005). Response of active tectonics on the alluvial Baghmati River, Himalayan foreland basin, eastern India. *Geomorphology, 70*(3), 339-356. doi:https://doi.org/10.1016/j.geomorph.2005.02.012

Japas, M. S., Ré, G. H., Oriolo, S., & Vilas, J. F. (2016). Basement-involved deformation overprinting thin-skinned deformation in the Pampean flat-slab segment of the southern Central Andes, Argentina. *Geological Magazine, 153*(5-6), 1042-1065. doi:https://doi.org/10.1017/S001675681600056X

Jessup, M., Law, R., Searle, M., & Hubbard, M. (2006a). Structural evolution and vorticity of flow during extrusion and exhumation of the Greater Himalayan Slab, Mount Everest Massif, Tibet/Nepal: implications for orogen-scale flow partitioning. *Geological Society, London, Special Publications, 268*(1), 379-413.

Jessup, M. J., Cottle, J. M., Searle, M. P., Law, R. D., Newell, D. L., Tracy, R. J., & Waters, D. J. (2008a). P–T–t–D paths of Everest Series schist, Nepal. *Journal of Metamorphic Geology, 26*(7), 717-739. doi:https://doi.org/10.1111/j.1525-1314.2008.00784.x

Jessup, M. J., Law, R. D., Searle, M. P., & Hubbard, M. S. (2006b). Structural evolution and vorticity of flow during extrusion and exhumation of the Greater Himalayan Slab, Mount Everest Massif, Tibet/Nepal: implications for orogen-scale flow partitioning. *Geological Society, London, Special Publications, 268*(1), 379-413. doi:doi:10.1144/GSL.SP.2006.268.01.18

Jessup, M. J., Newell, D. L., Cottle, J. M., Berger, A. L., & Spotila, J. A. (2008b). Orogen-parallel extension and exhumation enhanced by denudation in the trans-Himalayan Arun River gorge, Ama Drime Massif, Tibet-Nepal. *Geology, 36*(7), 587-590. doi:https://doi.org/10.1130/g24722a.1

Jordan, T. E., Isacks, B., Ramos, V. A., & Allmendinger, R. W. (1983). Mountain building in the Central Andes. *Episodes, 3*(3), 20-26.

Joudaki, M., Farzipour-Saein, A., & Nilfouroushan, F. (2016). Kinematics and surface fracture pattern of the Anaran basement fault zone in NW of the Zagros fold–thrust belt. *International Journal of Earth Sciences, 105*(3), 869-883. doi:https://doi.org/10.1007/s00531-015-1209-8

Kang, S., Mayewski, P. A., Qin, D., Sneed, S. A., Ren, J., & Zhang, D. (2004). Seasonal differences in snow chemistry from the vicinity of Mt. Everest, central Himalayas. *Atmospheric Environment, 38*(18), 2819-2829.

Kapp, P., & DeCelles, P. G. (2019). Mesozoic–Cenozoic geological evolution of the Himalayan-Tibetan orogen and working tectonic hypotheses. *American Journal of Science, 319*(3), 159. doi:10.2475/03.2019.01

Karlstrom, K. E., & Houston, R. S. (1984). The Cheyenne belt: Analysis of a Proterozoic suture in southern Wyoming. *Precambrian Research, 25*(4), 415-446. doi:https://doi.org/10.1016/0301-9268(84)90012-3

Kaspari, S. D., Schwikowski, M., Gysel, M., Flanner, M., Kang, S., Hou, S., & Mayewski, P. A. (2011). Recent increase in black carbon concentrations from a Mt. Everest ice core spanning 1860–2000 AD. *Geophysical Research Letters, 38*(4).

Kellett, D. A., Cottle, J. M., & Larson, K. P. (2019). The South Tibetan detachment system: History, advances, definition and future directions. In P. J. Treloar & M. P. Searle (Eds.), *Himalayan Tectonics: A Modern Synthesis* (Vol. 483, pp. 377-400). London: Geological Society, Special Publication.

Kellett, D. A., & Godin, L. (2009). Pre-Miocene deformation of the Himalayan superstructure, Hidden valley, central Nepal. *Journal of the Geological Society, 166*(2), 261-275. doi:doi:10.1144/0016-76492008-097

Kendrick, E., Bevis, M., Smalley Jr, R., Brooks, B., Vargas, R. B., Lauría, E., & Fortes, L. P. S. (2003). The Nazca–South America Euler vector and its rate of change. *Journal of South American earth sciences, 16*(2), 125-131. doi:https://doi.org/10.1016/S0895-9811(03)00028-2

Kent, P. E. (1979). The emergent Hormuz salt plugs of southern Iran. *Journal of petroleum Geology, 2*(2), 117-144. doi:https://doi.org/10.1111/j.1747-5457.1979.tb00698.x

Keppie, J. D., & Krogh, T. E. (1999). U-Pb Geochronology of Devonian Granites in the Meguma Terrane of Nova Scotia, Canada: Evidence for Hotspot Melting of a Neoproterozoic Source. *The Journal of Geology, 107*(5), 555-568. doi:10.1086/314369

Khadivi, S., Mouthereau, F., Larrasoaña, J. C., Vergés, J., Lacombe, O., Khademi, E., Beamud, E., Melinte-Dobrinescu, M., & Suc, J. P. (2010). Magnetochronology of synorogenic Miocene foreland sediments in the Fars arc of the Zagros Folded Belt (SW Iran). *Basin Research, 22*(6), 918-932. doi:https://doi.org/10.1111/j.1365-2117.2009.00446.x

Kley, J., Rossello, E. A., Monaldi, C. R., & Habighorst, B. (2005). Seismic and field evidence for selective inversion of Cretaceous normal faults, Salta rift, northwest Argentina. *Tectonophysics, 399*(1-4), 155-172. doi:https://doi.org/10.1016/j.tecto.2004.12.020

Kohn, M. J. (2008). P-T-t data from central Nepal support critical taper and repudiate large-scale channel flow of the Greater Himalayan Sequence. *GSA bulletin, 120*(3-4), 259-273. doi:10.1130/b26252.1

Kohn, M. J., Paul, S. K., & Corrie, S. L. (2010). The lower Lesser Himalayan sequence: A Paleoproterozoic arc on the northern margin of the Indian plate. *GSA bulletin, 122*(3-4), 323-335. doi:10.1130/b26587.1

Kokkalas, S., & Doutsos, T. (2004). Kinematics and strain partitioning in the southeast Hellenides (Greece). *Geological Journal, 39*(2), 121-140. doi:https://doi.org/10.1002/gj.947

Koop, W. J., & Stoneley, R. (1982). Subsidence history of the Middle East Zagros basin, Permian to recent. *Philosophical Transactions of the Royal Society A Mathematical and Physical Sciences, 305*(1489), 149-168. doi:https://doi.org/10.1098/rsta.1982.0031

Korup, O., & Weidinger, J. T. (2011). Rock type, precipitation, and the steepness of Himalayan threshold hillslopes. *Geological Society, London, Special Publications, 353*(1), 235-249. doi:https://doi.org/10.1144/sp353.12

Kralik, M., Klima, K., & Riedmüller, G. (1987). Dating fault gouges. *Nature*, *327*(6120), 315-317. doi:https://doi.org/10.1038/327315a0

Kuiper, Y. D. (2016). Development of the Norumbega fault system in mid-Paleozoic New England, USA: An integrated subducted oceanic ridge model. *Geology*, *44*(6), 455-458. doi:https://doi.org/10.1130/G37599.1

Kuiper, Y. D., & Wakabayashi, J. (2018). A comparison between mid-Paleozoic New England, USA, and the modern western USA: Subduction of an oceanic ridge-transform fault system. *Tectonophysics, 745*, 278-292. doi:https://doi.org/10.1016/j.tecto.2018.08.020

Kwon, S., & Mitra, G. (2004). Strain distribution, strain history, and kinematic evolution associated with the formation of arcuate salients in fold-thrust belts: The example of the Provo salient, Sevier orogen, Utah. In A. J. Sussman & A. B. Weil (Eds.), *Orogenic Curvature: Integrating Paleomagnetic and Structural Analyses* (Vol. 383, pp. 205-223): Geological Society of America Special Paper.

Kwon, S., & Mitra, G. (2006). Three-dimensional kinematic history at an oblique ramp, Leamington zone, Sevier belt, Utah. *Journal of Structural Geology*, *28*(3), 474-493. doi:https://doi.org/10.1016/j.jsg.2005.12.011

Lacombe, O., Mouthereau, F., Angelier, J., & Deffontaines, B. (2001). Structural, geodetic and seismological evidence for tectonic escape in SW Taiwan. *Tectonophysics*, *333*(1-2), 323-345. doi:https://doi.org/10.1016/S0040-1951(00)00281-X

Lacombe, O., Mouthereau, F., Kargar, S., & Meyer, B. (2006). Late Cenozoic and modern stress fields in the western Fars (Iran): implications for the tectonic and kinematic evolution of central Zagros. *Tectonics*, *25*(1), 1-27. doi:https://doi.org/10.1029/2005TC001831

Larson, K., Cottle, J., Lederer, G., & Rai, S. M. (2017). Defining shear zone boundaries using fabric intensity gradients: An example from the east-central Nepal Himalaya. *Geosphere*, *13*(3), 771-781. doi:10.1130/ges01373.1

Larson, K., Piercey, S., & Cottle, J. (2019a). Preservation of a Paleoproterozoic rifted margin in the Himalaya: Insight from the Ulleri-Phaplu-Melung orthogneiss. *Geoscience Frontiers*, *10*(3), 873-883. doi:https://doi.org/10.1016/j.gsf.2017.05.010

Larson, K. P. (2012). The geology of the Tama Kosi and Rolwaling valley region, East-Central Nepal. *Geosphere*, *8*(2), 507-517. doi:10.1130/ges00711.1

Larson, K. P. (2018). Refining the structural framework of the Khimti Khola region, east-central Nepal Himalaya, using quartz textures and c-axis fabrics. *Journal of Structural Geology*, *107*, 142-152. doi:https://doi.org/10.1016/j.jsg.2017.12.014

Larson, K. P., Camacho, A., Kumar, K. C., & Shrestha, S. (2019b). Kinematic implications of regional 40Ar/39Ar ages, east-central Nepal. *Journal of Asian Earth Sciences, 172*, 383-392. doi:https://doi.org/10.1016/j.jseaes.2018.09.023

Larson, K. P., Cottle, J. M., & Godin, L. (2011). Petrochronologic record of metamorphism and melting in the upper Greater Himalayan sequence, Manaslu–Himal Chuli Himalaya, west-central Nepal. *Lithosphere, 3*(6), 379-392. doi:10.1130/l149.1

Larson, K. P., Cottle, J.M. (2014). Midcrustal discontinuities and the assembly of the Himalayan midcrust. *Tectonics, 33*, 718-740. doi:https://doi.org/10.1002/2013TC003452

Larson, K. P., Kellett, D. A., Cottle, J. M., King, J., Lederer, G., & Rai, S. M. (2016). Anatexis, cooling, and kinematics during orogenesis: Miocene development of the Himalayan metamorphic core, east-central Nepal. *Geosphere, 12*(5), 1575-1593. doi:10.1130/ges01293.1

Larson, K. P., Price, R. A., & Archibald, D. A. (2006). Tectonic implications of 40Ar/39Ar muscovite dates from the Mt. Haley stock and Lussier River stock, near Fort Steele, British Columbia. *Canadian Journal of Earth Sciences, 43*(11), 1673-1684. doi:https://doi.org/10.1139/E06-048

Larson, K. P., Shrestha, S., Soret, M., & Smit, M. (2022). The P-T-t-D evolution of the Mahabharat, east-central Nepal: The out-of-sequence development of the Himalaya. *Geoscience Frontiers, 13*(2), 101057. doi:https://doi.org/10.1016/j.gsf.2020.08.001

Laubscher, H. P. (1971). Das Alpen-Dinariden-Problem und die Palinspastik der südlichen tethys. *Geologische rundschau, 60*(3), 813-833. doi:https://doi.org/10.1007/BF02046522

Laubscher, H. P. (1985). Large-scale, thin-skinned thrusting in the southern Alps: Kinematic models. *Geological Society of America Bulletin, 96*(6), 710-718. doi:https://doi.org/10.1130/0016-7606(1985)96<710:LTTITS>2.0.CO;2

Lavé, J., & Avouac, J. P. (2000). Active folding of fluvial terraces across the Siwaliks Hills, Himalayas of central Nepal. *Journal of Geophysical Research: Solid Earth, 105*(B3), 5735-5770. doi:https://doi.org/10.1029/1999JB900292

Law, R. D., Searle, M. P., & Simpson, R. L. (2004). Strain, deformation temperatures and vorticity of flow at the top of the Greater Himalayan Slab, Everest Massif, Tibet. *Journal of the Geological Society, 161*(2), 305-320. doi:10.1144/0016-764903-047

Lawton, T. F., Sprinkel, D. A., Decelles, P. G., Mitra, G., Sussman, A. J., & Weiss, M. P. (1997). Stratigraphy and structure of the Sevier thrust belt and proximal foreland-basin system in central Utah: A transect from the Sevier Desert to the Wasatch Plateau. In K. P. Link & B. J. Kowallis (Eds.), *Brigham Young University Geology Studies Field Trip Guide Book, Part 2* (Vol. 42, pp. 33-68): Geological Society of America Annual Meeting.

Le Fort, P. (1975). Himalayas:Collided range:Present knowledge of continental arc. *American Journal of Science, 275 (A)*, 1-44.

Le Fort, P., & Raï, S. M. (1999). Pre-Tertiary felsic magmatism of the Nepal Himalaya: recycling of continental crust. *Journal of Asian Earth Sciences, 17*(5), 607-628. doi:https://doi.org/10.1016/S1367-9120(99)00015-2

Le Garzic, E., Vergés, J., Sapin, F., Saura, E., Meresse, F., & Ringenbach, J. (2019). Evolution of the NW Zagros Fold-and-Thrust Belt in Kurdistan Region of Iraq from balanced and restored crustal-scale sections and forward modeling. *Journal of Structural Geology, 124*, 51-69. doi:https://doi.org/10.1016/j.jsg.2019.04.006

Lee, J.-Y., Marti, K., Severinghaus, J. P., Kawamura, K., Yoo, H.-S., Lee, J. B., & Kim, J. S. (2006). A redetermination of the isotopic abundances of atmospheric Ar. *Geochimica et Cosmochimica Acta, 70*(17), 4507-4512. doi:https://doi.org/10.1016/j.gca.2006.06.1563

Leier, A., McQuarrie, N., Garzione, C., & Eiler, J. (2013). Stable isotope evidence for multiple pulses of rapid surface uplift in the Central Andes, Bolivia. *Earth and Planetary Science Letters, 371*, 49-58. doi:https://doi.org/10.1016/j.epsl.2013.04.025

Lemieux, S., Ross, G. M., & Cook, F. A. (2000). Crustal geometry and tectonic evolution of the Archean crystalline basement beneath the southern Alberta Plains, from new seismic reflection and potential-field studies. *Canadian Journal of Earth Sciences, 37*(11), 1473-1491. doi:https://doi.org/10.1139/e00-065

Li, Z. X., Bogdanova, S. V., Collins, A. S., Davidson, A., De Waele, B., Ernst, R. E., Fitzsimons, I. C. W., Fuck, R. A., Gladkochub, D. P., Jacobs, J., Karlstrom, K. E., Lu, S., Natapov, L. M., Pease, V., Pisarevsky, S. A., Thrane, K., & Vernikovsky, V. (2008). Assembly, configuration, and break-up history of Rodinia: A synthesis. *Precambrian Research, 160*(1), 179-210. doi:https://doi.org/10.1016/j.precamres.2007.04.021

Likerman, J., Burlando, J. F., Cristallini, E. O., & Ghiglione, M. C. (2013). Along-strike structural variations in the Southern Patagonian Andes: insights from physical modeling. *Tectonophysics, 590*, 106-120. doi:https://doi.org/10.1016/j.tecto.2013.01.018

Lin, S., Staal, C. R. v., & Dubé, B. t. (1994). Promontory-promontory collision in the Canadian Appalachians. *Geology, 22*(10), 897-900. doi:https://doi.org/10.1130/0091-7613(1994)022<0897:PPCITC>2.3.CO;2

Linzer, H.-G., Ratschbacher, L., & Frisch, W. (1995). Transpressional collision structures in the upper crust: the fold-thrust belt of the Northern Calcareous Alps. *Tectonophysics, 242*(1-2), 41-61. doi:https://doi.org/10.1016/0040-1951(94)00152-Y

Llambías, E. J., Kleinman, L. E., & Salvarradi, J. A. (1993). El magmatismo Gondwánico. In V. Ramos (Ed.), *Rela- torio Geología y Recursos Naturales de Mendoza* (Vol. 1, pp. 53-64). Buenos Aires: Servicio Geológico Minero Argentino (SEGEMAR).

Lombardo, B., Pertusati, P., & Borghi, S. (1993). Geology and tectonomagmatic evolution of the eastern Himalaya along the Chomolungma-Makalu transect. In P. J. Treloar & M. P. Searle (Eds.), *Himalayan Tectonics* (Vol. 74, pp. 341-355): Geological Society, London, Special Publications.

Long, S., McQuarrie, N., Tobgay, T., & Grujic, D. (2011). Geometry and crustal shortening of the Himalayan fold-thrust belt, eastern and central Bhutan. *GSA bulletin, 123*(7-8), 1427-1447. doi:10.1130/b30203.1

Long, S., McQuarrie, N., Tobgay, T., Grujic, D. (2011). Geometry and crustal shortening of the Himalayan fold-thrust belt, eastern and central Bhutan. *Geological Society of America Bulletin, 123*(7/8), 1427-1447. doi:https://doi.org/10.1130/B30203.1

Long, S. P., & Robinson, D. M. (2021). Construction of the Lesser Himalayan–Subhimalayan thrust belt: The primary driver of thickening, exhumation, and high elevations in the Himalayan orogen since the middle Miocene. *Geology, 49*(11), 1283-1288. doi:10.1130/g48967.1

Lupi, M., Trippanera, D., Gonzalez, D., D'amico, S., Acocella, V., Cabello, C., Stef, M. M., & Tassara, A. (2020). Transient tectonic regimes imposed by megathrust earthquakes and the growth of NW-trending volcanic systems in the Southern Andes. *Tectonophysics, 774*, 228204. doi:https://doi.org/10.1016/j.tecto.2019.228204

Mahoney, L., Hill, K., McLaren, S., & Hanani, A. (2017). Complex fold and thrust belt structural styles: Examples from the Greater Juha area of the Papuan Fold and Thrust Belt, Papua New Guinea. *Journal of Structural Geology, 100*, 98-119. doi:https://doi.org/10.1016/j.jsg.2017.05.010

Malekzade, Z., Bellier, O., Abbassi, M. R., Shabanian, E., & Authemayou, C. (2016). The effects of plate margin inhomogeneity on the deformation pattern within west-Central Zagros Fold-and-Thrust Belt. *Tectonophysics, 693*, 304-326. doi:http://dx.doi.org/10.1016/j.tecto.2016.01.030

Malusà, M. G. (2004). *Post-metamorphic evolution of the Western Alps: kinematic constraints from a multidisciplinary approach.* (PhD). University of Turin, Turin, Italy.

Mancktelow, N., Zwingmann, H., Campani, M., Fügenschuh, B., & Mulch, A. (2015). Timing and conditions of brittle faulting on the Silltal-Brenner fault zone, Eastern Alps (Austria). *Swiss Journal of Geosciences, 108*(2-3), 305-326. doi:https://doi.org/10.1007/s00015-015-0179-y

Mancktelow, N. S. (1992). Neogene lateral extension during convergence in the Central Alps: evidence from interrelated faulting and backfolding around the Simplonpass (Switzerland). *Tectonophysics, 215*(3-4), 295-317. doi:https://doi.org/10.1016/0040-1951(92)90358-D

Mancktelow, N. S., Stöckli, D. F., Grollimund, B., Müller, W., Fügenschuh, B., Viola, G., Seward, D., & Villa, I. M. (2001). The DAV and Periadriatic fault systems in the Eastern Alps south of the Tauern window. *International Journal of Earth Sciences, 90*(3), 593-622. doi:https://doi.org/10.1007/s005310000190

Mandal, S., Robinson, D. M., Khanal, S., & Das, O. (2015). Redefining the tectonostratigraphic and structural architecture of the Almora klippe and the Ramgarh–Munsiari thrust sheet in NW India. *Geological Society, London, Special Publications, 412*(1), 247-269. doi:doi:10.1144/SP412.6

Manea, V. C., Pérez-Gussinyé, M., & Manea, M. (2012). Chilean flat slab subduction controlled by overriding plate thickness and trench rollback. *Geology, 40*(1), 35-38. doi:10.1130/g32543.1

Marshak, S., & Wilkerson, M. S. (1992). Effect of overburden thickness on thrust belt geometry and development. *Tectonics, 11*(3), 560-566. doi:https://doi.org/10.1029/92TC00175

Martin, A. J. (2017). A review of Himalayan stratigraphy, magmatism, and structure. *Gondwana Research, 49*, 42-80. doi:https://doi.org/10.1016/j.gr.2017.04.031

Maruo, Y., & Kizaki, K. (1981). Structure and metamorphism in eastern Nepal. In P. S. Saklani (Ed.), *Metamorphic Tectonites of the Himalaya* (pp. 175-230). New Delhi: Today and Tomorrow's Printers and Publishers.

McGugan, A. (1987). "Horses" and transverse faults in the Lewis thrust sheet, Elk range, Kananaskis valley, Rocky mountain front ranges, Southwestern Alberta. *Bulletin of Canadian Petroleum Geology, 35*(3), 358-361. doi:https://doi.org/10.35767/gscpgbull.35.3.358

McMechan, M. (2001). Large-scale duplex structures in the McConnell thrust sheet, Rocky Mountains, Southwest Alberta. *Bulletin of Canadian Petroleum Geology, 49*(3), 408-425. doi:https://doi.org/10.2113/49.3.408

McMechan, M. (2007). Nature, origin and tectonic significance of anomalous transverse structures, southeastern Skeena Fold Belt, British Columbia. *Bulletin of Canadian Petroleum Geology, 55*(4), 262-274. doi:https://doi.org/10.2113/gscpgbull.55.4.262

McMechan, M. E. (2000). Walker Creek fault zone, central Rocky Mountains, British Columbia—southern continuation of the Northern Rocky Mountain Trench fault zone. *Canadian Journal of Earth Sciences, 37*(9), 1259-1273. doi:https://doi.org/10.1139/e00-038

McMechan, M. E. (2012). Deep transverse basement structural control of mineral systems in the southeastern Canadian Cordillera. *Canadian Journal of Earth Sciences, 49*(5), 693-708. doi:https://doi.org/10.1139/E2012-013

McMechan, M. E., & Price, R. A. (1982). Transverse folding and superposed deformation, Mount Fisher area, southern Canadian Rocky Mountain thrust and fold belt. *Canadian Journal of Earth Sciences, 19*(5), 1011-1024. doi:https://doi.org/10.1139/e82-084

McQuarrie, N. (2004). Crustal scale geometry of the Zagros fold–thrust belt, Iran. *Journal of Structural Geology, 26*(3), 519-535. doi:https://doi.org/10.1016/j.jsg.2003.08.009

McQuarrie, N., Stock, J. M., Verdel, C., & Wernicke, B. P. (2003). Cenozoic evolution of Neotethys and implications for the causes of plate motions. *Geophysical Research Letters*, *30*(20). doi: https://doi.org/10.1029/2003GL017992

McQuarrie, N., & van Hinsbergen, D. J. J. (2013). Retrodeforming the Arabia-Eurasia collision zone: Age of collision versus magnitude of continental subduction. *Geology, 41*(3), 315-318. doi:https://doi.org/10.1130/G33591.1

McQuillan, H. (1991). The role of basement tectonics in the control of sedimentary facies, structural patterns and salt plug emplacements in the Zagros fold belt of southwest Iran. *Journal of Southeast Asian Earth Sciences, 5*(1-4), 453-463. doi:https://doi.org/10.1016/0743-9547(91)90061-2

Medlicott, H. B. (1864). *On the geological Structure and relations of the Himalayan ranges, between the rivers Ganges and Ravee*. Retrieved from

Mejdahl, V. (1979). Thermoluminescence dating: beta-dose attenuation in quartz grains. *Archaeometry*, *21*(pt1), 61-72. Retrieved from http://inis.iaea.org/search/search.aspx?orig_q=RN:10451974

Mendoza, M. M., Ghosh, A., Karplus, M. S., Klemperer, S. L., Sapkota, S. N., Adhikari, L. B., & Velasco, A. (2019). Duplex in the Main Himalayan Thrust illuminated by aftershocks of the 2015 Mw 7.8 Gorkha earthquake. *Nature geoscience, 12*(12), 1018-1022. doi:10.1038/s41561-019-0474-8

Mendoza, M. M., Ghosh, A., Karplus, M.S., Klemperer, S.L., Sapkota, S.N., Adhikari, L.B., Velasco, A. (2019). Duplex in the Main Himalayan Thrust illuminated by aftershocks of the 2015 Mw 7.8 Gorkha earthquake. *Nature geoscience, 12*, 1018-1022. doi:https://doi.org/10.1038/s41561-019-0474-8

Mescua, J. F., & Giambiagi, L. B. (2012). Fault inversion vs. new thrust generation: a case study in the Malargüe fold-and-thrust belt, Andes of Argentina. *Journal of Structural Geology, 35*, 51-63. doi:https://doi.org/10.1016/j.jsg.2011.11.011

Miller, C., Klötzli, U., Frank, W., Thöni, M., & Grasemann, B. (2000). Proterozoic crustal evolution in the NW Himalaya (India) as recorded by circa 1.80 Ga mafic and 1.84 Ga granitic magmatism. *Precambrian Research, 103*(3), 191-206. doi:https://doi.org/10.1016/S0301-9268(00)00091-7

Mitra, S. (1988). Three-dimensional geometry and kinematic evolution of the Pine Mountain thrust system, southern Appalachians. *Geological Society of America Bulletin, 100*(1), 72-95. doi:https://doi.org/10.1130/0016-7606(1988)100<0072:TDGAKE>2.3.CO;2

Moffat, I. W., & Spang, J. H. (1984). Origin of transverse faulting, Rocky Mountain Front Ranges, Canmore, Alberta. *Bulletin of Canadian Petroleum Geology, 32*(2), 147-161. doi:https://doi.org/10.35767/gscpgbull.32.2.147

Mogk, D. W., Mueller, P. A., & Wooden, J. L. (1992). The nature of Archean terrane boundaries: an example from the northern Wyoming Province. *Precambrian Research, 55*(1-4), 155-168. doi:https://doi.org/10.1016/0301-9268(92)90020-O

Molnar, P., & Tapponnier, P. (1975). Cenozoic Tectonics of Asia: Effects of a Continental Collision. *Science, 189*(4201), 419-426. doi:doi:10.1126/science.189.4201.419

Molnar, P., & Tapponnier, P. (1978). Active tectonics of Tibet. *Journal of Geophysical Research: Solid Earth, 83*(B11), 5361-5375. doi:https://doi.org/10.1029/JB083iB11p05361

Monod, B., Dhont, D., & Hervouët, Y. (2010). Orogenic float of the Venezuelan Andes. *Tectonophysics, 490*(1-2), 123-135. doi:https://doi.org/10.1016/j.tecto.2010.04.036

Monsalve, G., Sheehan, A., Schulte-Pelkum, V., Rajaure, S., Pandey, M. R., & Wu, F. (2006). Seismicity and one-dimensional velocity structure of the Himalayan collision zone: Earthquakes in the crust and upper mantle. *Journal of Geophysical Research: Solid Earth, 111*(B10). doi:https://doi.org/10.1029/2005JB004062

Montemagni, C., Montomoli, C., Iaccarino, S., Carosi, R., Jain, A. K., Massonne, H.-J., & Villa, I. M. (2019). Dating protracted fault activities: microstructures, microchemistry and geochronology of the Vaikrita Thrust, Main Central Thrust zone, Garhwal Himalaya, NW India. In R. Sharma, I. M. Villa, & S. Kumar (Eds.), *Crustal Architecture and Evolution of the Himalaya–Karakoram–Tibet Orogen* (Vol. 481): The Geological Society of London.

Morgan, L. E., Mark, D. F., Imlach, J., Barfod, D., & Dymock, R. (2014). FCs-EK: a new sampling of the Fish Canyon Tuff 40Ar/39Ar neutron flux monitor. In F. Jourdan, D. F. Mark, & C. Verati (Eds.), *Advances in 40Ar/39Ar Dating: from Archaeology to Planetary Sciences* (Vol. 378, pp. 63-67): Geological Society of London, Special Publications.

Mouthereau, F., Deffontaines, B., Lacombe, O., & Angelier, J. (2002). Variations along the strike of the Taiwan thrust belt: Basement control on structural style, wedge geometry, and kinematics. In T. Byrne & C.-S. Liu (Eds.), *Geology and Geophysics of an Arc-Continent collision, Taiwan, Republic of China* (Vol. 358, pp. 35-58). Boulder, Colorado: Geological Society of America Special Paper.

Mouthereau, F., & Lacombe, O. (2006). Inversion of the Paleogene Chinese continental margin and thick-skinned deformation in the Western Foreland of Taiwan. *Journal of Structural Geology, 28*(11), 1977-1993. doi:https://doi.org/10.1016/j.jsg.2006.08.007

Mouthereau, F., Lacombe, O., & Vergés, J. (2012). Building the Zagros collisional orogen: timing, strain distribution and the dynamics of Arabia/Eurasia plate convergence. *Tectonophysics*, *532*, 27-60. doi:https://doi.org/10.1016/j.tecto.2012.01.022

Mpodozis, C., & Ramos, V. (1989). The Andes of Chile and Argentina. In G. Ericksen, M. Cañas, & J. Reinemund (Eds.), *Geology of the Andes and its Relation to Hydrocarbon and Mineral Resources* (Vol. 11, pp. 59-90): Circum-Pacific Council for Energy and Mineral Resources.

Mücher, H., van Steijn, H., & Kwaad, F. (2018). Chapter 2 - Colluvial and Mass Wasting Deposits. In G. Stoops, V. Marcelino, & F. Mees (Eds.), *Interpretation of Micromorphological Features of Soils and Regoliths (Second Edition)* (pp. 21-36): Elsevier.

Mueller, P. A., Heatherington, A. L., Kelly, D. M., Wooden, J. L., & Mogk, D. W. (2002). Paleoproterozoic crust within the Great Falls tectonic zone: Implications for the assembly of southern Laurentia. *Geology*, *30*(2), 127-130. doi:https://doi.org/10.1130/0091-7613(2002)030<0127:PCWTGF>2.0.CO;2

Mugnier, J. L., Jouanne, F., Bhattarai, R., Cortes-Aranda, J., Gajurel, A., Leturmy, P., Robert, X., Upreti, B., & Vassallo, R. (2017). Segmentation of the Himalayan megathrust around the Gorkha earthquake (25 April 2015) in Nepal. *Journal of Asian Earth Sciences, 141*, 236-252. doi:https://doi.org/10.1016/j.jseaes.2017.01.015

Mugnier, J. L., Leturmy, P., Huyghe, P., & Chalaron, E. (1999a). The Siwaliks of western Nepal: II. Mechanics of the thrust wedge. *Journal of Asian Earth Sciences, 17*(5), 643-657. doi:https://doi.org/10.1016/S1367-9120(99)00039-5

Mugnier, J. L., Leturmy, P., Mascle, G., Huyghe, P., Chalaron, E., Vidal, G., Husson, L., & Delcaillau, B. (1999b). The Siwaliks of western Nepal 1: Geometry and kinematics. *Journal of Asian Earth Sciences, 17*, 629-642. doi:https://doi.org/10.1016/S1367-9120(99)00038-3

Mukherjee, S., Talbot, C. J., & Koyi, H. A. (2010). Viscosity estimates of salt in the Hormuz and Namakdan salt diapirs, Persian Gulf. *Geological Magazine, 147*(4), 497-507. doi:https://doi/org/10.1017/S001675680999077X

Mukhopadhyay, D. K., Chakraborty, S., Trepmann, C., Rubatto, D., Anczkiewicz, R., Gaidies, F., Dasgupta, S., & Chowdhury, P. (2017). The nature and evolution of the Main Central Thrust: Structural and geochronological constraints from the Sikkim Himalaya, NE India. *Lithos, 282-283*, 447-463. doi:https://doi.org/10.1016/j.lithos.2017.01.015

Mukul, M. (2010a). First-order kinematics of wedge-scale active Himalayan deformation: insights from Darjiling-Sikkim-Tibet (DaSiT) wedge. *Journal of Asian Earth Sciences, 39*, 645-657. doi:https://doi.org/10.1016/j.jseaes.2010.04.029

Mukul, M. (2010b). First-order kinematics of wedge-scale active Himalayan deformation: Insights from Darjiling–Sikkim–Tibet (DaSiT) wedge. *Journal of Asian Earth Sciences, 39*(6), 645-657. doi:https://doi.org/10.1016/j.jseaes.2010.04.029

Mukul, M., Jade, S., Ansari, K., Matin, A., & Joshi, V. (2018). Structural insights from geodetic Global Positioning System measurements in the Darjiling-Sikkim Himalaya. *Journal of Structural Geology, 114*, 346-356. doi:https://doi.org/10.1016/j.jsg.2018.03.007

Mukul, M., Jade, S., Ansari, K., Matin, A, Joshi, V. (2018). Structural insights from geodetic Global Positioning System measurements in the Darjiling-Sikkim Himalaya. *Journal of Structural Geology, 114*, 346-356. doi:https://doi.org/10.1016/j.jsg.2018.03.007

Muller, F. (1980). *Present and late Pleistocene equilibrium line altitudes in the Mt. Everest region-An application of the glacier inventory.* Paper presented at the Proceedings of the Riederalp Workshop.

Müller, W., Mancktelow, N. S., & Meier, M. (2000). Rb–Sr microchrons of synkinematic mica in mylonites: an example from the DAV fault of the Eastern Alps. *Earth and Planetary Science Letters, 180*(3-4), 385-397. doi:https://doi.org/10.1016/S0012-821X(00)00167-9

Müller, W., Prosser, G., Mancktelow, N. S., Villa, I. M., Kelley, S. P., Viola, G., & Oberli, F. (2001). Geochronological constraints on the evolution of the Periadriatic Fault System (Alps). *International Journal of Earth Sciences, 90*(3), 623-653. doi:https://doi.org/10.1007/s005310000187

Murphy, J. B., & Keppie, J. D. (2005). The Acadian Orogeny in the Northern Appalachians. *International Geology Review, 47*(7), 663-687. doi:https://doi.org/10.2747/0020-6814.47.7.663

Murphy, J. B., Waldron, J. W., Kontak, D. J., Pe-Piper, G., & Piper, D. J. (2011). Minas Fault Zone: Late Paleozoic history of an intra-continental orogenic transform fault in the Canadian Appalachians. *Journal of Structural Geology, 33*(3), 312-328. doi:https://doi.org/10.1016/j.jsg.2010.11.012

Musumeci, G. (2002). Sillimanite-bearing shear zones in syntectonic leucogranite: fluid-assisted brittle–ductile deformation under amphibolite facies conditions. *Journal of Structural Geology, 24*(9), 1491-1505. doi:https://doi.org/10.1016/S0191-8141(01)00153-5

Nabelek, J., G. Hetenyi, J. Vergne, S. Sapkota, B. Kafle, M. Jiang, H. Su, J. Chen, and B.-S. Huang, and the Hi-CLIMB Team. (2009). Underplating in the Himalaya-Tibet collision zone revealed by the Hi-CL IMB experiment. *Science, 325*, 1371-1374. doi:https://doi.org/10.1126/science.1167719

Nábělek, J., Hetényi, G., Vergne, J., Sapkota, S., Kafle, B., Jiang, M., Su, H., Chen, J., Huang, B.-S., & Team, t. H.-C. (2009). Underplating in the Himalaya-Tibet Collision Zone Revealed by the Hi-CLIMB Experiment. *Science, 325*(5946), 1371-1374. doi:doi:10.1126/science.1167719

Nakajima, T., Sakai, H., Iwano, H., Danhara, T., & Hirata, T. (2020). Northward younging zircon fission-track ages from 13 to 2 Ma in the eastern extension of the Kathmandu nappe and underlying Lesser Himalayan sediments distributed to the south of Mt. Everest. *Island Arc, 29*(1), e12352. doi:https://doi.org/10.1111/iar.12352

Nakayama, K., & Ulak, P. D. (1999). Evolution of fluvial style in the Siwalik Group in the foothills of the Nepal Himalaya. *Sedimentary Geology, 125*(3), 205-224. doi:https://doi.org/10.1016/S0037-0738(99)00012-3

Nelson, K. D., Zhao, W., Brown, L. D., Kuo, J., Che, J., Liu, X., Klemperer, S. L., Makovsky, Y., Meissner, R., Mechie, J., Kind, R., Wenzel, F., Ni, J., Nabelek, J., Leshou, C., Tan, H., Wei, W., Jones, A. G., Booker, J., Unsworth, M., Kidd, W. S. F., Hauck, M., Alsdorf, D., Ross, A., Cogan, M., Wu, C., Sandvol, E., & Edwards, M. (1996). Partially Molten Middle Crust Beneath Southern Tibet: Synthesis of Project INDEPTH Results. *Science, 274*(5293), 1684-1688. doi:doi:10.1126/science.274.5293.1684

Norris, D. (2001). Slickenlines and the kinematics of the Crowsnest Deflection in the southern Rocky Mountains of Canada. *Journal of Structural Geology, 23*(6-7), 1089-1102. doi:https://doi.org/10.1016/S0191-8141(00)00180-2

O'Brien, T. M., & van der Pluijm, B. A. (2012). Timing of Iapetus Ocean rifting from Ar geochronology of pseudotachylytes in the St. Lawrence rift system of southern Quebec. *Geology, 40*(5), 443-446. doi:10.1130/g32691.1

O'Neill, J. M., & Lopez, D. A. (1985). Character and regional significance of Great Falls tectonic zone, east-central Idaho and west-central Montana. *AAPG Bulletin, 69*(3), 437-447. doi:https://doi.org/10.1306/AD462506-16F7-11D7-8645000102C1865D

Ojha, T. P., Butler, R. F., DeCelles, P. G., & Quade, J. (2009). Magnetic polarity stratigraphy of the Neogene foreland basin deposits of Nepal. *Basin Research, 21*(1), 61-90. doi:https://doi.org/10.1111/j.1365-2117.2008.00374.x

Oldham, R. D. (1917). Structure of the Himalayas and Indo-Gangetic plains. *Memoir of the Geological Survey of India, 156*.

Oldow, J. S., Bally, A. W., Lallemant, H. G. A., & Leeman, W. P. (1989). Phanerozoic evolution of the North American Cordillera, United States and Canada. In A. W. Bally & A. R. Palmer (Eds.), *The geology of North America: an overview* (Vol. A, pp. 139-232): Geological Society of America, The Geology of North America.

Oriolo, S., Japas, M. S., Cristallini, E. O., & Giménez, M. (2014). Cross-strike structures controlling magmatism emplacement in a flat-slab setting (Precordillera, Central Andes of Argentina). *Geological Society, London, Special Publications, 394*(1), 113-127. doi:https://doi.org/10.1144/sp394.6

Orme, D. A., Carrapa, B., & Kapp, P. (2015). Sedimentology, provenance and geochronology of the upper Cretaceous–lower Eocene western Xigaze forearc basin, southern Tibet. *Basin Research, 27*(4), 387-411. doi:https://doi.org/10.1111/bre.12080

Oswald, P., Ortner, H., & Gruber, A. (2019). Deformation around a detached half-graben shoulder during nappe stacking (Northern Calcareous Alps, Austria). *Swiss Journal of Geosciences, 112*(1), 23-37. doi:https://doi.org/10.1007/s00015-018-0333-4

Owen, L. A., Robinson, R., Benn, D. I., Finkel, R. C., Davis, N. K., Yi, C., Putkonen, J., Li, D., & Murray, A. S. (2009a). Quaternary glaciation of Mount Everest. *Quaternary Science Reviews, 28*(15-16), 1412-1433.

Owen, L. A., Robinson, R., Benn, D. I., Finkel, R. C., Davis, N. K., Yi, C., Putkonen, J., Li, D., & Murray, A. S. (2009b). Quaternary glaciation of Mount Everest. *Quaternary Science Reviews, 28*(15), 1412-1433. doi:https://doi.org/10.1016/j.quascirev.2009.02.010

Pandey, M. R., Tandukar, R. P., Avouac, J. P., Lavé, J., & Massot, J. P. (1995). Interseismic strain accumulation on the Himalayan crustal ramp (Nepal). *Geophysical Research Letters, 22*(7), 751-754. doi:https://doi.org/10.1029/94GL02971

Pandey, M. R., Tandukar, R. P., Avouac, J. P., Vergne, J., & Héritier, T. (1999). Seismotectonics of the Nepal Himalaya from a local seismic network. *Journal of Asian Earth Sciences, 17*(5), 703-712. doi:https://doi.org/10.1016/S1367-9120(99)00034-6

Pantet, A., Epard, J.-L., & Masson, H. (2020). Mimicking Alpine thrusts by passive deformation of synsedimentary normal faults: a record of the Jurassic extension of the European margin (Mont Fort nappe, Pennine Alps). *Swiss Journal of Geosciences, 113*(1), 13. doi:10.1186/s00015-020-00366-2

Parrish, R. R., & Hodges, V. (1996). Isotopic constraints on the age and provenance of the Lesser and Greater Himalayan sequences, Nepalese Himalaya. *GSA bulletin, 108*(7), 904-911. doi:10.1130/0016-7606(1996)108<0904:Icotaa>2.3.Co;2

Pash, R. R., Sarkarinejad, K., Ghoochaninejad, H. Z., Motamedi, H., & Yazdani, M. (2020). Accommodation of the different structural styles in the foreland fold-and-thrust belts: northern Dezful Embayment in the Zagros belt, Iran. *International Journal of Earth Sciences*, 1-12. doi:https://doi.org/10.1007/s00531-020-01844-6

Passchier, C. W., & Trouw, R. A. (2005). *Micro-tectonics*: Springer.

Paul, H., Mitra, S., Bhattacharya, S. N., & Suresh, G. (2015). Active transverse faulting within underthrust Indian crust beneath the Sikkim Himalaya. *Geophysics Journal International, 201*(2), 1070-1081. doi:https://doi.org/10.1093/gji/ggv058

Paul, H., Mitra, S., Bhattacharya, S.N., Suresh, G. (2015). Active transverse faulting within underthrust Indian crust beneath the Sikkim Himalaya. *Geophysics Journal International, 201*(2), 1070-1081. doi:https://doi.org/10.1093/gji/ggv058

Paulsen, T., & Marshak, S. (1997). Structure of the Mount Raymond transverse zone at the southern end of the Wyoming salient, Sevier fold-thrust belt, Utah. *Tectonophysics, 280*(3-4), 199-211. doi:https://doi.org/10.1016/S0040-1951(97)00205-9

Paulsen, T., & Marshak, S. (1998). Charleston transverse zone, Wasatch Mountains, Utah: Structure of the Provo salient's northern margin, Sevier fold-thrust belt. *Geological Society of America Bulletin, 110*(4), 512-522. doi:https://doi.org/10.1130/0016-7606(1998)110<0512:CTZWMU>2.3.CO;2

Paulsen, T., & Marshak, S. (1999). Origin of the Uinta recess, Sevier fold–thrust belt, Utah: influence of basin architecture on fold–thrust belt geometry. *Tectonophysics, 312*(2-4), 203-216. doi:https://doi.org/10.1016/S0040-1951(99)00182-1

Pearson, O. N., & DeCelles, P. G. (2005). Structural geology and regional tectonic significance of the Ramgarh thrust, Himalayan fold-thrust belt of Nepal. *Tectonics, 24*(4). doi:https://doi.org/10.1029/2003TC001617

Pêcher, A. (1989). The metamorphism in the Central Himalaya. *Journal of Metamorphic Geology, 7*(1), 31-41. doi:https://doi.org/10.1111/j.1525-1314.1989.tb00573.x

Perello, P., Delle Piane, L., Piana, F., Morelli, M., Damiano, A., & Venturini, G. (2004). New constraints on late to post-Oligocene deformation history of the Western Alps: data from Middle Susa valley and High Maurienne valley. *Abstract, 32nd IGC—Firenze, 247.*

Perez-Estaun, A., Alvarez-Marron, J., Brown, D., Puchkov, V., Gorozhanina, Y., & Baryshev, V. (1997). Along-strike structural variations in the foreland thrust and fold belt of the southern Urals. *Tectonophysics, 276*(1-4), 265-280. doi:https://doi.org/10.1016/S0040-1951(97)00060-7

Pérez-Flores, P., Cembrano, J., Sánchez-Alfaro, P., Veloso, E., Arancibia, G., & Roquer, T. (2016). Tectonics, magmatism and paleo-fluid distribution in a strike-slip setting: Insights from the northern termination of the Liquiñe–Ofqui fault System, Chile. *Tectonophysics, 680*, 192-210. doi:http://dx.doi.org/10.1016/j.tecto.2016.05.016

Perrone, G., Cadoppi, P., Tallone, S., & Balestro, G. (2011). Post-collisional tectonics in the Northern Cottian Alps (Italian Western Alps). *International Journal of Earth Sciences, 100*(6), 1349-1373. doi:https://doi.org/10.1007/s00531-010-0534-1

Petrinovic, I., Riller, U., Brod, J., Alvarado, G., & Arnosio, M. (2006). Bimodal volcanism in a tectonic transfer zone: evidence for tectonically controlled magmatism in the southern Central Andes, NW Argentina. *Journal of Volcanology and Geothermal Research, 152*(3-4), 240-252. doi:https://doi.org/10.1016/j.jvolgeores.2005.10.008

Pfiffner, O. A. (2014). *Geology of the Alps*: John Wiley & Sons.

Picotti, V., Casolari, E., Castellarin, A., Mosconi, A., Cairo, E., Pessina, C., & Sella, M. (1997). Structural evolution of the eastern Lombardian Prealps: Alpine inversion of a Mesozoic rifted margin. *Agip SpA, San Donato Milanese, 102*.

Pilger, R. H. J. (1981). Plate reconstructions, aseismic ridges, and low-angle subduction beneath the Andes. *GSA bulletin, 92*(7), 448-456. doi:10.1130/0016-7606(1981)92<448:Praral>2.0.Co;2

Pilkington, M., Miles, W., Ross, G., & Roest, W. (2000). Potential-field signatures of buried Precambrian basement in the Western Canada Sedimentary Basin. *Canadian Journal of Earth Sciences, 37*(11), 1453-1471. doi:https://doi.org/10.1139/e00-020

Piquer, J., Rivera, O., Yañez, G., & Oyarzun, N. (2020). The Piuquencillo Fault System: a long-lived, Andean-transverse fault system and its relationship with magmatic and hydrothermal activity. *Solid Earth Discussions*, 1-34. doi:https://doi.org/10.5194/se-2020-142

Pizzi, A., & Galadini, F. (2009). Pre-existing cross-structures and active fault segmentation in the northern-central Apennines (Italy). *Tectonophysics, 476*(1-2), 304-319. doi:https://doi.org/10.1016/j.tecto.2009.03.018

Plint, H. E., & Jamieson, R. A. (1989). Microstructure, metamorphism and tectonics of the western Cape Breton Highlands, Nova Scotia. *Journal of Metamorphic Geology, 7*(4), 407-424. doi:https://doi.org/10.1111/j.1525-1314.1989.tb00606.x

Pognante, U., & Benna, P. (1993). Metamorphic zonation, migmatization and leucogranites along the Everest transect of Eastern Nepal and Tibet: record of an exhumation history. *Geological Society, London, Special Publications, 74*(1), 323-340. doi:doi:10.1144/GSL.SP.1993.074.01.22

Polinski, R. K., & Eisbacher, G. H. (1992). Deformation partitioning during polyphase oblique convergence in the Karawanken Mountains, southeastern Alps. *Journal of Structural Geology, 14*(10), 1203-1213. doi:https://doi.org/10.1016/0191-8141(92)90070-D

Pomella, H., Stipp, M., & Fügenschuh, B. (2012). Thermochronological record of thrusting and strike-slip faulting along the Giudicarie fault system (Alps, Northern Italy). *Tectonophysics, 579*, 118-130. doi:https://doi.org/10.1016/j.tecto.2012.04.015

Posch, E., Bell, R., Weidinger, J. T., & Glade, T. (2015). Geomorphic Processes, Rock Quality and Solid Waste Management—Examples from the Mt. Everest Region of Nepal. *Journal of Water Resource and Protection, 7*(16), 18. doi:https://doi.org/10.4236/jwarp.2015.716105

Prey, S. (1989). Ein steilstehendes Störungssystem als Westbegrenzung des Tauernfensters. *Journal of Geologische Bundesanstalt, 132*(4), 745-749.

Price, R. A. (1981). The Cordilleran foreland thrust and fold belt in the southern Canadian Rocky Mountains. *Geological Society, London, Special Publications, 9*(1), 427-448. doi:https://doi.org/10.1144/GSL.SP.1981.009.01.39

Pride, K. R., Lecouteur, P. C., & Mawer, A. B. (1986). Geology and mineralogy of the Aley carbonatite, Ospika River area, British Columbia. *Canadian Institute of Mining Bulletin, 79*(891), 32-32.

Prosser, G. (1998). Strike-slip movements and thrusting along a transpressive fault zone: The North Giudicarie line (Insubric line, northern Italy). *Tectonics, 17*(6), 921-937. doi:https://doi.org/10.1029/1998TC900010

Quincey, D., Luckman, A., & Benn, D. (2009a). Quantification of Everest region glacier velocities between 1992 and 2002, using satellite radar interferometry and feature tracking. *Journal of Glaciology, 55*(192), 596-606.

Quincey, D. J., Luckman, A., & Benn, D. (2009b). Quantification of Everest region glacier velocities between 1992 and 2002, using satellite radar interferometry and feature tracking. *Journal of Glaciology, 55*(192), 596-606. doi:https://doi.org/10.3189/002214309789470987

Raiverman, V., Kunte, S.V., and Mukherjea, A. (1983). Basin geometry, Cenozoic sedimentation and hydrocarbon in northwestern Himalaya and Indo-Gangetic plains. *Petroleum Geology of Asia Journal, 6*(4), 67-92.

Rajaure, S., Sapkota, S. N., Adhikari, L. B., Koirala, B., Bhattarai, M., Tiwari, D. R., Gautam, U. G., Shrestha, P., Maske, S., Avouac, J. P., Bollinger, L., & Pandey, M. R. (2013). Double difference relocation of local earthquakes in the Nepal Himalaya. *Journal of Nepal Geological Society, 46*(0), 133–142. doi:10.3126/jngs.v46i0.31590

Rajaure, S., Sapkota, S.N., Adhikari, L.B., Koirala, B., Bhattarai, M., Tiwari, D.R., Gautam, U., Shrestha, P., Maske, S., Avouac, J.P., Bollinger, L., Pandey, M.R. (2013). Double difference relocation of local earthquakes in the Nepal Himalaya. *Journal of the Nepal Geological Society, 46*, 133-142.

Ramos, V. A. (1988). The tectonics of the Central Andes (30°–33°S latitude). In S. Clark, D. Burchfiel, & D. Suppe (Eds.), *Processes in Continental Lithospheric Deformation* (Vol. 218, pp. 31-54): Geological Society of America Special Paper.

Ramos, V. A., Cristallini, E. O., & Pérez, D. J. (2002). The Pampean flat-slab of the Central Andes. *Journal of South American earth sciences, 15*(1), 59-78. doi:https://doi.org/10.1016/S0895-9811(02)00006-8

Ramos, V. A., & Folguera, A. (2009). Andean flat-slab subduction through time. *Geological Society, London, Special Publications, 327*(1), 31-54. doi:10.1144/sp327.3

Rankin, D. W. (1976). Appalachian salients and recesses: Late Precambrian continental breakup and the opening of the Iapetus Ocean. *Journal of Geophysical Research, 81*(32), 5605-5619. doi:https://doi.org/10.1029/JB081i032p05605

Rao, M. B. R. (1973). The subsurface geology of the Indo-Gangetic plains. *Journal of The Geological Society of India, 14*(3), 217-242.

Ratschbacher, L., Merle, O., Davy, P., & Cobbold, P. (1991). Lateral extrusion in the Eastern Alps, part 1: boundary conditions and experiments scaled for gravity. *Tectonics, 10*(2), 245-256. doi:https://doi.org/10.1029/90TC02622

Rees-Jones, J. (1995). Optical dating of young sediments using fine-grain quartz. *Ancient TL, 13*(2), 9-14.

Regard, V., Bellier, O., Thomas, J.-C., Bourles, D., Bonnet, S., Abbassi, M., Braucher, R., Mercier, J., Shabanian, E., & Soleymani, S. (2005). Cumulative right-lateral fault slip rate across the Zagros—Makran transfer zone: role of the Minab—Zendan fault system in accommodating Arabia—Eurasia convergence in southeast Iran. *Geophysical Journal International*, *162*(1), 177-203. doi:https://doi.org/10.1111/j.1365-246X.2005.02558.x

Reiter, F., Freudenthaler, C., Hausmann, H., Ortner, H., Lenhardt, W., & Brandner, R. (2018). Active seismotectonic deformation in front of the Dolomites indenter, Eastern Alps. *Tectonics, 37*(12), 4625-4654. doi:https://doi.org/10.1029/2017TC004867

Renne, P. R., Balco, G., Ludwig, K. R., Mundil, R., & Min, K. (2011). Response to the comment by W. H. Schwarz et al. on "Joint determination of 40K decay constants and the 40Ar*/40K for the Fish Canyon sanidine, and improved accuracy for 40Ar/39Ar geochronology" by P.R. Renne et al. (2010). *Geochimica et Cosmochimica Acta, 75*, 5097-5100.

Renne, P. R., Cassata, W. S., & Morgan, L. E. (2009). The isotopic composition of atmospheric argon and 40Ar/39Ar geochronology: Time for a change? *Quaternary Geochronology, 4*(4), 288-298. doi:https://doi.org/10.1016/j.quageo.2009.02.015

Reynolds, M. W. (1979). Character and Extent of Basin-Range Faultin, Western Montana and East-Central Idaho. In G. W. Newman & H. D. Goode (Eds.), *Basin and Range Symposium and Great Basin Field Conference* (pp. 185-193). Denver: Rocky Mountain Association of Geologists.

Ribes, C., Manatschal, G., Ghienne, J.-F., Karner, G. D., Johnson, C. A., Figueredo, P. H., Incerpi, N., & Epin, M.-E. (2019). The syn-rift stratigraphic record across a fossil hyper-extended rifted margin: the example of the northwestern Adriatic margin exposed in the Central Alps. *International Journal of Earth Sciences, 108*(6), 2071-2095. doi:10.1007/s00531-019-01750-6

Richards, B. W., Benn, D. I., Owen, L. A., Rhodes, E. J., & Spencer, J. Q. (2000a). Timing of late Quaternary glaciations south of Mount Everest in the Khumbu Himal, Nepal. *Geological Society of America Bulletin, 112*(10), 1621-1632.

Richards, B. W. M., Benn, D. I., Owen, L. A., Rhodes, E. J., & Spencer, J. Q. (2000b). Timing of late Quaternary glaciations south of Mount Everest in the Khumbu Himal, Nepal. *GSA bulletin, 112*(10), 1621-1632. doi:https://doi.org/10.1130/0016-7606(2000)112<1621:Tolqgs>2.0.Co;2

Ring, U. (1994). The kinematics of the late Alpine Muretto fault and its relation to dextral transpression across the Periadriatic Line. *Eclogae Geologicae Helvetiae, 87*(3), 811-831.

Ring, U., & Gerdes, A. (2016). Kinematics of the Alpenrhein-Bodensee graben system in the Central Alps: Oligocene/Miocene transtension due to formation of the Western Alps arc. *Tectonics, 35*(6), 1367-1391. doi:https://doi.org/10.1002/2015TC004085

Rivers, T. (2008). Assembly and preservation of lower, mid, and upper orogenic crust in the Grenville Province—Implications for the evolution of large hot long-duration orogens. *Precambrian Research, 167*(3), 237-259. doi:https://doi.org/10.1016/j.precamres.2008.08.005

Rivers, T. (2012). Upper-crustal orogenic lid and mid-crustal core complexes: signature of a collapsed orogenic plateau in the hinterland of the Grenville Province 1This article is one of a series of papers published in CJES Special Issue: In honour of Ward Neale on the theme of Appalachian and Grenvillian geology. *Canadian Journal of Earth Sciences, 49*(1), 1-42. doi:https://doi.org/10.1139/e11-014

Rivers, T. (2015). Tectonic Setting and Evolution of the Grenville Orogen: An Assessment of Progress Over the Last 40 Years. *Geoscience Canada, 42*(1), 77-124. doi:10.12789/geocanj.2014.41.057

Robertson, A. H. F., Clift, P. D., Degnan, P. J., & Jones, G. (1991). Palaeogeographic and palaeotectonic evolution of the Eastern Mediterranean Neotethys. *Palaeogeography, Palaeoclimatology, Palaeoecology, 87*(1-4), 289-343. doi:https://doi.org/10.1016/0031-0182(91)90140-M

Robinson, D. M., DeCelles, P. G., & Copeland, P. (2006a). Tectonic evolution of the Himalayan thrust belt in western Nepal: Implications for channel flow models. *GSA bulletin, 118*(7-8), 865-885. doi:10.1130/b25911.1

Robinson, D. M., DeCelles, P. G., Patchett, P. J., & Garzione, C. N. (2001). The kinematic evolution of the Nepalese Himalaya interpreted from Nd isotopes. *Earth and Planetary Science Letters, 192*(4), 507-521. doi:https://doi.org/10.1016/S0012-821X(01)00451-4

Robinson, D. P., Das, S., & Watts, A. B. (2006b). Earthquake rupture stalled by a subducting fracture zone. *Science, 312*(5777), 1203-1205. doi:https://doi.org/10.1126/science.1125771

Robl, J., & Stüwe, K. (2005). Continental collision with finite indenter strength: 2. European Eastern Alps. *Tectonics, 24*(4). doi:https://doi.org/10.1029/2004TC001741

Rodgers, J. (1990). Fold-and-thrust belts in sedimentary rocks. Part 1: Typical examples. *American Journal of Science, 290*(4), 321-359. doi:https://doi.org/10.2475/ajs.290.4.321

Ronemus, C. B., Orme, D. A., Campbell, S., Black, S. R., & Cook, J. (2020). Mesoproterozoic−Early Cretaceous provenance and paleogeographic evolution of the Northern Rocky Mountains: Insights from the detrital zircon record of the Bridger Range, Montana, USA. *GSA bulletin*. doi:10.1130/b35628.1

Root, K. G. (1987). *Geology of the Delphine Creek area, southeastern British Columbia: implications for the Proterozoic and Paleozoic development of the Cordilleran Divergent Margin.* (Ph.D.). University of Calgary, Calgary, Alberta.

Roquer, T., Arancibia, G., Rowland, J., Iturrieta, P., Morata, D., & Cembrano, J. (2017). Fault-controlled development of shallow hydrothermal systems: Structural and mineralogical insights from the Southern Andes. *Geothermics*, *66*, 156-173. doi:http://dx.doi.org/10.1016/j.geothermics.2016.12.003

Rosenberg, C. L., Brun, J.-P., & Gapais, D. (2004). Indentation model of the Eastern Alps and the origin of the Tauern Window. *Geology, 32*(11), 997-1000. doi:https://doi.org/10.1130/G20793.1

Rosenberg, C. L., & Garcia, S. (2011). Estimating displacement along the Brenner Fault and orogen-parallel extension in the Eastern Alps. *International Journal of Earth Sciences, 100*(5), 1129-1145. doi:https://doi.org/10.1007/s00531-011-0645-3

Ross, G., Parrish, R., Villeneuve, M., & Bowring, S. (1991). Geophysics and geochronology of the crystalline basement of the Alberta Basin, western Canada. *Canadian Journal of Earth Sciences*, *28*(4), 512-522. doi:https://doi.org/10.1139/e91-045

Röthlisberger, F., & Geyh, M. A. (1985). Glacier variations in Himalayas and Karakorum. *Zeitschrift für Gletscherkunde und Glazialgeologie, 21*, 237-249.

Royden, L., Horváth, F., Nagymarosy, A., & Stegena, L. (1983). Evolution of the Pannonian basin system: 2. Subsidence and thermal history. *Tectonics, 2*(1), 91-137. doi:https://doi.org/10.1029/TC002i001p00091

Royden, L. H. (1993). Evolution of retreating subduction boundaries formed during continental collision. *Tectonics, 12*(3), 629-638. doi:https://doi.org/10.1029/92TC02641

Sadeghi, S., & Yassaghi, A. (2016). Spatial evolution of Zagros collision zone in Kurdistan, NW Iran: Constraints on Arabia–Eurasia oblique convergence. *Solid Earth, 7*(2), 659-659. doi:https://doi.org/10.5194/se-7-659-2016

Sahoo, P. K., Kumar, S., & Singh, R. P. (2000). Neotectonic study of Ganga and Yamuna tear faults, NW Himalaya, using remote sensing and GIS. *International Journal of Remote Sensing, 21*(3), 499-518. doi:10.1080/014311600210713

Sahoo, P. K., Kumar, S., and Singh, R.P. (2000). Neotectonic study of Ganga and Yamuna tear faults, NW Himalaya, using remote sensing and GIS. *International Journal of Remote Sensing, 21*(3), 499-518. doi:https://doi.org/10.1080/014311600210713

Sakai, H. (1983). Geology of the Tansen Group of the Lesser Himalaya in Nepal. *Memoirs of the Faculty of Science, Kyūsyū University. Series D, Geology, 23*, 27-74. doi:https://doi.org/10.5109/1546083

Sakai, H., Iwano, H., Danhara, T., Takigami, Y., Rai, S. M., Upreti, B. N., & Hirata, T. (2013). Rift-related origin of the Paleoproterozoic Kuncha Formation, and cooling history of the Kuncha nappe and Taplejung granites, eastern Nepal Lesser Himalaya: a multichronological approach. *Island Arc, 22*(3), 338-360. doi:https://doi.org/10.1111/iar.12021

Saleeby, J. B. (2003). Segmentation of the Laramide slab—Evidence from the southern Sierra Nevada region. *Geological Society of America Bulletin, 115*(6), 655-668. doi:https://doi.org/10.1130/0016-7606(2003)115<0655:SOTLSF>2.0.CO;2

Saleeby, J. B., Busby-Spera, C., Oldow, J. S., Dunne, G. C., Wright, J. E., Cowan, D. S., Walker, R. W., & Alllmendinger, R. W. (1992). Early Mesozoic tectonic evolution of the western US Cordillera. In B. C. Burchfiel, W. Lipman, & M. L. Zoback (Eds.), *The Cordilleran Orogen, Conterminous U.S., The Geology of North America G3* (pp. 107-168): Geological Society of America.

Salfity, J. A., & Marquillas, R. A. (1994). Tectonic and sedimentary evolution of the Cretaceous-Eocene Salta Group basin, Argentina. In J. A. Salfity (Ed.), *Cretaceous tectonics of the Andes* (pp. 266-315): Vieweg+Teubner Verlag, Wiesbaden.

Sarkarinejad, K., Pash, R. R., Motamedi, H., & Yazdani, M. (2018). Deformation and kinematic evolution of the subsurface structures: Zagros foreland fold-and-thrust belt, northern Dezful Embayment, Iran. *International Journal of Earth Sciences, 107*(4), 1287-1304. doi:https://doi.org/10.1007/s00531-017-1532-3

Sastri, V. V., Bhandari, L. L., Raju, A. T. R., & Datta, A. K. (1971). *Tectonic Framework and Subsurface Stratigraphy of the Ganga Basin*.

Sastri, V. V., Bhandari, L.L., Raju, A.T.R., Datta, A.K. (1971). Tectonic framework and subsurface stratigraphy of the Ganga Basin. *Journal of The Geological Society of India, 12*(3), 222-233.

Satolli, S., Pace, P., Viandante, M. G., & Calamita, F. (2014). Lateral variations in tectonic style across cross-strike discontinuities: an example from the Central Apennines belt (Italy). *International Journal of Earth Sciences*, *103*(8), 2301-2313. doi:https://doi.org/10.1007/s00531-014-1052-3

Schelling, D. (1992). The tectonostratigraphy and structure of the eastern Nepal Himalaya. *Tectonics, 11*(5), 925-943. doi:https://doi.org/10.1029/92TC00213

Schepers, G., Van Hinsbergen, D. J., Spakman, W., Kosters, M. E., Boschman, L. M., & McQuarrie, N. (2017). South-American plate advance and forced Andean trench retreat as drivers for transient flat subduction episodes. *Nature communications, 8*, 15249. doi:https://doi.org/10.1038/ncomms15249

Schmid, S. M., Aebli, H. R., Heller, F., & Zingg, A. (1989). The role of the Periadriatic Line in the tectonic evolution of the Alps. *Geological Society, London, Special Publications, 45*(1), 153-171. doi:https://doi.org/10.1144/gsl.Sp.1989.045.01.08

Schmid, S. M., Fügenschuh, B., Kissling, E., & Schuster, R. (2004). Tectonic map and overall architecture of the Alpine orogen. *Eclogae Geologicae Helvetiae, 97*(1), 93-117. doi:https://doi,org/10.1007/s00015-004-1113-x

Schmid, S. M., Pfiffner, O.-A., Froitzheim, N., Schönborn, G., & Kissling, E. (1996). Geophysical-geological transect and tectonic evolution of the Swiss-Italian Alps. *Tectonics, 15*(5), 1036-1064. doi: https://doi.org/10.1029/96TC00433

Schönborn, G. (1992). Kinematics of a transverse zone in the Southern Alps, Italy. In K. R. McClay (Ed.), *Thrust Tectonics* (pp. 299-310). Dordrecht: Springer Netherlands.

Schultz, M. H., Hodges, K. V., Ehlers, T. A., van Soest, M., & Wartho, J.-A. (2017). Thermochronologic constraints on the slip history of the South Tibetan detachment system in the Everest region, southern Tibet. *Earth and Planetary Science Letters, 459*, 105-117. doi:https://doi.org/10.1016/j.epsl.2016.11.022

Schumacher, M. E. (1990). Alpine basement thrusts in the Eastern Seengebirge, Southern Alps (Italy Switzerland). *Eclogae Geologicae Helvetiae, 83*(3), 645-663.

Scrocca, D. (2006). Thrust front segmentation induced by differential slab retreat in the Apennines (Italy). *Terra nova, 18*(2), 154-161. doi: https://doi.org/10.1111/j.1365-3121.2006.00675.x

Searle, M. P. (1999). Extensional and compressional faults in the Everest–Lhotse massif, Khumbu Himalaya, Nepal. *Journal of the Geological Society, 156*(2), 227-240. doi:https://doi.org/10.1144/gsjgs.156.2.0227

Searle, M. P. (2010). Low-angle normal faults in the compressional Himalayan orogen; Evidence from the Annapurna–Dhaulagiri Himalaya, Nepal. *Geosphere, 6*(4), 296-315. doi:10.1130/ges00549.1

Searle, M. P., Law, R. D., Godin, L., Larson, K. P., Streule, M. J., Cottle, J. M., & Jessup, M. J. (2008). Defining the Himalayan Main Central Thrust in Nepal. *Journal of the Geological Society, 165*(2), 523-534. doi:10.1144/0016-76492007-081

Searle, M. P., Law, R. D., & Jessup, M. J. (2006). Crustal structure, restoration and evolution of the Greater Himalaya in Nepal-South Tibet: implications for channel flow and ductile extrusion of the middle crust. *Geological Society, London, Special Publications, 268*(1), 355-378. doi:doi:10.1144/GSL.SP.2006.268.01.17

Searle, M. P., & Rex, A. J. (1989). Thermal model for the Zanskar Himalaya. *Journal of Metamorphic Geology, 7*(1), 127-134. doi:https://doi.org/10.1111/j.1525-1314.1989.tb00579.x

Searle, M. P., Simpson, R. L., Law, R. D., Parrish, R. R., & Waters, D. J. (2003). The structural geometry, metamorphic and magmatic evolution of the Everest massif, High Himalaya of Nepal–South Tibet. *Journal of the Geological Society, 160*(3), 345-366. doi:doi:10.1144/0016-764902-126

Sears, J. W., Hendrix, M., Waddell, A., Webb, B., Nixon, B., King, T., Roberts, E., & Lerman, R. (2000). Structural and stratigraphic evolution of the Rocky Mountain foreland basin in central-western Montana. In S. Roberts & D. Winston (Eds.), *Geologic Field Trips, Western Montana and Adjacent Areas. Edited by S. Roberts and D. Winston. Rocky Mountain Section Geological Society of America Annual Meeting* (pp. 131-156). Missoula: University of Montana.

Sears, J. W., & Hendrix, M. S. (2004). Lewis and Clark line and the rotational origin of the Alberta and Helena salients, North American Cordillera. In A. Sussman & A. Weil (Eds.), *Orogenic Curvature: Integrating Paleomagnetic and Structural Analyses: Geological Society of America Special Paper* (Vol. 383, pp. 173-186).

Seifert, N. (2019). *Structural analysis of the Benkar Fault Zone, a cross structure in the Higher Himalaya of the Khumbu Region, eastern Nepal.* (MS). Montana State University, Bozeman, Montana.

Séjourné, S., & Malo, M. (2007). Pre-, syn-, and post-imbrication deformation of carbonate slices along the southern Quebec Appalachian front—implications for hydrocarbon exploration. *Canadian Journal of Earth Sciences, 44*(4), 543-564. doi:https://doi.org/10.1139/E06-106

Selverstone, J. (1988). Evidence for east-west crustal extension in the Eastern Alps: Implications for the unroofing history of the Tauern Window. *Tectonics, 7*(1), 87-105. doi:https://doi.org/10.1029/TC007i001p00087

Sepehr, M., Cosgrove, J., & Moieni, M. (2006). The impact of cover rock rheology on the style of folding in the Zagros fold-thrust belt. *Tectonophysics, 427*(1-4), 265-281. doi:https://doi.org/10.1016/j.tecto.2006.05.021

Sepehr, M., & Cosgrove, J. W. (2004). Structural framework of the Zagros fold–thrust belt, Iran. *Marine and Petroleum Geology, 21*(7), 829-843. doi:https://doi.org/10.1016/j.marpetgeo.2003.07.006

Sherpa, S. F., Wagnon, P., Brun, F., Berthier, E., Vincent, C., Lejeune, Y., Arnaud, Y., Kayastha, R. B., & Sinisalo, A. (2017). Contrasted surface mass balances of debris-free glaciers observed between the southern and the inner parts of the Everest region (2007–15). *Journal of Glaciology, 63*(240), 637-651. doi:https://doi.org/10.1017/jog.2017.30

Sielfeld, G., Ruz, J., Brogi, A., Cembrano, J., Stanton-Yonge, A., Pérez-Flores, P., & Iturrieta, P. (2019). Oblique-slip tectonics in an active volcanic chain: A case study from the Southern Andes. *Tectonophysics, 770*, 228221. doi:https://doi.org/10.1016/j.tecto.2019.228221

Silver, C. R. P., Murphy, M. A., Taylor, M. H., Gosse, J., & Baltz, T. (2015). Neotectonics of the Western Nepal Fault System: Implications for Himalayan strain partitioning. *Tectonics, 34*(12), 2494-2513. doi:https://doi.org/10.1002/2014TC003730

Simony, P. S., & Carr, S. D. (1997). Large lateral ramps in the Eocene Valkyr shear zone: extensional ductile faulting controlled by plutonism in southern British Columbia. *Journal of Structural Geology, 19*(6), 769-784. doi:https://doi.org/10.1016/S0191-8141(97)00011-4

Simpson, R. L., Parrish, R. R., Searle, M. P., & Waters, D. J. (2000). Two episodes of monazite crystallization during metamorphism and crustal melting in the Everest region of the Nepalese Himalaya. *Geology, 28*(5), 403-406. doi:10.1130/0091-7613(2000)28<403:Teomcd>2.0.Co;2

Sims, P. K., Bankey, V., & Finn, C. (2001). *Preliminary Precambrian basement map of Colorado: A geologic interpretation of the aeromagnetic map*: U.S. Geological Survey.

Skourlis, K., & Doutsos, T. (2003). The Pindos Fold-and-thrust belt (Greece): inversion kinematics of a passive continental margin. *International Journal of Earth Sciences, 92*(6), 891-903. doi:https://doi.org/10.1007/s00531-003-0365-4

Sobornov, K. O. (1996). Lateral variations in structural styles of tectonic wedging in the northeastern Caucasus, Russia. *Bulletin of Canadian Petroleum Geology, 44*(2), 385-399.

Sorgi, C., Deffontaines, B., Hippolyte, J. C., & Cadet, J. P. (1998). An integrated analysis of transverse structures in the northern Apennines, Italy. *Geomorphology*, *25*(3-4), 193-206. doi:https://doi.org/10.1016/S0169-555X(98)00041-5

Soucy La Roche, R., and Godin, L. (2019). Inherited cross-strike faults and Oligocene-early Miocene segmentation of the Main Himalayan Thrust, West Nepal. *Journal of Geophysical Research Solid Earth*, *124*, 7429-7444. doi:https://doi.org/10.1029/2019JB017467

Soucy La Roche, R., & Godin, L. (2019). Inherited Cross-Strike Faults and Oligocene-Early Miocene Segmentation of the Main Himalayan Thrust, West Nepal. *Journal of Geophysical Research: Solid Earth*, *124*(7), 7429-7444. doi:https://doi.org/10.1029/2019JB017467

Southworth, C. S. (1986). Side-looking airborne radar image map showing cross-strike structural discontinuities and lineaments of the central Appalachians. In *Miscellaneous Field Studies Map. doi: https://doi.org/10.3133/mf1891*.

Sperner, B., Ratschbacher, L., & Nemčok, M. (2002). Interplay between subduction retreat and lateral extrusion: Tectonics of the Western Carpathians. *Tectonics, 21*(6), 1-1-1-24. doi:https://doi.org/10.1029/2001TC901028

Srivastava, V., Mukul, M., Barnes, J. B., & Mukul, M. (2018). Geometry and kinematics of Main Frontal thrust-related fault propagation folding in the Mohand Range, northwest Himalaya. *Journal of Structural Geology, 115*, 1-18. doi:https://doi.org/10.1016/j.jsg.2018.06.022

Srivastava, V., Mukul, M., & Mukul, M. (2017). Quaternary deformation in the Gorubathan recess: Insights on the structural and landscape evolution in the frontal Darjiling Himalaya. *Quaternary International, 462*, 138-161. doi:https://doi.org/10.1016/j.quaint.2017.05.004

Srivastava, V., Mukul, M., Barnes, J.B., Mukul, M. (2018). Geometry and kinematics of Main Frontal thrust-related fault propagation folding in the Mohand Range, northwest Himalaya. *Journal of Structural Geology, 115*, 1-18. doi:https://doi.org/10.1016/j.jsg.2018.06.022

Stampfli, G. M., & Borel, G. D. (2002). A plate tectonic model for the Paleozoic and Mesozoic constrained by dynamic plate boundaries and restored synthetic oceanic isochrons. *Earth and Planetary Science Letters, 196*(1), 17-33. doi:https://doi.org/10.1016/S0012-821X(01)00588-X

Stanton-Yonge, A., Griffith, W., Cembrano, J., St. Julien, R., & Iturrieta, P. (2016). Tectonic role of margin-parallel and margin-transverse faults during oblique subduction in the Southern Volcanic Zone of the Andes: Insights from Boundary Element Modeling. *Tectonics, 35*(9), 1990-2013. doi:https://doi.org/10.1002/2016TC004226

Steck, A. (2008). Tectonics of the Simplon massif and Lepontine gneiss dome: deformation structures due to collision between the underthrusting European plate and the Adriatic indenter. *Swiss Journal of Geosciences, 101*(2), 515-546. doi:https://doi.org//10.1007/s00015-008-1283-z

Stevens, V. L., & Avouac, J.-P. (2016). Millenary Mw > 9.0 earthquakes required by geodetic strain in the Himalaya. *Geophysical Research Letters, 43*(3), 1118-1123. doi:https://doi.org/10.1002/2015GL067336

Stipp, M., Stünitz, H., Heilbronner, R., & Schmid, S. M. (2002). The eastern Tonale fault zone: a 'natural laboratory' for crystal plastic deformation of quartz over a temperature range from 250 to 700°C. *Journal of Structural Geology, 24*(12), 1861-1884. doi:https://doi.org/10.1016/S0191-8141(02)00035-4

Stocklin, J. (1968). Structural history and tectonics of Iran: A review. *AAPG Bulletin, 52*(7), 1229-1258. doi:https://doi.org/10.1306/5D25C4A5-16C1-11D7-8645000102C1865D

Stöcklin, J. (1980). Geology of Nepal and its regional frame. *Journal of the Geological Society, 137*(1), 1-34. doi:doi:10.1144/gsjgs.137.1.0001

Stöcklin, J., & Bhattarai, K. D. (1977). *Geology of the Kathmandu area and central Mahabharat range, Nepal Himalaya*. Retrieved from

Streule, M. J., Carter, A., Searle, M. P., & Cottle, J. M. (2012). Constraints on brittle field exhumation of the Everest-Makalu section of the Greater Himalayan Sequence: Implications for models of crustal flow. *Tectonics, 31*(3). doi:https://doi.org/10.1029/2011TC003062

Styron, R. H., Taylor, M. H., & Murphy, M. A. (2011). Oblique convergence, arc-parallel extension, and the role of strike-slip faulting in the High Himalaya. *Geosphere, 7*(2), 582-596. doi:10.1130/ges00606.1

Sue, C., & Tricart, P. (2003). Neogene to ongoing normal faulting in the inner western Alps: a major evolution of the late alpine tectonics. *Tectonics, 22*(5). doi:https://doi.org/10.1029/2002TC001426

Szulc, A. G., Najman, Y., Sinclair, H. D., Pringle, M., Bickle, M., Chapman, H., Garzanti, E., Andò, S., Huyghe, P., Mugnier, J. L., Ojha, T., & DeCelles, P. (2006). Tectonic evolution of the Himalaya constrained by detrital 40Ar–39Ar, Sm–Nd and petrographic data from the Siwalik foreland basin succession, SW Nepal. *Basin Research, 18*(4), 375-391. doi:https://doi.org/10.1111/j.1365-2117.2006.00307.x

Talbot, C. J., & Alavi, M. (1996). The past of a future syntaxis across the Zagros. *Geological Society, London, Special Publications, 100*(1), 89-109.

Tavarnelli, E., Butler, R. W. H., Decandia, F. A., Calamita, F., Grasso, M., Alvarez, W., Renda, P., Crescenti, U., & D'offizi, S. (2004). *Implications of fault reactivation and structural inheritance in the Cenozoic tectonic evolution of Italy*. Paper presented at the International Geological Congress 32.

Tchalenko, J., & Braud, J. (1974). Seismicity and structure of the Zagros (Iran): the Main Recent Fault between 33 and 35 N. *Philosophical Transactions of the Royal Society of London. Series A, Mathematical and Physical Sciences, 277*(1262), 1-25. doi:https://doi.org/10.1098/rsta.1974.0044

Thomas, W. A. (1977). Evolution of Appalachian-Ouachita salients and recesses from reentrants and promontories in the contineral margin. *American Journal of Science, 277*, 1233-1278. doi:http://dx.doi.org/10.2475/ajs.277.10.1233.

Thomas, W. A. (1990). Controls on locations of transverse zones in thrust belts. *Eclogae Geologicae Helvetiae, 83*(3), 727-744.

Thomas, W. A. (1991). The Appalachian-Ouachita rifted margin of southeastern North America. *Geological Society of America Bulletin, 103*(3), 415-431. doi:https://doi.org/10.1130/0016-7606(1991)103<0415:TAORMO>2.3.CO;2

Thomas, W. A. (2007). Role of the Birmingham basement fault in thin-skinned thrusting of the Birmingham anticlinorium, Appalachian thrust belt in Alabama. *American Journal of Science, 307*(1), 46-62. doi:https://doi.org/10.2475/01.2007.03

Thomas, W. A. (2014). A mechanism for tectonic inheritance at transform faults of the Iapetan margin of Laurentia. *Geoscience Canada*, 321-344. doi:http://dx.doi.org/10.12789/geocanj.2014.41.048

Thomas, W. A., & Bayona, G. (2002). Palinspastic restoration of the Anniston transverse zone in the Appalachian thrust belt, Alabama. *Journal of Structural Geology, 24*(4), 797-826. doi:https://doi.org/10.1016/S0191-8141(01)00117-1

Thompson, R. I. (1989). Stratigraphy, tectonic evolution and structural analysis of the Halfway River map area (94B), northern Rocky Mountains, British Columbia. *Geological Survey of Canada, 425*, 1-119.

Thomson, S. N. (2002). Late Cenozoic geomorphic and tectonic evolution of the Patagonian Andes between latitudes 42˚ S and 46˚ S: An appraisal based on fission-track results from the transpressional intra-arc Liquiñe-Ofqui fault zone. *Geological Society of America Bulletin, 114*(9), 1159-1173. doi:https://doi.org/10.1130/0016-7606(2002)114<1159:LCGATE>2.0.CO;2

Tiwari, R. K., Paudyal, H., & Shanker, D. (2022). On the spatio-temporal variation in b-value after 25 April 2015 Gorkha, Nepal earthquake. *Geodesy and Geodynamics, 13*(5), 525-533. doi:https://doi.org/10.1016/j.geog.2022.01.006

Tokuoka, T. (1986). The Churia (Siwalik) Group of the Arung Khola, West Central Nepal. *Memoir of the Faculty of Science, Shimane University, 20*, 135-210. Retrieved from https://cir.nii.ac.jp/crid/1573668925765389184

Tricart, P. (1984). From passive margin to continental collision; a tectonic scenario for the Western Alps. *American Journal of Science, 284*(2), 97-120. doi:https://doi.org/10.2475/ajs.284.2.97

Tsukamoto, S., Asahi, K., Watanabe, T., & Rink, W. J. (2002). Timing of past glaciations in Kanchenjunga Himal, Nepal by optically stimulated luminescence dating of tills. *Quaternary International, 97-98*, 57-67. doi:https://doi.org/10.1016/S1040-6182(02)00051-4

Tull, J. F., & Holm, C. S. (2005). Structural evolution of a major Appalachian salient-recess junction: Consequences of oblique collisional convergence across a continental margin transform fault. *Geological Society of America Bulletin, 117*(3-4), 482-499. doi:https://doi.org/10.1130/B25578.1

Upreti, B. N. (1999). An overview of the stratigraphy and tectonics of the Nepal Himalaya. *Journal of Asian Earth Sciences, 17*(5), 577-606. doi:https://doi.org/10.1016/S1367-9120(99)00047-4

Upreti, B. N., Rai, S. M., Sakai, H., Koirala, D. R., & Takigam, Y. (2003). Early Proterozoic granite of the Taplejung Window, far eastern Lesser Nepal Himalaya. *Journal of Nepal Geological Society*, *28*(0), 9–18. doi:10.3126/jngs.v28i0.31720

Urbanek, C., Frank, W., Grasemann, B., & Decker, K. (2002). Eoalpine versus Tertiary deformation: Dating of heterogeneously partitioned strain (Tauern Window, Austria). Pangeo Austria: Erdwissenschaften in€ Osterreich 28.-30.6. 2002 (Program and abstract). *Institute for geology and paleontology University of Salzburg*.

Valdiya, K. S. (1976). Himalayan transverse faults and folds and their parallelism with subsurface structures of North Indian plains. *Tectonophysics, 32*, 353-386. doi:https://doi.org/10.1016/0040-1951(76)90069-X

Valdiya, K. S. (2002). Emergence and evolution of Himalaya: reconstructing history in the light of recent studies. *Progress in Physical Geography: Earth and Environment*, *26*(3), 360-399. doi:10.1191/0309133302pp342ra

Valensise, G., & Pantosti, D. (2001). The investigation of potential earthquake sources in peninsular Italy: a review. *Journal of Seismology*, *5*(3), 287-306. doi:https://doi.org/10.1023/A:1011463223440

van der Beek, P., Litty, C., Baudin, M., Mercier, J., Robert, X., Hardwick, E. (2016). Contrasting tectonically driven exhumation and incision patterns, western versus central Nepal Himalaya. *Geology, 44*(4), 327-330. doi:https://doi.org10.1130/G37579.1

van Staal, C. R., Whalen, J. B., McNicoll, V. J., Pehrsson, S., Lissenberg, C. J., Zagorevski, A., van Breemen, O., & Jenner, G. A. (2007). The Notre Dame arc and the Taconic orogeny in Newfoundland. In R. D. Hatcher, Jr., M. P. Carlson, J. H. McBride, & J. R. Martínez Catalán (Eds.), *4-D Framework of Continental Crust: Geological Society of America Memoir 200* (pp. 511-552).

Vannay, J. C., & Hodges, K. V. (1996). Tectonometamorphic evolution of the Himalayan metamorphic core between the Annapurna and Dhaulagiri, central Nepal. *Journal of Metamorphic Geology, 14*(5), 635-656. doi:https://doi.org/10.1046/j.1525-1314.1996.00426.x

Vargas, G., Rebolledo, S., Sepúlveda, S. A., Lahsen, A., Thiele, R., Townley, B., Padilla, C., Rauld, R., Herrera, M. J., & Lara, M. (2013). Submarine earthquake rupture, active faulting and volcanism along the major Liquiñe-Ofqui Fault Zone and implications for seismic hazard assessment in the Patagonian Andes. *Andean Geology, 40*(1), 141-171. doi:https://doi.org/10.5027/andgeoV40n1-a07

Vergani, G., Tankard, J., Belotti, J., & Welsink, J. (1995). Tectonic evolution and paleogeography of the Neuquén Basin, Argentina. In A. Tankard, R. Suárez, & H. Welsink (Eds.), *Petroleum Basins of South America* (Vol. 62): American Association of Petroleum Geologists.

Vernant, P., & Chéry, J. (2006). Mechanical modelling of oblique convergence in the Zagros, Iran. *Geophysical Journal International, 165*(3), 991-1002. doi:https://doi.org/10.1111/j.1365-246X.2006.02900.x

Vernant, P., Nilforoushan, F., Hatzfeld, D., Abbassi, M., Vigny, C., Masson, F., Nankali, H., Martinod, J., Ashtiani, A., & Bayer, R. (2004). Present-day crustal deformation and plate kinematics in the Middle East constrained by GPS measurements in Iran and northern Oman. *Geophysical Journal International, 157*(1), 381-398. doi:https://doi.org/10.1111/j.1365-246X.2004.02222.x

Viola, G., Mancktelow, N. S., & Seward, D. (2001). Late Oligocene-Neogene evolution of Europe-Adria collision: New structural and geochronological evidence from the Giudicarie fault system (Italian Eastern Alps). *Tectonics, 20*(6), 999-1020. doi:https://doi.org/10.1029/2001tc900021

Viskupic, K., & Hodges, K. V. (2001). Monazite–xenotime thermochronometry: methodology and an example from the Nepalese Himalaya. *Contributions to Mineralogy and Petrology, 141*(2), 233-247. doi:10.1007/s004100100239

Waldron, J. W., Barr, S. M., Park, A. F., White, C. E., & Hibbard, J. (2015). Late Paleozoic strike-slip faults in Maritime Canada and their role in the reconfiguration of the northern Appalachian orogen. *Tectonics, 34*(8), 1661-1684. doi:https://doi.org/10.1002/2015TC003882

Wallace, C. A., Lidke, D. J., & Schmidt, R. G. (1990). Faults of the central part of the Lewis and Clark line and fragmentation of the Late Cretaceous foreland basin in west-central Montana. *Geological Society of America Bulletin, 102*(8), 1021-1037. doi:https://doi.org/10.1130/0016-7606(1990)102<1021:FOTCPO>2.3.CO;2

Wallinga, J., Murray, A., & Wintle, A. (2000). The single-aliquot regenerative-dose (SAR) protocol applied to coarse-grain feldspar. *Radiation measurements, 32*(5), 529-533. doi:https://doi.org/10.1016/S1350-4487(00)00091-3

Wang, A., Garver, J. I., Wang, G., Smith, J. A., & Zhang, K. (2010). Episodic exhumation of the Greater Himalayan Sequence since the Miocene constrained by fission track thermochronology in Nyalam, central Himalaya. *Tectonophysics, 495*(3-4), 315-323.

Wang, J.-M., Rubatto, D., & Zhang, J.-J. (2015). Timing of Partial Melting and Cooling across the Greater Himalayan Crystalline Complex (Nyalam, Central Himalaya): In-sequence Thrusting and its Implications. *Journal of Petrology, 56*(9), 1677-1702. doi:10.1093/petrology/egv050

Webb, A. A. G., Schmitt, A. K., He, D., & Weigand, E. L. (2011). Structural and geochronological evidence for the leading edge of the Greater Himalayan Crystalline complex in the central Nepal Himalaya. *Earth and Planetary Science Letters, 304*(3), 483-495. doi:https://doi.org/10.1016/j.epsl.2011.02.024

Weidinger, J. T., & Korup, O. (2009). Frictionite as evidence for a large Late Quaternary rockslide near Kanchenjunga, Sikkim Himalayas, India — Implications for extreme events in mountain relief destruction. *Geomorphology, 103*(1), 57-65. doi:https://doi.org/10.1016/j.geomorph.2007.10.021

Weil, A. B., Yonkee, A., & Schultz, M. (2016). Tectonic evolution of a Laramide transverse structural zone: Sweetwater Arch, south central Wyoming. *Tectonics, 35*(5), 1090-1120. doi:https://doi.org/10.1002/2016TC004122

Weinberg, R. F. (2016). Himalayan leucogranites and migmatites: nature, timing and duration of anatexis. *Journal of Metamorphic Geology, 34*(8), 821-843. doi:https://doi.org/10.1111/jmg.12204

Wessels, R. L., Kargel, J. S., & Kieffer, H. H. (2002a). ASTER measurement of supraglacial lakes in the Mount Everest region of the Himalaya. *Annals of Glaciology, 34*, 399-408. doi:https://doi.org/10.3189/172756402781817545

Wessels, R. L., Kargel, J. S., & Kieffer, H. H. (2002b). ASTER measurement of supraglacial lakes in the Mount Everest region of the Himalaya. *Annals of Glaciology, 34*, , 399-408.

West Jr, D. P., & Hubbard, M. S. (1997). Progressive localization of deformation during exhumation of a major strike-slip shear zone: Norumbega fault zone, south-central

Maine, USA. *Tectonophysics*, *273*(3-4), 185-201. doi:https://doi.org/10.1016/S0040-1951(96)00306-X

Wheeler, R. L. (1980). Cross-strike structural discontinuities: possible exploration tool for natural gas in Appalachian overthrust belt. *AAPG Bulletin*, *64*(12), 2166-2178. doi:https://doi.org/10.1306/2F91975B-16CE-11D7-8645000102C1865D

Whisner, S. C., Schmidt, C. J., & Whisner, J. B. (2014). Structural analysis of the Lombard thrust sheet and adjacent areas in the Helena salient, southwest Montana, USA. *Journal of Structural Geology*, *69*, 351-376. doi:http://dx.doi.org/10.1016/j.jsg.2014.08.006

Whitmeyer, S. J., & Karlstrom, K. E. (2007). Tectonic model for the Proterozoic growth of North America. *Geosphere*, *3*(4), 220-259. doi:https://doi.org/10.1130/GES00055.1

Williams, H., & Cawood, P. (1986). Relationships along the eastern margin of the Humber Arm allochthon between Georges Lake and Corner Brook, Newfoundland. *Current Research, Part A. Geological Survey of Canada, Paper*, *86*, 759-765.

Wintle, A. G. (1997). Luminescence dating: laboratory procedures and protocols. *Radiation measurements*, *27*(5), 769-817. doi:https://doi.org/10.1016/S1350-4487(97)00220-5

Wooden, J., & Mueller, P. (1988). Pb, Sr, and Nd isotopic compositions of a suite of Late Archean, igneous rocks, eastern Beartooth Mountains: implications for crust-mantle evolution. *Earth and Planetary Science Letters*, *87*(1-2), 59-72. doi:https://doi.org/10.1016/0012-821X(88)90064-7

Wu, C., Nelson, K. D., Wortman, G., Samson, S. D., Yue, Y., Li, J., Kidd, W. S. F., & Edwards, M. A. (1998). Yadong cross structure and South Tibetan Detachment in the east central Himalaya (89°–90°E). *Tectonics*, *17*(1), 28-45. doi:https://doi.org/10.1029/97TC03386

Wu, F.-Y., Ji, W.-Q., Wang, J.-G., Liu, C.-Z., Chung, S.-L., & Clift, P. D. (2014). Zircon U–Pb and Hf isotopic constraints on the onset time of India-Asia collision. *American Journal of Science*, *314*(2), 548. doi:10.2475/02.2014.04

Yeats, R. S., and Lillie, R.J. (1991). Contemporary tectonics of the Himalayan frontal fault system: folds, blind thrusts and the 1905 Kangra earthquake. *Journal of Structural Geology*, *13*(2), 215-225.

Yin, A. (2006). Cenozoic tectonic evolution of the Himalayan orogen as constrained by along-strike variation of structural geometry, exhumation history, and foreland sedimentation. *Earth-Science Reviews*, *76*(1), 1-131. doi:https://doi.org/10.1016/j.earscirev.2005.05.004

Yonkee, W. A., & Weil, A. B. (2015). Tectonic evolution of the Sevier and Laramide belts within the North American Cordillera orogenic system. *Earth-Science Reviews*, *150*, 531-593. doi:http://dx.doi.org/10.1016/j.earscirev.2015.08.001

Yoshida, K., Nakajima, T., Matsumoto, Y., Osaki, A., Rai, L. K., Cruz, J. W., & Sakai, H. (2021). Miocene provenance change in Himalayan foreland basin and Bengal Fan sediments, with special reference to detrital garnet chemistry. *Island Arc, 30*(1), e12408. doi:https://doi.org/10.1111/iar.12408

Zanchetta, S., D'Adda, P., Zanchi, A., Barberini, V., & Villa, I. M. (2011). Cretaceous-Eocene compression in the central Southern Alps (N Italy) inferred from 40Ar/39Ar dating of pseudotachylytes along regional thrust faults. *Journal of Geodynamics, 51*(4), 245-263. doi:https://doi.org/10.1016/j.jog.2010.09.004

Zanchi, A., D'Adda, P., Zanchetta, S., & Berra, F. (2012). Syn-thrust deformation across a transverse zone: the Grem–Vedra fault system (central Southern Alps, N Italy). *Swiss Journal of Geosciences, 105*(1), 19-38. doi:https://doi.rog/10.1007/s00015-011-0089-6

Zerlauth, M., Ortner, H., Pomella, H., Pfiffner, O. A., & Fügenschuh, B. (2014). Inherited tectonic structures controlling the deformation style: an example from the Helvetic nappes of the Eastern Alps. *Swiss Journal of Geosciences, 107*(2-3), 157-175. doi:https://doi.org/10.1007/s00015-014-0167-7

Zhao, W., K. D. Nelson, the Project INDEPTH Team. (1993). Deep seismic reflection evidence for continental underthrusting beneath southern Tibet. *Nature geoscience, 366*, 557-559. doi:https://doi.org/10.1038/366557a0

Zhu, D.-C., Wang, Q., Zhao, Z.-D., Chung, S.-L., Cawood, P. A., Niu, Y., Liu, S.-A., Wu, F.-Y., & Mo, X.-X. (2015). Magmatic record of India-Asia collision. *Scientific reports, 5*(1), 14289. doi:10.1038/srep14289

APPENDICES

APPENDIX A

GOOGLE EARTH IMAGES OF LINEAMENTS

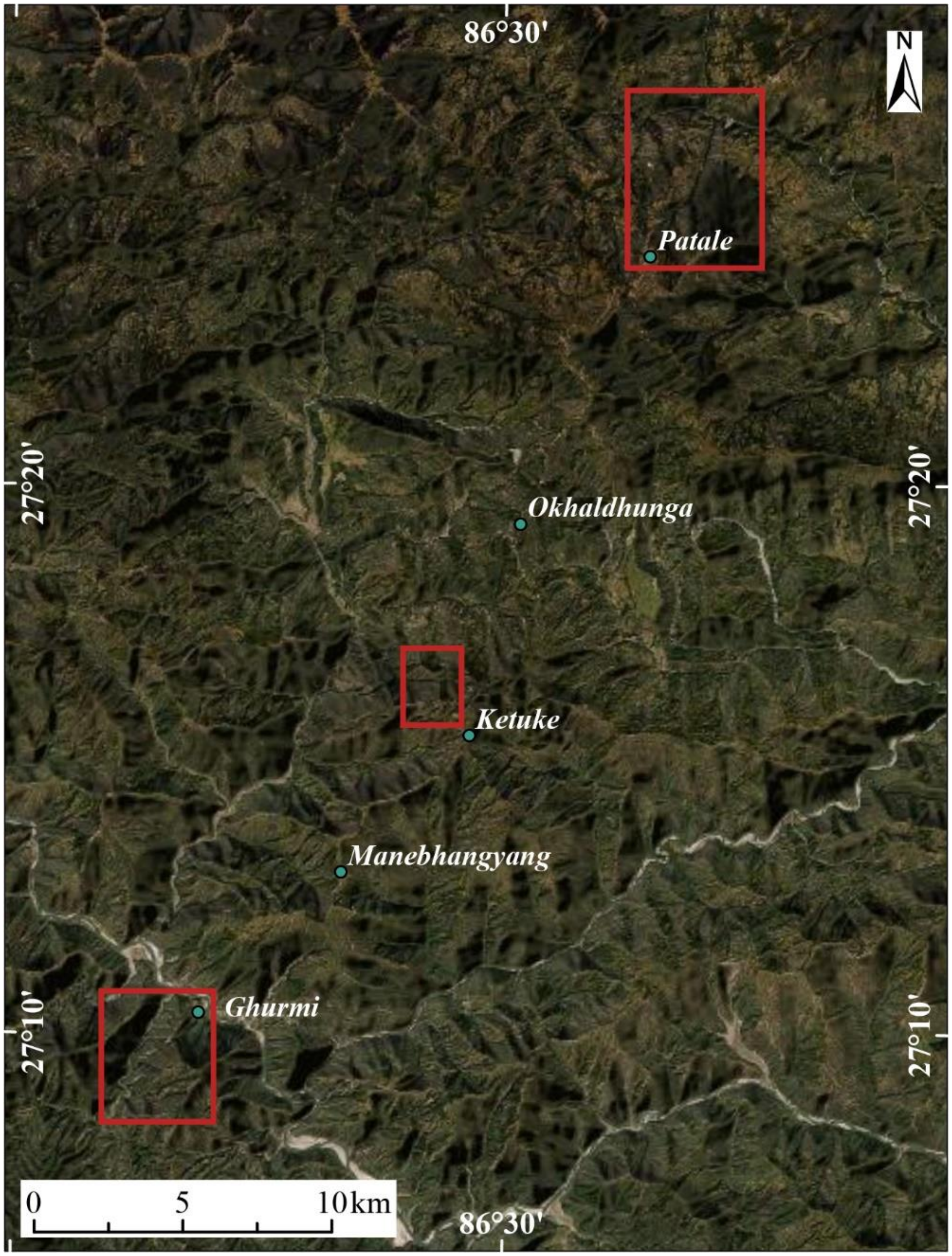

Figure A1: Locations of areas shown in subsequent maps.

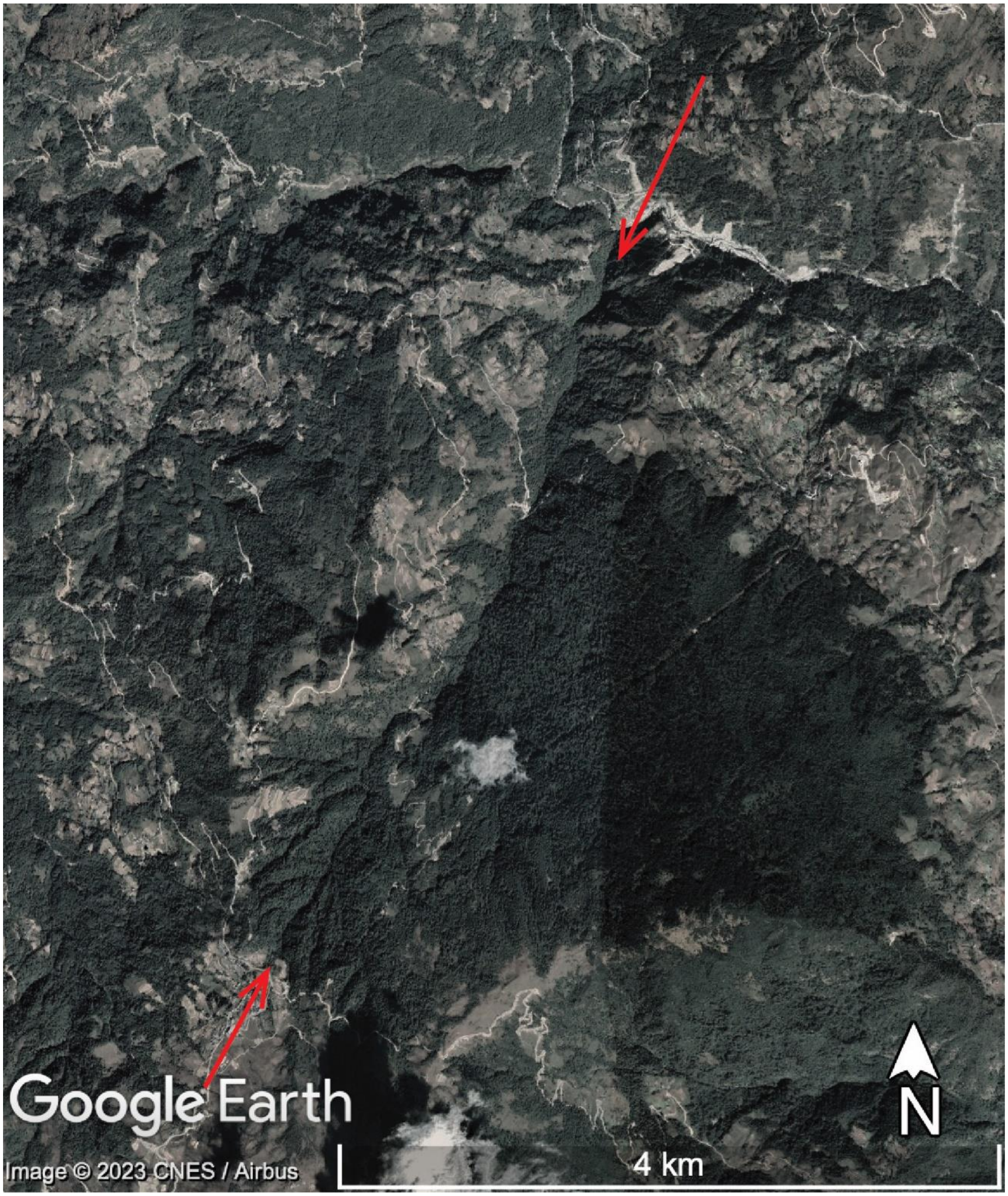

Figure A2: Lineament near Patale. See Figure A1 for location.

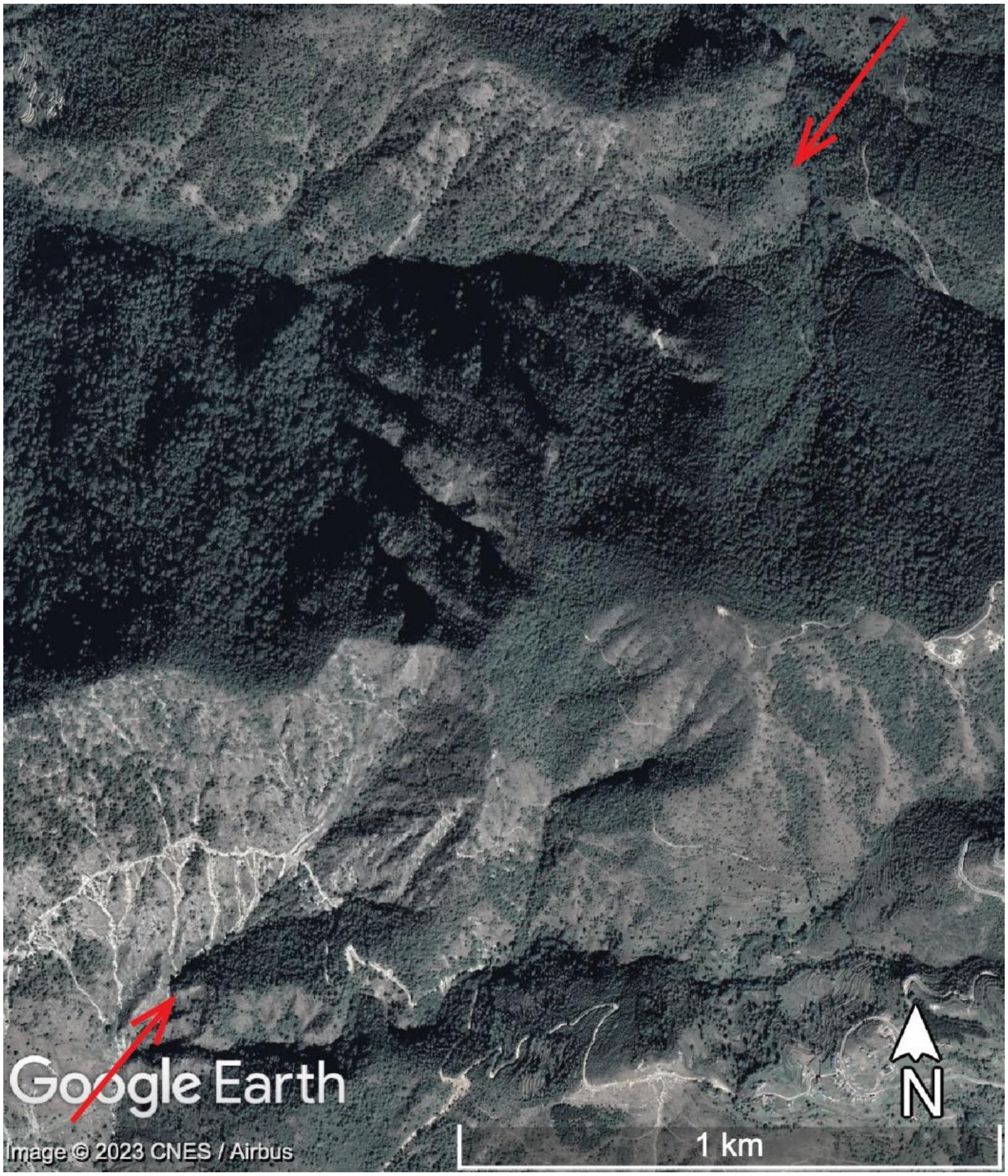

Figure A3: Lineament near Ketuke. See Figure A1 for location.

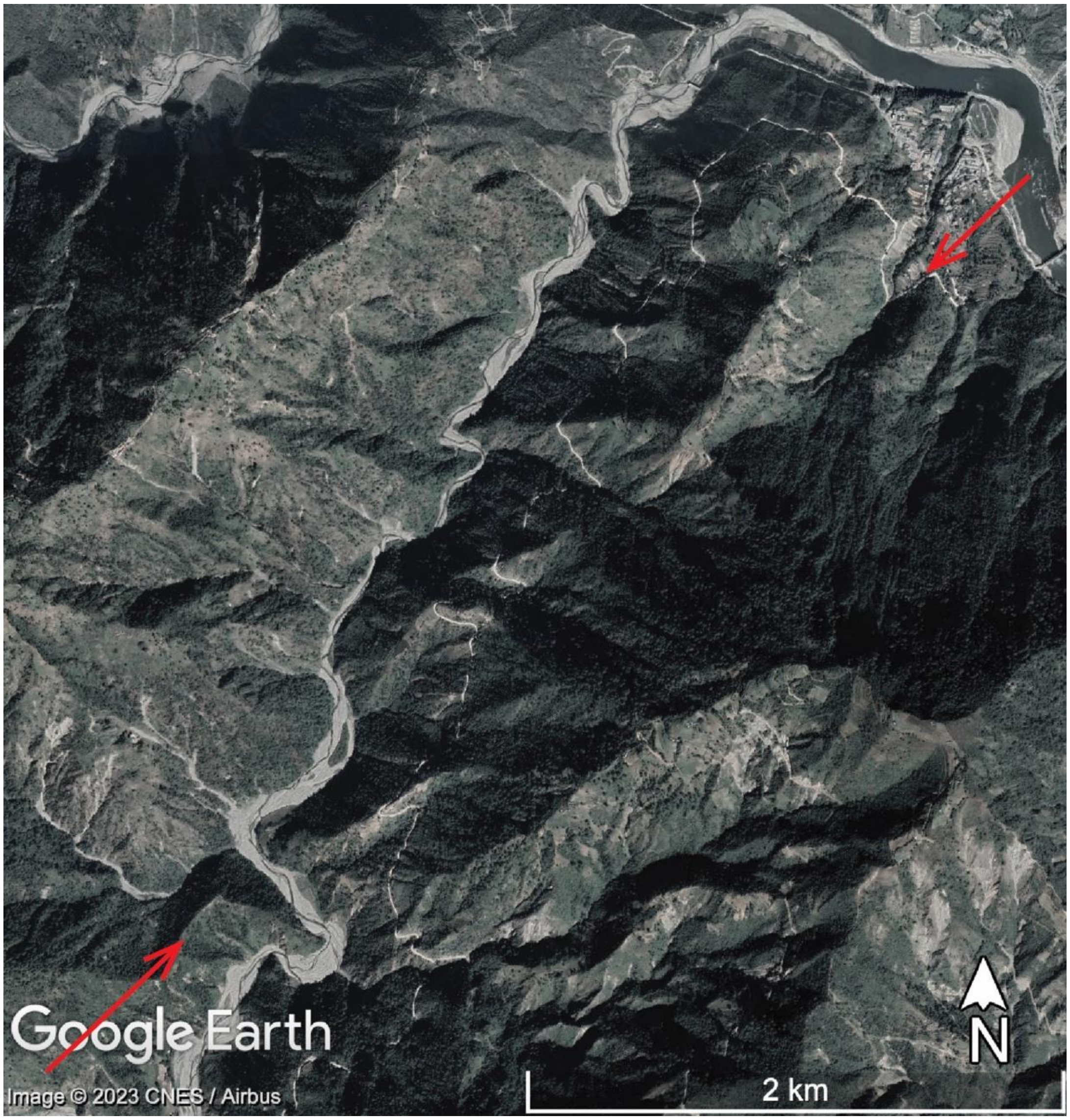

Figure A4: Lineament near Ghurmi. See Figure A1 for location.

APPENDIX B

$^{40}Ar/^{39}Ar$ EXPERIMENTAL DATA

Standard

Standards: FC EK Lab Id: 1214 Age[3]: 28.294 ± 0.036 Ma Heating 15s

Irradiation coordinates: A1, Weighted mean J: 0.00009341 ± 0.00000024 (0.26% 1SD)

Run ID	1214-01	1214-02	1214-03	1214-04	1214-05	1214-06	1214-07	1214-08	1214-09	1214-10
Power (watts)	0.60	0.60	0.60	0.60	0.60	0.60	0.60	0.60	0.60	0.60
^{40}Ar*(cps)	112007.88	50978.939	112915.85	103038.88	393922.27	484857.3	39851.51	65262.452	15762.16	211371.2
± σ (cps)	559.53419	552.92836	621.70961	497.17788	717.18622	717.82482	556.63979	580.03108	563.47078	549.52899
^{39}Ar (cps)	679.24765	298.59306	661.52942	598.41353	2322.4164	2883.1175	230.35365	390.01252	92.066279	1254.3823
± σ (cps)	5.0863063	4.1123422	5.5493831	4.7636256	8.7668143	9.8430696	3.1165524	4.032841	3.1316118	6.5557966
^{38}Ar (cps)	1.8857478	1.8663437	2.7399227	2.4595556	0.3099179	0.8715887	2.7699809	6.2000635	2.6410435	-1.4828399
± σ (cps)	0.6160649	0.5897446	0.5903097	0.6071072	0.7553072	0.864089	0.6167983	0.6013353	0.5377745	0.7124678
^{37}Ar (cps)	9.8999888	2.6573867	7.9963869	6.0418142	15.767608	21.974114	8.0750887	12.416878	4.87754	16.200481

± σ (cps)	2.405392	2.4064997	2.4012634	2.5533766	2.7248423	2.7979102	2.7137423	3.008356	3.1076834	2.6446797
^{36}Ar (cps)	0.2400511	-0.6628812	7.4722779	6.9417976	6.7444751	7.4387144	4.717999	10.691545	4.1980846	-16.652659
± σ (cps)	1.8539098	1.8446679	2.0660089	1.6454283	2.2745737	2.1831075	1.8584897	1.9341237	1.8828571	1.7380344
D1	1.0022389	1.0021018	1.0019646	1.0018274	1.0016902	1.0029139	1.0028945	1.002875	1.0028556	1.0028362
± σ	0.0014474	0.0014274	0.0014073	0.0013873	0.0013673	0.001254	0.0012541	0.0012541	0.0012542	0.0012542
%40Ar*	99.936055	100.38973	98.062539	98.028242	99.491425	99.544036	96.586035	95.336951	92.633909	102.40883
40Ar*/39 ArK	164.89992	170.73049	170.68908	172.18676	169.61741	168.17119	173.00143	167.33425	171.20449	168.5062
±σ	1.484349	2.9929948	1.7127364	1.6028211	0.7108632	0.6258023	3.364182	2.2815961	8.4481149	0.9836126
Ca/K	0.0271094	0.0165534	0.0224832	0.0187793	0.0126281	0.0141763	0.0652026	0.0592171	0.0985401	0.0240221
± σ	0.0122572	0.0278857	0.0125628	0.0147644	0.00406	0.0033586	0.0407898	0.0267099	0.1169446	0.0072978
Δt (days)	29	29	29	29	29	30	30	30	30	30

Blank Type[2]	LR	LR	LR	LR	LR	LR	LR	LR	LR	LR
^{40}Ar(cps)	13234.88	13341.44	13445.56	13443.21	13440.86	12252.5	12147.11	12041.44	11874.25	11811.09
± σ(cps)	17.68059	17.168	16.28347	14.85722	16.71335	20.94766	16.83001	16.44053	18.26749	17.04168
^{39}Ar (cps)	168.5212	168.6504	168.9268	169.0558	169.185	166.5485	166.6732	166.7983	166.7402	166.5534
± σ (cps)	0.8816162	0.8085284	0.8018973	0.8697008	0.9723617	0.747817	0.7553542	0.8472018	0.8568017	0.7629723
^{38}Ar (cps)	10.18258	10.10523	10.12494	10.21027	10.29578	8.658098	8.681918	8.705804	8.75294	8.77676
± σ (cps)	0.4406604	0.4684886	0.4657447	0.4484599	0.527684	0.5825631	0.5086832	0.4578793	0.453858	0.5012078
^{37}Ar (cps)	190.7832	190.1261	188.892	188.3867	187.8803	191.1238	190.9604	190.7965	190.9084	191.1898
± σ (cps)	0.7746981	0.7762987	0.7702701	0.7742941	0.939057	0.9597695	0.8841814	1.01908	1.103973	0.945693
^{36}Ar (cps)	49.01553	49.45767	50.11619	50.30532	50.49484	45.11702	44.6095	44.10059	43.82204	44.05597
± σ (cps)	1.061305	1.177455	1.144754	0.9883722	1.05033	1.189833	1.060679	1.184756	1.102412	0.9933082

Irradiation coordinates: A3, Weighted mean *J*: 0.00009318 ± 0.00000027 (0.29% 1SD)

Run ID	1216-01	1216-04	1216-06	1216-07	1216-08	1216-09	1216-10
Power (watts)	0.60	0.60	0.60	0.60	0.60	0.60	0.60
40Ar*(cps)	205644.03	75969.445	195062.62	270923.06	251513.82	40992.787	73661.299
± σ (cps)	579.25729	570.23764	567.69462	613.65639	595.83458	548.89405	631.69359
39Ar (cps)	1222.28	447.4562	1154.6866	1600.1833	1477.9658	242.69284	435.51224
± σ (cps)	6.5520451	4.1324584	6.4344176	6.9739554	7.2213485	3.8060706	3.7632552
38Ar (cps)	1.3041951	2.1800695	2.3036833	3.0713665	3.9557864	3.6242396	3.9789127
± σ (cps)	0.6577033	0.6283342	0.6638967	0.7159883	0.6769413	0.5626785	0.6981448
37Ar (cps)	19.247333	7.2773483	16.794007	27.383288	19.520199	10.776813	61.988845
± σ (cps)	2.3708791	2.4990764	2.6762177	2.4214439	2.6875423	2.779375	3.0846476
36Ar (cps)	4.3789757	2.9358547	4.6649939	9.1642801	12.977819	3.8649107	4.3333864
± σ (cps)	1.9040385	1.900964	1.8574482	1.9831798	1.9210451	1.8315862	2.1056355
D1	1.0029139	1.0028556	1.0033902	1.0039636	1.004537	1.0051104	1.0056839
± σ	0.001254	0.0012542	0.0012563	0.0012584	0.0012604	0.0012625	0.0012645
%40Ar*	99.368264	98.859369	99.291045	99.000184	98.482838	97.262163	98.273932
40Ar*/39Ar K	168.24625	169.78074	168.93123	169.30751	170.17567	168.90811	169.13715
±σ	1.0188198	2.0205742	1.062012	0.8315842	0.9240582	3.4831068	2.0590906
Ca/K	0.0292896	0.0302507	0.0270522	0.0318294	0.0245659	0.0825936	0.264744
± σ	0.006717	0.0193291	0.0080232	0.0052415	0.0062949	0.0396933	0.0248704

Δt (days)	30	30	30	30	30	30	30
Blank Type2	LR	LR	LR	LR	LR	LR	LR
40Ar(cps)	11680.46	11429.31	11399.48	11425.69	11604.37	11759.68	11914.98
± σ(cps)	16.71297	23.55984	18.40078	19.64341	21.12437	17.7494	18.50532
39Ar (cps)	166.167	166.3017	167.3844	167.5947	168.2233	168.6486	169.0739
± σ (cps)	0.8072078	0.8136216	0.768599	0.8273446	0.8009362	0.7429379	0.8608378
38Ar (cps)	8.830367	8.90152	8.609929	8.605094	8.595496	8.590667	8.585839
± σ (cps)	0.4424956	0.4926207	0.5142887	0.4565284	0.4303198	0.466654	0.5291514
37Ar (cps)	191.7717	192.9761	193.8985	194.0976	194.4929	194.6918	194.8907
± σ (cps)	0.8526168	0.8136216	0.9603513	0.8580797	0.831373	0.9118261	1.039592
36Ar (cps)	44.04358	42.95906	43.45589	43.55017	43.73733	43.83149	43.92565
± σ (cps)	1.13669	1.132482	1.052697	0.9589399	0.9981926	1.123357	1.295901

Irradiation coordinates: A5, Weighted mean *J*: 0.00009341 ± 0.00000030 (0.31% 1SD)

Run ID	1218-01	1218-02	1218-03	1218-04	1218-05	1218-06	1218-07	1218-08	1218-09	1218-10
Power (watts)	0.60	0.60	0.60	0.60	0.60	0.60	0.60	0.60	0.60	0.60
^{40}Ar*(cps)	22753.365	392559.71	31080.573	193421.37	35801.113	63523.274	196264.73	86866.605	87114.203	20119.787
± σ (cps)	507.58806	570.38838	565.79923	569.03183	562.82535	553.08382	575.15895	531.6442	590.24556	547.51361

^{39}Ar (cps)	132.77004	2313.7	178.42244	1146.1109	212.24773	371.32923	1162.2427	517.48134	497.42957	121.84418
± σ (cps)	3.7132621	10.059565	3.5510951	6.6197325	4.3303371	4.1812027	6.4485596	4.3515852	4.5319045	3.2289764
^{38}Ar (cps)	2.2538563	0.8482419	0.4357216	1.0125143	0.4973966	0.7806934	2.7781596	-1.4541081	1.3659423	-2.3533566
± σ (cps)	0.5905933	0.7548104	0.9012089	1.0365914	0.9125072	0.9230192	1.0699916	0.9766386	0.9035026	0.7738916
^{37}Ar (cps)	-4.6543593	22.427177	12.809847	20.646664	7.6985232	9.5324136	26.173496	8.5144843	2.8961989	-3.8302026
± σ (cps)	2.8296404	2.8472148	2.8202973	2.8514944	2.8171357	2.9593856	2.785261	2.8103868	2.6742394	2.9117119
^{36}Ar (cps)	-0.1327343	11.838019	11.787007	6.7713629	0.8631261	4.5146687	5.709507	13.385967	6.4267951	3.3118339
± σ (cps)	1.6959518	1.7163931	1.8898143	1.8625043	1.8797093	1.8442732	1.883263	1.7677136	1.968402	1.8302889
D1	1.0037632	1.0037931	1.0038229	1.0038528	1.0038827	1.0038907	1.0038689	1.003847	1.0038252	1.0038033

± σ	0.0011752	0.0011753	0.0011753	0.0011754	0.0011754	0.0011828	0.0011902	0.0011975	0.0012049	0.0012123
%40Ar*	100.17447	99.107697	89.82902	98.965602	99.285348	97.92219	99.138942	95.60161	97.844862	95.315736
40Ar*/39ArK	171.37425	169.66751	174.19654	168.76322	168.67607	171.06995	168.86726	167.86423	175.12872	165.12719
±σ	6.1309039	0.777788	4.6985123	1.0939068	4.3445117	2.4349568	1.0595995	1.7458794	1.9883996	6.2722834
Ca/K	-0.0652038	0.0180294	0.1335388	0.033507	0.0674648	0.0477482	0.0418869	0.0306039	0.0108295	-0.0584696
± σ	-0.0738102	0.0042598	0.0549084	0.0086149	0.0459901	0.0275901	0.008302	0.0187948	0.0186001	-0.0827243
Δt (days)	33	33	33	33	33	33	33	33	33	33
Blank Type[2]	LR	LR	LR	LR	LR	LR	LR	LR	LR	LR
^{40}Ar(cps)	10254.25	10228.69	10178.08	10152.55	10126.97	9849.388	9826.215	9803.027	9753.161	9725.909
± σ(cps)	17.34979	15.10571	12.95656	13.40728	14.83612	20.16312	16.1403	15.64161	14.20914	14.154

^{39}Ar (cps)	166.6211	166.5403	166.587	166.7172	166.8476	166.2425	166.2654	166.2884	166.334	166.3572
± σ (cps)	0.8337948	0.9738138	0.951671	0.8485435	0.9474791	1.072297	0.9605944	0.8747849	0.8120363	0.8434617
^{38}Ar (cps)	8.715099	8.965161	9.258885	9.303226	9.347658	9.156924	9.175212	9.193512	8.635728	8.04175
± σ (cps)	0.5073358	0.4783329	0.5003964	0.4489923	0.5045261	0.5228966	0.4632387	0.5133559	0.4875483	0.4901747
^{37}Ar (cps)	189.9665	189.733	189.1841	188.8626	188.5405	188.4853	188.8886	189.2923	189.8327	189.9695
± σ (cps)	0.8337948	0.9738138	0.951671	0.8485435	0.9474791	0.9380587	0.7821601	0.8062153	0.8248093	0.7414115
^{36}Ar (cps)	39.0062	39.05334	39.14668	39.19375	39.24092	37.02128	36.18743	35.353	34.80283	35.10466
± σ (cps)	1.049708	0.9465045	0.9497349	1.055374	1.210971	1.023639	1.090448	1.259808	1.094619	1.000212

<u>Sample 18N5d</u>

Lab Id: 1219 Muscovite Irradiation coordinates: A6 J: 0.00009542 ± 0.00000027 (0.28% 1SD)

Run ID	1219-01A	1219-01B	1219-01C	1219-01D	1219-01E	1219-01F	1219-01G	1219-01H	1219-01I	1219-01J	1219-01K	1219-01L

Power (watts)	0.5	0.8	0.9	1.0	1.1	1.2	1.3	1.5	1.8	2.0	5.0	10
^{40}Ar*(cps)	4505.7823	56016.266	37759.885	27789.659	23698.408	18250.546	8734.3153	3734.9996	1488.8478	3671.3297	7645.0923	9089.6824
± σ (cps)	801.70896	2121.5607	877.67347	765.95426	619.95187	877.30051	682.00917	534.62797	475.77274	522.29849	505.9309	546.55339
^{40}Ar(cps)	43146.145	283226.53	78668.533	65441.157	37681.778	60839.087	23793.188	6140.2732	3744.2969	4023.4826	9603.7583	11065.836
± σ(cps)	42.142505	170.79096	59.008502	45.422044	43.614132	41.217487	37.483732	24.940254	25.519708	26.41958	31.017234	29.873859
^{39}Ar (cps)	51.059743	797.13654	535.50295	397.86019	336.46315	259.11004	122.22506	46.14784	39.169578	52.181435	122.95198	145.44474
± σ (cps)	2.743523	4.5154796	4.3769644	4.0456822	4.4044816	3.5224897	3.3590405	2.5616675	2.7383136	2.7456768	2.8711728	3.2006288
^{38}Ar (cps)	23.533297	142.14112	26.119231	23.331409	10.801529	24.941683	10.36984	0.6240598	0.2766987	0.7024985	0.6447938	-0.9962019
± σ (cps)	1.0766727	2.2956898	1.2107873	1.0821629	1.0688286	1.3030719	1.0287751	0.8015868	0.7181769	0.7944658	0.8062976	0.875911
^{37}Ar (cps)	-2.8186483	1.3157576	-3.6177872	1.7539357	1.0457038	-0.5274088	0.7750585	0.5726097	-3.6177125	-7.0259168	0.1229003	-4.4459219

± σ (cps)	2.9899247	2.9601346	2.8186641	2.9785195	2.5699542	2.8796302	3.4781816	3.0191645	2.909243	2.65342	3.0084754	3.0496754
^{36}Ar (cps)	129.42244	761.02046	137.01985	126.11032	46.836046	142.64651	50.438347	8.0562486	7.5544252	1.1795046	6.5603763	6.6189495
± σ (cps)	2.6781706	7.0386998	2.9295846	2.5576306	2.0707575	2.9314554	2.2802746	1.7887195	1.5912448	1.7471521	1.691369	1.8278821
D1	1.0060242	1.0056351	1.005246	1.0048569	1.0044678	1.0040786	1.0040881	1.0044866	1.0048851	1.0052837	1.0056822	1.0060807
± σ	0.0012517	0.0012527	0.0012538	0.0012548	0.0012559	0.0012569	0.0012636	0.0012692	0.0012748	0.0012804	0.0012861	0.0012917
%40Ar*	10.443071	19.777902	47.998715	42.465109	62.890897	29.998059	36.70931	60.827906	39.763079	91.24756	79.605214	82.14185
40Ar*/39ArK	88.245299	70.271859	70.512935	69.847799	70.43389	70.4355	71.460922	80.935525	38.010309	70.35701	62.179498	62.49578
±σ	16.40171	2.6910808	1.7373524	2.0520226	2.06037	3.5186183	5.9154688	12.42576	12.433753	10.67196	4.3635384	4.0015607
Age (Ma)	15.161424	12.0837	12.125016	12.011022	12.111469	12.111745	12.287474	13.910349	6.5461429	12.098293	10.696273	10.750519
±1σ (Ma)	2.8065243	0.4624751	0.2997217	0.3533391	0.354771	0.6039983	1.0142951	2.1277803	2.1375526	1.8293006	0.7490249	0.6869821
1σ (-J) (Ma)	2.8061961	0.4612059	0.2977461	0.3516962	0.3531073	0.6030225	1.0136974	2.1274156	2.1374718	1.8289793	0.748411	0.6863059

±2σ (Ma)	5.6130487	0.9249501	0.5994433	0.7066783	0.7095419	1.2079966	2.0285902	4.2555606	4.2751052	3.6586011	1.4980498	1.3739642
2σ (-J) (Ma)	5.6123922	0.9224118	0.5954923	0.7033925	0.7062146	1.2060451	2.0273949	4.2548312	4.2749437	3.6579587	1.496822	1.3726118
Ca/K	-0.1026775	0.0030701	-0.0125659	0.0081997	0.0057807	-0.003786	0.0117947	0.0230792	-0.1717901	-0.2504378	0.0018592	-0.0568561
± σ	-0.1210521	0.0155565	-0.0077304	0.02373	0.0349911	-0.1129153	0.2378565	0.6428989	-0.1231036	-0.0488971	1.1141258	-0.0280034
Δt (days)	36	36	36	36	36	36	36	36	36	36	36	36
Blank Corrections												
Blank Type[2]	LR	LR	LR	LR	LR	LR	LR	LR	LR	LR	LR	LR
^{40}Ar(cps)	9036.95	8993.383	8950.112	8886.302	8865.287	8844.286	8810.299	8805.522	8800.699	8795.912	8791.129	8786.349
± σ(cps)	15.96843	16.41804	18.60116	17.2963	14.87254	15.965	15.78069	14.90021	14.50019	14.62854	15.26659	16.35382
^{39}Ar (cps)	166.8575	167.0526	167.2464	167.6174	167.7984	167.9793	167.8558	167.2665	166.6715	166.0809	165.4907	164.901

± σ (cps)	0.818438	0.829573	0.931977	0.864815	0.743627	0.79825	0.960579	0.858624	0.81226	0.831839	0.912517	1.040064
^{38}Ar (cps)	7.381005	7.321708	7.262814	7.264118	7.325454	7.386748	7.542491	7.568172	7.5941	7.619834	7.64555	7.671249
± σ (cps)	0.453518	0.41015	0.464713	0.468564	0.420716	0.473159	0.514183	0.455786	0.424136	0.425907	0.460336	0.520931
^{37}Ar (cps)	190.4388	190.3449	190.2524	190.0122	189.8613	189.7106	190.295	190.0716	189.8461	189.6222	189.3985	189.1749
± σ (cps)	0.937371	0.781366	0.807568	0.800867	0.742995	0.861261	1.072486	0.961045	0.874685	0.823123	0.812109	0.84315
^{36}Ar (cps)	35.07238	34.85048	34.63009	34.3829	34.35525	34.32761	34.38639	34.30702	34.22689	34.14736	34.06789	33.98846
± σ (cps)	0.81889	0.819557	1.006107	1.030728	0.919248	1.026893	1.166347	1.061385	0.997461	0.983916	1.022038	1.106406
Inverse Isochron												
^{39}Ar/^{40}Ar	1.18E-03	2.81E-03	6.81E-03	6.08E-03	8.93E-03	4.26E-03	5.14E-03	7.52E-03	1.05E-02	1.30E-02	1.28E-02	1.31E-02
1SD	6.36E-05	1.60E-05	5.59E-05	6.20E-05	1.17E-04	5.80E-05	1.41E-04	4.18E-04	7.35E-04	6.88E-04	3.02E-04	2.91E-04
^{36}Ar/^{40}Ar	3.00E-03	2.69E-03	1.74E-03	1.93E-03	1.24E-03	2.34E-03	2.12E-03	1.31E-03	2.02E-03	2.93E-04	6.83E-04	5.98E-04

1SD	6.21E-05	2.49E-05	3.73E-05	3.91E-05	5.50E-05	4.82E-05	9.59E-05	2.91E-04	4.25E-04	4.34E-04	1.76E-04	1.65E-04

Plateau Age: 12.08 ± 0.34 (2SD), Steps: A-H

Run ID	1219-02A	1219-02B	1219-02C	1219-02D	1219-02E	1219-02F	1219-02G	1219-02H	1219-02I	1219-02J	1219-02K	1219-02L
Power (watts)	0.5	0.8	0.9	1.0	1.1	1.2	1.3	1.5	1.8	2.0	5.0	10
^{40}Ar*(cps)	14018.738	49116.382	38505.363	20690.365	12141.615	2868.7306	2311.9289	1715.2617	1155.7354	934.773	2766.3025	12283.273
± σ (cps)	1172.3064	1734.3899	740.01993	757.28183	627.8511	533.00321	559.98895	523.50562	489.47258	476.45119	498.07084	499.58287
^{40}Ar(cps)	95095.484	223295.93	76987.643	45122.108	19571.31	3615.1918	2520.6576	2066.2293	1611.5473	1289.7326	3237.2975	15438.287
± σ(cps)	66.873086	140.64515	54.918724	42.496654	32.728612	25.765095	24.094048	25.725797	26.392666	27.319849	25.78457	29.452448
^{39}Ar (cps)	156.6294	678.22281	547.86597	294.88363	170.60815	40.573388	32.623646	26.247585	16.335497	13.099188	43.461599	175.8588
± σ (cps)	3.2155075	5.5449349	4.2595538	4.4138685	3.7032937	2.5655951	2.7410026	2.3801915	2.5258626	2.4971748	2.7296948	3.4225551

^{38}Ar (cps)	51.074719	109.68851	25.232566	15.185335	5.8610993	-0.0119712	-0.4053698	1.5634533	0.5648182	0.8188775	2.1071886	2.1965629
± σ (cps)	1.5715834	1.9892672	1.3085114	1.1478672	1.0171077	0.7910952	0.8023922	0.7034126	0.7165911	0.770769	0.803009	0.8940564
^{37}Ar (cps)	7.7696873	8.5725046	7.8205995	1.9567037	-0.6551818	0.4545163	0.3945562	-0.5735996	3.9755382	0.1337112	1.0403541	-2.1097795
± σ (cps)	2.9180319	3.3647755	3.5640073	3.4776325	2.9418703	3.3961472	3.5546061	3.1100874	3.2707569	3.154477	3.2516607	3.3860287
^{36}Ar (cps)	271.5593	583.39881	128.89296	81.831939	24.885098	2.5002048	0.6991182	1.1755344	1.5267012	1.1889056	1.5775556	10.567438
± σ (cps)	3.9099879	5.7582779	2.4681699	2.5310249	2.099913	1.7831576	1.8738958	1.7513163	1.6370588	1.5932045	1.6660059	1.6703617
D1	1.0036155	1.0040511	1.0044866	1.0049222	1.0053578	1.0057933	1.0059662	1.0057034	1.0054407	1.0051779	1.0049152	1.0046524
± σ	0.0013522	0.0013603	0.0013684	0.0013765	0.0013845	0.0013926	0.0013969	0.0013931	0.0013893	0.0013855	0.0013816	0.0013778
%40Ar*	14.741749	21.996094	50.014991	45.854162	62.037826	79.352101	91.719275	83.014104	71.715885	72.478045	85.450982	79.563703
40Ar*/39ArK	89.502598	72.419243	70.282449	70.164508	71.166681	70.704734	70.866663	65.349315	70.74994	71.361141	63.649349	69.847359

±σ	7.7068288	2.6249033	1.457074	2.7745227	3.9911521	13.876731	18.168469	20.806659	31.898302	38.833398	12.137261	3.1493053
Age (Ma)	15.376524	12.451688	12.085515	12.065302	12.237051	12.157886	12.185636	11.239862	12.165633	12.270375	10.948357	12.010946
±1σ (Ma)	1.3191359	0.4511541	0.2520547	0.4767386	0.6848365	2.3783898	3.1137854	3.5677175	5.4666925	6.6547938	2.0816599	0.5408315
1σ (-J) (Ma)	1.3184175	0.4497727	0.2497177	0.4755113	0.6839582	2.3781403	3.1135939	3.5675753	5.4665838	6.6547029	2.0814286	0.5397596
±2σ (Ma)	2.6382717	0.9023081	0.5041095	0.9534773	1.3696729	4.7567796	6.2275707	7.1354351	10.933385	13.309588	4.1633198	1.081663
2σ (-J) (Ma)	2.6368349	0.8995453	0.4994354	0.9510226	1.3679164	4.7562807	6.2271879	7.1351506	10.933168	13.309406	4.1628572	1.0795192
Ca/K	0.0922663	0.0235098	0.0265509	0.0123421	-0.0071429	0.0208363	0.0224952	-0.0406474	0.4526646	0.0189861	0.0445234	-0.0223144
± σ	0.0149083	0.0038142	0.0057205	0.0391704	-0.144167	1.1646268	1.8276955	-1.1986641	0.3763876	10.570711	0.4377436	-0.0579112
Δt (days)	41	41	41	41	41	41	41	41	41	41	41	41
Blank Corrections												
Blank Type[2]	LR	LR	LR	LR	LR	LR	LR	LR	LR	LR	LR	LR

^{40}Ar(cps)	8323.8	8323.8	8323.8	8291.761	8259.072	8226.384	8140.429	8122.878	8105.351	8087.68	8087.558	8087.435
± σ(cps)	15.71654	13.45582	14.38979	14.3515	13.08289	14.92783	16.01634	14.8599	17.22129	18.61113	16.27403	15.5707
^{39}Ar (cps)	166.7744	166.4495	166.1286	165.6489	165.4876	165.3263	165.4432	165.5455	165.6477	165.8007	165.8523	165.9041
± σ (cps)	0.778014	0.696499	0.78147	0.793851	0.739571	0.860367	0.811454	0.870093	1.008631	0.937143	0.781712	0.807361
^{38}Ar (cps)	7.089699	6.996773	6.904981	6.810903	6.808763	6.806624	6.798664	6.796523	6.794385	6.790142	6.788003	6.785859
± σ (cps)	0.403556	0.421096	0.480917	0.535278	0.503363	0.475705	0.422886	0.424736	0.433626	0.470227	0.496837	0.52794
^{37}Ar (cps)	184.7443	184.679	184.6146	184.4429	184.3336	184.2243	184.4712	184.6022	184.733	184.9927	185.1236	185.2548
± σ (cps)	0.81142	0.870601	1.00899	0.944183	0.814304	0.877076	0.849574	0.798672	0.778105	0.832489	0.902139	0.993211
^{36}Ar (cps)	33.17814	33.15889	33.13987	33.10213	33.08308	33.06402	33.11603	30.14217	31.16828	31.22008	31.2462	33.27238
± σ (cps)	1.081331	1.016103	0.990279	1.059739	1.148421	1.264063	1.179241	1.11468	1.061855	0.998399	0.98995	0.998105
Inverse Isochron												

$^{39}Ar/^{40}Ar$	1.65E-03	3.04E-03	7.12E-03	6.54E-03	8.72E-03	1.12E-02	1.29E-02	1.27E-02	1.01E-02	1.02E-02	1.34E-02	1.14E-02
1SD	3.38E-05	2.49E-05	5.56E-05	9.80E-05	1.90E-04	7.14E-04	1.09E-03	1.16E-03	1.58E-03	1.95E-03	8.50E-04	2.23E-04
$^{36}Ar/^{40}Ar$	2.86E-03	2.61E-03	1.67E-03	1.81E-03	1.27E-03	6.92E-04	2.77E-04	5.69E-04	9.47E-04	9.22E-04	4.87E-04	6.84E-04
1SD	4.12E-05	2.58E-05	3.21E-05	5.61E-05	1.07E-04	4.93E-04	7.43E-04	8.48E-04	1.02E-03	1.24E-03	5.15E-04	1.08E-04

Plateau Age: 12.13 ± 0.36 (2SD), Steps: B-L

Run ID	1219-03A	1219-03B	1219-03C	1219-03D	1219-03E	1219-03F	1219-03G	1219-03H	1219-03I	1219-03J	1219-03K	1219-03L
Power (watts)	0.5	0.8	0.9	1.0	1.1	1.2	1.3	1.5	1.8	2.0	5.0	10
^{40}Ar*(cps)	2543.4517	117789.31	27210.866	22883.762	11328.874	7388.3837	3389.828	2648.9422	2637.9167	1209.8817	5532.5077	9392.4324
± σ (cps)	798.97305	2342.9203	684.48619	793.97786	527.42219	506.7071	464.22414	524.46712	541.7519	493.41379	476.16432	493.9921
^{40}Ar(cps)	30278.431	371961.19	43724.589	56864.65	14819.327	8975.5398	4117.9647	2998.721	2805.6089	2000.4345	6362.645	10319.029
± σ(cps)	42.885868	240.67241	44.169637	41.727232	35.312382	28.645869	27.894556	24.297012	26.677089	25.805796	27.337893	27.080043

^{39}Ar (cps)	48.823886	1682.4236	384.53726	321.30439	162.04642	98.599761	41.573561	28.598746	29.93833	14.682722	87.178359	138.97159
± σ (cps)	2.8624697	7.9083545	3.931744	4.0193187	3.4263124	2.9602178	2.8230186	2.6845851	2.1822272	2.8255216	2.7428362	3.4457471
^{38}Ar (cps)	20.217426	159.89543	12.624612	21.205665	2.7141131	-0.1248267	1.0568075	0.5768657	1.1842358	-1.4425732	2.2466122	-0.0504232
± σ (cps)	1.0365033	2.3117011	0.9925719	1.0855977	0.8222092	0.821116	0.8029196	0.6786288	0.7167983	0.7726696	0.7160294	0.8043665
^{37}Ar (cps)	8.3633532	6.3024784	2.2564777	4.8624952	0.0945331	-6.7988134	-2.8350964	3.509056	-2.3681208	-2.4492374	3.8323179	-8.1783867
± σ (cps)	3.3790191	3.2171571	3.0820769	2.9042468	3.0283184	3.571553	3.3285466	3.2269632	3.6117622	3.6334669	3.2909887	3.454952
^{36}Ar (cps)	92.895831	851.32596	55.311239	113.81594	11.690961	5.3160372	2.4388288	1.1715528	0.56167	2.6478857	2.7804705	3.103551
± σ (cps)	2.6704895	7.7556779	2.287126	2.6530519	1.7625477	1.6944468	1.5520656	1.7547692	1.8123481	1.6503812	1.5922365	1.6520912
D1	1.0044367	1.0044837	1.0045307	1.0045777	1.0046247	1.0046717	1.0050633	1.0054079	1.0057526	1.0060972	1.0064418	1.0067864
± σ	0.0013582	0.0013425	0.0013267	0.0013109	0.0012951	0.0012794	0.0012669	0.0012703	0.0012736	0.001277	0.0012803	0.0012837

%40Ar*	8.4002098	31.667097	62.23241	40.24251	76.446615	82.316873	82.318044	88.335734	94.022967	60.480947	86.952953	91.02051
40Ar*/39ArK	52.094414	70.011686	70.762623	71.221443	69.911287	74.933079	81.53807	92.62442	88.111684	82.401732	63.461939	67.585271
±σ	16.646965	1.4309439	1.9214507	2.6268121	3.5747102	5.6098753	12.46366	20.295574	19.201547	37.158488	5.8154635	3.9298233
Age (Ma)	8.9657053	12.03911	12.167807	12.246435	12.021903	12.882378	14.013508	15.9105	15.138563	14.161362	10.916217	11.623205
±1σ (Ma)	2.8580465	0.2476069	0.3310889	0.4514862	0.6136123	0.9617062	2.1341519	3.4712579	3.285546	6.3611517	0.997796	0.6744818
1σ (-J) (Ma)	2.8579334	0.2452457	0.329289	0.4501508	0.612666	0.9610135	2.1337828	3.4709657	3.2852665	6.3610253	0.9973162	0.673677
±2σ (Ma)	5.716093	0.4952138	0.6621778	0.9029723	1.2272246	1.9234124	4.2683037	6.9425157	6.5710921	12.722304	1.9955921	1.3489636
2σ (-J) (Ma)	5.7158668	0.4904915	0.6585779	0.9003017	1.2253321	1.922027	4.2675657	6.9419314	6.570533	12.722051	1.9946324	1.3473541
Ca/K	0.3186112	0.0069677	0.0109145	0.0281485	0.0010851	-0.1282538	-0.1268421	0.2282213	-0.1471259	-0.3102682	0.0817647	-0.1094598
± σ	0.070689	0.0018483	0.0204741	0.0103937	1.113529	-0.0392436	-0.1834516	0.2144261	-0.3529555	-0.7425459	0.0628695	-0.0222486

Δt (days)	41	41	41	41	41	41	41	41	41	41	41	41
Blank Corrections												
Blank Type[2]	LR	LR	LR	LR	LR	LR	LR	LR	LR	LR	LR	LR
^{40}Ar(cps)	8093.304	8099.633	8105.971	8118.487	8124.816	8131.15	8152.731	8157.066	8161.398	8153.064	8140.106	8127.157
± σ(cps)	19.87958	17.978	16.43036	14.83785	14.93199	15.63924	15.7831	13.79655	15.08864	14.99797	13.09047	14.29436
^{39}Ar (cps)	166.3769	166.6287	166.881	167.379	167.6309	167.8829	168.65	168.7289	168.8077	168.9637	169.0426	169.1215
± σ (cps)	0.907079	0.832685	0.784698	0.784409	0.832051	0.906263	1.059447	0.935224	0.839011	0.769898	0.807031	0.887092
^{38}Ar (cps)	6.785902	6.791924	6.797954	6.818731	6.833813	6.848907	6.617125	6.526295	6.435527	6.391009	6.438326	6.485611
± σ (cps)	0.491184	0.405703	0.413449	0.412803	0.397162	0.474296	0.410245	0.410888	0.458185	0.457749	0.402794	0.389912
^{37}Ar (cps)	187.0485	187.353	187.6579	188.0476	188.135	188.2225	188.5286	188.609	188.6894	188.7895	188.8097	188.8298
± σ (cps)	0.862839	0.733764	0.777274	0.779879	0.732788	0.858795	0.81145	0.870068	1.008727	1.019252	0.904508	0.888343
^{36}Ar (cps)	33.36954	33.39568	33.42186	33.47338	33.49935	33.52533	33.6219	33.64786	31.67381	33.2871	32.86492	32.44302

± σ (cps)	1.160005	1.231836	1.312448	1.2645	1.140898	1.037557	0.935163	0.995407	1.085959	0.951933	0.848542	0.94748
Inverse Isochron												
$^{39}Ar/^{40}Ar$	1.61E-03	4.52E-03	8.79E-03	5.65E-03	1.09E-02	1.10E-02	1.01E-02	9.54E-03	1.07E-02	7.34E-03	1.37E-02	1.35E-02
1SD	9.46E-05	2.15E-05	9.04E-05	7.08E-05	2.33E-04	3.32E-04	6.89E-04	8.99E-04	7.84E-04	1.42E-03	4.35E-04	3.36E-04
$^{36}Ar/^{40}Ar$	3.07E-03	2.29E-03	1.26E-03	2.00E-03	7.89E-04	5.92E-04	5.92E-04	3.91E-04	2.00E-04	1.32E-03	4.37E-04	3.01E-04
1SD	8.83E-05	2.09E-05	5.23E-05	4.67E-05	1.19E-04	1.89E-04	3.77E-04	5.85E-04	6.46E-04	8.25E-04	2.50E-04	1.60E-04

Plateau Age: 12.08 ± 0.33 (2SD), Steps: A-L

<u>18N10c</u>

Lab Id: 1217 Muscovite Irradiation coordinates: A4 J: 0.00009519 ± 0.00000026 (0.27% 1SD)

Run ID	1217-01A	1217-01B	1217-01C	1217-01D	1217-01E	1217-01F	1217-01G	1217-01H	1217-01I	1217-01J	1217-01K	1217-01L
Power (watts)	0.5	0.8	0.9	1.0	1.1	1.2	1.3	1.5	1.8	2.0	5.0	10
$^{40}Ar^*$(cps)	4755.0348	27346.841	19205.741	18333.141	40343.755	32765.871	40676.351	39154.744	21697.282	6263.2127	20756.074	24.585822

± σ (cps)	728.73699	771.51731	1185.8957	815.30511	1169.435	910.17139	647.80476	737.74654	679.34087	512.88318	594.13275	502.40674
^{40}Ar(cps)	29692.467	47717.951	118843.93	55361.089	131982.97	74082.746	56566.024	76626.636	36688.353	7926.011	24667.095	327.7459
± σ(cps)	41.449651	48.525965	74.589821	48.380705	84.025849	57.79659	40.968986	58.82107	38.082159	30.368399	37.903445	26.76627
^{39}Ar (cps)	25.243443	271.66861	246.62736	237.84828	513.34277	442.08547	552.09233	516.42178	277.63607	77.015768	257.40969	0.9992109
± σ (cps)	2.5198372	4.21166	3.4079506	3.2236726	4.4249388	3.9494364	3.9611683	4.0638848	3.576644	2.8709242	4.1076116	2.4667261
^{38}Ar (cps)	15.815785	14.422461	60.880679	23.820647	61.799355	24.003213	8.5113566	24.635013	9.362709	2.3463128	0.9194016	0.0646701
± σ (cps)	1.0271661	1.0432492	1.5741583	1.291698	1.479508	1.2998132	0.9892112	1.096697	1.042538	0.8033008	0.783606	0.7800925
^{37}Ar (cps)	9.371427	4.6434061	11.08788	3.4722525	-0.2774292	6.7244188	7.1218237	10.660884	3.8730591	7.9277221	0.3437225	1.982573
± σ (cps)	2.7081674	3.0542144	2.5917551	2.9052724	2.5866032	2.7229606	2.8490899	2.9298011	2.9217945	3.082441	3.0935382	2.993773
^{36}Ar (cps)	83.525699	68.231211	333.7292	124.0218	306.93737	138.38718	53.221036	125.50875	50.211252	5.5693942	13.099615	1.0154075

± σ (cps)	2.4353441	2.5780385	3.9490128	2.722936	3.8937732	3.0389899	2.1647153	2.4596996	2.2712152	1.7148326	1.9858942	1.6803763
D1	1.0028115	1.0032989	1.0030552	1.0035426	1.0037863	1.0040299	1.0038963	1.0035189	1.0031416	1.0027642	1.0023869	1.0020095
± σ	0.0012562	0.0012424	0.0012493	0.0012355	0.0012286	0.0012217	0.0012433	0.0012717	0.0013002	0.0013286	0.0013571	0.0013855
%40Ar*	16.01428	57.309335	16.160473	33.115571	30.567393	44.228748	71.909511	51.098085	59.139427	79.020994	84.144785	7.5014889
40Ar*/39ArK	188.36712	100.6625	77.873521	77.079142	78.590286	74.116597	73.676718	75.819312	78.150084	81.323771	80.634395	24.605238
±σ	34.451973	3.2404489	4.9273866	3.5834962	2.3766701	2.1626673	1.2869412	1.5481631	2.6458988	7.3169969	2.6425513	506.45926
Age (Ma)	32.134146	17.243353	13.354006	13.21828	13.476462	12.712016	12.636834	13.003007	13.401257	13.943391	13.825644	4.2300543
±1σ (Ma)	5.826124	0.5547963	0.8427802	0.6135421	0.4079869	0.3715392	0.2231252	0.2673458	0.4537829	1.2503949	0.4532191	86.967101
1σ (-J) (Ma)	5.8253548	0.5524462	0.8418518	0.612292	0.4060304	0.3696264	0.2199632	0.2645575	0.4520442	1.2497131	0.4513663	86.9671
±2σ (Ma)	11.652248	1.1095925	1.6855604	1.2270842	0.8159738	0.7430783	0.4462503	0.5346916	0.9075659	2.5007898	0.9064381	173.9342
2σ (-J) (Ma)	11.65071	1.1048925	1.6837037	1.2245839	0.8120607	0.7392527	0.4399264	0.529115	0.9040884	2.4994262	0.9027327	173.9342

Ca/K	0.6905102	0.0317914	0.0836219	0.0271534	-0.0010052	0.0282919	0.0239934	0.0383974	0.0259472	0.1914616	0.0024837	3.690498
± σ	0.1265924	0.0142471	0.0057244	0.0193777	-0.0873888	0.0048919	0.0040121	0.0032021	0.0151009	0.0360822	0.2012225	17.525834
Δt (days)	35	35	35	35	35	35	35	35	35	35	35	35
Blank Corrections												
Blank Type[2]	LR	LR	LR	LR	LR	LR	LR	LR	LR	LR	LR	LR
^{40}Ar(cps)	9504.33	9311.221	9407.544	9194.236	9173.372	9152.508	9037.919	8985.84	8933.618	8900.051	8918.978	8937.854
± σ(cps)	18.68351	15.45216	15.31801	14.98975	13.08981	14.29845	15.31201	14.52302	17.15374	17.24064	14.54892	15.24576
^{39}Ar (cps)	165.3255	164.9691	165.1469	165.0235	165.2605	165.4976	165.2181	165.0283	164.8379	164.3718	164.0894	163.8077
± σ (cps)	0.7416428	0.8312346	0.7445087	0.7867004	0.7362142	0.8596776	0.8114473	0.8699089	1.008828	0.9447478	0.8144319	0.8760175
^{38}Ar (cps)	7.545001	7.680349	7.612837	7.625198	7.499995	7.374792	7.200057	7.131805	7.063367	7.003219	7.011504	7.019766

± σ (cps)	0.3964566	0.4723623	0.4135844	0.4463582	0.4066273	0.4636455	0.4686263	0.4207109	0.473159	0.4767963	0.4277765	0.4803053
^{37}Ar (cps)	187.4445	187.0948	187.2693	186.5788	186.231	185.8832	185.3284	185.7346	186.1419	186.5665	186.5854	186.6041
± σ (cps)	0.7787541	0.9278545	0.8123979	0.9307257	0.8137731	0.7785039	0.88023	0.8135646	0.9402253	0.9447478	0.8144319	0.8760175
^{36}Ar (cps)	34.83407	34.618	34.72578	34.66882	34.83074	34.99267	35.26749	35.30898	35.35058	35.43273	35.47431	35.51577
± σ (cps)	1.102648	1.035048	0.9555101	1.038649	0.9549193	1.098001	1.111219	1.03528	0.9819393	0.9570738	0.9872684	1.043489
Inverse Isochron												
^{39}Ar/^{40}Ar	8.50E-04	5.69E-03	2.08E-03	4.30E-03	3.89E-03	5.97E-03	9.76E-03	6.74E-03	7.57E-03	9.72E-03	1.04E-02	3.05E-03
1SD	8.49E-05	8.85E-05	2.87E-05	5.84E-05	3.36E-05	5.35E-05	7.04E-05	5.33E-05	9.78E-05	3.64E-04	1.67E-04	7.53E-03
^{36}Ar/^{40}Ar	2.81E-03	1.43E-03	2.81E-03	2.24E-03	2.33E-03	1.87E-03	9.41E-04	1.64E-03	1.37E-03	7.03E-04	5.31E-04	3.10E-03
1SD	8.21E-05	5.40E-05	3.33E-05	4.92E-05	2.95E-05	4.10E-05	3.83E-05	3.21E-05	6.19E-05	2.16E-04	8.05E-05	5.13E-03

Plateau Age: 12.95 ± 0.27 (2SD), Steps: C-K

Run ID	1217-02A	1217-02B	1217-02C	1217-02D	1217-02E	1217-02F	1217-02G	1217-02H	1217-02I	1217-02J	1217-02K	1217-02L
Power (watts)	0.5	0.8	0.9	1.0	1.1	1.2	1.3	1.5	1.8	2.0	5.0	10
$^{40}Ar^*$(cps)	14545.008	45689.583	34679.789	45491.344	21303.265	25455.636	3140.8172	4039.2196	8572.1292	2499.3159	9010.6658	4803.2381
± σ (cps)	1058.9473	1199.6012	835.02833	680.05835	632.37471	683.29523	502.41793	479.20182	568.46722	500.45785	507.73626	463.10378
^{40}Ar(cps)	76669.072	128251.67	68285.728	64712.695	36172.846	50848.734	4227.1066	5569.9255	9953.4586	2854.6239	11247.286	5329.8062
± σ(cps)	58.401396	84.257687	54.370521	49.578487	39.059623	47.043764	29.39605	37.949489	37.251913	30.888396	31.309157	27.928282
^{39}Ar (cps)	125.20224	511.9311	460.39144	606.16595	299.69809	356.13582	42.568402	53.181718	100.78065	20.701616	99.894	56.475431
± σ (cps)	3.2736274	4.5346911	3.9409663	4.7546748	3.5137214	4.1978535	2.436993	2.8551847	2.9765266	2.6080622	2.8426597	3.0197257
^{38}Ar (cps)	37.207166	54.999443	22.082626	9.9659941	8.7487847	14.614741	0.9768486	0.7329072	1.7486678	-0.3299924	0.6611515	1.057893
± σ (cps)	1.4073233	1.4917446	1.0778341	0.9870147	0.9946575	0.9828829	0.6973352	0.6845002	0.7656875	0.7047569	0.7217509	0.724914

^{37}Ar (cps)	9.506203	10.909309	9.4220599	11.657228	6.4949448	4.4155794	5.0855933	1.3088533	5.2997705	1.9816982	7.2852005	-4.5456106
± σ (cps)	3.6520298	3.2298501	3.457442	3.1321185	2.831276	3.2115618	2.8480475	3.7044095	5.1548079	3.0337987	3.1132392	3.0542962
^{36}Ar (cps)	208.07899	276.53431	112.56009	64.380195	49.804332	85.05191	3.6384291	5.1269624	4.6266392	1.1900722	7.491358	1.7636925
± σ (cps)	3.5348548	3.9977356	2.7884694	2.2707497	2.1134057	2.2814971	1.6799168	1.5999938	1.8999314	1.6730426	1.697363	1.5483004
D1	1.0026225	1.0027343	1.0028462	1.002958	1.0030698	1.0031816	1.0038134	1.0043335	1.0048535	1.0053735	1.0058935	1.0064136
± σ	0.0012535	0.0012518	0.0012501	0.0012484	0.0012467	0.001245	0.0012531	0.001263	0.0012728	0.0012826	0.0012924	0.0013023
%40Ar*	18.971155	35.624943	50.786291	70.297403	58.892973	50.061494	74.301822	72.518378	86.122117	87.553247	80.114137	90.120316
40Ar*/39ArK	116.1721	89.249478	75.326745	75.047673	71.082417	71.477324	73.782831	75.95128	85.05729	120.73047	90.202273	85.050048
±σ	8.9867956	2.4730542	1.9249424	1.2669594	2.268655	2.0954726	12.535688	9.8903389	6.1747598	28.561644	5.6941325	9.3766845
Age (Ma)	19.885569	15.296563	12.918833	12.871141	12.193363	12.260875	12.65497	13.025558	14.580948	20.661399	15.459167	14.579712

±1σ (Ma)	1.5310009	0.4244929	0.3311764	0.2198503	0.3895306	0.3600679	2.1428982	1.6905273	1.0551352	4.8605047	0.9727962	1.6015176
1σ (-J) (Ma)	1.529872	0.4220716	0.3289586	0.2165198	0.3878522	0.3582313	2.1425703	1.6900871	1.0542519	4.8601211	0.9717196	1.6009358
±2σ (Ma)	3.0620018	0.8489859	0.6623528	0.4397005	0.7790612	0.7201357	4.2857964	3.3810546	2.1102705	9.7210094	1.9455924	3.2030352
2σ (-J) (Ma)	3.059744	0.8441431	0.6579172	0.4330397	0.7757044	0.7164627	4.2851407	3.3801742	2.1085038	9.7202422	1.9434392	3.2018717
Ca/K	0.1412238	0.0396368	0.0380655	0.0357698	0.0403092	0.0230614	0.2222119	0.0457764	0.0978122	0.1780517	0.1356485	-0.1497082
± σ	0.0245356	0.0038254	0.0054515	0.0028628	0.0081324	0.0124713	0.0824127	0.3691464	0.0954234	0.439728	0.0286319	-0.075595
Δt (days)	40	40	40	40	40	40	40	40	40	40	40	40
Blank Corrections												
Blank Type[2]	LR	LR	LR	LR	LR	LR	LR	LR	LR	LR	LR	LR
^{40}Ar(cps)	8547.845	8477.281	8406.624	8332.152	8328.173	8324.199	8300.609	8296.769	8292.931	8281.174	8273.104	8265.028
± σ(cps)	16.57477	14.50371	15.87934	18.49395	17.33938	16.64679	22.43051	24.47782	26.6778	23.53918	18.84843	15.84263

^{39}Ar (cps)	163.7834	164.0823	164.3816	164.7875	164.8964	165.0052	166.2086	166.432	166.6552	166.6817	166.4808	166.2797
± σ (cps)	1.010166	0.82112	0.816958	0.857847	0.752519	0.70489	1.023689	0.88498	0.955851	0.982525	0.822224	0.763712
^{38}Ar (cps)	6.826389	6.814558	6.802712	6.779238	6.767384	6.755545	6.71182	6.710153	6.708487	6.705185	6.703518	6.70185
± σ (cps)	0.508976	0.463061	0.425211	0.383277	0.382499	0.395953	0.444052	0.42243	0.405145	0.385797	0.38433	0.388596
^{37}Ar (cps)	187.452	187.291	187.1298	186.8104	186.6491	186.488	185.5317	185.3761	185.2205	185.0983	185.1324	185.1666
± σ (cps)	1.127182	1.056912	0.991356	0.879813	0.835247	0.800443	0.83781	0.881219	0.93231	0.90589	0.836657	0.788455
^{36}Ar (cps)	33.24309	32.85905	32.47451	32.04109	31.99081	31.94059	31.85451	32.02259	32.19056	30.29331	32.22658	32.15981
± σ (cps)	0.959357	0.884249	1.01915	1.150905	1.028663	0.947854	1.023689	0.88498	0.955851	0.996535	0.888333	0.916218
Inverse Isochron												
$^{39}Ar/^{40}Ar$	1.63E-03	3.99E-03	6.74E-03	9.37E-03	8.29E-03	7.00E-03	1.01E-02	9.55E-03	1.01E-02	7.25E-03	8.88E-03	1.06E-02
1SD	4.27E-05	3.55E-05	5.80E-05	7.38E-05	9.75E-05	8.28E-05	5.81E-04	5.17E-04	3.01E-04	9.17E-04	2.54E-04	5.69E-04

$^{36}Ar/^{40}Ar$	2.71E-03	2.16E-03	1.65E-03	9.95E-04	1.38E-03	1.67E-03	8.61E-04	9.20E-04	4.65E-04	4.17E-04	6.66E-04	3.31E-04
1SD	4.62E-05	3.12E-05	4.09E-05	3.51E-05	5.84E-05	4.49E-05	3.97E-04	2.87E-04	1.91E-04	5.86E-04	1.51E-04	2.91E-04

Plateau Age: 12.72 ± 0.30 (2SD), Steps: C-J

Run ID	1217-03A	1217-03B	1217-03C	1217-03D	1217-03E	1217-03F	1217-03G	1217-03H	1217-03I	1217-03J	1217-03K	1217-03L
Power (watts)	0.5	0.8	0.9	1.0	1.1	1.2	1.3	1.5	1.8	2.0	5.0	10
$^{40}Ar^*$(cps)	3322.962	37807.61	31560.726	52137.685	1005.8279	1203.6846	3712.7206	3297.9603	2203.5553	1585.2539	4852.6603	4613.1917
± σ (cps)	714.86959	1308.6627	695.22264	925.86522	463.68319	514.72197	539.95909	484.15765	541.98775	494.02716	442.52956	481.28087
^{40}Ar(cps)	29713.35	142504.65	53722.622	88104.239	1178.9826	1717.0833	5238.1806	5058.8862	2313.1908	1729.072	4909.921	5386.464
± σ(cps)	42.454566	91.03837	48.019269	62.947905	26.299621	26.819427	25.37609	27.121254	26.461457	26.705837	26.817338	30.38217
^{39}Ar (cps)	33.6069	498.18046	418.37766	694.077	13.782085	16.325269	52.069987	46.334805	30.903585	18.879809	47.841741	58.228098
± σ (cps)	2.6252058	4.4502546	4.2660287	4.5061849	2.2545556	2.2878198	2.7221849	2.7225199	2.6522756	2.5431996	2.917299	2.8655667

^{38}Ar (cps)	18.606288	67.814387	14.893285	19.490381	0.7698103	1.0883761	0.8866287	1.317082	1.0579189	0.9415163	1.8303469	1.3209054
± σ (cps)	0.9712655	1.905073	1.0728838	1.1289754	0.7035408	0.726566	0.8196709	0.8559769	0.770974	0.7683101	0.7903414	0.757236
^{37}Ar (cps)	6.2282054	6.6524226	4.3984282	9.8766663	2.7036129	0.0787964	2.5670142	-0.9116693	1.7027322	5.7275761	2.9431058	2.5343846
± σ (cps)	3.2261505	3.3538	3.5078781	3.3423617	3.3452722	3.4097944	3.0566522	3.1061587	3.6471002	3.5470807	3.3808334	3.1763643
^{36}Ar (cps)	88.392241	350.67336	74.229288	120.46676	0.5799662	1.7195829	5.1093917	5.8980638	0.3672143	0.481706	0.1917899	2.5900063
± σ (cps)	2.3884028	4.3574434	2.3217459	3.0913976	1.5505651	1.7216724	1.8065385	1.6190848	1.8131745	1.6522802	1.479489	1.6087897
D1	1.0068432	1.0067529	1.0066625	1.0065722	1.0064819	1.0063915	1.0056733	1.0050454	1.0044175	1.0037896	1.0031617	1.0025338
± σ	0.0013066	0.0013011	0.0012956	0.0012902	0.0012847	0.0012792	0.0012626	0.0012514	0.0012403	0.0012292	0.0012181	0.0012069
%40Ar*	11.183398	26.530791	58.747553	59.177271	85.313209	70.100538	70.878056	65.191431	95.260422	91.682351	98.833774	85.644157
40Ar*/39ArK	98.877374	75.891395	75.435973	75.118013	72.980818	73.731383	71.302507	71.176738	71.304197	83.965568	101.43151	79.226213

±σ	22.63039	2.7129551	1.8311025	1.4203065	35.699349	33.179097	11.01951	11.254978	18.575038	28.506813	11.127239	9.138887
Age (Ma)	16.938992	13.015325	12.937499	12.883162	12.517887	12.646177	12.230989	12.209488	12.231278	14.394543	17.374454	13.585101
±1σ (Ma)	3.8591052	0.4651993	0.3152562	0.2457058	6.1022242	5.6710447	1.8842189	1.9244884	3.1757526	4.8678189	1.8975803	1.561712
1σ (-J) (Ma)	3.8587798	0.4635995	0.3129188	0.2427248	6.1021115	5.670921	1.8838705	1.9241484	3.1755459	4.8676324	1.8968841	1.5611938
±2σ (Ma)	7.7182103	0.9303987	0.6305124	0.4914116	12.204448	11.342089	3.7684378	3.8489767	6.3515051	9.7356379	3.7951605	3.1234241
2σ (-J) (Ma)	7.7175595	0.927199	0.6258377	0.4854496	12.204223	11.341842	3.767741	3.8482969	6.3510917	9.7352648	3.7937682	3.1223876
Ca/K	0.3447049	0.0248374	0.0195543	0.0264677	0.3648737	0.0089776	0.0916967	-0.0365968	0.1024827	0.564269	0.1144226	0.0809567
± σ	0.1194158	0.0065347	0.012637	0.0032029	0.6183081	16.812608	0.1348076	-0.4269807	0.4789635	0.2924243	0.1579671	0.1311494
Δt (days)	40	40	40	40	40	40	40	40	41	41	41	41
Blank Corrections												
Blank Type[2]	LR	LR	LR	LR	LR	LR	LR	LR	LR	LR	LR	LR

^{40}Ar(cps)	8203.597	8186.901	8170.205	8137.189	8120.516	8103.808	8071.904	8066.309	8060.706	8075.304	8095.874	8116.43
± σ(cps)	14.22639	13.71075	13.77861	15.53829	17.07835	18.92833	14.24591	14.37228	16.09996	15.13941	13.7902	15.71866
^{39}Ar (cps)	165.3051	165.0933	164.8815	164.3931	164.1107	163.8276	163.633	163.6653	163.6976	163.878	164.0287	164.1793
± σ (cps)	0.73705	0.794873	0.924267	0.872335	0.777829	0.86885	0.747652	0.755496	0.847156	0.809389	0.780426	0.933047
^{38}Ar (cps)	6.694005	6.692336	6.690667	6.680936	6.672709	6.664465	6.633801	6.625525	6.617238	6.600811	6.592529	6.584253
± σ (cps)	0.475309	0.504476	0.536197	0.482688	0.423341	0.407269	0.554756	0.530561	0.508072	0.469605	0.453816	0.440809
^{37}Ar (cps)	185.3274	185.3616	185.3958	185.2805	185.128	184.9752	184.4077	184.2553	184.1027	183.9863	184.0233	184.0602
± σ (cps)	0.906654	0.992811	1.091691	1.085584	0.986026	0.909357	0.908156	0.984079	1.083272	1.018755	0.904395	0.888345
^{36}Ar (cps)	32.01213	32.00645	32.00076	31.98952	31.98385	31.97816	31.95704	31.95136	31.94568	28.99691	32.05485	32.11276
± σ (cps)	1.094762	1.034832	0.985756	0.927048	0.919239	0.926838	1.077257	1.143849	1.218568	1.099728	0.961625	0.920055
Inverse Isochron												

$^{39}Ar/^{40}Ar$	1.13E-03	3.50E-03	7.79E-03	7.88E-03	1.17E-02	9.51E-03	9.94E-03	9.16E-03	1.34E-02	1.09E-02	9.74E-03	1.08E-02
1SD	8.84E-05	3.13E-05	7.97E-05	5.15E-05	1.93E-03	1.34E-03	5.22E-04	5.40E-04	1.16E-03	1.48E-03	5.97E-04	5.35E-04
$^{36}Ar/^{40}Ar$	2.97E-03	2.46E-03	1.38E-03	1.37E-03	4.92E-04	1.00E-03	9.75E-04	1.17E-03	1.59E-04	2.79E-04	3.91E-05	4.81E-04
1SD	8.05E-05	3.06E-05	4.32E-05	3.51E-05	1.32E-03	1.00E-03	3.45E-04	3.20E-04	7.84E-04	9.56E-04	3.01E-04	2.99E-04

Plateau Age: 12.92 ± 0.36 (2SD), Steps: A-J

<u>18N11c</u>

Lab Id: 1215 Muscovite Irradiation coordinates: A2 J: 0.00009229 ± 0.00000026 (0.28% 1SD)

Run ID	1215-01A	1215-01B	1215-01C	1215-01D	1215-01E	1215-01F	1215-01G	1215-01H	1215-01I	1215-01K	1215-01L	1215-01M
Power (watts)	0.5	0.8	0.9	1.0	1.1	1.2	1.3	1.5	2.0	10	15	20
^{40}Ar*(cps)	6535.8097	39758.38	38478.616	37279.421	30656.384	33990.365	39881.009	66601.341	125545.06	286.90424	2046.7541	679.17917
± σ (cps)	820.93648	1151.326	807.80159	832.00686	653.26885	652.13866	565.84594	776.46577	968.07631	497.40758	508.1221	581.71696

^{40}Ar(cps)	37013.045	109909.33	64853.172	68862.994	62505.79	50583.341	50665.82	94209.185	177225.59	759.20347	2831.5816	1502.7579
± σ(cps)	40.088414	64.485727	48.793117	46.42922	51.232789	44.832847	44.049677	59.965667	111.45313	28.316592	29.050253	28.896207
^{39}Ar (cps)	51.419183	347.84417	342.94867	337.14307	277.87875	314.88586	378.75705	622.07955	1181.3718	5.1504924	13.661008	10.822068
± σ (cps)	2.9229517	3.832104	4.2448274	3.8696481	4.324616	3.3406393	4.1265724	4.9680266	6.3986364	2.3559782	3.1422717	2.4311569
^{38}Ar (cps)	20.207887	44.55375	17.726551	20.768883	22.113653	9.8552242	9.3609679	16.899095	34.458627	1.6460486	0.7100552	0.9654386
± σ (cps)	1.2172319	1.3995321	1.1123742	1.313324	1.2397179	0.9468105	0.9607047	1.2007759	1.5082005	0.8367756	0.9643454	0.7818339
^{37}Ar (cps)	6.5000966	8.7031839	3.6183277	2.9347192	9.843142	6.6189666	7.1317482	7.9542915	11.886866	-5.52886	-5.3560147	-3.1738096
± σ (cps)	2.7584908	2.8348713	2.9410632	2.9419138	2.8619507	5.2641931	3.3401649	2.9056043	2.8762657	2.4906969	2.8243217	2.9759117
^{36}Ar (cps)	102.08077	234.96434	88.339215	105.78635	106.67674	55.576691	36.122757	92.470002	173.09931	1.581924	2.6287093	2.7585032
± σ (cps)	2.7443268	3.8424727	2.6991609	2.7802212	2.1785123	2.1783481	1.8891265	2.5911571	3.2159059	1.6633195	1.6991236	1.9460014

D1	1.0053744	1.0047704	1.0041663	1.0035623	1.0029583	1.0023542	1.0022879	1.0028257	1.0033634	1.0044389	1.0049766	1.0055144
± σ	0.0012203	0.0012371	0.001254	0.0012709	0.0012877	0.0013046	0.001326	0.0013306	0.0013351	0.0013443	0.0013488	0.0013534
%40Ar*	17.658125	36.173798	59.331895	54.135637	49.045671	67.196756	78.713834	70.695167	70.839126	37.790165	72.283071	45.195516
40Ar*/39ArK	127.10839	114.2994	112.19935	110.57448	110.32288	107.94503	105.29443	107.06242	106.27057	55.704235	149.82453	62.758722
±σ	17.524494	3.5413234	2.7343718	2.7750403	2.911136	2.3665676	1.8835973	1.5129449	1.0014014	99.879672	50.706225	55.571032
Age (Ma)	21.087601	18.973666	18.626847	18.358459	18.316897	17.924053	17.486048	17.778215	17.647365	9.2717596	24.830499	10.442568
±1σ (Ma)	2.8910804	0.5872266	0.4546619	0.4613171	0.4836615	0.3942762	0.3151804	0.2549788	0.1728073	16.582064	8.3464242	9.2199894
1σ (-J) (Ma)	2.8904698	0.5847851	0.4516183	0.4584033	0.4808957	0.3910225	0.3112978	0.2500005	0.1654845	16.582044	8.3461316	9.2199422
±2σ (Ma)	5.7821608	1.1744531	0.9093238	0.9226341	0.9673231	0.7885523	0.6303608	0.5099576	0.3456146	33.164129	16.692848	18.439979
2σ (-J) (Ma)	5.7809395	1.1695701	0.9032366	0.9168066	0.9617915	0.7820449	0.6225956	0.5000011	0.3309691	33.164087	16.692263	18.439884

Ca/K	0.2351298	0.0465379	0.0196242	0.0161907	0.0658857	0.0390976	0.0350226	0.0237831	0.0187152	-1.9966401	-0.7292425	-0.5454859
± σ	0.0557119	0.0054503	0.0132083	0.016456	0.0065953	0.0251453	0.0080639	0.0033634	0.0011971	-1.3185195	-0.3705147	-0.6021233
Δt (days)	34	34	34	34	34	34	34	34	34	34	34	34
Blank Corrections												
Blank Type[2]	LR	LR	LR	LR	LR	LR	LR	LR	LR	LR	LR	LR
^{40}Ar(cps)	10013.35	9961.331	9909.312	9806.271	9754.181	9702.126	9569.641	9580.451	9591.291	9687.696	9720.077	9747.341
± σ(cps)	19.54689	17.73158	16.2717	14.82135	14.9599	15.68388	16.10509	15.22764	17.93876	15.02762	14.79585	16.09319
^{39}Ar (cps)	165.9224	166.1538	166.3852	166.4348	166.2492	166.0638	165.3723	165.187	165.0012	165.6803	166.0075	166.283
± σ (cps)	0.7779156	0.8173237	0.9325416	0.9951958	0.9039286	0.8337925	0.8325742	0.9021462	0.9931473	0.8119158	0.8785074	1.001602
^{38}Ar (cps)	7.799375	7.734126	7.668877	7.53963	7.474291	7.408998	7.276463	7.25187	7.22721	7.444706	7.536317	7.613452
± σ (cps)	0.4865089	0.4640353	0.4596246	0.5042061	0.5493265	0.605459	0.4525775	0.4551425	0.5088381	0.4278383	0.452509	0.5106887

^{37}Ar (cps)	191.6735	191.6212	191.5689	190.4842	189.4302	188.377	187.953	187.7341	187.5147	187.6881	187.8366	187.9616
± σ (cps)	0.8495836	0.7784526	0.8767693	0.8803105	0.8135762	0.9397658	0.9516365	0.8485426	0.947707	0.849083	0.8931416	1.005407
^{36}Ar (cps)	36.65674	36.56438	36.47202	36.28908	36.1966	36.10418	35.74217	35.64344	35.54445	35.91999	36.09949	36.25062
± σ (cps)	1.298481	1.154091	1.04705	0.9896925	1.047565	1.15496	0.9529539	1.017692	1.177561	0.9905968	1.041999	1.172975
Inverse Isochron												
^{39}Ar/^{40}Ar	1.39E-03	3.16E-03	5.29E-03	4.90E-03	4.45E-03	6.23E-03	7.48E-03	6.60E-03	6.67E-03	6.78E-03	4.82E-03	7.20E-03
1SD	7.90E-05	3.49E-05	6.56E-05	5.63E-05	6.93E-05	6.63E-05	8.17E-05	5.29E-05	3.63E-05	3.11E-03	1.11E-03	1.62E-03
^{36}Ar/^{40}Ar	2.76E-03	2.14E-03	1.36E-03	1.54E-03	1.71E-03	1.10E-03	7.13E-04	9.82E-04	9.77E-04	2.08E-03	9.28E-04	1.84E-03
1SD	7.42E-05	3.50E-05	4.16E-05	4.04E-05	3.49E-05	4.31E-05	3.73E-05	2.75E-05	1.82E-05	2.19E-03	6.00E-04	1.30E-03

Plateau Age: 17.76 ± 0.25 (2SD), Steps: D-L

Run ID	1215-02A	1215-02B	1215-02C	1215-02D	1215-02E	1215-02F	1215-02G	1215-02H	1215-02I	1215-02J	1215-02K	1215-02L

Power (watts)	0.5	0.8	0.9	1.0	1.1	1.2	1.3	1.5	1.8	2.0	5.0	10
^{40}Ar*(cps)	6843.4304	37817.087	46972.985	259610.14	44544.987	27336.382	84298.245	4575.4069	6333.2442	2329.3448	22734.246	2590.7368
± σ (cps)	657.71271	931.14073	730.47146	1343.7536	700.87131	615.84275	620.13291	509.98842	492.91999	489.06158	520.55626	503.56013
^{40}Ar(cps)	17339.278	84202.09	71906.736	376978	60170.567	33253.897	96314.347	5954.0875	6994.7153	2451.8173	25377.308	2933.3686
± σ(cps)	30.214153	64.20421	56.788227	240.43876	46.118802	39.544078	63.548689	28.566205	31.036561	24.616082	35.498639	28.261177
^{39}Ar (cps)	35.154784	346.6612	446.7834	2474.8142	422.74995	262.17316	821.19162	43.650948	54.946185	16.63941	202.0343	13.576557
± σ (cps)	2.451024	4.11845	4.6216532	9.3346548	3.8550395	3.6551377	5.4311127	2.5142585	2.9584639	2.5580224	3.7303571	2.398988
^{38}Ar (cps)	4.7049526	31.146871	14.670739	79.143882	9.6920587	4.841345	7.322675	1.09573	-1.6560867	0.1691255	0.167604	-1.4575092
± σ (cps)	1.0088632	1.3334399	1.1344443	1.996436	0.8795154	0.8151044	1.11646	0.771749	0.7842917	0.779643	0.8256693	0.7144173
^{37}Ar (cps)	6.8934422	11.574354	7.4022748	15.562403	12.849727	8.2812817	-0.3035834	-0.3521467	-3.0766413	-5.7908811	0.4379073	-5.4304073

± σ (cps)	3.154723	3.385544	2.9755244	3.2151813	2.6713315	2.6635335	2.982099	3.0667405	3.325086	3.0468138	2.9119389	2.89783
^{36}Ar (cps)	35.154903	155.36242	83.513368	393.11315	52.336484	19.820188	40.246857	4.6177674	2.2155382	0.4102105	8.8526992	1.1476144
± σ (cps)	2.2003214	3.107165	2.4377023	4.4092948	2.3417875	2.0583505	2.0657222	1.705472	1.6477138	1.6359916	1.7394735	1.6839708
D1	1.0041624	1.0041355	1.0041086	1.0040817	1.0040548	1.0040279	1.0041462	1.0042915	1.0044367	1.004582	1.0047273	1.0048725
± σ	0.0013367	0.0013213	0.001306	0.0012906	0.0012752	0.0012598	0.0012414	0.0012383	0.0012352	0.0012322	0.0012291	0.001226
%40Ar*	39.467792	44.91229	65.324874	68.866125	74.03119	82.205047	87.524079	76.844804	90.543274	95.00483	89.58494	88.319512
40Ar*/39ArK	194.66569	109.08947	105.13592	104.90086	105.36958	104.26842	102.65356	104.81804	115.26267	139.98963	112.52666	190.82429
±σ	23.113529	2.9823476	1.9636344	0.6718437	1.9162047	2.7624166	1.0154811	13.151075	10.908417	36.428406	3.3099135	50.126404
Age (Ma)	32.19623	18.113136	17.459851	17.421002	17.498468	17.316473	17.049544	17.407314	19.132726	23.210971	18.680907	31.566405
±1σ (Ma)	3.7900482	0.4953554	0.3282451	0.1214242	0.3205073	0.4591861	0.1746203	2.1740971	1.8019753	6.0017633	0.5491921	8.2204936
1σ (-J) (Ma)	3.7889689	0.4927148	0.32453	0.1110381	0.3166846	0.4565811	0.1678667	2.1735426	1.8011678	6.0014073	0.5466604	8.2200152

±2σ (Ma)	7.5800964	0.9907107	0.6564903	0.2428484	0.6410146	0.9183723	0.3492406	4.3481942	3.6039506	12.003527	1.0983841	16.440987
2σ (-J) (Ma)	7.5779379	0.9854296	0.6490601	0.2220761	0.6333691	0.9131621	0.3357335	4.3470853	3.6023357	12.002815	1.0933209	16.44003
Ca/K	0.3647243	0.0621018	0.0308163	0.0116963	0.0565358	0.0587519	-0.0006876	-0.0150052	-0.1041483	-0.647321	0.0040315	-0.7439705
± σ	0.1018151	0.0060511	0.0052982	0.0005434	0.0029589	0.0068969	-0.0663536	-1.1388838	-0.1272555	-0.2787079	0.1783411	-0.3433142
Δt (days)	37	37	37	37	37	37	37	37	37	37	37	37
Blank Corrections												
Blank Type[2]	LR	LR	LR	LR	LR	LR	LR	LR	LR	LR	LR	LR
^{40}Ar(cps)	8926.318	8880.574	8835.018	8774.039	8758.389	8742.706	8608.468	8565.008	8521.549	8476.941	8475.711	8474.48
± σ(cps)	13.56079	12.37661	14.13869	14.5187	13.81824	16.36258	13.94401	13.82129	15.30582	14.35101	13.08256	14.92294
^{39}Ar (cps)	166.6534	166.5979	166.5426	166.4329	166.3776	166.3222	166.2559	166.3434	166.431	166.6041	166.6915	166.7789
± σ (cps)	0.814102	0.779576	0.76823	0.81563	0.87094	0.94302	1.085368	0.985733	0.909198	0.84876	0.87055	0.925465

^{38}Ar (cps)	7.796987	7.769334	7.741793	7.687183	7.659642	7.632045	7.529239	7.50166	7.474082	7.545123	7.645563	7.746072
± σ (cps)	0.586489	0.545721	0.509823	0.456746	0.44132	0.434701	0.488453	0.520577	0.558118	0.509456	0.452244	0.444167
^{37}Ar (cps)	186.5299	186.5503	186.5707	186.611	186.6313	186.6517	186.7275	186.7479	186.7682	186.6994	186.6085	186.5176
± σ (cps)	1.024309	0.954084	0.893159	0.806706	0.784276	0.777931	0.892167	0.953005	1.022894	0.934317	0.830553	0.817621
^{36}Ar (cps)	35.37024	34.99171	34.61472	33.86721	33.49022	33.11246	33.35401	33.04204	32.73008	30.58548	32.75557	32.92577
± σ (cps)	1.32665	1.179171	1.074807	1.039579	1.113926	1.238633	1.095611	0.922594	0.965084	0.944146	0.814342	0.876837
Inverse Isochron												
$^{39}Ar/^{40}Ar$	2.03E-03	4.12E-03	6.21E-03	6.56E-03	7.03E-03	7.88E-03	8.53E-03	7.33E-03	7.86E-03	6.79E-03	7.96E-03	4.63E-03
1SD	1.41E-04	4.90E-05	6.45E-05	2.51E-05	6.43E-05	1.10E-04	5.67E-05	4.24E-04	4.24E-04	1.05E-03	1.47E-04	8.19E-04
$^{36}Ar/^{40}Ar$	2.03E-03	1.85E-03	1.16E-03	1.04E-03	8.70E-04	5.96E-04	4.18E-04	7.76E-04	3.17E-04	1.67E-04	3.49E-04	3.91E-04
1SD	1.27E-04	3.69E-05	3.39E-05	1.17E-05	3.89E-05	6.19E-05	2.14E-05	2.86E-04	2.36E-04	6.67E-04	6.85E-05	5.74E-04

Plateau Age: 17.36 ± 0.19 (2SD), Steps: B-K

Run ID	1215-03A	1215-03B	1215-03C	1215-03D	1215-03E	1215-03F	1215-03G	1215-03H	1215-03I	1215-03J	1215-03K	1215-03L
Power (watts)	0.5	0.8	0.9	1.0	1.1	1.2	1.3	1.5	1.8	2.0	5.0	10
$^{40}Ar^{*}$(cps)	5844.0754	50206.806	20391.101	36442.905	31124.133	35691.157	54616.023	59188.279	16208.078	29573.186	2203.0816	4830.3411
± σ (cps)	701.00755	1055.7491	664.4386	1006.1582	570.28726	607.55788	765.44646	1237.0803	541.53748	530.41308	480.77783	514.28628
^{40}Ar(cps)	26141.248	123505.42	44412.36	90149.776	43941.419	47010.326	76303.97	83423.892	19205.051	31161.404	2450.987	5041.3283
± σ(cps)	31.713652	72.16126	45.3521	61.550268	43.046116	47.618843	49.685912	101.00205	34.906966	40.173285	25.623243	25.907013
^{39}Ar (cps)	46.865124	473.75215	193.29369	350.42611	295.52403	345.87867	516.89529	565.67203	157.13556	284.26483	19.798085	45.515879
± σ (cps)	2.875529	4.3358147	3.6322462	4.0348276	3.8121996	3.9336061	4.4449642	8.0060357	3.712859	4.3318334	2.8885711	2.8328262
^{38}Ar (cps)	12.608564	46.393614	13.969024	34.002471	7.4864444	4.8416753	12.889256	15.654644	0.1903916	1.4462187	-0.733385	0.3847639
± σ (cps)	1.0954196	1.6983136	0.9970135	1.2770591	0.8593638	0.8074645	1.0792387	1.6826812	0.8475424	0.8613574	0.6748056	0.7372432

^{37}Ar (cps)	8.4441091	11.993869	7.6308534	8.3940798	7.4808974	-1.2487819	4.4477318	5.7533972	5.2665269	10.467083	0.218125	-4.3553843
± σ (cps)	3.2714032	2.9570897	3.1851276	3.109988	3.3096397	2.8201058	2.8953932	3.0424784	2.8801923	2.9275211	2.840945	2.8690633
^{36}Ar (cps)	67.983564	245.50716	80.457058	179.88636	42.930354	37.912543	72.641838	81.17502	10.038093	5.3195942	0.8303369	0.7066828
± σ (cps)	2.3444957	3.5186455	2.2187152	3.3585354	1.9041553	2.0283187	2.5572754	4.1287963	1.8100292	1.7714595	1.6080335	1.7203687
D1	1.0048231	1.0046285	1.0044339	1.0042392	1.0040446	1.0038499	1.0038649	1.0040745	1.0042842	1.0044938	1.0047034	1.004913
± σ	0.0012087	0.0011944	0.0011801	0.0011659	0.0011516	0.0011373	0.0011653	0.0012075	0.0012498	0.001292	0.0013342	0.0013765
%40Ar*	22.355763	40.651499	45.913122	40.424842	70.830968	75.921952	71.576909	70.948834	84.39487	94.903253	89.885488	95.814849
40Ar*/39ArK	124.69988	105.97695	105.49284	103.99597	105.31845	103.18982	105.66168	104.63356	103.1471	104.03392	111.27751	106.12431
±σ	16.801286	2.4304041	3.9681005	3.110922	2.3600189	2.1125222	1.7373895	2.6411496	4.2210158	2.4484573	29.21145	13.087949
Age (Ma)	20.690301	17.598842	17.518838	17.271442	17.490017	17.138189	17.54674	17.376824	17.131128	17.277714	18.474586	17.623194

±1σ (Ma)	2.7724068	0.4046976	0.6576458	0.5164986	0.3931412	0.3525292	0.2913586	0.439266	0.6994059	0.4076213	4.8253518	2.1634222
1σ (-J) (Ma)	2.7717936	0.4016422	0.6557869	0.514196	0.390034	0.3491989	0.2871247	0.4365231	0.6977345	0.4046975	4.8250706	2.1628512
±2σ (Ma)	5.5448135	0.8093953	1.3152916	1.0329972	0.7862824	0.7050584	0.5827171	0.878532	1.3988117	0.8152426	9.6507036	4.3268444
2σ (-J) (Ma)	5.5435872	0.8032845	1.3115739	1.0283919	0.7800681	0.6983977	0.5742495	0.8730462	1.395469	0.8093951	9.6501412	4.3257023
Ca/K	0.3351329	0.0470892	0.0734291	0.0445543	0.0470841	-0.0067155	0.0160048	0.0189179	0.0623394	0.0684882	0.0204925	-0.1779822
± σ	0.070864	0.0032934	0.0141729	0.0066289	0.0098231	-0.0343242	0.0069201	0.005558	0.0201178	0.0064012	3.4792318	-0.0883105
Δt (days)	37	37	37	37	37	37	37	37	37	37	37	38
Blank Corrections												
Blank Type[2]	LR	LR	LR	LR	LR	LR	LR	LR	LR	LR	LR	LR
^{40}Ar(cps)	8480.247	8482.827	8485.42	8507.088	8526.55	8546.038	8592.576	8587.049	8579.633	8544.767	8514.811	8484.897
± σ(cps)	12.83572	12.89369	14.41572	13.72718	13.11366	15.57415	16.11489	14.19201	16.04669	15.64905	13.13585	13.68113

^{39}Ar (cps)	166.9255	166.8305	166.735	166.3149	165.9834	165.6515	165.2604	165.2386	165.2092	165.1658	165.1439	165.122
± σ (cps)	0.944677	0.814432	0.877238	0.872214	0.777828	0.86885	0.865487	0.822982	0.814477	0.903213	0.985503	1.085801
^{38}Ar (cps)	8.000607	7.979324	7.957924	7.915793	7.894538	7.873255	7.982006	7.918843	7.834093	7.708763	7.64547	7.582264
± σ (cps)	0.573258	0.503392	0.445928	0.391446	0.40163	0.436222	0.50797	0.461601	0.413803	0.384936	0.392597	0.414572
^{37}Ar (cps)	186.2101	186.1504	186.0905	185.9724	185.9129	185.8532	185.6666	185.6428	185.6108	185.4761	185.3629	185.2499
± σ (cps)	1.085675	0.986053	0.909129	0.848764	0.870583	0.925565	0.953519	0.78766	0.795323	0.829724	0.758136	0.778942
^{36}Ar (cps)	33.19297	33.22858	33.26439	33.37143	33.44425	33.51718	33.56059	33.70382	33.89601	34.18022	34.32375	32.46709
± σ (cps)	0.880598	0.987547	1.171126	1.102689	0.955626	1.03508	1.178918	1.070235	0.956409	0.88202	0.895302	0.941915
Inverse Isochron												
$^{39}Ar/^{40}Ar$	1.79E-03	3.84E-03	4.35E-03	3.89E-03	6.73E-03	7.36E-03	6.77E-03	6.78E-03	8.18E-03	9.12E-03	8.08E-03	9.03E-03
1SD	1.10E-04	3.52E-05	8.19E-05	4.48E-05	8.70E-05	8.40E-05	5.84E-05	9.63E-05	1.94E-04	1.40E-04	1.18E-03	5.64E-04

$^{36}Ar/^{40}Ar$	2.60E-03	1.99E-03	1.81E-03	2.00E-03	9.77E-04	8.06E-04	9.52E-04	9.73E-04	5.23E-04	1.71E-04	3.39E-04	1.40E-04
1SD	8.97E-05	2.85E-05	5.00E-05	3.73E-05	4.33E-05	4.32E-05	3.35E-05	4.95E-05	9.43E-05	5.68E-05	6.56E-04	3.41E-04

Plateau Age: 17.41 ± 0.29 (2SD), Steps: A-L

Explanations

D1: Mass discrimination per AMU based on power law (Renne et al., 2009)

Blank Type2: Ave = average; LR = linear regression versus time

Δt = Time interval (days) between end of irradiation and analysis

N.D. = negative values indicate that the value is indistinguishable from the background

Constants Used

Atmospheric argon ratios $(^{40}Ar/^{36}Ar)_{Air}$: 298.56 ± 0.31 from Lee et al. (2006)

Interfering Isotope Production Ratios

Derived from co-irradiated Fe-doped kalsilite and from CaF_2

$(^{40}Ar/^{39}Ar)K$	0.000104 ± 0.000024
$(^{38}Ar/^{39}Ar)K$	0.012201 ± 0.000045
$(^{37}Ar/^{39}Ar)K$	0.0001676 ± 0.0000028
$(^{39}Ar/^{37}Ar)Ca$	0.0006689 ± 0.000055
$(^{38}Ar/^{37}Ar)Ca$	0.0000316 ± 0.0000012
$(^{36}Ar/^{37}Ar)Ca$	0.0003058 ± 0.0000031
$(^{36}Cl/^{38}Cl)Cl$	263 ± 2

Decay Constants

$^{40}K\ \lambda_{\varepsilon}$	5.757E-11 ± 0.016E-11	Renne et al., (2011)
$^{40}K\ \lambda_{\beta}$	4.9548E-10 ± 0.0134E-10	Renne et al., (2011)
^{39}Ar	2.58E-3 ± 2.87E-05 a^{-1}	Stoenner et al. (1965)
^{37}Ar	7.24E0 ± 1.66E-02 a^{-1}	Renne & Norman (2001)
$^{36}Cl\ \lambda_{\beta}$	(2.305)E-6 a^{-1}	Endt (1998)

References for $^{40}Ar/^{39}Ar$ Experimental Data

Endt, P. M. (1998). Supplement to energy levels of A = 21–44 nuclei (VII). *Nuclear Physics A, 633*(1), 1-220. doi:https://doi.org/10.1016/S0375-9474(97)00613-1

Lee, J.-Y., Marti, K., Severinghaus, J. P., Kawamura, K., Yoo, H.-S., Lee, J. B., & Kim, J. S. (2006). A redetermination of the isotopic abundances of atmospheric Ar. *Geochimica et Cosmochimica Acta, 70*(17), 4507-4512. doi:https://doi.org/10.1016/j.gca.2006.06.1563

Renne, P. R., Balco, G., Ludwig, K. R., Mundil, R., & Min, K. (2011). Response to the comment by W. H. Schwarz et al. on "Joint determination of 40K decay constants and the 40Ar*/40K for the Fish Canyon sanidine, and improved accuracy for 40Ar/39Ar geochronology" by P.R. Renne et al. (2010). *Geochimica et Cosmochimica Acta, 75*, 5097-5100.

Renne, P. R., Cassata, W. S., & Morgan, L. E. (2009). The isotopic composition of atmospheric argon and 40Ar/39Ar geochronology: Time for a change? *Quaternary Geochronology, 4*(4), 288-298. doi:https://doi.org/10.1016/j.quageo.2009.02.015

Renne, P. R., & Norman, E. B. (2001). Determination of the half-life of 37Ar by mass spectrometry. *Physical Review C, 63*(4), 047302. doi:10.1103/PhysRevC.63.047302

Stoenner, R. W., Schaeffer, O. A., & Katcoff, S. (1965). Half-Lives of Argon-37, Argon-39, and Argon-42. *Science, 148*(3675), 1325-1328. doi:doi:10.1126/science.148.3675.1325